Investigating mtDNA replication in neurons; implications for mtDNA deletion formation

Elizabeth Dona Stephen

BSc (Hons) MRes

This thesis is submitted for the degree of Doctor of Philosophy at Newcastle University

Author's declaration

This thesis is submitted for the degree of Doctor of Philosophy at Newcastle University. The research was conducted in the Wellcome Trust Centre for Mitochondrial Research, Institute of Neuroscience, and is my own work if not stated otherwise. The research was completed under the supervision of Prof Sir D.M. Turnbull and Dr A.K. Reeve. All work is my own unless otherwise stated.

I certify that none of the material offered in this thesis has been previously submitted by me for a degree or any other qualification at any other university.

Abstract

Mitochondria contain their own DNA (mtDNA) which can be damaged, leading to the formation of mtDNA deletions (ΔmtDNA). These are particularly prominent in post mitotic tissues and progressively accumulate with advancing age. Within the brain, ΔmtDNA may reach levels of 50% and has been linked to COX-deficiency and neurodegeneration. Although these ΔmtDNA are well characterised, the definitive mechanism for their formation and accumulation to high levels is unknown. One of the suggestions for deletion formation is inadequate replication. This study aimed to further understand how mtDNA replication differs between neurons and with age, and whether such changes could be associated with the formation and accumulation of mtDNA deletions.

This was investigated in different ways. Various regions of the brain differ in the levels of deletions. Therefore, the mtDNA replication levels in different regions were investigated via thymidine analogue labelling to identify any alterations. Significant differences were noticed between different regions with cerebellum generally presenting increased signal and the SN presenting the lowest. Since ageing and disease is a risk factor of ΔmtDNA accumulation, aged mice and *PolgA*$^{mut/mut}$ mice were used, demonstrated a general decrease in thymidine analogue signalling with increased age and with a replication defect. The replication levels obtained from this study were compared to another study from the literature investigating the levels of deletions from different brain regions. No correlation was observed suggesting that although mtDNA replication is altered within different regions in the brain, there could be other mechanisms effecting the formation and accumulation of ΔmtDNA.

Additionally, the thymidine analogue labelling was developed and optimised for *in vitro* use on HeLa cells and was used to label iPSCs and differentiated neurons from a patient with a large scale mtDNA deletion. Two isogenic cell lines of varying heteroplasmy (>10% and 40%) were used for this study to see the effect of altered ΔmtDNA on replication. The methodology was optimised successfully for further use.

Along with the total replication levels, the location of replication was also investigated to understand the impact of this on the accumulation of ΔmtDNA. This is due to previous theories

that have suggested that since replication and mitophagy happen in close proximity to the nucleus and each other, this increases the chances of a dysfunctional mitochondria, containing ΔmtDNA, replicating. The results suggested that majority of the replication happened in the perinuclear region, and preliminary data on the location of mitophagy also showed a perinuclear increase.

To further investigate the health and connectivity of the mitochondria in the perinuclear region I compared them to distal mitochondria. This novel 'proof-of-concept' study investigated the morphology and structural connectivity of mitochondria in human brain tissue using electron microscopy techniques. This study was successful and preliminary data from dopaminergic neurons are discussed.

In conclusion although mtDNA replication levels and replication location varies between neurons, ageing and genotype suggesting implications for ΔmtDNA formation.

Dedicated to all individuals that have donated to scientific research in any form.

Acknowledgements

'I can do all things through him who strengthens me' – Thanks to the big G.

Firstly, thanks to all the sponsors who have funded this thesis.

Thank you to my supervisors. Doug, thank you for your input and insight that is unparalleled. Your need to 'tell a story' has helped me in many ways with my research. Amy, starting with my masters you have always been there. You saw potential in me when I often couldn't and I'll forever be in debt and thankful for your patience, scientific knowledge, encouragement and chats. Thank you also to my assessors Prof Bobby McFarland, Dr Laura Greaves and Dr Helen Tuppen for all your insights and guidance regarding my projects.

Amy V, thank you for being a 'surrogate' supervisor in times of need. You are someone I often confide in science and science-related life problems and thank you so much for being friendly and offering sound advice. Helen, even though we couldn't finish that project, thank you so much for helping me become a better scientist in techniques and writing. Thank you also for a lot of funny chats. Ollie, thanks for being so clever. You always have the answer for everything and a great fashion sense #GreenShirtSquad. Hannah Rosa, thanks for making work bearable on the days when real-time failed #GoneButNeverForgotten (Don't worry, she is still alive, just left the lab).

A number of people have made these past three years more vibrant and exciting that even an introvert like me, enjoyed it. My main gals Char, Nisa, Chun, G, T'dwag, Carla[2], Hulio, Pavan, Hannah and Shawn. Work doesn't feel that tough with you guys around. Thank you for the endless hours of funny conversations, pick-me-ups and venting times. Thank you also, for proof-reading. Thank you also to my mallu squad, you know who you are #StartedFromTheBottomNowWeHere #TooManyToName. Thanks Lily mumma and BLC for all their support.

Finally, my OG's, Pappadom, Paco, Chinnol and Linin. You guys are exceptional human beings. Papa and mamma, you have put aside so much for a better life for Chinnu and me, and I am forever grateful for your love and in awe of your selflessness. Chinnu, thanks for constantly

being worried about me and checking up on me. Libin, thanks for all the distractions that I needed and giving me hope when I didn't have any.

Contents

List of figures

List of tables

List of equations

Abbreviations

3D	Three-dimensional
ADP	Adenosine diphosphate
AIFM1	Apoptosis Inducing Factor Mitochondria Associated
AMPK	AMP-activated protein kinase
ANT	Adenine nucleotide Translocator
ATP	Adenosine Triphosphate
ATPase	Adenosine Triphosphate synthase
BAG3	BCL2-Associated Athanogene 3
BCL2	B-cell lymphoma 2
BER	base excision repair
C	Cytosine
Ca2+	Calcium ion
CBC	Comparative Biology Centre
CCCP	Carbonyl cyanide m-chlorophenyl hydrazone
cDNA	Coding DNA
CER	cerebellum
CFV	Cresyl Fast Violet
CldU	5-Chloro-2-deoxyuridine thymidine
CM	cristae membrane
CO_2	Carbon dioxide
COR	cortex

COX   Cytochrome c oxidase

CPEO   Chronic Progressive External Opthalmoplegia

dH2O   Distilled water

D-Loop   Displacement loop

DMSO   Dimethyl Sulfoxide

DNA   Deoxyribonucleic Acid

dNTP   Deoxynucleotide

DRP   Dynamin-related proteins

DRP   dynamin-like protein

DSB   Double strand break

E site   Exit site

EM   electron microscopy

ERR   Estrogen Related Receptor

ETC   Electron transport chain

FADH   Flavin adenine dinucleotide

Fe-S   Iron-sulphur

FIS   Fission

G   Guanine

GAPDH   Glyceraldehyde 3-phosphate dehydrogenase

GFM1   by G Elongation Factor Mitochondrial 1

GTP   Guanosine triphosphate

H strand   Heavy strand

H+	Protons
H2O	Water
HCl	Hydrochloric acid
HIP	hippocampus
HMG	high mobility group
HR	heptad repeats
HSP	Heavy strand promoters
HVR	Hypervariable region
IBM	inner boundary membrane
IdU	Iodo-2-deoxyuridine
IHC	Immunohistochemistry
IMM	Inner mitochondrial membrane
IMS	Intermembrane space
Kb	Kilobase
kDa	Kilo daltons
KSS	Kearn-Sayre Syndrome
L strand	Light strand
LC3	Light chain 3
LFB	Luxol Fast Blue staining
LIR	LC3-interacting region
LONP	Mitochondrial Lon peptidase
LSP	Light strand promotor

M   Molar

MALM   Mieap-induced accumulation of lysosome-like organelles

MCU   mitochondrial Ca^{2+} uniporter

MELAS   Mitochondrial Enchephalomyopathy, Lactic Acidosis and Stroke-like episodes

MFF   mitochondrial fission factor

MFN   Mitofusion

MiD   mitochondrial dynamic

ml   millilitre

mM   millimolar

MMR   mismatch repair

mRNA   messenger Ribonucleic Acid

MT   Microtubules

mtDNA   Mitochondrial DNA

mtEFT   translation elongation factor

mtIF   Mitochondrial Translational Initiation Factor

mtSSB   Mitochondrial Single Strand Binding protein

mtTFB   mitochondrial transcription factor B

mt-tRNA   mitochondrial transfer Ribonucleic Acid

mtTUFM   Tu Translation Elongation Factor, Mitochondrial

mV   millivolts

Na+   Sodium ion

NADH   Nicotinamide adenine dinucleotide

NaOH	Sodium hydroxide
NBTR	Newcastle brain tissue resource
ND	NADH dehydrogenase
nDNA	nuclear DNA
NER	nucleotide excision repair
NGS	Normal goat serum
NH_3	Ammonia
NIX	NIP3-like protein X
nM	nanomolar
NRF	Nuclear respiratory factors
O_2	oxygen
OH	Origin of heavy strand replication
OL	Origin of light strand replication
OMM	Outer mitochondrial membrane
OPA1	Optic Atrophy 1
OXPHOS	Oxidative phosphorylation
P site	peptidyl-tRNA binding site
PARL	presenilins-associated rhomboid-like protein
PBS	Phosphate buffered saline
PCR	Polymerase Chain Reaction
PEO	Progressive External Opthalmoplegia
PEO	progressive external ophthalmoplegia

PGC-1α	Peroxisome proliferator-activated receptor γ, coactivator 1α
Pi	Inorganic Phosphate
PINK1	PTEN-induced putative kinase 1
PM	Post-mortem
PO	PolgA$^{mut/mut}$ old
POLG	Polymerase Gamma
POLMRT	Mitochondrial RNA polymerase
POLRMT	mtRNA polymerase
Polγ	Polymerase Gamma
PPARγ	Peroxisome Proliferator Activated Receptor Gamma
PY	PolgA$^{mut/mut}$ young
Rcf	Relative Centrifugal Force
RITOLS	Ribonucleotide incorporation throughout the lagging strand
RNA	Ribonucleic Acid
ROI	Region of interest
ROS	Reactive oxygen species
RRM2B	Ribonucleotide Reductase subunit M2 B
RT	Room temperature
SBF-SEM	Serial Block Face Scanning Electron Microscopy
SD	Standard Deviation
SDH	Succinate Dehydrogenase
SDM	strand-displacement

SIRT1   Situins

SLC   solute carrier

smPCR   Single molecule PCR

SN   Substantia nigra

SPATA18   Spermatogenesis Associated 18

SPATA18   Spermatogenesis Associated 18

T   Thymidine

TCA   Tricarboxylic Acid

TEM   Transmission Elctron Microscopy

TFAM   Transcription Factor A, Mitochondrial

TIM   translocases of the inner membrane

Tm   Melting temperature

TOM   translocases of the outer membrane

tRNA   transfer ribonucleic acid

TSFM   Tu Translation Elongation Factor, Mitochondrial

TWINKLE   Twinkle helicase

UNG   Uracil-N glycoslyase

UV   ultra violet

VDAC   Voltage Dependant Anion Channel

VGLUT   Vesicular glutamate transporter

WO   wildtype old

WT   Wild-type

WY   wildtype young

ΔmtDNA   mtDNA deletion

μl   microlitre

μm   micromolar

Chapter 1 : Introduction

1.1 Origin of Mitochondria

Mitochondria are dynamic organelles present within the cytoplasm of all mammalian nucleated cells. The origin of mitochondria has been theorised to arise due to an endosymbiotic relationship, where a primitive free-living prokaryote with the ability to utilise oxygen available in the atmosphere as an energy source, was engulfed by a pre-eukaryotic cell. This was brought to light in 1971 (Margulis, 1971), and explained that the reason for this symbiotic relationship was that the free-living prokaryote received a secure and stable environment and in return ATP (adenosine triphosphate) as the result of respiration, was provided for the host cell (Martin et al., 2015). The main evidence for this theory is the prokaryotic-like properties of the mitochondrion including its double membrane, circular genome, ability to undergo fission and fusion and the ability to independently synthesise proteins. Alongside this, a high proportion of genes required for mitochondrial structure, function and quality control are found in the nuclear genome (Gray, 2012, Gray et al., 1999).

The hydrogen hypothesis theory proposes another basis for mitochondrial origin (Martin and Müller, 1998). This theory suggests that the host cell was a methanogenic archezoa which engulfed a eubacterium with the ability to produce H_2 and CO_2. When the host was in an environment with a lack of H_2, a symbiotic relationship was formed between the two species. Selective pressures within this environment selected the host cells with this symbiotic relationship (Martin et al., 2001). This theory suggests that the formation of the nucleus occurred following this symbiotic event. However this theory is not completely accepted as a 'true archezoa', a eukaryotic cell without a mitochondria, has not been identified and molecular analysis has identified mitochondrial genes present within the nuclear DNA of this group (Clark and Roger, 1995, Roger, 1999).

The ancestor of mitochondria has been suggested to be the intracellular parasite *Rickettsia prowazekii,* identified by whole genome sequencing (Andersson et al., 1998). This analysis found genes encoding for components of the tricarboxylic acid (TCA) cycle and complexes of the respiratory chain within its genome, allowing *Rickettsia prowazekii* to produce ATP, similar

to mitochondria. However, due to inconsistencies in phylogenetic trees during analysis and a fast evolution rate, it has been suggested that this might not be the true ancestor of mitochondria but simply a lineage relative (Degli Esposti, 2018, Degli Esposti, 2016). In other studies, a few other organisms have been suggested to be the evolutionary ancestor of mitochondria (Yang et al., 1985, Atteia et al., 2009, Williams et al., 2007, Degli Esposti, 2018), despite this, all studies are consistent in their agreement for a prokaryotic origin for the mitochondrion (Gray, 2015).

1.2   Mitochondrial Structure

In concurrence with their prokaryote ancestors, mitochondria have been observed through electron microscopy as consisting of a double membrane structure with an outer mitochondrial (OMM) and an inner mitochondrial membrane (IMM) separated by the intermembrane space (Palade, 1953, Mannella et al., 1994). Figure 1.1 presents a cartoon illustration of a mitochondrion highlighting its integral structures (figure 1.1a), and an image obtained from electron microscopy (EM, figure 1.1b). Although typically illustrated as a rod shaped organelle (figure 1.1a), the shape and size of mitochondria vary due to their dynamic nature and ability to form a reticular network. Initial studies, using EM, measured mitochondrial length to be in the range of 1-4µm and with diameters ranging between 0.3-0.7µm (Palade, 1953). This is consistent with the EM image (figure 1.1b) produced for the purpose of this thesis. Further studies looking at 3D models have demonstrated consistent values within the range of 0.75 to 3µm^2 for the size of mitochondria (Rafelski and Marshall, 2008, Bereiter-Hahn, 1990, Wiemerslage and Lee, 2016). The number of mitochondria per cell also varies depending on the cell type due to differential energy requirements (Nass, 1969). Analysis of five different mammalian cell types demonstrated an average of 83 mitochondria per cell (Robin and Wong, 1988). However, these measures are not fixed since mitochondria can undergo fission and fusion constantly merging or separating.
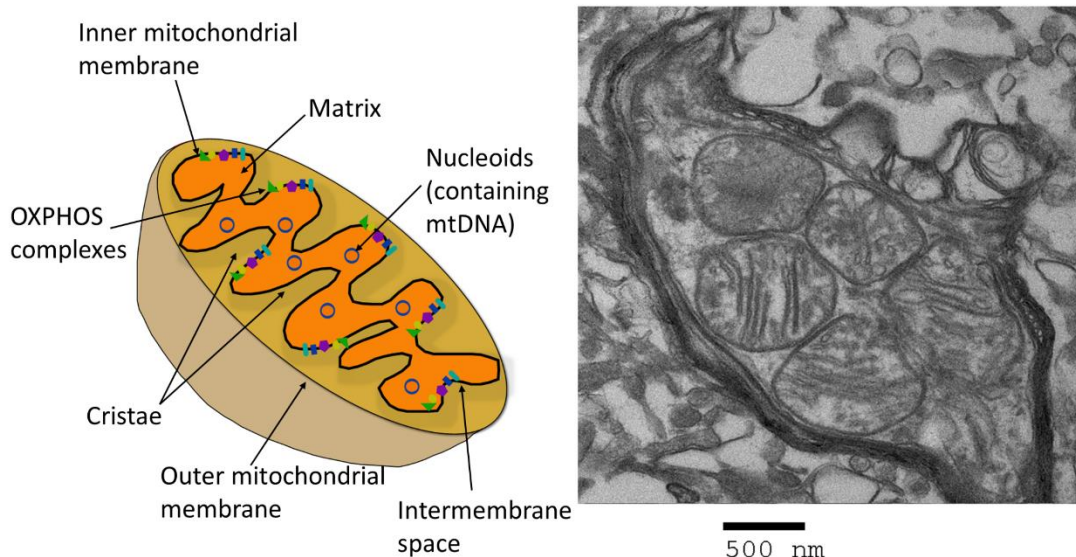
Figure 1.1 The structure of the mitochondrion. Image A presents the cartoon representation of a mitochondrion with its structural components labelled. Image B presents an electron microscopy image of multiple mitochondria presented within an axon. The image shows clearly the cristae and double membrane structures of the mitochondria

The double membrane of the mitochondrion has a similar structure to the phospholipid bilayer of the cell membrane and functions in a similar way to allow selective permeabilisation. The OMM is a smooth lipid membrane separating the free flow of molecules between the mitochondrial interior and the cytoplasm of the cell. The membrane contains voltage-dependent anion channels (VDAC), also known as mitochondrial porin. These channels allow the exchange of molecules and ions <10kDa to pass (Alberts et al., 2002, Szabo and Zoratti, 2014). VDAC remains open at a membrane potential of 0mV, but when the potential reaches 30mV (for both positive and negative potential), it closes (Blachly-Dyson and Forte, 2001).

Compared to the OMM, the IMM is highly selective in terms of permeabilisation, only allowing O_2, CO_2, H_2O and NH_3 to pass freely. The IMM has an increased protein to lipid ratio due to the presence of cardiolipin and the IMM bound oxidative phosphorylation (OXPHOS) complexes I – V (also termed respiratory complexes), that are required for ATP production (Fleischer et al., 1961). Cardiolipin is a protein required for the function of the respiratory chain enzymes and also provides structural support for the IMM (Pfeiffer et al., 2003). Due to this high protein content, the IMM is less permeable then the OMM. Alongside this, the IMM is also folded into convoluted structures called cristae (Frey and Mannella, 2000). The

convolution provides an increased surface area, which is beneficial for oxidative phosphorylation (OXPHOS) protein assembly and to maximise ATP production. Originally, according to the baffle model, the IMM was thought to be folded back on itself to form internal ridges with broad openings (Palade, 1953). However, with better resolution and 3D EM, structures termed 'pediculi cristae' were discovered. They demonstrated that the IMM contained an inner boundary membrane (IBM) and a cristae membrane (CM) that were connected together via narrow and tubular openings called cristae junctions (Daems and Wisse, 1966, Mannella et al., 1997, Frey and Mannella, 2000). As mentioned before, the IMM is highly selective in terms of permeabilisation, and hence for protein transport it contains adenine nucleotide translocator (ANT) which is responsible for the transport of ATP out of the mitochondrial matrix into the cytoplasm and the transport of adenosine diphosphate (ADP) from the cytoplasm into the matrix in a 1:1 ratio (Pfaff et al., 1969, Lauquin et al., 2017).

Certain molecules over 10kDa, including pyruvate produced as the result of glycolysis in the cytoplasm and various nuclear encoded proteins, are required within mitochondria. These proteins contain N-terminal sequences that target them to mitochondria but they require assistance to cross the membranes. To facilitate this, the OMM and IMM also contain the translocases of the outer membrane (TOM) and inner membrane (TIM) that allow protein transport across the mitochondrial membranes and into the matrix (Alberts et al., 2002, Endo and Yamano, 2010, Ahmed and Fisher, 2009).

Surrounded by the inner membrane, is the matrix, containing a mixture of substances that makes it more viscous than the cytoplasm (Palade, 1953). They included various nuclear encoded proteins and multiple copies of the mitochondrial DNA (mtDNA) packed together in nucleoids. Initially studies discovered an average of 2.6 mtDNA molecules per mitochondria, and within the whole cell the range was from 220-1720 in various mammalian cell types (Robin and Wong, 1988). In human carcinoma cell lines, for example, mtDNA copy number was suggested to be in the range of 1-15 mtDNA molecules or an average of 4.6 mtDNA molecules within each mitochondrion (Satoh and Kuroiwa, 1991). This was consistent with later studies using more developed techniques such as quantitative-PCR and immune-EM which demonstrated a similar range of 2-10 mtDNA molecules per mitochondrion (Legros et al., 2004, Iborra et al., 2004).

As mentioned above, a number of nuclear encoded proteins required for mitochondrial function are also transported into the matrix. This includes proteins required for the transcription, translation and general maintenance of the mtDNA. The majority of the proteins required for this purpose are coded for by the nuclear DNA and transported into the matrix. Mitochondria contain mitochondrial ribosomes for translation. The matrix is also the site of iron-sulphur cluster biogenesis, pyruvate oxidisation, β-oxidation of fatty acids and Krebs cycle, hence electron carriers, enzymes required for these processes and their by-products are also present within the matrix (McCommis and Finck, 2015, Braymer and Lill, 2017, Wanders et al., 2010).

1.3   Mitochondrial dynamics

Mitochondrial dynamics is a term that describes various characteristics of mitochondria including their biogenesis, fission, fusion, transport and finally their degradation, through the process of mitophagy.

1.3.1   *Mitochondrial biogenesis*

This is the process by which, new mitochondria are formed. This normally occurs in response to the requirement for energy within cells, for example an increase in the demand for more ATP would stimulate the production of more mitochondria (Handschin and Spiegelman, 2006). One of the most studied proteins within the biogenesis pathway is Peroxisome Proliferator-Activated Receptor Gamma, Coactivator 1 Alpha (PGC1α). This is activated upon phosphorylation by AMP-activated protein kinase (AMPK) in response to an increase in the AMP/ATP ratio, or by Sirtuin (SIRT1)-dependent deacetylation, which then functions to activate production of more PGC1α in a feedback loop (Jäger et al., 2007, Handschin et al., 2003, Cantó et al., 2010).

PGC1α then induces downstream production of various transcription factors that activate this biogenesis pathway via other signalling proteins such as Peroxisome Proliferator Activated Receptor Gamma (PPARγ), Nuclear respiratory factors 1 and 2 (NRF1, NRF2), Estrogen Related Receptor (ERR) all of which function to assist in mitochondrial biogenesis (Zong et al., 2002, Hardie et al., 2012, Fan and Evans, 2015, Jäger et al., 2007).

PGC1α deficient mice have been described as being "blunted" which includes effects such as a diminished mitochondrial number and respiratory capacity (Leone et al., 2005). While overexpression of PGC1α *in vitro* has demonstrated an increase in mitochondrial density, oxygen consumption, oxidative phosphorylation genes and mtDNA levels all indicating an increased level of biogenesis (Wu et al., 1999).

A more specific discussion of mitochondrial biogenesis in neurons can be found in chapter 5.

1.3.2 *Mitochondrial fusion*

As mentioned above, originally, with EM, mitochondria were observed to be simple rod shaped organelles and were thought to be distinct, individual mitochondrion (Palade, 1953). However, with advances such as live cell imaging, it was discovered that mitochondria are dynamic organelles that undergo simultaneous and continuous fission and fusion resulting in altered morphology to form complex networks with one another (Johnson et al., 1981, Rizzuto et al., 1996, van der Bliek et al., 2013). These mechanisms determine the shape and size of mitochondria. Fusion is the merging of multiple mitochondria to form the connected mitochondrial network observed in many cells. The main purpose of fusion is to share contents between mitochondria such as mtDNA and other vital molecules (including NADH, FADH and cAMP), to provide mtDNA stability and at times, to compensate for mitochondrial dysfunction and avoid degradation (Olichon et al., 2003, Twig et al., 2006, Nunnari and Suomalainen, 2012, Chen et al., 2010).

This process requires the fusion of both the OMM and IMM and is mediated by mitofusin proteins 1 and 2 (mfn1 and mfn2) and mitochondrial dynamin like GTPase, also called opa1 due the involvement of this gene in dominant optical atrophy, which is the neurodegeneration of the optic nerve (Delettre et al., 2000, Santel and Fuller, 2001). These are GTPases which hydrolyse guanosine triphosphate (GTP) for their energy requirements. Mfn1 and 2 mediate the fusion of OMM as they contain hydrophobic heptad repeats (HR) which tethers them to the OMM. Although the exact mechanism of fusion is unclear, the mitofusins can also bind to HR regions on adjacent mitochondria which eventually leads to the fusion of the phospholipid bilayer using the energy obtained from GTP hydrolysis (Koshiba et al., 2004, Formosa and Ryan, 2016, Westermann, 2010). Studies have shown that they are present together within a

cell and have certain structural and functional differences, however they are capable of facilitating successful fusion individually as well (Chen et al., 2003a). This was also highlighted by a study showing mRNA expression of mfn1 and mfn2 in most human tissues examined, including skeletal muscle, heart, brain and pancreas, however their expression levels differed in different tissues suggesting differential affinity for either protein based on tissue (Santel et al., 2003). Following OMM fusion, is the fusion of the IMM.

The opa1 protein is involved in the fusion of IMM. Studies have observed that *OPA1* mutations (or their yeast orthologs), resulted in fusion of the OMM, but not the IMM (Meeusen et al., 2006, Meeusen et al., 2004, Malka et al., 2005, Westermann, 2010). Similar to mfn1 and mfn2, the exact mechanism of action of opa1 is still undetermined. However, it is known that it is imported into the mitochondria, again due a mitochondria targeting sequence, and can be tethered to the IMM of both mitochondria that are undergoing fusion (Escobar-Henriques and Anton, 2013, Westermann, 2010).

Although the mechanism of action is not completely clear, several studies have identified the importance of these proteins in mitochondrial fusion. Studies on patient fibroblasts with mutations in the OPA1 gene have demonstrated complete inhibition of mitochondrial fusion in some cases (Zanna et al., 2007). Further highlighting the importance of the fusion process is that mutations in the genes that code for mfn2 and opa1 are involved in neuropathies such as optic atrophy or axonal neuropathy (Züchner et al., 2006, Williams et al., 2010). Other studies have also observed a lack of tubular network and the presence of fragmented mitochondria in cells with mutations in mfn1, mfn2 or opa1 (Chen et al., 2003a, Olichon et al., 2003). Alongside this, knockdowns of OPA1 using siRNA in HeLa cells has demonstrated increased mitochondrial fragmentation and apoptosis (Olichon et al., 2003), with Mfn1 knockout displaying similar characteristics. Over expression of mfn1 cDNA results in a highly complex mitochondrial network and the presence of mfn1 containing a point mutation results in fragmented mitochondria *in vitro* (Santel et al., 2003). Over expression of Mfn2 also gives similar results, leading to a highly connected network of mitochondria in most cases, however in some cases, they also produced clusters of fragmented mitochondria within the perinuclear region and causing the release of cytochrome *c* (Huang et al., 2007). This could be because

Mfn2 has also been identified as being involved in the removal of damaged mitochondria and cellular apoptosis (Chen and Dorn, 2013, Wan-Xin et al., 2012).

1.3.3 *Mitochondrial fission*

Fission is the process by which individual mitochondria separate from the network, typically for transport to distal regions or for degradation purposes (Simcox et al., 2013). The fission process of the IMM is still inconclusive, however, the main protein conducting this is dynamin-like protein 1 (drp1), which is a GTPase (Smirnova et al., 2001). Mutations in the drp1 gene lead to perinuclear clusters of highly connected mitochondria as observed with overexpression of mfn2 (Huang et al., 2007). The method of action of this protein is to form a multimeric structure with itself which encloses the site of fission and allows cleavage of the OMM (Smirnova et al., 2001). Other proteins such as fission protein 1 (FIS1), mitochondrial fission factor (mff), mitochondrial dynamic proteins (MiD49 and MiD51) also have roles in fission by recruiting drp1 from the cytoplasm to the OMM (Losón et al., 2013, Mozdy et al., 2000). Studies looking at knock down of fis1 in human cell lines has not demonstrated an effect on fission, however mff was demonstrated as having an effect on drp1 and fission, as drp1 was not recruited to mitochondria (Otera et al., 2010).

Knockout of drp1 in mice leads to the presence of extremely large individual mitochondria instead of a tubular network (Wakabayashi et al., 2009). Drp1 knockout mice in this study also demonstrated embryonic lethality and this was determined as being due to developmentally regulated apoptosis not occurring during neural tube formation. Other studies using drp1 knockout mice have also demonstrated the need for this protein in cytochrome *c* release and apoptosis (Ishihara et al., 2009). This is because fission is required for targeted removal of damaged mitochondria, also termed mitophagy (Twig et al., 2008). In support of this, patient fibroblasts with parkin mutations (a protein involved in mitophagy, see section 1.3.5) have demonstrated increased mitochondrial branching, suggesting that they experienced increased fusion (Mortiboys et al., 2008).

Mitochondrial transport

Mitochondrial transport occurs due to the demand for ATP in various regions of a cell. Mitochondria move along the cytoskeleton of the cell on microtubules (MT) which have a negative or positive charge that facilitates the movement and transport direction of cargo. This movement uses ATP as an energy source and utilises the proteins kinesin, dynein and myosin (Frederick and Shaw, 2007). Disruption of these proteins in HeLa cells has been observed as causing defective mitochondrial movement leading to perinuclear clustering of mitochondria and formation of highly branched mitochondria (Varadi et al., 2004). Mitochondrial movement is particularly important in neurons due to their architecture, they are the longest cells in the human body and are highly branched with a number of processes and axons. Dopaminergic neurons, for example, can have a total length of 4.5m when all their processes are added up (Bolam and Pissadaki, 2012, Matsuda et al., 2009).

Transport of mitochondria into distal regions of the neuron such as axons is termed anterograde and the movement back towards the cell body or the perinuclear region is retrograde (figure 1.2). The cytoskeletal structure of neurons is comprised of cytoskeletal elements termed the microtubules (MT) which consist of α and β-tubulin. Each MT has a negatively charged end directed towards the cell body and a positively charged end towards the distal regions which allows bi-directional transport based on their polarity and driven by the hydrolysis of ATP (Hirokawa et al., 2010). This transport is mediated by two motors: kinesins for anterograde movements as they travel towards the positively charged end of the MT, and dynein motors for retrograde movement as they travel to the negatively charged end (Ligon and Steward, 2000, Tanaka et al., 1998). Dynein can also mediate anterograde movement and kinesin is required for dynein mediated retrograde transport (Hirokawa et al., 1990, Pilling et al., 2006, Haghnia et al., 2007). The attachment of mitochondria to these motors is facilitated by two proteins: Miro and Trak1 (Milton) (van Spronsen et al., 2013, Schwarz, 2013). These act as a connection between the motor proteins and the mitochondria, forming a motor-adaptor-receptor complex, allowing bi-directional movement of the mitochondria. Miro is a GTPase found on the OMM, which binds to Trak1 which then interacts with kinesins. The interaction between mitochondria and dynein remains unclear, however it has been suggested that dynein can bind with proteins present on the OMM, for example

VDAC, but it is also thought to interact with Miro as loss of Miro impacts on both anterograde and retrograde mitochondrial transport (Russo et al., 2009, Schwarzer et al., 2002).
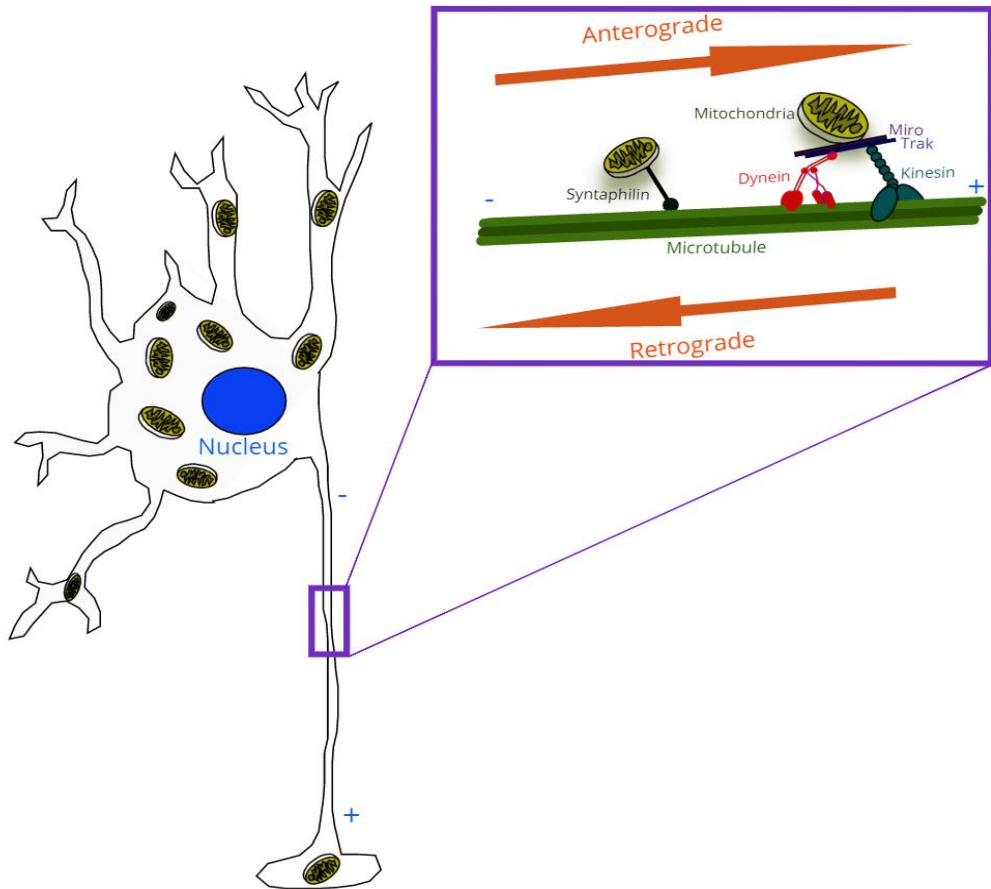
Figure 1.2 Mitochondrial transport machinery in neurons. Miro1, Trak2, Kinesin and Dynein are involved in the anterograde and retrograde movement of mitochondria along the microtubules that form the cytoskeleton of a neuron. The negative and positive charge of the microtubules is also highlighted in the image. Syntaphilin halts mitochondrial movement and anchoring them to

Mitochondria are not always moving, they can remain stationary for a period of time, in fact evidence suggests that the majority of the mitochondria are stationary (Sun et al., 2013). There have been multiple mechanisms suggested for the stalling of mitochondria, one of which involves syntaphilin (SNPH, figure 1.2) (Kang et al., 2008). Other suggested methods include anchoring to the microtubules by myosin present on the mitochondrial surface, inhibiting Miro or the motor complexes and disassociation from the motor complexes which in turn blocks the movement mediated by them (Schwarz, 2013, Sheng, 2014, Pathak et al.,

2010). SNPH is a protein specific to neurons and capable of binding to the MT and the OMM, but it is not capable of moving along the MT which in turn 'anchors' the mitochondria to the microtubule. As further evidence, knockout of this gene in mouse models has demonstrated an increase in mitochondrial movement (Sheng and Cai, 2012).

1.3.4 *Mitochondrial degradation (Mitophagy)*

The specific degradation of mitochondria is termed mitophagy. This is the process by which dysfunctional mitochondria are removed from the reticular network and degraded by lysosomes. This process is connected to fission as this is required to remove the damaged mitochondria from the network in order for mitophagy to occur (Duvezin-Caubet et al., 2006, Frank et al., 2012). This term was coined by a study that used GFP tagged Light chain 3 (LC3) protein in hepatocytes (Kim et al., 2007). This study demonstrated that when cells were exposed to laser induced photo damaged, there was a loss of membrane potential and following this loss, there was an increase in GFP tagged LC3 intensity over time.

One of the suggested pathways of mitophagy, is the PTEN-induced putative kinase 1 (PINK1) and parkin pathway. PINK1 contains a mitochondrial targeting sequence and localises within the inner membrane space. Usually in healthy mitochondria, PINK1 undergoes proteolysis by presenilins-associated rhomboid-like protein (PARL). In cases of mitochondrial damage such as a loss of membrane potential or an increase in reactive oxygen species (ROS), PARL does not cleave PINK1, which in turn transfers to and accumulates within the OMM (Narendra et al., 2008). This accumulation activates and recruits the E3 ubiqutin ligase protein, parkin, from the cytoplasm which ubiquitinates OMM proteins (including VDAC1 and DRP1) and recruits lysis proteins such as p62, LC3 and autophagosomes (Narendra et al., 2010). This relationship of PINK1 and parkin is further evidenced by overexpression studies, where overexpression of parkin in PINK1 deficient cells was beneficial, rescuing the ensuing defects, however overexpression of PINK1 in parkin deficient cells did not have the same effect suggesting that parkin was required for the recruitment of further mitophagy related proteins (Clark et al., 2006, Exner et al., 2007, Park et al., 2006). In the absence of PINK1, it has been suggested that VDAC is abundant within the OMM alters to be accessible for parkin translocation and

mitophagy, suggesting that parkin mediated mitophagy can occur even in the absence of PINK1 (Geisler et al., 2010)

Another pathway of mitophagy uses NIP3-like protein X (NIX) which has been studied in erythrocytes since their differentiation involves the complete removal of mitochondria and through the action of this pathway (Aerbajinai et al., 2003). Mice lacking NIX in these cells retain their mitochondria as the cells mature (Sandoval et al., 2008). In this pathway, NIX localises to the OMM and then in turn binds to LC3 present in the cytoplasm via the LC3-interacting region (LIR) on the NIX. LC3 then functions to recruit autophagosomes. In mice with NIX deficiency, there is a decrease in mitophagy, however decreasing the membrane potential of the IMM by treatment with the uncoupler Carbonyl cyanide m-chlorophenyl hydrazone (CCCP) can rescue mitophagy, suggesting stimulation of another pathway such as PINK1/Parkin (Zhang and Ney, 2009, Sandoval et al., 2008). BNIP3 has also been suggested to behave in a similar manner to NIX, as they both contain LIR allowing binding to LC3 (Chinnadurai et al., 2009, Rodger et al., 2018). *In vivo* models with loss of BNIP3 resulted in lower levels of mitophagy along with an accumulation of damaged mitochondria (Chourasia et al., 2015)

Mitophagy, and its importance for neurons is discussed in more detail in chapter 5.

1.4   Mitochondrial functions

1.4.1   *Tricarboxylic acid (TCA) cycle (Kreb's cycle)*

The initiation of glucose breakdown for ATP production occurs within the cytoplasm via the process of glycolysis. This reaction breaks down glucose through intermediate products, into pyruvate producing a net yield of two adenosine triphosphate (ATP) molecules and two molecules of reduced Nicotinamide adenine dinucleotide (NADH) (Berg, 2011) (figure 1.3).

When the conditions are hypoxic, this pyruvate is converted to lactic acid via anaerobic respiration, however in the presence of oxygen, the pyruvate is imported into the mitochondrial matrix and is converted into Acetyl CoA by pyruvate dehydrogenase (producing NADH as a by-product), which is used for the TCA cycle (Wang et al., 2010). Fatty acid

breakdown through the β-oxidation pathway, can also result in the production of Acetyl CoA for use within the TCA cycle (Houten and Wanders, 2010).

The TCA cycle consists of a series of enzyme mediated reactions through which Acetyl CoA is oxidised, in turn reducing several products such as GDP, NAD^+ and FAD into GTP, NADH, and $FADH_2$ respectively, which are required for downstream oxidative phosphorylation (Krebs and Eggleston, 1940b, Krebs and Eggleston, 1940a). Figure 1.3 presents all the intermediate products in glycolysis and the enzymes that mediate this process. Within this cycle, oxaloacetate is produced, which then combines with a new molecule of Acetyl CoA to go through the same series of oxidative reactions again. The name citric acid cycle comes from the formation of citrate from oxaloacetate and Acetyl CoA.
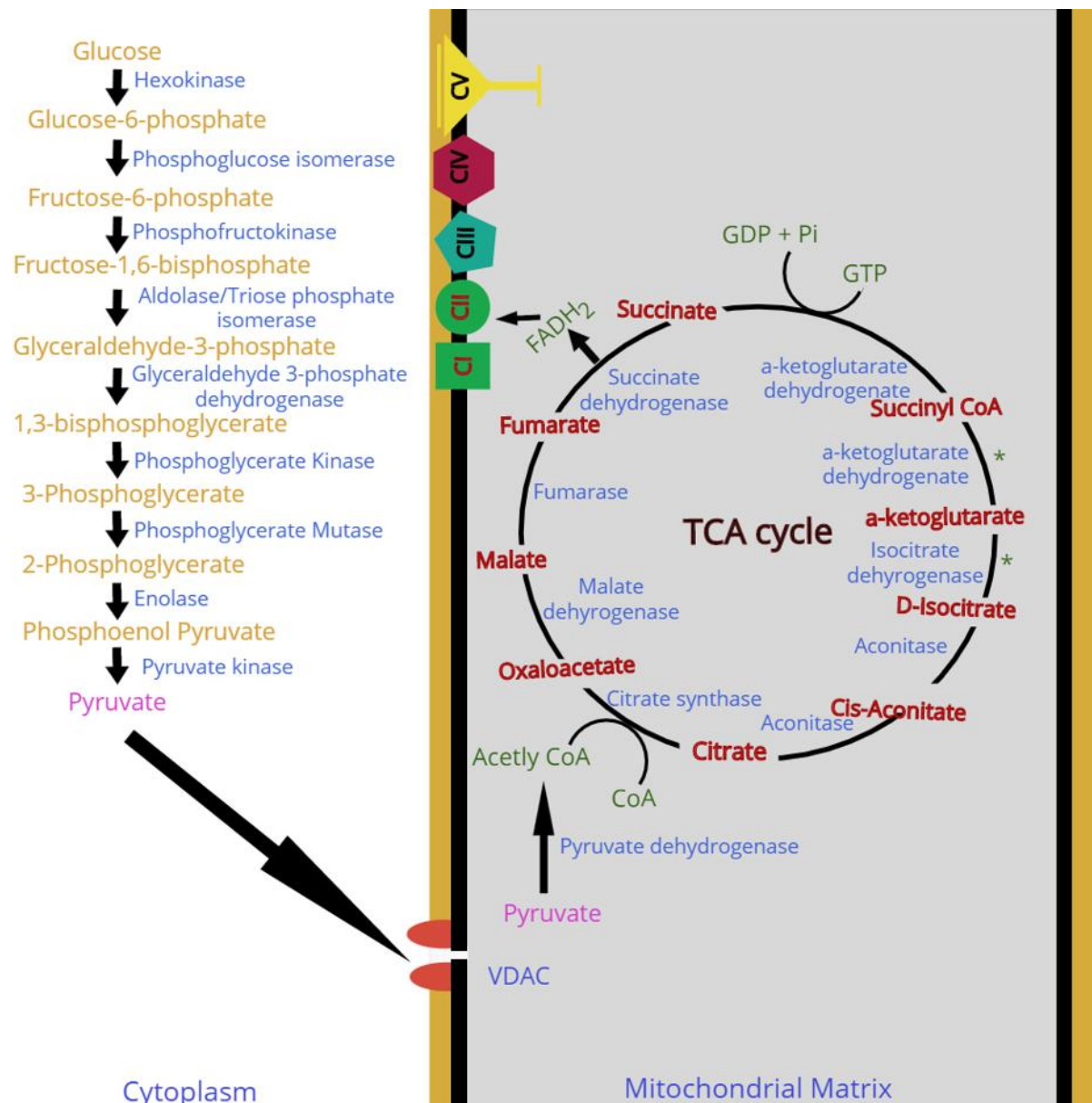
Figure 1.3 The reactions of glycolysis and the TCA cycle. This presents the breakdown of glucose to pyruvate through glycolysis, which happens in the cytoplasm. It also presents the transport of pyruvate into the mitochondrial matrix, where it is converted into Acetyl CoA, and enters the TCA cycle. All the intermediates are named for both the processes. All the enzymes mediating the reactions are presented in blue. The green asterisks represent the production of NADH. The image also shows the production of FADH2 from succinate which is used by complex II of the OXPHOS system

1.4.2 *Oxidative phosphorylation (OXPHOS)*

As the final process of ATP production, mitochondria contain the electron transport chain within their inner membrane. This enables OXPHOS, which requires complexes I – V (figure

1.4). The OXPHOS processes utilise redox reactions which transport electrons across the complexes and transfers protons into the IMS, thereby establishing a proton gradient and allowing the maintenance of a negative membrane potential across the IMM (Mimaki et al., 2012). The protons are then utilised by complex V to phosphorylate ADP to form ATP.

Complex I, or NADH ubiquinone oxidoreductase, is the largest of the 5 OXPHOS complexes containing around 45-46 subunits (Hirst et al., 2003, Sazanov, 2007), 7 of which are coded for by the mammalian mitochondrial DNA (mtDNA) (MTND1, MTND2, MTND3, MTND4L, MTND4, MTND5 and MTND6). The remaining subunits are encoded by the nuclear genome and translocate into the mitochondria to be assembled in the inner membrane, to produce the full enzyme complex with the mitochondrially encoded subunits. This complex oxidises NADH produced in the TCA cycle into NAD^+ transferring four protons into the intermembrane space and transferring electrons to reduce Coenzyme Q (Janssen et al., 2006) (equation 1.1). This complex is also a site of reactive oxygen species (ROS) production, as it can produce superoxide radicles as a result of electron leakage (Hirst et al., 2008).

$$NADH + Q + 5H^+_{(matrix)} \rightarrow NAD^+ + QH_2 + 4H^+_{(IMS)}$$
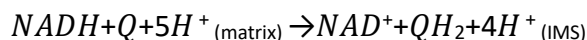
Equation 1.1 Complex I reaction

Complex II is also called Succinate dehydrogenase, and functions in oxidising succinate to fumarate (this reaction is part of the TCA cycle) and produces $FADH_2$ (Cecchini, 2003). The oxidation of $FADH_2$ into FAD, by the iron sulphur clusters within this complex, produces electron that are passed on reducing Coenzyme Q (equation 1.2). Complex II is the smallest of all the complexes and is completely coded for by the nuclear DNA.

$$succinate + Q \rightarrow fumarate + QH_2$$
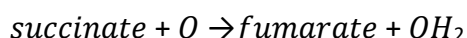
Equation 1.2 Complex II reaction
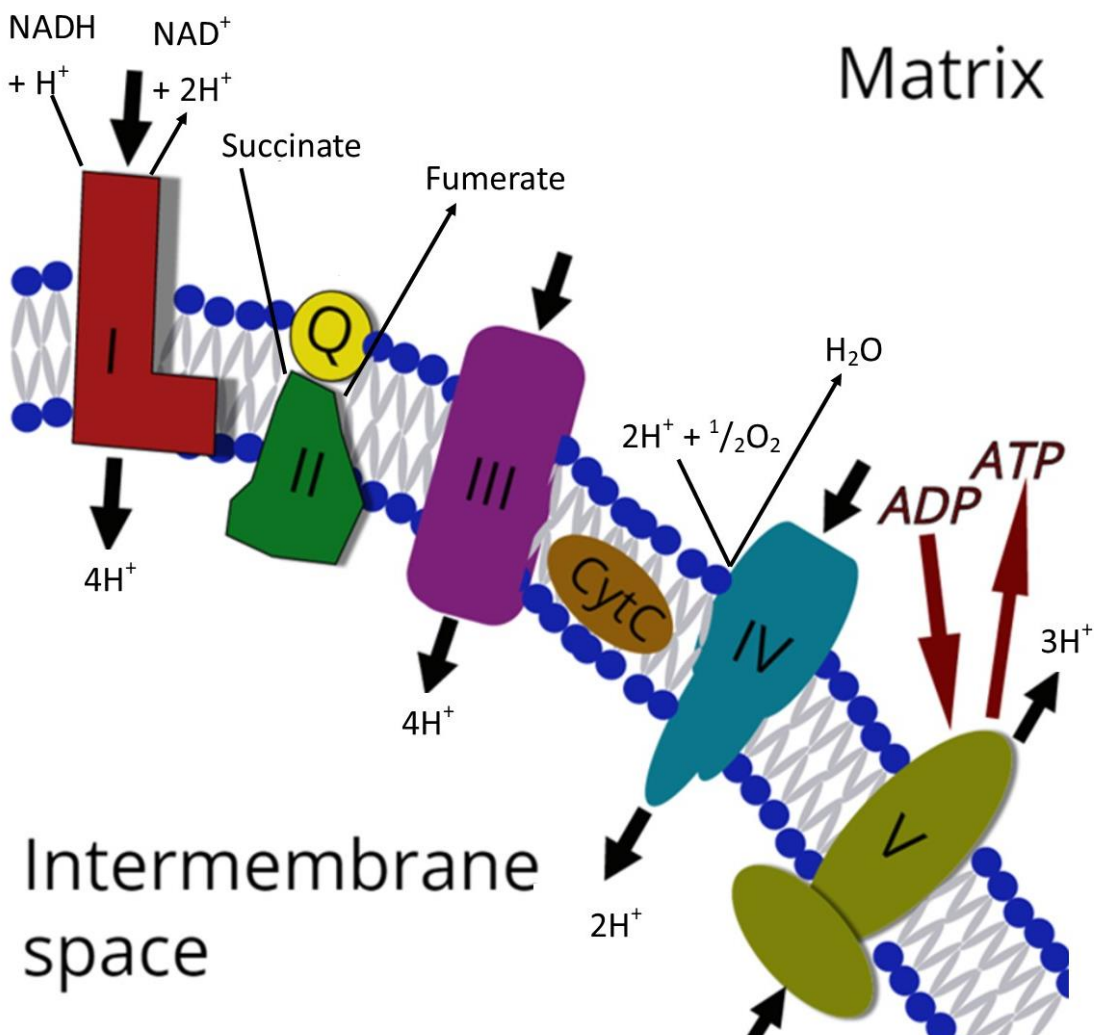
Figure 1.4 Oxidative phosphorylation. Highlighted on the figure are the complexes (I-V) embedded in the inner mitochondrial membrane and functions within the OXPHOS system. This system functions by transporting electrons from complex I and II to complex IV with the help of cytochrome C. This process releases protons into the intermembrane space creating a proton gradient that is then utilised by complex V to convert ADP into ATP. More details about the individual processes are present in section 1.4.2.

Electrons produced from oxidation of NADH and $FADH_2$ from Complex I and II respectively, are transferred on to Coenzyme Q that is then oxidised by complex III. This complex, also known as ubiquinol cytochrome *c* oxidoreductase, consists of 11 subunits, one of which; cytochrome b (gene: MTCYB), is coded for by mtDNA (Schägger et al., 1995). This complex is responsible for transferring electrons from Coenzyme Q to cytochrome *c*. This complex also releases 4

protons into the intermembrane space (van den Heuvel and Smeitink, 2001). Cytochrome *c* is then responsible for transferring electrons from Complex III to complex IV.

$$2QH_2+Q+2Cytc_{(oxidised)}+2H^+_{(matrix)} \rightarrow 2Q+QH_2+2Cytc_{(reduced)}+4H^+_{(IMS)}$$
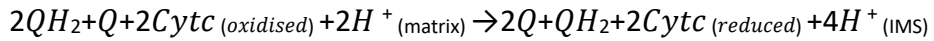
Equation 1.3 Complex III reaction

Complex IV (Cytochrome *c* oxidase; COX) is comprised of 13 subunits, 3 of which; COXI, COXII and COXIII, are coded for by the mtDNA (van den Heuvel and Smeitink, 2001). This complex accepts electrons from cytochrome *c* and transfers them to oxygen (the terminal electron acceptor), producing H_2O. This also releases two protons into the intermembrane space further adding to the proton gradient (Capaldi, 1990, Diaz, 2010).

$$4Cytc_{(reduced)}+8H^+_{(matrix)}+O_2 \rightarrow 4Cytc_{(oxidised)}+2H_2O+4H^+_{(IMS)}$$
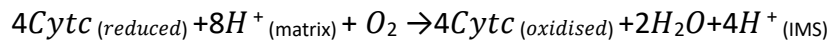
Equation 1.4 Complex IV reaction

The final complex, complex V is also termed ATP synthase. This contains 17 subunits, 2 of which; ATP6 and ATP8, are present on mtDNA. This molecule is responsible for phosphorylating ADP into ATP using the protons pumped out into the IMS by the other complexes. This protein contains two main domains: F_O and F_1. The protons in the intermembrane space travel down their concentration gradient into the matrix through the F_O subunit of ATP synthase causing this to rotate. This leads to the rotation of the F_1 subunit which functions to catalyses the phosphorylation of ADP into ATP and the release of this ATP molecule into the matrix (Boyer, 1997). The ATP synthase can also function in reverse converting ATP into ADP and releasing protons to IMS in the process (Abramov et al., 2010). This usually occurs as a response to loss of membrane potential in order to regain this, and to avoid mitophagy (Gottlieb et al., 2003, Safiulina et al., 2006).

$$ADP+Pi+2.7H^+_{(IMS)}+ \rightarrow ATP+2.7H^+_{(matrix)}$$
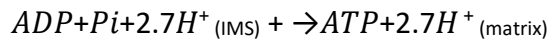
Equation 1.5 Complex V reaction

1.4.3 *Biogenesis of molecules in mitochondria*

Iron is transported into the mitochondria using mitoferrin present on the IMM (Shaw et al., 2006, Zhu et al., 2016). This is used within mitochondria for haem synthesis which is a catalyst for redox reactions occurring in complexes I-III, by acting as an electron carrier. Iron is also important for the movement of electrons in the OXPHOS system as it is used for Fe-S cluster biogenesis. These are required within the OXPHOS complexes to accept electrons, for example the Fe-S cluster within Complex II accepts electrons from $FADH_2$ (Lill et al., 2012, Wang and Pantopoulos, 2011). Fe-S clusters are formed and matured using various mitochondrial proteins (such as Isu1/2, Isa1/2, Nfu, Grx5 and Abcb7), which obtain the iron through frataxin, and forms Fe-S clusters. The sulphur for this process is produced from cysteine mediated by the enzyme cysteine disulfurase (Tong and Rouault, 2000). Mitochondria also function to regulate iron homeostasis within the cell (Rouault and Tong, 2005).

Although the mechanisms remain unclear, mitochondria are also the site of steroid hormone synthesis from cholesterol (Miller, 2013).

1.4.4 *Calcium buffering*

Mitochondria assist the cell with calcium buffering and the regulation of this ion is particularly important within neurons for action potential generation (Bean, 2007, Surmeier and Schumacker, 2013). Mitochondria contain the mitochondrial Ca^{2+} uniporter (MCU) in their IMM and VDAC on the OMM, which together are capable of importing calcium ions from the cytoplasm into the mitochondrial matrix regulating the calcium ion concentration within the cell. This is based on a calcium gradient and when there is large concentration of calcium within the cell, it is sequestered down its concentration gradient into mitochondria, which can sequester large quantities of calcium, up to 1000nmol per mitochondrion (Kirichok et al., 2004). Ca^{2+} is required for various signalling pathways and functions within the cell such as ATP production, however at large concentrations it can be detrimental and lead to apoptosis of the cell (Griffiths and Rutter, 2009, Orrenius et al., 2003, Mattson and Chan, 2003). Calcium is released into the cell through an exchange with Na^+ ions at a ratio of 3 Na^+ for each Ca^{2+} molecule.

1.4.5 *Reactive oxygen species (ROS) production*

Reactive oxygen species can be produced from the mitochondrial OXPHOS system due to the leakage of electrons from complex I and III (Chen et al., 2003b). These electrons can react with oxygen molecules in the vicinity (produced from complex IV) to produce the superoxide anion ($^\bullet O_2^-$). Although initially thought to be detrimental, recent studies discovered that at low levels, ROS are beneficial for cells though various pathways such as cell signalling, differentiation and immunity (Sena and Chandel, 2012). However, at higher levels, ROS can have negative effects, and therefore the mitochondria possess antioxidant enzymes to minimise this risk and regulate ROS. Superoxide dismutase (SOD), present within the matrix and IMS, converts the $^\bullet O_2^-$ into H_2O_2, which is then converted into H_2O by gluthathione peroxidase (GPx) or peroxiredoxins (PRX) (Sabharwal and Schumacker, 2014). Although this system is beneficial, H_2O_2 can itself be converted into the hydroxyl radical ($^\bullet OH$) upon reaction with $^\bullet O_2^-$ (Sena and Chandel, 2012). ROS scavengers such as uric acid and vitamin C can also function to protect from ROS related damage (Valko et al., 2007). ROS can be detrimental as it can also cause the oxidation of proteins, lipids and DNA within the cells and mitochondria (Lyras et al., 1997, Slupphaug et al., 2003). Since mitochondria are a site of ROS production, mtDNA can be particularly damaged due to its close proximity to the source of ROS, leading to mtDNA damage (Indo et al., 2007, Liang and Godley, 2003). An accumulation of this damage can eventually lead to apoptosis of the cell (Kim et al., 2010).

1.4.6 *Apoptosis*

Cellular damage, such as oxidative stress, DNA damage and high levels of intercellular calcium can lead to cell death. Apoptosis is the process by which a damaged or unrequired cell is degraded. The IMM contains Apoptosis Inducing Factor Mitochondria Associated (AIFM1). This generally functions as a NADH oxidoreductase, however in the case of damage, this protein translocates to the nucleus in order to cause chromosome condensation and DNA fragmentation leading to apoptosis (Kettwig et al., 2015). This protein can also induce the release of cytochrome c.

Within the IMM, cytochrome c is present and functions as an electron transporter for the OXPHOS system. The release of cytochrome c from the IMM is generally regulated by the Bcl-

2 family of proteins. BNIP3L is involved in mitochondrial quality control by interacting with Spermatogenesis Associated 18 (SPATA18, or Mieap) which can regulate the translocation of lysosomal proteins into the mitochondrial matrix to degrade damaged proteins, a process termed Mieap-induced accumulation of lysosome-like organelles (MALM) (Nakamura and Arakawa, 2017). BNIP3L can also bind to Bcl-2. Bcl-2 is capable of interacting with VDAC to increase the membrane permeability and also influence cytochrome c release which induces apoptosis. This is in response to high levels of damage, where cytochrome c released to trigger caspase-9 leading to apoptosis (Wang and Youle, 2009, Hüttemann et al., 2011).

1.5   Mitochondrial DNA

Mitochondria are the only other organelle that contain their own DNA, which like the organelle in which is it found is maternally inherited (Giles et al., 1980). As mentioned, the subunits required for OXPHOS are coded for by both the nuclear and the mitochondrial genomes. The mtDNA of humans was first sequenced in 1981, which was later revised in 1999 to include any polymorphisms and correct any errors (Anderson et al., 1981, Andrews et al., 1999). MtDNA contains 37 genes coding for 13 proteins, 22 tRNA's and 2 rRNA's within 16,569 base pairs (figure 1.5). It is a circular DNA molecule that consists of a heavy (H) strand on the outside that gets this name, as it is rich in purines, which are heavier than pyrimidines. This H strand is paired with the light (L) strand on the inside.
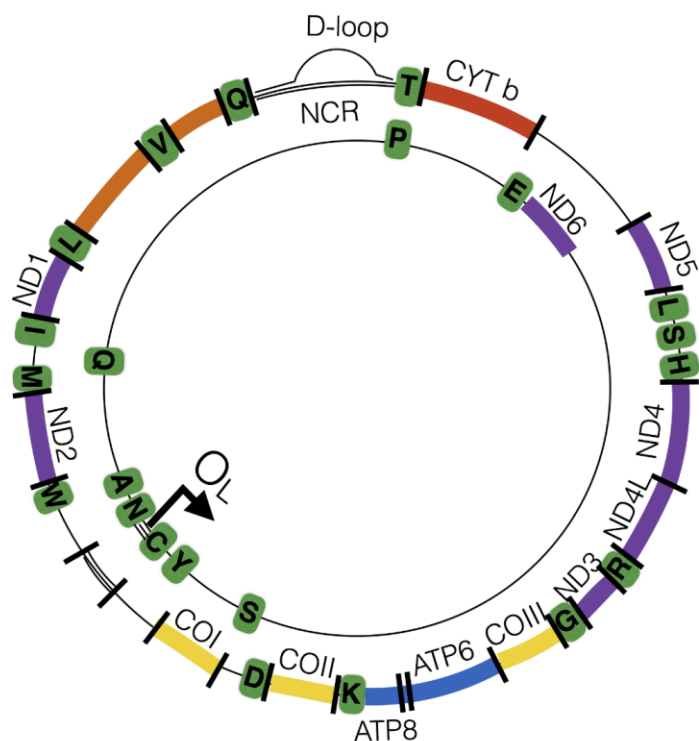
Figure 1.5 Mitochondrial DNA. Highlighted on the figure are the protein encoding genes in colour and the genes are stated on the image. The orange sites code for rRNAs and the green stadium shapes demonstrate the tRNAs. The OL and OH regions are also indicated, along with the D-loop. Image taken with permission from (Vincent, 2017)

MtDNA is supercoiled and arranged into structures called nucleoids (which average 100nm in diameter), within the mitochondrial matrix, causing this molecule to be highly compact (Satoh and Kuroiwa, 1991, Gilkerson et al., 2013). Although previous studies have eluded to a higher number of mtDNA molecules within these nucleoids, recent advances in electron microscopy discovered that each nucleoid contained an average of 1-3 mtDNA molecules (Kukat et al., 2011, Brown et al., 2011). Super resolution fluorescence imaging was also used to identify that each nucleoid, in addition to mtDNA, also contains mtDNA maintenance proteins, such as those involved in transcription and replication (Brown et al., 2011). One such example of a nucleoid protein is mitochondrial transcription factor A (TFAM). This is involved in mtDNA transcription; however, it also has an additional function in the appropriate packaging of

mtDNA. TFAM can generate U-shaped bends with the mtDNA, due to the presence of a high mobility group (HMG) box, allowing mtDNA to be compacted within the nucleoid (Alam et al., 2003, Ngo et al., 2011b).

MtDNA contains a non-coding displacement-loop (D-loop) which consists of the origin of replication (OH) for the heavy strand. For replication to initiate, a complementary strand binds to the D-loop displacing the H strand from the L strand. This exposes OH where replication for the H strand is initiated. The origin of replication for the light strand (OL) is present further into the strand. The region from OH to OL is the major arc and the remaining bases pairs from OL to OH are termed the minor arc. The 13 genes present are all essential for OXPHOS and all the genes are expressed as there are no introns in the mtDNA and some genes even have overlapping regions; therefore any damage to mtDNA could be severe. As mentioned in the previous section, high levels of ROS are also produced within the mitochondria from the OXPHOS system. As a result, mtDNA is also highly susceptible to damage which accumulates with age (Castro et al., 2012, Manczak et al., 2005, Corral-Debrinski et al., 1992b, Yen et al., 1991, Fayet et al., 2002).

Unlike the nuclear DNA, cells and indeed individual mitochondria harbour multiple copies of mtDNA. A single cell has been estimated to contain 10^3-10^4 copies of mtDNA, however the number can vary based on age, tissue and cell (Wiesner et al., 1992, Lightowlers et al., 1997, Miller et al., 2003). Individuals with inherited mtDNA mutations commonly harbour wild type and mutant genomes within most cells, a situation termed heteroplasmy. If the mtDNA genomes present are all the same, this is termed homoplasmy. For a mutation within mtDNA to have a biochemical defect, a certain threshold level of mutant mtDNA has to be achieved, at which point the wild type mtDNA could not compensate for the mutated mtDNA. This is termed the biochemical threshold effect (Rossignol et al., 2003). Due to this threshold, there is often some residual function of the OXPHOS system in cells harbouring mtDNA mutations, as wild type mtDNA might be present (Brunelle et al., 2005).

1.5.1   *MtDNA replication*

MtDNA replication will be discussed in more detail in chapter 4, therefore this brief introduction will focus on the replication machinery and the modes of replication.

As mentioned before, a nucleoid contains mtDNA molecules alongside a few replication machinery related proteins. These include TFAM, mitochondrial transcription factor B (mtTFB), mtRNA polymerase (POLRMT), DNA Polymerase gamma (Polγ), mitochondrial single strand binding protein (mtSSB), Twinkle and Mitochondrial Lon peptidase (LONP) (Bogenhagen et al., 2008, Gilkerson et al., 2013). TFAM, as discussed above, is involved in transcription and packaging of mtDNA. TFAM, mtTFB and POLRMT are involved in mtDNA transcription (section 1.5.2). POLRMT also has roles in replication initiation by providing RNA primers at the at the site of OH (Fuste et al., 2010). Polγ is the DNA polymerase, specific to mitochondria, that carries out mtDNA synthesis based on template sequence and is also suggested to have roles in repair. The importance of Polγ was noticed when transgenic knockdown mice displayed an accelerated ageing phenotype and when a number of diseases were associated with Polγ mutations (Trifunovic et al., 2004, Wong et al., 2008). MtSSB is a single strand DNA binding protein, and has been thought to provide stability to single stranded mtDNA during replication. An increase in mtDNA replication was associated with an increase in mtSBB protein levels indicating this is involved in mtDNA replication and repair (Schultz et al., 1998, Ruhanen et al., 2010). Twinkle is a mtDNA helicase capable of unwinding short stretches of DNA in a 5' to 3' direction in response to stimulation from mtSSB, and mutations within this gene are associated with mtDNA deletions (ΔmtDNA) and multiple disease conditions (Korhonen et al., 2003, Goffart et al., 2008, Tyynismaa et al., 2005). LONP is a protease and functions to degrade damaged nucleotides (Lu et al., 2007).

Although the definitive mechanism of replication is uncertain, a few theories exist, which have postulated potential mechanisms. The first theory to be proposed suggests that mtDNA replication occurs through the strand-displacement method (SDM). This mechanism was initially described in a paper looking at mouse mitochondria isolated using caesium chloride density centrifugation (Kasamatsu and Vinograd, 1973). This led to the development of the SDM model of replication which has also been referred to as the asynchronous model of mtDNA replication (Clayton, 1982). The SDM mechanism suggests that replication begins at 'OH' of the leading strand (heavy strand), as the D-loop is displaced. This heavy strand is then replicated from 5' to 3', once approximately 2/3rd of the strand has been replicated, 'OL', the origin of replication of the lagging strand (light strand) becomes exposed. This allows

replication of the lagging strand to begin (Krishnan et al., 2008) in an opposing direction from 5' to 3' until both strands have been replicated (figure 1.6). Further evidence supporting this was obtained when the origin of replication sites OH and OL were found on opposite strands with a distance of over 11kb between them (Clayton, 1982). This suggests that replication is initiated at different locations within both the strands. The 11kb distance supports the original idea that 2/3rd of the H strand is replicated before replication begins at the L strand.

Another proposed theory is the coupled leading-lagging-strand replication (Holt et al., 2000) also termed the synchronous model which was observed using 2D-neutral agarose gel electrophoresis. This theory suggests that replication is initiated at the zone of replication (OriZ) that is present at the same loci for both the leading and the lagging strand. This region is broad and said to be between the bases 12337 and 15887 containing the genes ND5, ND6 and CYB. In this model, replication proceeds bidirectionally (Bowmaker et al., 2003). However, the coupled leading-lagging theory was observed after mtDNA in human cultured cells was depleted using 2'3' dideoxycytidine (ddC) or ethidium bromide, hence this mode of replication could be the result of damage. This study also investigated an untreated control cell line which presented with a different replication intermediate to the ddC or ethidium bromide treatments. This suggested that multiple modes of replication could exist.

Nonetheless this, and SDM, have been challenged by the discovery of multiple 'OL' sites within the L strand suggesting multiple origins of replication (Brown et al., 2005). Another challenge for the SDM model came when mitochondrial RNA polymerase was found to have RNA primase activity in the mitochondria and to be capable of producing primers for the OL region. This can initiate replication of the L strand even without H strand exposing the OL site as suggested by SDM (Fusté et al., 2010). This primase can start replication at any one of the multiple OL sites and the gap between these strands can then be filled in by poly (Wanrooij et al., 2008). As mentioned above, the study (Holt et al., 2000) discovered two replication intermediates, one with and one without mtDNA depletion, one of these was vulnerable to single stranded nuclease digestion as suggested by SDM, which was initially used to support SDM and couple-leading lagging theory co-existing (Holt et al., 2000). However upon further study using a purer preparation of mitochondria, these single stranded intermediates were found to not be DNA but RNA:DNA hybrids (Yang et al., 2002, Yasukawa et al., 2006). The led

to the postulation of the 'RNA incorporation throughout the lagging strand' model (the RITOLS model) (figure 1.6) (Holt and Reyes, 2012, Yasukawa et al., 2006). This is similar to the SDM method where the H strand replicates as normal from OH, whereas the single stranded L strand replicates as segments of RNA of about 2.5kb in length, which hybridises with the H strand, and is then matured into DNA.

Recently a 'bootlace' mechanism of replication was also put forward after analysis of replication forks on 2D gel electrophoresis (Reyes et al., 2013). This theory is similar to RITOLS, however it suggests that RNA transcripts complementary to the L-strand are produced prior to replication. This was verified as RNA chain terminators did not block the labelling of mtDNA replication intermediates however DNA chain terminators did, hence RNA transcripts was produced beforehand. Once the D-loop is displaced and DNA synthesis begins at 'OH' on the H strand, these RNA transcripts bind to the L strand discontinuously. This is later processed into DNA through a maturation process which is as yet unclear. This also explains the single stranded regions noticed by (Holt et al., 2000) as the RNA transcripts are discontinuous, therefore short single strands of DNA are present between the DNA:RNA hybrid regions.
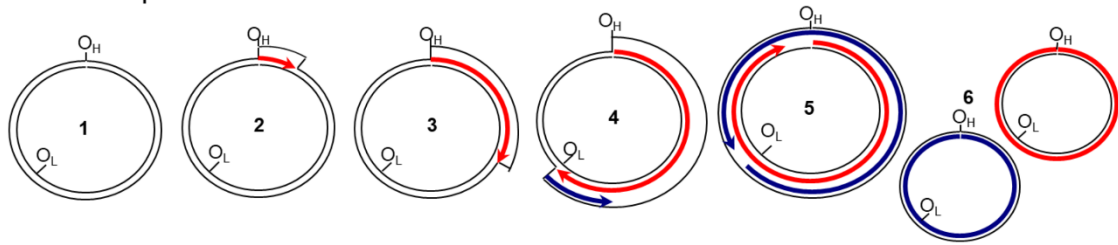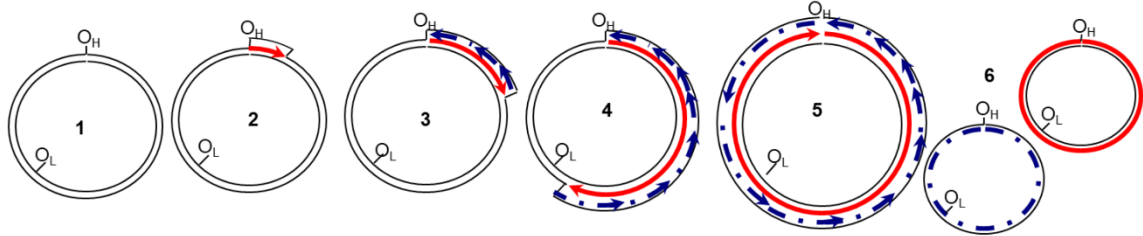
Figure 1.6 Models of replication for the mtDNA. In the top image, SDM starts replication at the OH and as the OL strand is revealed, replication of the lagging strand begins. The bottom image demonstrates the RITOLS model where the replication of both strand is initiated at the OH region, and the lagging start replicates using RNA fragments. Image taken with permission from (Reeve, 2007)

1.5.2 *MtDNA repair*

DNA can undergo various chemical modifications that result in damage. Over the evolutionary period, sufficient repair mechanisms have been developed to combat this damage. Although an abundance of information is available regarding the repair of nuclear DNA, DNA repair within mtDNA remains relatively unknown (Houtgraaf et al., 2006). Until recently mtDNA was believed to have no repair system at all due to the increased DNA mutations observed in mtDNA compared to nuclear DNA (Yakes and Van Houten, 1997, Mecocci et al., 1993). However this was because most of the mtDNA is coding and polycistronic, hence mutations have a higher chance of leading to a biochemical defect, and due to the high oxidative stress present within mitochondria, high levels of DNA damage were inevitable. Recent advances however have paved the way to better understand the repair mechanisms present in mtDNA (Alexeyev et al., 2013, Bowmaker et al., 2003). A list of proteins involved in mammalian mtDNA repair and their function in presented in table 1.1

Protein	Gene	Function	Pathway	Reference
Oxoguanine glycosylase	OGG1	DNA glycosylase	BER	(Hashiguchi et al., 2004, Cotter et al., 2004, Karahalil et al., 2003)
MYH glycosylase	MUTYH	DNA glycosylase	BER	(Cotter et al., 2004, Ohtsubo et al., 2000)
Uracil-DNA glycosylase	UNG1	DNA glycosylase	BER	(Chatterjee and Singh, 2001, Cotter et al., 2004)
Nuclease-sensitive element-binding protein 1	YB-1	Endonucleolytic activity – create double strand DNA breaks at site of mismatch	MMR	(de Souza-Pinto et al., 2009)
Polymerase γ	POLG	Insert new base pairs at damaged sites	All	(Copeland and Longley, 2003, Cotter et al., 2004)
7,8-dihydro-8-oxoguanine triphosphatase	MTH1	Triphosphatase - hydrolyse damaged dNTPs so it does not get incorporated into DNA	Non-specific	(Kang et al., 1995, Nakabeppu, 2001)
Apurinic-Apyrimidinic endonuclease	APE1	Multifunctional – Repair of AP sites, Generate single strand breaks at site of damage, 3'-5' exoribonuclease activity	BER/MMR	(Tell et al., 2001)
Endonuclease III-like protein 1	NTHL1	DNA glycosylase	BER	(Karahalil et al., 2003)

Endonuclease 8-like 1 and 2	NEIL1, NEIL2	DNA glycosylase	BER	(Mandal et al., 2012, Hu et al., 2005)
Polynucleotide kinase 3'-phosphatase	PKNP	DNA Nucleases	BER	(Mandal et al., 2012, Tahbaz et al., 2011)
Flap endonuclease 1	FEN1	DNA Nucleases	BER	(Kalifa et al., 2009)
DNA replication ATP-dependent nuclease	DNA2	DNA Nucleases	BER	(Copeland and Longley, 2008, Zheng et al., 2008)
Nuclease EXOG	EXOG	endonuclease	BER	(Kalifa et al., 2009)
DNA ligase	LIG3	DNA Ligase	All	(Akbari et al., 2014, Lakshmipathy and Campbell, 1999)
Deoxyuridine 5'-triphosphate nucleotidohydrolase	DUT1	Produces thymidine nucleotide precursors so uracil concentration decreases and does not get incorporated into DNA	Non-specific	(Ladner and Caradonna, 1997)
DNA repair protein RAD51 homolog 1	RAD51	Recombination of double stranded breaks	Non-specific	(Sage et al., 2010)

Table 1.1 List of proteins associated with the DNA (and RNA) repair of mitochondrial DNA and their functions. BER refers to base excision repair and MMR to mismatched repair

Since each type of DNA damage is different in terms of its chemical or physical properties, a different mechanism of repair is required for each type of damage. This includes nucleotide excision repair (NER), base excision repair (BER), mismatch repair (MMR) and recombination repair. The most reported type of repair in mitochondria is BER where the damaged base pair

is exchanged for an undamaged base pair, therefore BER is responsible for the repair of smaller modifications.

Although BER happens in the nucleus as well as mitochondria, they can be differentiated by the fact that the proteins involved in the mitochondrial BER pathway are specific isoforms or splice variants from the nuclear versions of the same enzymes. In the BER pathway, a damaged DNA base is recognised and cleaved at the site of a glycolytic bond by DNA glycosylases such as OGG1, MUTYH or UNG1. This produces an abasic (AP) site. Endonucleases such as APE1 then function to break the phosphodiester bonds and remove the damaged base pair. The repair activity of Polγ functions to insert the correct base pair and the strand is ligated through the action of DNA ligase III (Bohr, 2002, Bohr et al., 2002)

A number of DNA glycosylases associated with the BER pathway have been identified as localising to the mitochondria, these include OGG1, MUTYH and UNG1. OGG1 is involved in the initial stages of the BER pathway and is responsible for cleaving DNA at the damaged base. It has two splice variants; OGG1α and OGG1β. OGG1β is mitochondrial specific; however both contain an N-terminal targeting sequence for mitochondrial localisation (Nishioka et al., 1999, Takao et al., 1998). Other evidence suggests that OGG1β does not have glycosylase activity and OGG1α is responsible for this activity in both the nucleus and mitochondria (Hashiguchi et al., 2004). MUTYH is also a DNA glycosylase involved in the BER pathway. It recognises and cleaves adenine that is paired inappropriately. The isoform p57 of MUTYH localises to mitochondria (Ohtsubo et al., 2000). UNG1 also functions as a DNA glycosylase and localises to the mitochondria. It is responsible for removing uracil from DNA and in turn activating the BER pathway (Nilsen et al., 1997). Following the activity of such DNA glycosylases, the remaining damaged site is processed by APE1 which is also identified as localising to the mitochondria (Tell et al., 2005). Following this, the correct base pair is inserted by catalytic subunit of polγ (Copeland and Longley, 2003). The DNA is then ligated back together by DNA ligase III which also contains mitochondrial encoded proteins (Muftuoglu et al., 2014). This process mostly explains short-patch BER which is the correction of a single base pair. A long-patch BER also exists, which repairs up to 12 base pairs. Although not extensive, there is evidence of this pathway occurring in the mitochondria as well (Szczesny et al., 2008, Liu et al., 2008, Akbari et al., 2008).

The MMR pathway also has shown activity in the mitochondria (Mason et al., 2003, de Souza-Pinto et al., 2009). However, unlike the proteins involved in nuclear MMR pathway such as the endonuclease EXO1, the mitochondria uses YB-1 a DNA binding protein which can bind to mismatched base pairs (de Souza-Pinto et al., 2009). This study also demonstrated that depletion of YB-1 leads to an increased level of mtDNA mutations as shown using a chloramphenicol-resistance selection assay. This selects specifically for cells with mutant mtDNA as chloramphenicol binds to ribosomal RNA and inhibits protein synthesis within the mitochondria. Mutated cells survived as ribosomal RNA genes would be mutated and hence not bound to.

The mtDNA is double stranded and hence prone to double stranded breaks, this form of damage requires recombination repair. Although not a lot of information is available on recombination repair of double strand breaks in the mitochondria, a recombination protein; RAD51, has been identified as localising to the mitochondria. This protein is involved in repair of double strand break repair and it was noticed as accumulating following oxidative stress (Sage et al., 2010).

TFAM, as mentioned before, has a role in the packaging of mtDNA by inducing a u-shaped bend in the mtDNA. Although this protects nucleotides from DNA damage, it also makes the DNA inaccessible for repair enzymes such as the ones involved in BER. Overexpression of TFAM has demonstrated excessive binding of TFAM with mtDNA in cultured cells (Maniura-Weber et al., 2004). This can shield mtDNA from the activity of OGG1, APE1 and can also prevent incorporation of new bases by poly (Canugovi et al., 2010). This study also demonstrated that inhibition of TFAM results in increased mtDNA repair as mtDNA was not 'hidden' from the enzymes involved in repair and TFAM knockdown showed an increase in mtDNA mutations measured using quantitative-PCR.

1.5.3 *MtDNA transcription and translation*

TFAM is a key protein involved in the transcription of mtDNA. Due to its involvement in the maintenance and packaging of mtDNA into nucleoids (Bogenhagen et al., 2008, Kaufman et al., 2007). TFAM initiates transcription by binding to sequences on the light and heavy strand promoter regionof mtDNA producing long transcripts coding for multiple proteins (Falkenberg

et al., 2007, Shi et al., 2012, Ngo et al., 2014, Ngo et al., 2011c). The sequences that TFAM binds to are present within the D-loop and are called L-strand promoter (LSP), Heavy strand promoter 1 and 2 (HSP1 and HSP2). LSP is used to transcribe the light chain and HSP1 and HSP2 for the heavy chain. HSP1 is responsible for transcribing short sequences of mRNA and HSP2 is responsible for transcribing the majority of the heavy strand (Montoya et al., 1983). This TFAM binding causes the mtDNA to alter its conformation allowing the transcription machinery to be recruited and initiate transcription (Ngo et al., 2011a, Rubio-Cosials et al., 2011). This machinery includes the RNA polymerase POLMRT, which is responsible for the synthesis of the new molecule, and the two transcription factors mtTFB1 and mtTFB22 (Falkenberg et al., 2002). The binding of these transcription factors initiates the transcription, and synthesis of the mRNA molecule then occurs simultaneously in both directions, matured by enzymes such as RNase P (Rossmanith and Karwan, 1998). This is particularly important due to the polycistronic nature of the mtDNA molecule. Termination of transcription is mediated by Mitochondrial Transcription Termination Factor (mTERF) (Yakubovskaya et al., 2010). The transcript produced from the LSP also produces RNA primers that also play a role in replication of the mtDNA suggesting a link between translation and replication since both use the same template (Fernández-Silva et al., 2003, Chang and Clayton, 1985).

Similar to nuclear mRNA translation, mitochondria also follows the steps of initiation, elongation and termination, however the mitochondria contain their own ribosomes for this purpose; the mitoribosomes. Initially the template mRNA strand is bound to the smaller subunit (28s) of the mitoribosome mediated by Mitochondrial Translational Initiation Factor 3 (mtIF3) (Koc and Spremulli, 2002). Synthesis is initiated by the AUA or AUG codon on the template mRNA, which codes for formylmethionyl-tRNA, which is recruited by Mitochondrial Translational Initiation Factor 2 (mtIF2) (Bilbille et al., 2011). This formylated version of methionine is only used at initiation of translation.

Following initiation, elongation occurs mediated by Tu Translation Elongation Factor, Mitochondrial (mtTUFM). This mediates aminoacylated tRNA binding and GTP hydrolysis at the Aminoacyl-tRNA binding site (A-site) of the ribosome. Mitochondrial translation elongation factor (mtEFT) binds to and mediates the recycling of TUFM by inducing the exchange of GDP to GTP, allowing it to bind more aminoacylated tRNAs (Emperador et al.,

2017). The elongation continues when the amino acid at the site moves into the peptidyl-tRNA binding site (P site) and Exit site (E site). The movement of these tRNAs through these sites are mediated by mitochondrial translation elongation factor G1 (Takeuchi et al., 2010).

The final step is termination. This is driven by recognition of the stop codons AGG, AGA, TAA or TAG at the A-site. Rather than an aminoacylated tRNA, this recruits Eukaryotic Translation Termination Factor 1 (ERF1), which mediates the release of the newly formed polypeptide chain from the mitoribosome (Janzen and Geballe, 2004, Guenet et al., 1999). The machinery is then recycled for the next mRNA template to be translated.

1.6 MtDNA deletions

Mitochondrial DNA can harbour a range of mutations including deletions (ΔmtDNA), point mutations and duplications. Mitochondrial DNA, due to its proximity to ROS, and intron-less nature, could be susceptible damage (Brown et al., 1979). Adding to this is the reduced accuracy of Polγ compared to DNA polymerases for the nuclear DNA (Kunkel and Loeb, 1981, Nissanka et al., 2018). MtDNA deletions caused by these can either remove a few base pairs or could be large scale effecting 1000s of basepairs (Damas et al., 2013). ΔmtDNA can be present as a single mtDNA deletion or as multiple mtDNA deletions within an individual cell. These can be transmitted through the germline, can arise sporadically over the life span of an individual, or as a result of mutations in mtDNA maintenance genes, e.g. POLG (Zeviani et al., 1988, Schon et al., 2012, Shanske et al., 2002, DiMauro and Davidzon, 2005, Longley et al., 2005, Hudson and Chinnery, 2006b, Naïmi et al., 2006). Deletions occurred in the germline or during the early stages of gestation and expanded to high levels as a result of genetic bottleneck. Since this deletion was present in germline, it may be present in every cell (Yamashita et al., 2008). The theory of genetic bottleneck suggests that, as a method of reducing replication of a damaged mtDNA molecule during oogenesis, only a small number of maternal mtDNA molecules undergo replication and amplify to high levels. This could then limit the probability of a damaged mtDNA molecule being passed on to the offspring (Marchington et al., 1998). However, if this is the case, if the maternal mtDNA molecules contain an mtDNA mutations such as deletion, this could then be amplified within the

offspring. In support of this theory was the data that suggested a lack of association between heteroplasmy levels between mothers, offsprings or siblings (Chinnery et al., 2004).

ΔmtDNA can also be the result of mutations in the nuclear genes which are responsible for the maintenance of mtDNA, e.g. POLG (Longley et al., 2005, Hudson and Chinnery, 2006b, Naïmi et al., 2006). Mutations in this gene can result in an unstable poly leading to errors in the mtDNA sequence causing an accumulation of deletions or depletion of mtDNA (Brandon et al., 2013, Hanisch et al., 2015). Similar to this, variants in the mitochondrial helicase, twinkle (section 1.5.1) are also associated with an accumulation of ΔmtDNA and depletion (Tyynismaa et al., 2005, Spelbrink et al., 2001). These deletions would differ between each cell as the mtDNA defect was not present in germline. An accumulation of multiple ntDNA deletions can also occurs as a result of ageing. Many studies have demonstrated an age-related increase in mtDNA deletions within various tissues such as brain, heart and muscle (Bender et al., 2006a, Bua et al., 2006, Kraytsberg et al., 2006a, Zhang et al., 1992). The deleted mtDNA, along with wildtype mtDNA, undergoes replication which would increase the number of deleted mtDNA molecules within a cell through a process known as clonal expansion (section 1.6.3).

A number of studies have demonstrated that the majority of mtDNA deletions lie within the major arc. One such deletion is the common 4977bp deletion. This is associated with ageing and a number of disease conditions such as Huntington's disease and Parkinson's disease (Horton et al., 1995, Ikebe et al., 1990, Taylor and Turnbull, 2005). This deletion removes 4977bps between two flanking 13bp direct repeat sequences present at m.8470-8482 and m.13447-13459 which results in the loss of subunits from complex I, complex IV and complex V, and a number of tRNAs. A vast number of other mtDNA deletions have also been thought to occur as a result of direct repeat sequences (Samuels et al., 2004). This is because the direct repeat sequences are complementary to each other and can bind with each other leading to the deletion of the sequences between the repeats. Other deletions can occur due to indirect repeats, which are not identical repeats of each other, for example there may be a difference of one or two base pairs within a sequence, AC*G*TGCTAAC rather than AC*T*TGCT*C*AC. A small number of deletions also occur without any repeat sequences (Samuels et al., 2004).

Multiple ∆mtDNAs are particularly fascinating due to their proposed involvement in ageing and many age related diseases such as neurodegenerative diseases (including Parkinson's disease) and sarcopenia (Krishnan et al., 2012, Aiken et al., 2002). An accumulation of ∆mtDNAs has been noticed in a number of tissues with ageing, which is particularly prominent with post-mitotic tissues such as brain and skeletal muscle (Bua et al., 2006, Bender et al., 2006c, Kraytsberg et al., 2006b, Lee et al., 1994). Due to the fact that mtDNA does not containing any non-coding regions, deletions will often cause a biochemical defect. Therefore it is important to understand the mechanism which leads to the formation of ∆mtDNA, which still remains unclear. Two theories have been put forward to explain this phenomena; Errors in replication and inaccurate repair.

1.6.1 *MtDNA deletion formation through replication*

In a previous study by our group, deletions from single substantia nigra neurons were analysed from PD patients, a ∆mtDNA disorder patient and aged matched individuals (Reeve et al., 2008). The distribution of the breakpoints was analysed. The 5' was set as being the region close to OH and 3' being close to OL. The results show there was no difference in distribution of the deletions between the three groups. A total of 89 deletions was observed within these three groups. Out of this, 80% involved direct repeats with ~42% being perfect repeats and ~38% being imperfect repeats. Only ~20% contained no direct repeats. With no differences in the types of deletion detected between the 3 groups, this suggested that the method of deletion formation is likely to be the same in the three groups. A further systematic review looking at human ∆mtDNA reported a total of 263 ∆mtDNA (Samuels et al., 2004). They discovered 90% of the sequences contained repeat sequences with 60% carrying perfect repeats and 30% imperfect repeats. This study (Samuels et al., 2004) also discovered that the mtDNA contains only 5 direct repeat sequences that have a length of 13bp's or over. Out of these, the pairs with both the direct repeat sequences within either the major arc or within the minor arc have been associated with deletions in patients. One of these was the common 4977bp deletion (Zhang et al., 2002, Moraes et al., 1991). This means that the deletion does not exclude the OL or the OH region, allowing the deleted molecule to replicate again. The remaining direct repeat sequences occur in either the major and minor arc and result in deletion of either the OL or the OH region and interestingly, they have never been associated

with a phenotype (Damas et al., 2013). This is because they eliminate one of the origins of replication hence replication of the deleted molecule cannot take place. However, deletions that remove OL have been discovered in post-mitotic tissues which opposes this theory (Baumer et al., 1994, Kajander et al., 2000, Rygiel et al., 2016).

This (Samuels et al., 2004) study also found that the 3' end of all deletions they analysed were located in close proximity to m.16070, with very few deletions described to have gone past this region. This could be due to the adjacent 'termination-associated sequence'. These pieces of evidence suggest that mtDNA replication could be involved in ΔmtDNA formation. However, although minimal, there have been deletions reported that span this region suggesting that there are other mechanisms of deletion formation (Kajander et al., 2000, Samuels et al., 2004, Bodyak et al., 2001, Bua et al., 2006).

A mechanism of deletion formation by mtDNA replication occurs as a result of slipped strand replication. This is because the light strand remains single stranded until the OL is exposed, during which repeat sequences can bind to each other, exposing the DNA in between (figure 1.7). However, this assumes mtDNA replicates via SDM and as mentioned above, and there are other well supported theories of replication. A major argument against ΔmtDNA formation through replication is that when analysed, human colonic crypt stem cells, although actively replicating contain clonally expanding point mutations, and no ΔmtDNAs (Taylor et al., 2003b). This is also not due to natural selection against deletions, as these tissues have shown very low evidence of selection (Greaves et al., 2012). If replication was the factor leading to deletions, the colonic crypt stem cells should contain higher levels of ΔmtDNA compared to post-mitotic tissue such as skeletal muscle and brain in which mitochondrial turnover is much slower (Wang et al., 1997). Additionally the discovery of deletions that extend into the minor arc and remove OL (Rygiel et al., 2016) also suggests that replication alone cannot explain deletion formation.
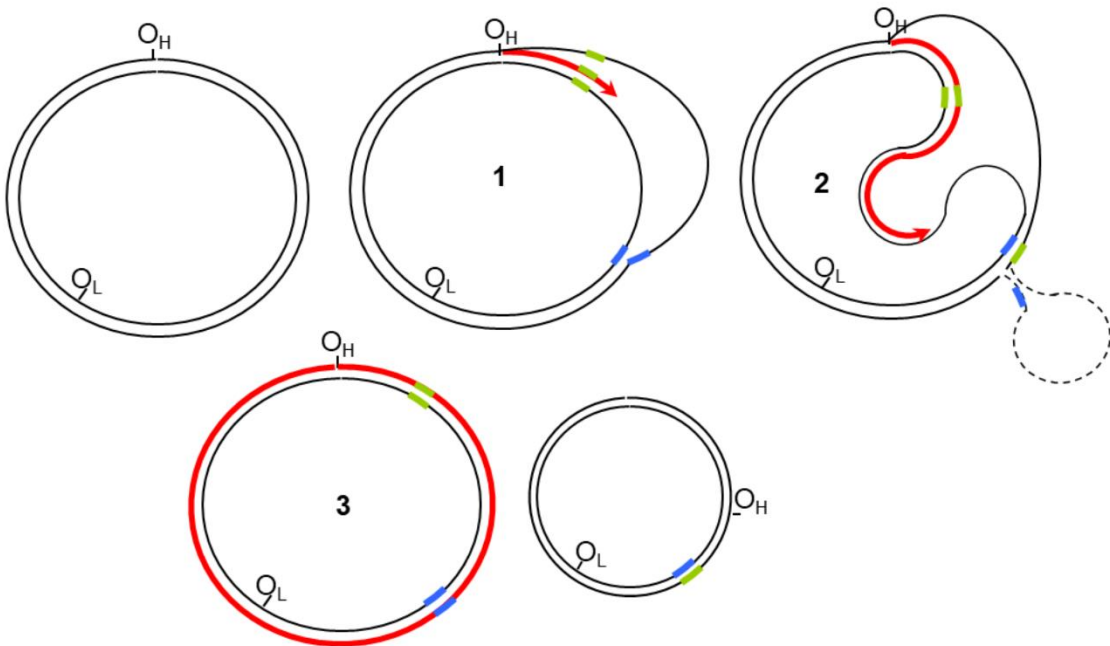
Figure 1.7 Slipped strand model of mtDNA deletion formation. 1) Initially the replication of heavy strand is initiated at OH, leaving the L-strand single stranded. 2) This allows complementary sequences on the light strand to bind to the region of the H-strand not being replicated. The DNA loop that is formed as a result of this mismatch is then degraded 3) this will result in two daughter molecule, one with the full 16kbp, and another with a deletion. Image taken with permission from (Reeve, 2007).

Another method of deletion formation through replication is due to replication stalling (Wanrooij et al., 2004). This was explained using recombinant baculovirus to analyse the Polγ fidelity via the Y955C mutation. This mutation, within the active site of the polymerase domain, structurally altered the active site and could lead to replication stalling which can lead to double strand breaks (DSB). The paper explains that this mutation resulted in a decreased affinity for nucleotides (Ponamarev et al., 2002), therefore when the polymerase reaches a region that contains repetition of the same nucleotide, due to this low affinity and a depletion of this nucleotide in the vicinity, replication cannot continue, leading to stalling and further DSBs. This study also reported an increased number of repeating nucleotides at the breakpoints of deletions. Furthermore one of the genes associated with ΔmtDNA in human patients is the TWNK gene, which encodes for the previously mentioned twinkle helicase. A mutation in this gene resulted in an accumulation of replication intermediates and accumulation of ΔmtDNA in a transgenic cell line and a mouse model, suggesting that

replication was stalled. The paper suggested that mtDNA depletion, associated with TWNK mutations, is due to this replication stalling and this is the mechanism of ΔmtDNA formation in these cells (Goffart et al., 2008).

Recently, copy-choice recombination has been put forward as the mechanism of deletion formation during mtDNA replication via SDM (Persson et al., 2019). This hypohthesis also suggests that during replication of the H-strand, the single stranded L-strand can bind to repeat sequences within itself forming a loop. When the L-strand is synthesised, the resulting loop is not replicated. This is similar to the previous replication stalling theory, however without the double strand breaks.

1.6.2 *MtDNA deletion formation through repair*

Another possible method of ΔmtDNA formation is through repair. Although, repair pathways exist to correct mtDNA damage, these are not infallible. As mentioned before the BER pathway is the major repair pathway that has been observed in mitochondria. During repair via BER, intermediates containing single strand breaks are recognised and cleaved by DNA glycosylases, processed and correct base pairs are inserted before ligating it back to the original strand. However if BER is interrupted, these breaks can accumulate as seen in yeast (Ma et al., 2008). This can then disrupt other processes such as replication which could potentially lead to an accumulation of mtDNA mutations. However, this is more specific for point mutations as BER is involved in the removal of a single base pair. It could be suggested that we see an accumulation of ΔmtDNA (Bender et al., 2006a, Kraytsberg et al., 2006a) as repair mechanisms for these mutations are absent or not adequate.

Another theory set forward by (Krishnan et al., 2008) is that deletion formation occurs through the repair of double strand breaks (DSB) (figure 1.8). They suggest that after a DSB is made, this is susceptible to 3'→5' exonuclease activity which is generally involved in proofreading activity and removes mismatched base pairs. This would then leave the mtDNA single stranded at the site of the break, allowing the DNA to mis-anneal to a direct repeat sequence forming a ΔmtDNA. Examples of 3'→5' exonucleases are POLG and RNA exonuclease 2, an oligoribonuclease, which localises to the mitochondria which could mediate this deletion formation (Nguyen et al., 2000, Hudson and Chinnery, 2006a). This hypothesis suggests that a

direct repeat is required for deletions to form, and while these are associated with the majority of mtDNA deletions, previously mentioned studies have identified breakpoints that do not correspond with a direct repeat (Reeve et al., 2008, Samuels et al., 2004).

Figure 1.8 MtDNA deletion formation through repair of double strand breaks. 1) Initially mtDNA is damaged as a result of insult such as ROS. 2) This requires repair which could initiate a double strand break for repair. 3) The DNA undergoes degradation 4) this leaves single strands of DNA. 5) this allows repeat sequences present on the single strand to anneal due to homologous recombination, and any remaining single stranded DNA could be degraded. 6) which leaves a deleted mtDNA molecule. Image taken with permission from (Reeve, 2007).

Another theory that could be suggested as to why there are more deletions in post-mitotic tissues than mitotic ones is that the nuclear genome has reduced transcription of mtDNA repair proteins. Due to this, these repair proteins would not be transcribed from the nuclear genome and thus would not be accessible for the mitochondria. Transcriptomic studies have demonstrated an age-related decrease in nuclear encoded mitochondrial proteins (Preston et al., 2008). This is also supported by a study (Imam et al., 2006) which demonstrated an age-dependent decrease in various DNA glycosylases in five brain regions; caudate nucleus, frontal cortex, hippocampus, cerebellum and brain stem. This was done on mice aged 6 and 18 months, mitochondrial as well as nuclear DNA glycosylases were identified. This is also supported by another study which demonstrated an age-dependent decrease of BER activity in the mitochondria in mice cerebral cortices (Chen et al., 2002). Since mtDNA is double

stranded and circular a further theory has suggested that the formation of DNA conformations such as a hairpin, cloverleaf or cruciform occur due to repeat sequences that are complementary with each other. These structures can also increase mtDNA vulnerability to deletions (Damas et al., 2012). This again points towards repair as a method of deletion formation since these structures are not described within any of the replication models.

Since Polγ is also involved in repair pathways, the *PolgA^{mut/mut}* mouse can be studied to understand repair as well. With inadequate repair, ΔmtDNA formation, especially in the case of Polγ mutations, is said to be due to ineffective proof reading activity of the polymerase resulting in incorporation of inaccurate nucleotides which are not correctly 'proof read'. This could lead to accumulation of point mutations and which will then be cleaved and possibly lead to DSB, which can lead to ΔmtDNA (Krishnan et al., 2008). However, a study using patient tissue containing the Polγ mutation Y955C showed that the levels of point mutation in the cytb encoding region did not differ significantly between patients and control individuals, suggesting that the accuracy in replication and or repair is not diminished (Wanrooij et al., 2004). However other mechanism could have a different mechanism of action.

1.6.3 *Clonal expansion of mtDNA deletions*

Clonal expansion of mtDNA mutations refers to the process by which ΔmtDNA or any other mutation might expand to high levels in a single cell. Once the deletion level crosses the threshold value, this leads to OXPHOS deficiency and mitochondrial dysfunction resulting in disease (Campbell et al., 2012, Fayet et al., 2002). There are three main theories for how mtDNA mutations clonally expands; survival of the smallest, survival of the slowest and random genetic drift.

I) Survival of the smallest

Survival of the smallest was the first theory to be suggested (Wallace, 1989, Wallace, 1992). This theory suggests that deleted mtDNA molecules, since they are smaller, replicate much faster allowing the deletion to accumulate. There has been evidence uncovered that both supports and disputes this theory. Initial support for this 'survival of the smallest' theory was put forth by an *in vitro* study on human fibroblasts containing both wildtype and a deleted

mtDNA molecule. They caused mtDNA depletion using ethidium bromide treatment, and when the mtDNA repopulated, there was an increase in ΔmtDNA within the cell lines that harboured them compared to the wildtype mtDNA molecules. This suggested that deleted mtDNA replenished their population significantly faster than full length, wild type mtDNA molecules (Moraes et al., 1999). This was replicated in another study which also demonstrated that deleted mtDNA accumulation (Diaz et al., 2002). They also used a cell line with point mutations and demonstrated that there was no increase of these mutations further suggesting a size advantage. One of the main criticisms for the original Moraes *et al* study was that the higher level of ΔmtDNA was due to the toxicity induced by ethidium bromide. However, the Diaz *et al* study also looked at normal conditions, which still showed a preferential accumulation of shorter mtDNA molecules. This study is also supported by another study that looked at iPSC cells reprogrammed from human fibroblasts (Russell et al., 2018). This revealed that the level of a ΔmtDNA increased with sequential passage, which was not observed in cells harbouring point mutations. This has also been investigated *in vivo* using mice (Fukui and Moraes, 2008). These mice expressed a restriction endonuclease, which was targeted specifically to the mitochondria in adult neurons. This restriction enzyme has the ability to induce double strand breaks by cleaving the mtDNA that will be repaired by DNA repair machinery forming ΔmtDNAs (section 1.6.2). Furthermore, they demonstrated that larger deletions, accumulated faster in adult neurons, than smaller deletions.

A major piece of evidence against this theory is that the accumulation of point mutations to high levels is also commonly seen. MtDNA molecules containing point mutations do not have the smaller size advantage yet they accumulate to high levels similar to those of ΔmtDNA particularly within mitotic tissues (Michikawa et al., 1999, Khaidakov et al., 2003, Trifunovic et al., 2004, Taylor et al., 2003a). A study of the colorectal epithelium demonstrated an accumulation of point mutations with ageing (Greaves et al., 2014). However, accumulation of ΔmtDNA with age, rather than point mutations is prominent in post-mitotic cells such as neurons; hence, survival of the smallest theory could still be the mechanism of ΔmtDNA accumulation in post-mitotic cells. In addition to this, there was a suggestion that faster replication is not advantageous for mtDNA, due to its long half-life (~6-31 days) compared to its short replication time (~1 hour) (Korr et al., 1998, Gross et al., 1969, Clayton, 1982). This

suggest that, even if replication occurs faster, there is no benefit since mtDNA molecules are present for a much longer time. Hence, replication time would not be the rate-limiting step in this process.

II) Survival of the slowest

The survival of the slowest theory takes into account mitochondria's ability to produce ROS as a by-product of OXPHOS. This theory suggests that in mitochondria with ΔmtDNA, the OXPHOS system, due to decrease in normal function, has a reduction in the amount of ROS produced. This in turn prevents the mitochondria from being targeted for mitophagy, hence the ΔmtDNA is allowed to replicate and accumulate (De Grey, 1997). However, evidence against this theory suggests that in mitochondria with OXPHOS dysfunction and mtDNA mutations including ΔmtDNA, there is an increase in ROS production (Indo et al., 2007). Also in cytoplasmic hybrids (cybrid) cells containing the common deletion causing an OXPHOS defect, an increase in ROS within the mitochondria was noticed (Peng et al., 2006).

III) Random drift

Another theory of clonal expansion suggests that there is no selective mechanism for mtDNA replication and that accumulation of ΔmtDNA is random (Elson et al., 2001). This was supported by a mathematical model that was developed that predicted that up to 4% of post mitotic cells will be COX negative by the 8th decade of life, which was concurrent with histochemical data. However, in neurons, by the 8th decade of life, over 50% deletion heteroplasmy is observed (Bender et al., 2006c, Kraytsberg et al., 2006b). This theory also supports and provides an explanation for the accumulation of point mutations. However, this theory does not explain clonal expansion in patients with multiple ΔmtDNA due to nuclear mutations, as they tend to have a younger age of onset and higher levels of COX deficiency (Campbell et al., 2014, Lax et al., 2012, Cottrell et al., 2000).

IV) Other possible theories

Recently, another theory has suggested that clonal expansion of deletions occurs due to the connection between replication and transcription, where transcription of the L-strand

produces an mRNA that can initiate replication. This study used bioinformatics analysis of ΔmtDNA to suggest a negative feedback loop where transcription levels are controlled by the availability of certain proteins coded by the mtDNA. In the case of ΔmtDNA, when these proteins are not available, mtDNA transcription is still upregulated, which can also lead to an increase in replication of this molecule. The analysis discovered that the mtDNA coded genes; ND4, ND5 and ND6, functioned in this feedback loop. Although most mtDNA deletions do remove these genes, ΔmtDNA has also been observed as accumulating in cases where these candidate genes are not deleted (Damas et al., 2013).

1.6.4 *MtDNA deletions in post-mitotic cells*

Although ΔmtDNA have been associated with diseases such as Kearns-Sayre syndrome (KSS), the age-dependent accumulation of ΔmtDNA was first reported in the early 90's, particularly in post-mitotic tissues (Cortopassi and Arnheim, 1990, Cooper et al., 1992, Cortopassi et al., 1992, Soong et al., 1992). Low levels of specific ΔmtDNA, previously described as being pathogenic in mitochondrial diseases, were discovered in tissue from heart and brain from aged individuals, however, these mutations were not observed in fetal heart and brain tissue suggesting they accumulate with age (Cortopassi and Arnheim, 1990). A fascinating factor uncovered was that the same tissue from different individuals contained more similar deletion loads than different tissues within the same individual (Cortopassi et al., 1992, Meissner et al., 2006), suggesting that the same tissues accumulate ΔmtDNA in a similar fashion. In support of this, a study comparing mtDNA mutations in the colon of *PolgA^{mut/mut}* mice and aged wild-type individuals showed that the location of the genes effected were not significantly different between both cases (Baines et al., 2014). Alongside this, ΔmtDNA have also been associated with normal ageing, and age associated conditions such as Parkinson's disease and muscle myopathies (Bender et al., 2006c, Cortopassi et al., 1992, Holt et al., 1988, Reeve et al., 2008). More evidence of ΔmtDNA association with ageing was established when a study comparing mtDNA mutations in *PolgA^{mut/mut}* mice and aged wild-type individuals showed that although the location of the genes effected were not significantly different, there was a significant difference in the type of mutation as point mutations were noticed in both groups, but ΔmtDNA was present only in aged individuals (Baines et al., 2014).

1.6.5 *MtDNA deletions in neurons*

Of all the post-mitotic cells, neurons seem to be particularly susceptible to ΔmtDNA. A study compared the level of the 'common' deletion which cleaves 4977 bps and demonstrated the highest levels in the brain compare to muscle and heart (Meissner et al., 2008). They also mentioned that in older individuals, compared to adolescent individuals, the deletion load increased by 3 fold. This increase in ΔmtDNA within neurons could be due to the complexity of these cells and their function, resulting in a high energy demand, thus increasing their dependence on mitochondria to produce this energy through OXPHOS activity. This high requirement for oxygen could also result in a higher level of oxidative stress, which has the potential to induce mtDNA damage. Damaged mtDNA can also result in mtDNA mutations and damaged OXPHOS function which results in a further increased in oxidative stress creating a vicious cycle of mtDNA damage and oxidative stress (Circu and Aw, 2010).

Clonal expansion of ΔmtDNA in neurons was investigated in two studies looking at dopaminergic neurons (Bender et al., 2006c, Kraytsberg et al., 2006b). Bender *et al* laser-microdissected individual neurons from the Substantia Nigra (SN) of PD patients and control (healthy aged) individuals and conducted long range PCR. They demonstrated that SN neurons from both groups contained multiple ΔmtDNA which had clonally expanded to high levels in both COX-deficient and COX-positive neurons. The presence of multiple deletions which were different in each neuron suggested that they were acquired, as an inherited mutation would produce the same ΔmtDNA species in all the cells studied from each patient. This age related increase in ΔmtDNA was also supported by Kraytsberg *et al*, further suggesting a role of clonal expansion. Both of these papers demonstrated a higher level of ΔmtDNA in COX-deficient neurons suggesting a link between the ΔmtDNA and mitochondrial dysfunction. Following this, a study by our group looked at the actual break points of these ΔmtDNA (Reeve et al., 2008). They found that similar break points were observed within the ΔmtDNA in 3 groups: PD patients, ΔmtDNA disorder patients and age matched controls. This suggested that the type of ΔmtDNA is similar in the three groups, suggesting a similar mechanism of ΔmtDNA accumulation.

ΔmtDNA, specifically the differences between brain regions is discussed in more detail in section 3.1 (chapter 3)

1.6.6 *MtDNA deletions and neurological disease*

As mentioned previously, ΔmtDNA are associated with a number of age associated neurodegenerative conditions such as Parkinson's disease, Huntington's disease and Alzheimer's disease (Aiken et al., 2002, Bender et al., 2006c, Krishnan et al., 2012). Mitochondrial diseases can also occur as a result of ΔmtDNA. Mitochondrial diseases are a set of conditions caused by inherited mutations (in both the nuclear and mitochondrial genomes) that lead to mitochondrial dysfunction. One such condition is progressive external ophthalmoplegia (PEO). This can be caused by an inherited mutation with the twinkle helicase protein or Polγ (section 1.5.1) that leads to the presence of multiple ΔmtDNA which accumulate within an individual (Spelbrink et al., 2001, Van Goethem et al., 2001). In these conditions, patients most commonly exhibit myopathies, however neuropathies have also been observed (Kiechl et al., 2004). Polγ mutations in humans are also associated with early onset Parkinsonism in a number of studies (Davidzon et al., 2006, di Poggio et al., 2013, Puschmann, 2013). A recent study conducted whole exome sequencing on a cohort of PD patients and identified variations within mtDNA maintenance genes such as POLG, POLRMT and OGG1 (Gaare et al., 2018). Single large scale deletions have also been associated with Kearns-Sayre syndrome (KSS), which is a neuromuscular disease, with neurological symptoms such as ataxia, cognitive decline and seizures (Khambatta et al., 2014). These studies suggest a direct association between ΔmtDNA and neuronal health and survival.

1.6.7 *Why are SN neurons particularly prone to accumulating mtDNA deletions?*

A reason for the sensitivity of SN dopaminergic neurons to these ΔmtDNA could be due to high oxidative stress as a result of their function. SN neurons are one of the largest neurons within the brain, and are highly arborized with a total axonal length of 4.5m (Bolam and Pissadaki, 2012). They also have an increased rate of oxygen consumption and more axonal mitochondria compared to dopaminergic neurons from the ventral tegmental area (VTA) (Pacelli et al., 2015). Due to this size and complex arborization, there is an increase in dependence on the OXPHOS system and oxidative stress (Haddad and Nakamura, 2015, Pacelli

et al., 2015). Studies have demonstrated increased oxo-8-dG levels in the midbrain (containing SN) compared to other regions such as cerebellum (Cardozo-Pelaez et al., 2000). This oxidative stress is further exaggerated by the metabolism of dopamine, which produces oxidative molecules such as dopaminergic quinines and H_2O_2 which can lead to oxidative stress if not properly degraded by glutathione peroxidase (Andersen, 2004). Hydroxide radicals and ions are produced from the Fenton reaction between H_2O_2 and iron, while ferritin, a protein that binds and stores iron, has been demonstrated to be decreased in the SN of PD patients suggesting an increase in cellular free iron levels to react with H_2O_2 (Dexter et al., 1991, James et al., 2015). In addition to this, neuromelanin, found within SN neurons, is also capable of binding iron. In PD and ageing, a decrease in neuromelanin levels is observed further elevating the levels of unbound iron (Mann and Yates, 1983, Kastner et al., 1992, Zucca et al., 2017). All of this suggests a toxic cycle between iron and dopamine within dopaminergic neurons adding to the high oxidative stress in these cells (Hare and Double, 2016). Furthermore, SN neurons exhibit a high rate of lipid peroxidation and protein nitration (Dexter et al., 1989, Good et al., 1998). Glutathione, one of the antioxidant enzymes within the mitochondria, is also reduced in the SN of PD patients further suggesting a link between the SN and increased oxidative stress (Bharath et al., 2002, Sofic et al., 1992).

1.6.8 *MtDNA deletions in PolgA$^{mut/mut}$ transgenic mice*

Tables 3.1 presents mtDNA deletion levels detected in *PolgA$^{mut/mut}$* transgenic mice. The mice used in this thesis were a gift from Dr Laura Greaves (Wellcome Centre for Mitochondrial Research), and have been described in detail in section 2.2.1. Briefly these mice demonstrate an accumulation of mtDNA deletions and point mutations alongside a premature ageing phenotype (Kujoth et al., 2005). In *PolgA$^{mut/mut}$* mice, ΔmtDNA form due to error prone replication instigated by defective DNA polymerase γ. Since this is the only polymerase which functions in the mitochondria, any mutations within this gene can have a large effect (Bolden et al., 1977, Luoma et al., 2004). The D257A mutation within the mice used for this study, codes for a missense mutation that affects the proof reading domain of the catalytic subunit which alters the 3'-5' exonuclease activity of the enzyme (Falkenberg et al., 2007). Normally this region is involved in identifying mismatched basepairs which are then repaired by exonuclease activity. Therefore the mutation results in mismatches being retained within the

genome. This mutation is also suggested to affect the ligation of the mtDNA following replication which will be discussed in detail later in this section (Macao et al., 2015).

These *PolgA^{mut/mut}* mice demonstrate the presence of multiple ΔmtDNA species, which increase with age, especially within the brain (refer to table 3.1). This renders it a good model to study ΔmtDNA, as in humans, patients with POLG mutations also lead to multiple deletions and often Parkinsonism (Bender et al., 2006b, Davidzon et al., 2006, Trifunov et al., 2018, Van Goethem et al., 2001). In patients with POLG mutations, the mtDNA deletions mtDNA molecules retain a circular structure, however, mtDNA deletions in *PolgA^{mut/mut}* mice are understood to be linear. A suggested mechanism of deletion formation in *PolgA^{mut/mut}* mice is through faulty ligation of the 5'- end (Macao et al., 2015). Studies have suggested that when replication of a single mtDNA strand is complete, 3'-5' exonuclease activity is required to produce a nick that is ligated when replication of both strands end. However in *PolgA^{mut/mut}* mice, the replication does not stop when it returns back to the origin of replication. Instead this is continued and due to this the remaining product cannot be ligated and it is left as a nick. When the next round of replication happens, this then produces a double strand break and a linear mtDNA molecule. It has also been suggested that the mutated version of Polγ does not require Twinkle to linearise the double stranded mtDNA, instead it can produce short fragments of mtDNA from the double strands (He et al., 2013, Farge et al., 2007). This will produce fragments observed as ΔmtDNA in a long range PCR experiment, however these might not be reflecting the accumulation of ΔmtDNA as these short fragments are linear and might prevent further replication due to disturbed origin of replication sites. Recent studies have demonstrated that these linear fragments are degraded quickly, even within 4 hours (Peeva et al., 2018, Nissanka et al., 2018), which could explain the association of POLG mutations and mtDNA depletion syndromes (Naviaux and Nguyen, 2004, Van Goethem et al., 2001, Mehta et al., 2011) and could be further evidence that these ΔmtDNA are in fact linear. However, this depletion can also be caused by inefficient polymerase gamma. Alongside this, *PolgA^{mut/mut}* mice demonstrate premature ageing phenotype Therefore, in this study, *PolgA^{mut/mut}* mice is used as a model for replication defect rather than a model for a particular disease.

1.7   Significance of this thesis

Although the field studying ΔmtDNA has seen much progress over the years, the mechanism of mtDNA formation and accumulation to high levels remain uncertain. One of the mechanism that have been theorised to lead to ΔmtDNA is mtDNA replication (section 1.6.1). This thesis aims to shed light on mtDNA replication, with particular emphasis on neurons due to the high levels of ΔmtDNA observed here. This would be beneficial in establishing the impact of mtDNA replication in mtDNA deletion formation. Therefore, the aims of this thesis were as follows;

1. To study mtDNA replication in various brain regions to correlate with the different levels of ΔmtDNA observed in these regions
2. To develop a model to study mtDNA replication *in vitro* within various cell lines
3. To study the location of mtDNA replication which could shed more light on expansion of ΔmtDNA

Chapter 2 : Materials and Methods

2.1 Equipment, software, reagents and consumables

2.1.1 *Equipment*

Equipment	Supplier
ABI Step-one Plus Real Time PCR system	Applied Biosystems
ABI veriti-96 well Thermo Cycler	Applied Biosystems
AMT CCD camera (for TEM)	Deban
Antigen Retrieval Unit	2100 Retriever
Autoclave	Prior Clave
Autoclave	Astell
Axioimager M1 microscope	Carl Zeiss
Bench-top Centrifuge 3-15	Sigma
Biorad Chemidoc	Biorad
Corning LSE Vortex mixer	Sigma Aldrich
Electrophoresis power supply	Cleaver scientific
Eppendorf Thermomixer	Eppendorf
Horizontal Agarose Gel Electrophoresis Systems	Amersham
Laminar flow hood	Jencons-PLS
Microtome	Microm
Nanodrop ND-1000 Spectrophotometer	Labtech International
Nikon A1R point scanning confocal microscope	Nikon
Pipette 1000-10µL (Gilson)	StarLab
Pipette boy	Integra
PURELAB flex	Elga
Rotatest shaker R100	Luckham
Serial block face scanning electron microscope	Zeiss Sigma

Stereology microscope	Olympus BX51
Sterilizing oven	Laboratory Thermal Equipment Ltd.
Transmission Electron Microscope	Philips CM100
UV hood	Bioair
Vortex genie 2	Scientific Industries

Table 2.1 List of equipment used in this thesis

2.1.2 *Software*

Software	Supplier
3view	Gatan
A1R scanning confocal system	Nikon
ABI Step one software v2.0	Applied Biosystems
Axiovison	Zeiss
Digital Micrograph v2.31.734.0	Gatan
ImageJ	Public domain, NIH
ImageLab software (v4.1)	Bio Rad
Imaris v7.7.2	Bitplane
Imaris v9.0	Bitplane
ND-1000 software	Labtech International
NIS-Elements Viewer v4.2	Nikon
Prism v7.0	Graph pad

Zeiss axioimager	Zeiss
ZEN blue	Zeiss

Table 2.2 List of softwares used in this thesis

2.1.3 *Reagents and consumables*

Reagents/Consumables	Supplier
"Mr Frosty" Freezing container	Thermo Scientific
0.2ml Thin-Walled PCR Tubes	Thermo Scientific
0.5ml PCR Tubes	Thermo Scientific
1.5ml Eppendorf Tubes	Thermo Scientific
1kb DNA ladder	Promega
2ml Eppendorf tubes	Thermo Scientific
5-Chloro-2-deoxyuridine thymidine (CldU)	Sigma-Aldrich
5-Iodo-2-deoxyuridine (IdU)	Sigma-Aldrich
60mm dishes	Fisher Scientific
6-well/12-well plates	Greiner Bio-One
96-well plate Semi-Skirted with Raised Rim	Starlabs
Agarose	Biolin
Aphidicolin	Bertin Pharma
Avidin/biotin blocking kit	Vector Laboratories
B27 supplement	GIBCO
bisBenzimide Hoechst 33258	Sigma Aldrich
Brain Derived Neurotrophic factor (BDNF)	R & D systems
Cellometer Auto T4	Nexcelom

Cellometer disposable counting chambers	Nexcelom
Concentrated HCl	Sigma-Aldrich
Coverslips (22mm and 13mm)	VWR International
Cryostor CS2 Freeze Media	Biolife solutions
Nunc Cryotube	Sigma-Aldrich
Dimethyl Sulfoxide (DMSO)	Sigma-Aldrich
DNA Away	Thermo Fisher
DNA extraction Kit	Qiagen
Doxycycline	Stemcell technologies
DPX	BDH
Dulbecco's Modified Eagle Medium (DMEM)	GIBCO
Dulbecco's Modified Eagle Medium/F-12 media	GIBCO
Dulbecco's Phosphate buffered saline (DPBS)	GIBCO
Eosin	CellPath
Ethanol	Fisher Scientific
Fetal Bovine Serum (FBS)	GIBCO
Filter pipette tips	Tip One
Formalin solution, neutral buffered, 10%	Sigma-Aldrich
Geneticin (G418)	Sigma Aldrich
Glial-cell derived neurotropic factor (GDNF)	R & D systems
Gloves	Ultrasense
GoTaq® Long PCR Master Mix	Promega
Haemotoxylin	TCS Biosciences Ltd.
Histoclear	National Diagnostics
Human Epidermal Growth Factor (hEGF)	GIBCO
Human Fibroblast Growth Factor (hFGF)	GIBCO
Human Neurotrophin-3 (hNT3)	R & D systems

Hydrochloric acid 37%	VWR
Laminin	Sigma Aldrich
L-Glutamine	GIBCO
Matrigel	Millipore
MitoTracker Green FM	Thermo Fisher
mTeSR1 media	Stem cell technologies
N2 supplement	GIBCO
Nomal goat serum (NGS)	Abcam
Normal donkey serum (NDS)	Abcam
Normal goat serum	Sigma-Aldrich
Nutristem	Biological industries
Parafilm	Pechiney plastic packaging
Paraformaldehyde solution 4% in PBS	Santa-Cruz Biotechnology
PBS tablets	Sigma-Aldrich
PCR Primers – long range	Eurofins
Pencillin/Streptomycin	GIBCO
Poly-D-Lysine (PDL)	Sigma Aldrich
ProLong® Gold Antifade Mountant	Life Technologies
Proteinase K solution	Fisher Scientific
Real Time PCR primers	Applied biosystems
Rock inhibitor (Y-2763-ROCKi)	Millipore
Scalpels	Swann Morton
Sodium Pyruvate	GIBCO
Sterilin™ 7ml Polystyrene Bijou Containers	Thermo Scientific
Superfrost plus glass microscope slides	Thermo Scientific
SYBR safe DNA gel stain	Invitrogen
T75cm^2 vented flasks	Corning
TAE buffer	Sigma-Aldrich

Tamara labelled probes (ND1, ND4, Dloop)	Applied biosystems
Taqman mastermix	Applied Biosystems
Tetramethylrhodamine, Methyl Ester, Perchlorate (TMRM)	Thermo Fisher
Tissue cassettes	CellPath
Tris-acetate EDTA buffer	Sigma-Aldrich
Tri-sodium citrate dihydrate	VWR
Trizma base	Sigma-Aldrich
Trypan Blue	GIBCO
Trypl-E Express	GIBCO
Tween®-20	Sigma-Aldrich
Uridine	Sigma Aldrich
X-VIVO media	Corning

Table 2.3 List of reagents and consumables used in this thesis

2.1.4 **Antibodies**

Primary Antibodies	Isotype	Supplier
Anti-CaMKIIα antibody (6G9)	Mouse IgG1	Santa Cruz
Anti-DAT antibody	Rat polyclonal	abcam
Anti-DNA antibody, double stranded, clone BV16-13	Mouse IgG2a	Merck Millipore
Anti-Grp75 antibody	Rabbit polyclonal	Abcam
Anti-MAP2 antibody (ab5392)	Rabbit polyclonal	Abcam

Anti-mtTFA antibody	Mouse IgG2b	Abcam
Anti-NDUFB8 antibody	IgG1	Abcam
Anti-Tyrosine Hydroxylase antibody	Rabbit polyclonal	Sigma
Anti-VDAC1 / Porin antibody [20B12AF2] (ab14734)	Mouse IgG2b	Abcam
CldU (Bromodeoxyuridine/BrdU Antibody (BU1/75 (ICR1))	Rat IgG2a	BD Biosciences
IdU (Purified Mouse Anti-BrdU)	Mouse IgG1	Novus biologicals
MitoTracker Red CMXRos	n/a	Thermofisher
Monoclonal anti b-tubulin	Mouse IgG2b	Sigma-Aldrich
PicoGreen	n/a	Thermofisher
Smi-31	Mouse IgG1	Cambridge Bioscience
Tom20 antibody	Mouse IgG2a	Santa Cruz
Tom20 antibody (FL-145): sc-11415	Rabbit polyclonal	Santa Cruz
Twinkle antibody	Rabbit polyclonal	Protein Tech

Table 2.4 List of antibodies used in this thesis

2.1.5 *Solutions*

Solution	content
COX-EM fixative	2% Glutaraldehyde 0.1M Sorrenson's buffer (pH7.4)
Differentiation media	100ml Neurobasal media 2ml B27 supplement 1ml N2 supplement 1ml Pencilin/Streptomycin (50µg/ml) 1ml Sodium Pyruvate (1mM) 0.2ml Uridine (50mg/ml) 10ng/ml Brain Derived Neurotrophic factor (BDNF) 10ng/ml Glial-cell derived neurotropic factor (GDNF) 10ng/ml Human Neurotrophin-3 (hNT3)
DNA electrophoresis gel buffer	100ml 10x Tris-acetate EDTA buffer 900ml Nanopure water
DNA electrophoresis running buffer	100ml 10x Tris-acetate EDTA buffer 900ml Nanopure water
Single cell lysis buffer	250µl 1% Tween 20 50µl 0.5M TrisHCl pH8.5

	195µl dH2O
	5µl proteinase K
MTeSR media	400ml mTesR base Medium
	100ml MTesR supplement
	5ml Pencilin/Streptomycin (50µg/ml)
	5ml Sodium Pyruvate (1mM)
	1ml Uridine (50µg/ml)
NutriStem Media	500ml Nutristem hPSC XF Medium
	5ml Pencilin/Streptomycin (50µg/ml)
	5ml Sodium Pyruvate (1mM)
	1ml Uridine (50µg/ml)
Phosphate Buffered Saline (PBS)	1 tablet in 100ml dH$_2$O
Proliferation media	100ml Dulbecco's Modified Eagle Medium (DMEM)/F12 media
	2ml B27 supplement
	1ml N2 supplement
	1ml Pencilin/Streptomycin
	1ml L-gutamine
	(filter through at this point, then add the following)
	10ng/ml Human Epidermal Growth Factor (hEGF)

	10ng/ml Human Fibroblast Growth Factor (hFGF)
Tris-Buffered Saline (TBS, pH 7.4)	1.2g Trizma Base 17g NaCl 2L dH$_2$O Concentrated HCl
Tris-Buffered Saline, Tween 20 (TBST, pH 7.4)	1.2g Trizma Base 17g NaCl 2L dH$_2$O Concentrated HCl 2ml Tween
TEM fixative (pH 7)	2% Glutaraldehyde 0.1 M Sodium Cacodylate
Tri-sodium citrate antigen retrieval buffer (pH 6.0)	2.9g tri-sodium citrate dehydrate (10mM) 1L dH$_2$O 0.5ml tween
Luxol fast blue solution	1g Luxol fast blue 95% alcohol

	10% acetic acid
Cresyl fast violet solution	0.2g Cresyl fast violet 100ml distilled water
Acetate buffer solution	13.5ml Acetic acid 23.5g Sodium acetate 2000ml distilled water
0.1% cresyl fast violet in 1% acetic acid	50ml Cresyl fast violet solution 500ml Acetate buffer solution 500ml Distilled water

Table 2.5 List solutions and their contents used in this thesis

2.2 Mouse brain tissue methods

2.2.1 *PolgA$^{mut/mut}$ mitochondrial mutator mice*

The *PolgA$^{mut/mut}$* mouse, originally produced by (Trifunovic et al., 2004), were a generous gift from Dr Laura Greaves (Wellcome centre for mitochondrial research, Newcastle University). These mice had a knock-in missense mutation which resulted an alanine to aspartate (D257A) conversion effecting the proof reading activity to produce a defective *PolγA*. These mice have an accelerated ageing phenotype resulting in a reduced life span. They also have observational phenotypes such as alopecia, weight loss, kyphosis, and many age related conditions such as anaemia and osteoporosis. They also have molecular age related changes such as increased mtDNA point mutations and deletions.

A total of 17 mice were used for this study. Prior to culling, they were housed in the Comparative Biology Centre (CBC) at Newcastle University. These mice were housed individually and kept in a constant temperature of 25°C with a 12 hour light/dark cycle. These

mice were cared for by Carla Bradshaw (Technican, Wellcome centre for mitochondrial research, Newcastle University). More details about the mice and their age are provided in the chapter (section 3.3.1)

2.2.2 *Thymidine analogue labelling of mouse tissue*

The mice were labelled with 5-Chloro-2-deoxyuridine thymidine (CldU, Sigma Aldrich) and 5-Iodo-2-deoxyuridine (IdU, Sigma Aldrich) by Dr Craig Stamp and Carla Bradshaw (Wellcome centre for mitochondrial research, Newcastle University). Thymidine analogues are incorporated into the cell during DNA replication and hence identify any replicating DNA. The timing and concentration of CldU and IdU labelling was developed and optimised for the mice with the help of Dr Craig Stamp who used this method to label replicating stem cells within colonic crypts (Stamp, 2016). CldU is made up in PBS at a concentration of 5mg/ml. The powder dissolves into the solution with vortexing. The pH is adjusted to 7.4 and the solution is passed through 22μm sterile filter and stored at 4°C until use.

 IdU is also made up at 5mg/ml, however solubilisation requires further steps as the solubility in PBS is at 2mg/ml. Hence IdU is left in a 55°C water bath for 8 hours, following this, 100 ul of 2M NaOH is added into solution dropwise until it is completely dissolved. This requires adjusting the pH back to 7.4 using 10M HCl. The volume of NaOH and HCl are also recorded to ensure a final concentration of 5mg/ml. This solution is passed through a 22μm sterile filter and stored at 55°C on the day of injection as it precipitates out of solution.

The mice are injected via the intra-peritonal cavity at a dose of 50mg/kg. The injection schedule is present in table 2.6. Briefly these mice were injected with 50mg/kg of CldU twice a day for 4 days at 10:00 hours and 18:00 hours. On day 4, they were injected with CldU as normal at 10 am, however at 6pm; they were injected with 50mg/kg of IdU and sacrificed after a further 14-16 hours. Therefore all the mitochondrial DNA which had replicated in the previous 4.5 days would be labelled with CldU and the last 15 hours with IdU.

	Day 1	Day 2	Day 3	Day 4	Day 5
Action 1	Injection: CldU – 50 mg/kg	Injection: CldU – 50 mg/kg	Injection: CldU – 50 mg/kg	Injection: CldU – 50 mg/kg	Animal sacrificed
Time of Action	10:00	10:00	10:00	10:00	8:00-10:00
Action 2	Injection: CldU – 50 mg/kg	Injection: CldU – 50 mg/kg	Injection: CldU – 50 mg/kg	Injection: **IdU** – 50 mg/kg	-
Time of Action	18:00	18:00	18:00	18:00	-

Table 2.6 Thymidine analogue labelling schedule

2.2.3 *Harvesting the mouse brain*

Mice were sacrificed by cervical neck dislocation and the brains were harvested as quickly as possible. The brain was cut down the midline in an anterior to posterior direction. One half was mounted in OCT and moved to -80°C immediately. This was intended to be used for molecular analysis. The other half was added to a cassette and left overnight in a 10% formalin solution, neutral buffered (Sigma Aldrich). This was then transferred into 70% ethanol and fixed in paraffin wax by Newcastle Brain Tissue Resource (NBTR, Newcastle University). This half was used for histological staining and immunohistochemistry.

2.2.4 *Haematoxylin and Eosin staining*

Mouse brain tissue was cut sagittally at 5μm using a microtome (Bright Instruments, 0TF5000) and stored at 37°C overnight and then at room temperature until use. For anatomical confirmation to identify different regions of the brain, every 5th section cut from the brains

was stained histologically using Haematoxylin and Eosin or Cresyl Fast Violet/Luxol Fast Blue staining.

Haematoxylin is used to stain the nuclei as it stains for acidic substances such as RNA and DNA giving it a blue colour. Following this, the section is stained with Eosin which stains for basic substances such as cells, organelles and proteins in pink.

Briefly, paraffin-fixed tissue sections were heated to 65°C for 20 minutes to melt the paraffin wax, and were then subjected to rehydration through histoclear and a graded ethanol series (100% x2, 95%, 70%) to distilled water. The slides were submerged in haematoxylin for 1 minute and then run under normal tap water until the water ran clear to ensure removal of excess staining. Following this, they were submerged in eosin for 30 seconds and washed in tap water again. The slides were then dehydrated through an ethanol series (70%, 95% and 100% x2), washed in histoclear and mounted under coverslip glass with DPX.

2.2.5 *Cresyl Fast Violet/Luxol Fast Blue staining*

The 5μm sections mentioned above were also stained with Cresyl Fast Violet (CFV) and Luxol Fast Blue staining (LFB) for further anatomical confirmation. The sections were heated and rehydrated according to the protocol metioned in the previous section in order to melt the paraffin wax. Following this, the sections were rinsed in 95% ethanol and left in luxol fast blue solution overnight at room temperature (this can also be done at 60°C for 3 hours). The stained sections were then washed in 95% ethanol and then in distilled water. The stain was then differentiated in lithium carbonate solution for 10-30 seconds, which also removes excess LFB staining. The differentiation was then continued in 70% ethanol. At this point, the grey and white matter are clearly distinguishable and the nuclei will be decolourised. If this is not the case, the differentiation is repeated with lithium carbonate solution and 70% ethanol. When the staining has reached optimal colour, the sections were stained in 0.1% cresyl fast violet in 1% acetic acid for 10-15 minutes, washed in distilled water and dehydrated using an ethanol series (70%, 95% and 100% x2) and finally washed in histoclear. Following this they were mounted under coverslip glass with DPX. Following this protocol, the myelin will be stained in blue with variation in the staining intensity, and the nuclei and nissl substances will stain in purple. Images are available in chapter 3

The 5μm sections mentioned above were also stained with Cresyl Fast Violet (CFV) and Luxol Fast Blue staining (LFB) for further anatomical confirmation. The sections were heated and rehydrated according to the protocol metioned in the previous section in order to melt the paraffin wax. Following this, the sections were rinsed in 95% ethanol and left in luxol fast blue solution overnight at room temperature (this can also be done at 60°C for 3 hours). The stained sections were then washed in 95% ethanol and then in distilled water. The stain was then differentiated in lithium carbonate solution for 10-30 seconds, which also removes excess LFB staining. The differentiation was then continued in 70% ethanol. At this point, the grey and white matter are clearly distinguishable and the nuclei will be decolourised. If this is not the case, the differentiation is repeated with lithium carbonate solution and 70% ethanol. When the staining has reached optimal colour, the sections were stained in 0.1% cresyl fast violet in 1% acetic acid for 10-15 minutes, washed in distilled water and dehydrated using an ethanol series (70%, 95% and 100% x2) and finally washed in histoclear. Following this they were mounted under coverslip glass with DPX. Following this protocol, the myelin will be stained in blue with variation in the staining intensity, and the nuclei and nissl substances will stain in purple. Images are available in chapter 3.

2.2.6 *Immunofluorescent labelling of mouse brain tissue*

Immunohistochemistry was performed using a method modified from previous protocols (Grünewald et al., 2014). Briefly, paraffin-fixed tissue sections were left at 37°C and rehydrated through histoclear and ethanol and washed with distilled water as mentioned for the H&E staining in section 2.2.4. Antigen retrieval was then performed for 40 minutes at pressure and at a high temperature in 10mM sodium citrate buffer with 0.05% Tween-20 (pH6). Antigen retrieval was extended with emersion in 1.5M HCl for another 40 minutes. The sections were rinsed with distilled water and incubated in 10% normal donkey serum and normal goat serum (NGS/NDS, Sigma). A combination of both was used since the secondary antibodies used were produced from both these species. The incubation lasts 1 hour and acts to block any non-specific targets which could react with the host species of the secondary antibody. The sections were also incubated with avidin and biotin respectively for 15 minutes each. Sections were subjected to primary antibodies Tom20 (Santa Cruz), CIdU (BD Biosciences) and IdU (Novusbio) (table 2.7) over night at 4°C, following by incubation with

fluorescently conjugated secondary antibodies (Life Technologies) and biotin for 2 hours at room temperature. Following this, streptavidin-546 was added for 2 hours, and then Hoechst (Life Technologies) for 20 minutes. The section were mounted in ProLong Gold (Invitrogen). Sections were also washed with TBST between each step and stored in -20°C until imaged. Images were captured using Nikon A1R point scanning confocal microscope.

Primary	Ig Subtype	Dilution	Secondary	Dilution	Streptavidin	Dilution	Fluorescence wavelength
Tom20	Rabbit IgG	1:400	Alexa Goat anti Rabbit	1:200	-	-	488
CldU	Rat IgG2a	1:200	Alexa Donkey anti Rat-	1:100	-	-	647
IdU	Mouse	1:100	Alexa Goat anti IgG1	1:200	Biotin-546	1:100	546

Table 2.7 Antibodies used for Immunofluorescence of mouse brain tissue, along with their species, isotype and dilution. For suppliers, refer to materials section 2.1.4.

2.2.7 *Analysis of thymidine analogue labelling*

Purkinje cells from the cerebellum, dopaminergic neurons from substantia nigra, pyramidal cells from the frontal cortex (layers 3 or 4) and CA1/CA2 regions of hippocampus were analysed to keep variability between different neurons in the same region to a minimum. Identification of specific neurons within these regions are mentioned in the chapter (section 3.3.3). The images were analysed using IMARIS (Bitplane) by creating a mitochondrial surface based on the Tom20 staining (figure 2.1). Initially the volume, area, intensity and number of voxels were the parameters analysed. These surfaces were masked on to the IdU and CldU channels to identify incorporation into the mtDNA. This was done individually for each cell. All of these channels were background corrected using the intensity values from a no primary control. Surfaces were created for both IdU and CldU. Once the surfaces are produced, IMARIS measures the surfaces and produces values for various parameters. The total sum of all of these values for an individual cell is calculated and expressed as a percentage of the total sum of values of the Tom20 channel of that cell. This provided a

percentage per cell of total mitochondria that have incorporated IdU and/or CldU into their mtDNA.
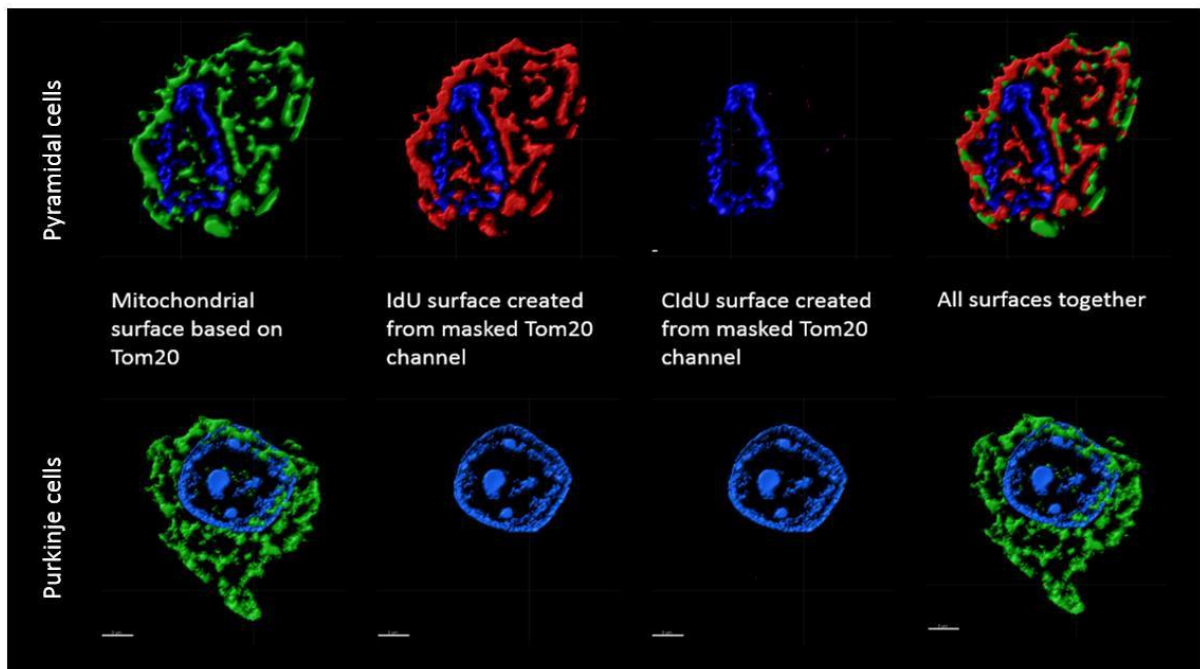
Figure 2.1 IdU and CldU channel surfaces created from masked mitochondrial surface based on Tom20 staining within individual cells. Scale bar represents 3µm.

2.3   Mammalian Cell culture

2.3.1   *HeLa cells*

HeLa cells were cultured in a T75 vented flasks in Dulbecco's Modified Eagle Medium (DMEM) media with the addition of 10% FBS, 2 mM L-glutamine, 1 mM Sodium Pyruvate, 50µg/ml uridine and 50µg/ml penicillin/streptomycin. The cells were placed in incubator at 37°C and with 5% CO_2 until they reached a confluency of 70% at which point they were passaged.

2.3.2   *HeLa cell passaging and freezing down*

The media from the HeLa cells was aspirated and the cells washed with Phosphate buffered saline (PBS) to remove dead cells and any excess media. Following this, 5ml of Trypl-E Express was added to the cells to disassociate the cells from the growing surface of the T75 flask. The

flask was then returned to the incubator at 37°C and 5% CO_2 for 3 minutes. The activity of Trypl-E Express was then quenched using 3ml of fresh media containing fetal bovine serum (FBS). This is because Trypl-E Express is a serine protease which allows it to break the matrix that adheres the cells to the flask and FBS contains serine protease inhibitors which inhibit Trypl-E Express from further activity which could lead to apoptosis of the cell. The cell and media suspension was then moved into a universal and centrifuged at 1200RPM for 4 minutes. The supernatant was then removed and the cells were re-suspended in 1ml of media. The cells were seeded into a new T75 flask at a total seeding density of $1x10^6$ per dish.

Cells were frozen down using freezing media containing FBS and 10% Dimethyl Sulfoxide (DMSO). A volume of 1ml of media containing $1x10^6$ cells were added to each cryotube to be frozen down. The cryotubes were then placed in a Mr Frosty Freezing container overnight in -80°C to freeze the cells in stages protecting their viability. Following this, the cryotubes are moved into a liquid nitrogen dewar for long term storage.

2.3.3 *Induced pluripotent stem cells*

All the cell lines used were a kind gift from Dr Oliver Russell (Wellcome centre for mitochondrial research, Newcastle University). Fibroblasts were obtained from a patient with Pearson's syndrome who had an mtDNA deletion of around 6kb (nt7777:nt13794). These were reprogrammed into induced Pluripotent Stem Cells (iPSC) according to the protocol using a sendai vector containing the reprogramming factors c-Myc, Sox2, Klf4 and Oct4 (Fusaki et al., 2009). These cells were used in a previously published paper (Russell et al., 2018). The reprogramming produced clones with varying levels of heteroplasmy. For this study, a high heteroplasmy clone (~40% mtDNA deletion) and a low heteroplasmy clone (>10% deletion) were used. The control cell line used was Human Dermal fibroblasts, adult (HDFa) which were reprogrammed according to the same protocol. Since these cells had no mDNA mutations, they acted as controls.

The stem cells were cultured in matrigel coated dishes at a seeding density of $1.7x10^4$ per cm^2. The high and low heteroplasmy cell lines were cultured in Nutristem media (see materials; solutions) with additional Rho-associated Kinase inhibitor (Rock inhibitor, 10μM) to aid the survival of cells as it blocks apoptosis and Geneticin (G418, 0.1 mg/ml) for antibiotic

selection for cells containing the construct. Nutristem media was required for the survival of the clones (Russell et al., 2018). HDFa cells were grown in mTeSR1 media (see materials; solutions) with additional Rock inhibitor (10µM) and Geneticin (G418, 0.1mg/ml). In both cases, media was replaced after 24 hours removing Rock inhibitor allowing cells to proliferate.

2.3.4 *Matrigel Preparations*

Matrigel is a gelatinous substance that provides a matrix-like structure for the stem cells to adhere to within a plastic dishes. Originally developed from a mouse sarcoma, it mimics the environment found within tissues and provides the stem cells with the support usually required from a feeder cell layer such as extracellular matrix proteins and growth factors.

Matrigel is prepared in aliquots, as per the manufacturer's instructions. This is different for each batch and the volume required for each batch is mentioned on the manufacturer's instruction for that batch. This is aliquoted out accordingly and stored at -80°C.

Before use, the 60mm dishes/6-well/12-well plates to be coated are placed in the freezer at -20°C over night to pre-chill in order for the matrigel to not set too quickly. On the day of coating, the matrigel aliquot is placed in ice alongside X-VIVO media (8ml per aliquot of matrigel). The matrigel is thawed on ice using cold X-VIVO media and added to appropriate dishes. A 60mm dish requires 3ml, a 6-well plate requires 1.5ml and a 12-well plate requires 1ml. The dishes are left at -4°C overnight for it to polymerase and produce a gel like substance to which the cells can adhere to. Before use, the matrigel dishes are checked under a light microscopy for properly formed matrix structure and any contaminations. These are then washed out with PBS before adding fresh media.

2.3.5 *Freezing down and defrosting cells*

The cells were initially collected using a centrifuge at 1200 RPM for 5 minutes. The supernatant is discarded and the cells suspended in Cryostor CS2 Freezing Media. This is moved into a cryotube with 1×10^6 cells placed in each cryotube and placed in a Mr Frosty Freezing container overnight in -80°C before being moved into a liquid nitrogen dewar.

The stem cells were defrosted by addition of 1 ml of nutristem media until thawed. This was transferred into a 20 ml universal flask and centrifuged as mentioned above. The supernatant is aspirated and the cell pellet is re-suspended in another 1ml of fresh nutristem media. This is then added into a 60 mm matrigel dish as mentioned above and left in incubator at 37°C and 5% C0$_2$. Each cryotube contains 1×10^6 cells and when defrosting, all of this is added to the dish as a number of cells are lost while defrosting.

2.3.6 *Cell culture*

Briefly, once the cells have reached 70% confluency, they were passaged and added to a 12 well plate on 13mm coverslips (VWR International). The seeding density was 150,000 cells per well for HeLa cells and 250,000 cells per well for the iPSCs. The coverslips were etched using 2M HCl (Sigma-Aldrich) for 6 hours on a magnetic stirrer, followed by 3 washes with distilled water before baking in the oven overnight. The coverslips were added to the 12 well plates using sterile tweezers and coated with PDL (0.01ng) (Sigma-Aldrich) and laminin (0.02ng) (Sigma-Aldrich) to allow cells to adhere. PDL and laminin were only used for HeLa cells; the iPSCs required matrigel (Millipore) coating.

2.3.7 *iPSC Cell Counting and passaging*

Similar to the passage of HeLa cells (section 2.3.2), iPSC cells were washed with PBS and 1ml of Trypl-E Express was added to the 60mm dish containing the cells, and left in the incubator for 3 minutes. The cells were gently pipetted up and down to disassociate the cells from matrigel before adding 1ml of fresh Nutristem media to block Trypl-E Express. The cells were centrifuged (1200RPM for 5 minutes) and the cell pellet was re-suspended in 1ml of fresh Nutristem media with Rock inhibitor and G418. The cells were then counted by adding 10µl of re-suspended pellet to 10µl of trypan blue to get a 1:1 ratio. Trypan blue is used to measure cell viability as live cells are not permeable to the dye. This was placed on to a cellometer disposable counting chamber and counted using the Cellometer Auto T4. The cells were transferred to a matrigel coated 60mm dishes at a seeding density of 5×10^5 per dish. Following 24hours, the media was replaced without rock inhibitor as described earlier. The cells are allowed to grow until 70% confluent which happened roughly after another 48 hours.

2.3.8 *Differentiating iPSC stem cells into neurons*

Neurons were generated using the transcription factor Neurogenin2 (ngn2) from human fibroblasts. Ngn2 is a transcription factor expressed in neural progenitor cells that allows differentiation into neuronal cells. The original fibroblasts mentioned in section 2.2.3 also contained an e-piggyBac vector with the neuronal specific transcription ngn2, transformed by Novartis following a published protocol (Zhang et al., 2013). This was under the control of a TET-ON system hence doxycycline was used to initiate transcription of ngn2.

Following passage, for proliferation, $2x10^6$ cells were seeded into 60mm matrigel coated dishes with Proliferation media (see materials; solutions) with additional Rock inhibitor (0.1 mg/ml) and doxycycline (1 μg/ml). Doxycycline is an antibiotic which acts to induce activation of ngn2 gene expression through the tetracycline controlled tet-on system. After 24 hours, the media was replaced without rock inhibitor as described earlier. The cells were allowed to proliferate for 72 hours after seeding into dishes.

After 72 hours, the cells were passaged as described (section 2.3.4) and seeded into 12-well plates containing 1ml of differentiation media (see materials; solutions). These wells contain 13mm round etched glass coverslips coated with Poly-D-Lysine (PDL) and laminin (see next section 2.3.8). A half media change was performed every 2 days and this involved removing 0.5ml of the media from the well and adding fresh 0.5ml of differentiation media. The cells were allowed to mature for 7 days prior to experimentation at which stage they became post-mitotic and active cell division is completely halted.

2.3.9 *Preparing coverslips and PDL/Laminin coating*

The neurons were grown on 13mm coverslips in 12-well plates. The purpose of this was to allow removal of the glass coverslips for experiments to stain the cells using immunofluorescence. The coverslips were initially etched in 1M HCl and left on a shaker for 1 hour. The purpose of etching is to smoothen the surface of the coverslips for the cells to grow on. The coverslips are then washed in distilled water to remove all HCl and put in the oven for 4 hours.

The coverslips were added to the 12-well plates using sterile tweezers. 0.01ng/ml of PDL was prepared in Dulbecco's Phosphate-Buffered Saline (DPBS) and 1ml was added to each well. This was incubated at room temperature for 1 hour which aids the cells in adhering to the surface of the coverslips and wells due to their polyatomic properties. Following three washes with DPBS, 0.02ng/ml, Laminin was prepared in DPBS and 1ml was added to each well. This was left for a minimum of 30 minutes or until use at room temperature. Laminin is a protein found within the extracellular matrix and aids with adhesion of cells to surface as well as with normal cell responses such as differentiation, evading apoptosis and proliferation (Esco et al., 2001). Before use the wells and coverslips were washed again with DPBS.

2.3.10 *MtDNA extraction and cell lysis*

DNA needed to be extracted from the cells in order to check the level of heteroplasmy in the cells to maintain consistency. Cells were centrifuged at 1200 RPM for 5 minutes and the supernatant discarded. PBS was added to the pellet to wash. This was then centrifuged again and PBS aspirated out. The cell pellets were flash frozen by dipping in liquid nitrogen before moving into -80°C for storage until used.

Single cell lysis buffer (500µl; see solutions section in 2.1.5) was added to the cell pellet and the mixture was moved into 5 PCR tubes with 100µl in each tube. The lysis mix was then vortexed and placed in an ABI Gene Amp 9700 Thermal cycler. Cell lysis was performed by subjecting the samples to 2 cycles at 56°C for 60 minutes, 1 cycle at 95°C for 10 minutes and finally cooled to 4°C until required.

Real-time PCR assay

Since the heteroplasmy in iPSC cells can vary with passage number, the heteroplasmy was confirmed with each passage utilising an established real time PCR assay (He et al., 2002). This technique analyses the levels of MTND1 and MTND4. The deletion within this cell line (base pairs nt7777:nt13794) removes ND4 however ND1 remains intact within the mtDNA. Therefore by comparing the levels of MTND4 to MTND1 will give an estimate of the level of deletion in the cells.

Briefly, this uses the 7D1-B2M plasmid to calculate the heteroplasmy levels. This plasmid contains single copies of MTND1, MTND4, the D-Loop region and B2M, hence this is used as a control to which the cell lines are compared to. B2M is also commonly used to analyse the copy number as this is a nuclear house-keeping gene and would reveal the total number of cells. This can be compared with the MTND1 which represents each mtDNA molecule.

Theoretically since this plasmid contains single copies of MTND1 and MTND4, this would contain no deletion when the levels of each are quantified. A standard curve is produced from serial dilutions of this plasmid with each dilution analysed in triplicate alongside cell samples. From this, a trend line is produced and assessed for efficiency and a gradient of '-3.36' has the highest efficiency. The heteroplasmy levels in the cell samples are calculated using this gradient.

The reagents required for the master mix are presented in table 2.8. A volume of 15µl of master mix is added to each well of a 96-well plate. Following this, 5µl of sample DNA is added to each well except the no template control, to which 5µl of autoclaved H_2O is added. As mentioned, all samples are run in triplicate. The plates are sealed, vortexed to mix all the reagents with the sample DNA and centrifuged. Real time PCR was conducted using an ABI Step-one Plus Real Time PCR system with the following conditions; 1 cycle at 50^OC for 2 min, 1 cycle of 95^OC for 10 minutes, 40 cycles of 95^OC for 15 secs and 60^OC for 1 minute.

Reagents	Volume (µl)	Final concentration	Manufacturer
Taqman Universal PCR mastermix	10	1X	Applied Biosystems
MTND1 forward primer	0.6	10µM	Eurofins MWG
MTND1 reverse primer	0.6	10µM	Eurofins MWG
MTND4 forward primer	0.6	10µM	Eurofins MWG
MTND4 reverse primer	0.6	10µM	Eurofins MWG

MTND1 probe VIC	0.4	5μM	Life Technologies
MTND4 probe FAM	0.4	5μM	Life Technologies
Autoclaved dH$_2$0	1.8	-	
Sample DNA	5	-	

Table 2.8 Reagents and DNA used for each sample to run the real time PCR. The manufacturers are also listed.

2.3.11 *Preparation of IdU and CldU*

All the methodology with preparing CldU and IdU in solution, and details of the cell lines used are all provided in section 2.3

CldU and IdU were purchased as powders (Sigma Aldrich). CldU has good solubility in distilled water and a stock solution of 1 mg/ml was prepared. IdU was more difficult to get into solution. The solubility for the powder was 2 mg/ml. A stock of 1 mg/ml was prepared in distilled water and left at 55°C in a water bath overnight. If the powder had not dissolved the following day, the solution was left in the water bath and vortexed at intervals of 20 minutes until all particles had completely dissolved. Other steps, which have been previously shown to facilitate dissolution, included the addition of 100 μl of 2 M NaOH (drop wise) until dissolved and balanced to pH 7, however this was not required for this study.

2.3.12 *Cell fixation and Immunofluorescent labelling of Cells*

All the cell lines used were treated the same for fixation and immunofluorescent labelling. Prior to staining, the cells were washed using PBS to remove dead cells and excess media. Following this, 4% paraformaldehyde at 4°C was added to the cells at a volume of per each well in a 12-well plate. This was left to incubate at 37°C for 20 minutes. Usually this can be left at room temperature, however since the remaining wells contained cultured cells, the plate was moved into the incubator to protect the viability of these cells. Following this, the cells were washed with DPBS 3 times. The cells can be left in PBS at 4°C for up to 2 weeks before staining.

Before staining, the PBS was aspirated. The coverslips were removed from the wells using tweezers and placed on a parafilm sheet. This has an hydrophobic surface, hence any liquids added to the coverslips will remain on the coverslip. Using DPBS, 3 washes were performed after each step. Antigen retrieval was performed using 1M HCl for 30 minutes. Since all the secondary antibodies in this case are raised in goat, the coverslips are blocked with 10% normal goat serum (NGS) for 1 hour. The primary antibodies were prepared in TBS and 10% NGS. A list of all the primary and secondary antibodies used for immunofluorescence in cells are mentioned in table 2.9. Incubations with the antibodies were performed overnight at 4°C. The following day, secondary antibodies were prepared again in TBS and 10% NGS, and incubated with the cells for 1 hour at room temperature. The sections were then labelled with Hoechst at 2.5µg/ml for 20 minutes before the coverslips were fixed with Prolong gold on to a glass slide and stored in -20°C until imaged. The coverslips were then imaged on the Nikon A1R confocal microscope and imaged at 40x magnification.

Primary	Supplier	Ig Subtype	Dilution	Secondary	Supplier	Dilution
Tom20	Santa Cruz	Rabbit	1:400	Goat anti Rabbit Alexa Fluro-488	Life Technologies	1:200
IdU	Novus biologicals	Mouse IgG1	1:100	Goat anti mouse IgG1 Alexa Fluro -546	Life Technologies	1:200
B-Tubulin	BD biosciences	Mouse IgG2b	1:200	Goat anti mouse IgG2b Alexa Fluro -647	Life Technologies	1:200

Table 2.9 Antibodies used for Immunofluorescence of HeLa cells/iPSC stem cells/Differentiated Neurons, along with their species, isotype and dilution.

2.3.13 *Analysis*

Analysis of the cells following immunolabelling with IdU was conducted in a similar manner to analysis carried out on mouse brain tissue in section 2.2.6. Briefly, IMARIS (Bitplane) was used to create surfaces based on the mitochondrial marker (tom20) and was done individually for each cell. This was then masked on to the IdU channel and a surface was created based on presence of IdU staining limited to the area of mitochondrial marker in the cell. This would identify the levels of IdU within the mitochondria for each cell. All of these channels were background corrected using the channel intensity values from a no primary control.

Chapter 3 : Understanding the possible link between mtDNA replication and mtDNA deletion load in the mouse brain

3.1 Introduction

3.1.1 *Variations in mtDNA deletion load between neuronal subtypes*

Neurons are particularly susceptible to ΔmtDNA (section 1.6.5). An increase in COX-deficiency with ageing is observed particularly in comparison to other post-mitotic cells such as muscle (Cottrell et al., 2001, Kraytsberg et al., 2006b). A study compared levels of the 'common' 4977bp deletion in different tissues and demonstrated the highest levels in the basal ganglia of the brain with a value of 2.9% which decreased to 0.00019% in muscle, with even lower levels detected in heart (Meissner et al., 2008). This study also found that in older individuals, compared to adolescent individuals, the deletion level increased by 3 fold. A suggested reason for the higher level of ΔmtDNA within neurons could be due to their complexity and function resulting in a high-energy demand, thereby increasing their dependence on mitochondria to produce ATP through OXPHOS activity. This high requirement for oxygen within neurons could also result in a higher level of oxidative stress, which has the potential to induce mtDNA damage. Damaged mtDNA could result in OXPHOS function decline which again adds to the increased oxidative stress creating a vicious cycle of mtDNA damage and oxidative stress (Circu and Aw, 2010, Linnane et al., 1989).

Even though neurons generally contain the highest ΔmtDNA level, variations between neuronal regions have been observed. Table 3.1 and 3.2 presents a literature review of studies that have assessed the levels of ΔmtDNA in different brain regions and the changes that occur in age and disease models. Although variations exist, the level of ΔmtDNA is generally the highest in the SN and the lowest in the cerebellum. This differential level of ΔmtDNA could possibly be due to variations in mitochondrial enzyme activity based on specific cellular requirements, mitochondrial membrane potential and PGC-1α expression all suggesting a varied dependence on the OXPHOS system (Pickrell et al., 2011). These variations could also potentially be the result of variation in mtDNA turnover, replication or repair, as they have been suggested to be involved in ΔmtDNA formation.

Although many previous investigations used homogenate tissue, studies at a single neuron level have also demonstrated similar results, with the SN presenting the highest level of ΔmtDNA when compared to the putamen and the frontal cortex (Bender et al., 2008) or cortex and cerebellum (Dölle et al., 2016). The ΔmtDNA load within the SN, compared to other regions, is further elevated with ageing and Parkinson's disease (Bender et al., 2006c, Kraytsberg et al., 2006b). These two studies also discovered that the total number of deleted mtDNA molecules can exceed more than 50% of total mtDNA within SN neurons, and suggested these could be causative of respiratory chain deficiency, possibly effecting neuronal survival leading to neurodegeneration (Bender et al., 2006c, Kraytsberg et al., 2006b).

Study/ Citation	Genotype	Age	Brain region and deletion information				Method of deletion analysis
(Brossas et al., 1994)	WT	2 weeks – 25 months (n=7)	Homogenate brain	Three specific ΔmtDNA with deletion sizes of 3726bp, 3867bp and 4236 were only noticed in aged mice.			Nested PCR
(Filburn et al., 1996)	WT	6 months – 22-25 months (n=7)	Homogenate Region	6 months	22-23 months	24-25 months	Competitive PCR – used to detect 4.8kb
			Striatum	6.0± 6.8%	111.5± 4.9%	121.2± 6.4%	values based on 4.8kb deletion/10^6 total genome
			Cerebral cortex	8.0± 1.5%	53.0± 1.8%	-	
			Hippocampus	3.2± 1.0%	30.0± 1.6%	-	
			Cerebellum	5.0±	13.1±	-	

			1.5%	6.6%		
(Kasahara et al., 2006)	WT or PolgA$^{(wt/mut)}$ mice	8-68 weeks aged	Deletion not quantified – band intensity highest in hippocampus, followed by cortex and lowest in cerebellum. Deletions also increased with age in WT and PolyA$^{(mut/mut)}$ mice			Long Range PCR
(Perier et al., 2013)	WT or PolgA$^{(mut/mut)}$ mutator mice	6- to 13-month-aged	Data obtained for this thesis and presented in section 3.5.4			Homogenate brain regions Real Time PCR
(Fuke et al., 2014)	WT vs PolgA$^{(mut/mut)}$ mice vs polgA$^{(wt/mut)}$ mice	WT – 48 weeks **(n=3)**, Poly mice 24 weeks **(n=4)**		Hippocampus	Cortex	Cerebellum	short extension qPCR Deletion values normalised to WT mice in previous generation
			WT	1.50%	1%	0.5	
			PolgA$^{mut/mut}$ mutator mice	50%	70%	15%	
			PolgA$^{wt/mut}$	4%	6%	2%	

Table 3.1 Brief literature review of the levels of ΔmtDNA observed within different brain regions in mice. The studies presented include various genotypes including wildtype (WT) and PolgA$^{mut/mut}$ mice. Many of these studies also looked at the levels of deletion at various ages, hence the ages of the mice are presented in the 'Age' column. The regions and deletions column presents the specific regions examined and the levels of ΔmtDNA observed within these regions. In some cases this column is divided by genotype and or age as indicated. The final column describes the method of deletion analysis. This was important to highlight as some techniques are more sensitive than other, and could explain variations in the data.

Study	Condition	Ages	Regions and deletions			Method
(Soong et al., 1992)	Young and aged individuals	Range of 39-82 years **(n=12)**	Region	39 years	82 years	Dilution-PCR to detect mtDNA[4977] Numbers represent the percentage of mtDNA[4977] to total mtDNA in each area
			SN	0.0030	0.46	
			Putamen	0.0010	0.19	
			Thalamus	0.0008	0.0085	
			Cerebellum	0.0001	0.0013	
(Corral-Debrinski et al., 1992a)	Healthy ageing	Range of 24-94 years **(n=6)**	Region	Young	Ageing	Histology stain to identify area Dilution-PCR to detect mtDNA[4977] Numbers represent proportion to total mtDNA
			Striatum	0.0016	0.12	
			Temporal cortex	0.000067	0.034	
			Frontal cortex	0.00063	0.0028	
			Occipital cortex	0.00013	0.0082	
			Parietal Cortex	0.00021	0.003	
			Cerebellum	0.000024	0.000067	
(Gu et al., 2002)	Parkinson's disease	PD - 79.4±3.6 years (n=5)	Region		total ΔmtDNA	homogenate brain Long range PCR,
			SN	12		

			Hippocampus	9		Numbers represent the total number of fragments observed via ethidium bromide staining
			Cerebellum	8		
			Cortex	7		
(Meissner et al., 2008)	Young and aged individuals	0.2-102 years	Regions	0-20 years	60-102 years	detected mtDNA[4977] Full table with individual values in paper
			SN	0.001021%	1.136334%	
			Putamen	0.001225%	0.446191%	
			Caudate nucleus	0.001722%	0.688275%	
			Frontal lobe	0.000851%	0.091737%	
			Cerebellum	0%	0.004938%	
(Dölle et al., 2016)	Parkinson's disease Patients and healthy ageing	PD - (69-95 years) (n=10),	Region	Control	PD	individual neurons Real-time PCR This is a visual estimate
			SN	32%	40%	
			Cortex	15%	15%	
			Cerebellum	13%	13%	

Table 3.2 Brief literature review of the levels of ΔmtDNA observed within different brain regions in humans. The column indicated as 'condition' presents the cases used such as healthy ageing (highlighted in grey) or Parkinson's disease. Many of these studies also looked at the levels of deletion at varying ages (the ages of the individuals

3.1.2 *Thymidine analogue*

Thymidine is one of the pyrimidine base pairs of DNA. Analogues of thymidine have been used to label and study nuclear DNA replication for many years (Taylor et al., 1957, Hendee et al., 1963), and it is one of the most commonly used techniques to do this (Van Laar et al., 2018). This technique has also been adapted to specifically study mitochondrial DNA (mtDNA) replication (Van Laar et al., 2018, Phillips et al., 2017). There are a number of analogues that are structurally similar to thymidine (figure 4.1); however, the methyl group on the fifth position of the pyrimidine ring is replaced in each case. Initial studies used radiolabelled isotopes such as tritium (H^3) to label thymidine, which was detected using autoradiography (Taylor et al., 1957). Later on, other analogues were developed based on the same model. One of the first employed was 5-bromo-2'-deoxyuridine (BrdU), followed by 5-chloro-2'-deoxyuridine (CldU), 5-Iodo-2'-deoxyuridine (IdU) and more recently 5-Ethynyl-2'-deoxyuridine (EdU) (Davis and Clayton, 1996, Lentz et al., 2010, Phillips et al., 2017). A further benefit of using a thymidine analogue to study DNA replication is that since uracil, rather than thymidine is used by RNA, RNA will not be labelled thus reducing false positive incorporation.

These analogues can be incorporated into the genome during replication substituting in for thymidine. Since these bases are halogenated in replacement for the methyl group, they can then be detected using specific antibodies (figure 3.1), targeted to each thymidine analogue. These primary antibodies were initially developed by immunising mice with these analogues, isolating the spleen from these animals and obtaining hybrid clones which were tested using ELISA assays for specificity to the thymidine analogues (Gratzner, 1982). These primary antibodies are a specific isotype that can be recognized by a secondary counterpart labelled with a fluorophore, which can be visualised using a specific wavelength where the fluorescence of the secondary antibody can then be observed with a microscope. This method has been used in many instances (Van Laar et al., 2018, Harris et al., 2018, Phillips et al., 2017, Davis and Clayton, 1996, Flory Jr and Vinograd, 1973), including *in-vivo* work on human cancer

patients (Eriksson et al., 1998). These patients received BrdU as part of their treatment, as high concentrations of BrdU can increase cell susceptibility to ionizing radiation making it beneficial when used in combination with chemotherapy or radiation treatment (Levkoff et al., 2008, Djordjevic and Szybalski, 1960, Prados et al., 2004). After post-mortem, their brains were used to investigate and identify adult neurogenesis in the dentate gyrus which had been previously reported in primates and rodents (Gould et al., 1998, Kuhn et al., 1996).
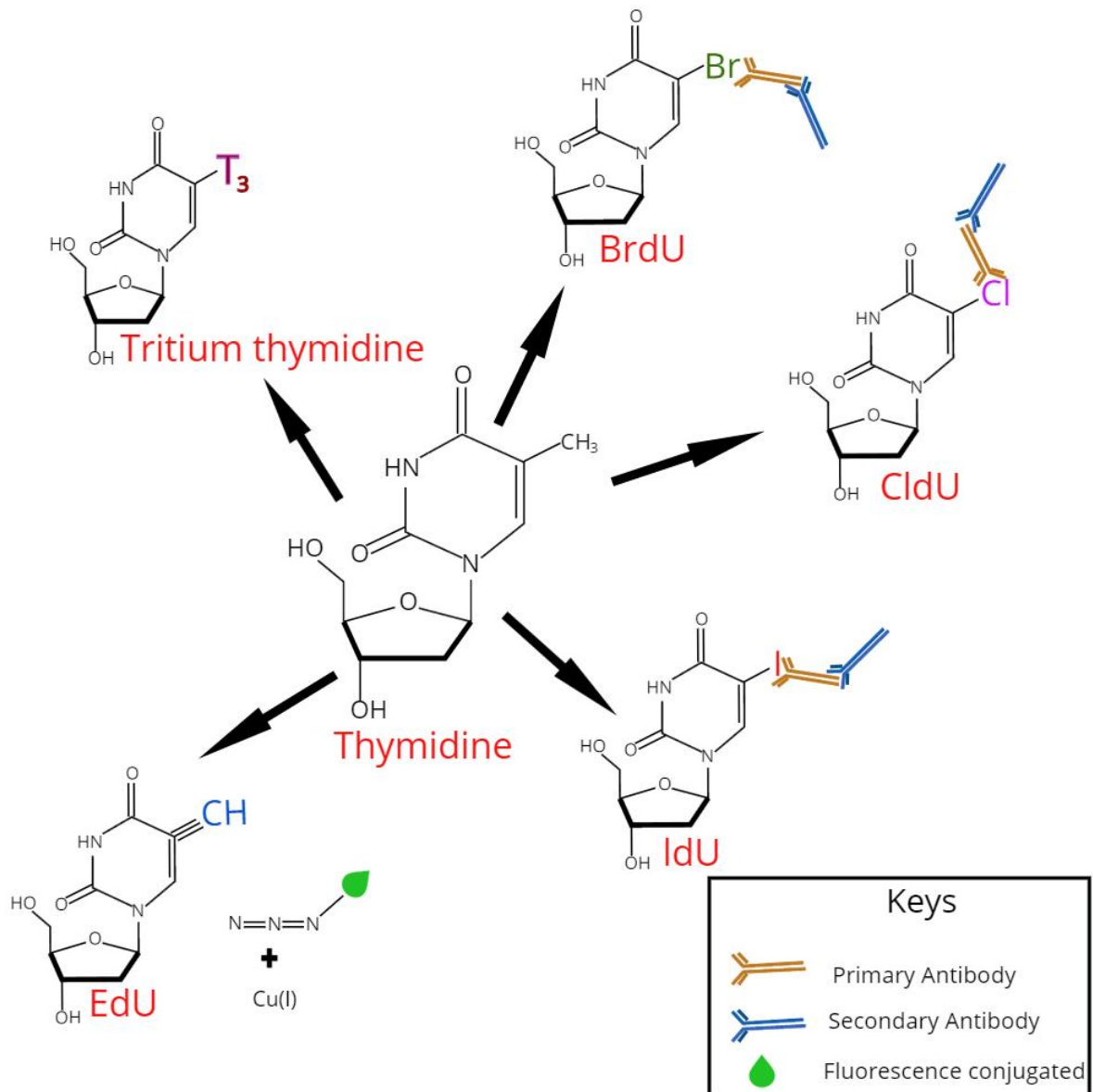
Figure 3.1 Thymidine analogues used for labelling DNA replication. Tritium thymidine uses autoradiography for detection. 5-bromo-2'-deoxyuridine (BrdU), 5-chloro-2'-deoxyuridine (CldU), 5-Iodo-2'-deoxyuridine (IdU) use antibodies that bind to the specific group. 5-Ethynyl-2'-deoxyuridine (EdU) utilises click chemistry where a fluorescence conjugated azide group forms a covalent bond with the alkyne group in a reaction catalysed by copper.

One of the limitations of this method is that these analogues can be incorporated during all processes involving DNA synthesis, including DNA repair (Taupin, 2007). Another limitation to take into consideration is that the thymidine analogue also fails to label around half of dividing cells for unknown reasons (Kee et al., 2002). This could be due to a low concentration of the analogue which can partially be avoided by increasing the concentration; however these analogues can be toxic at high doses (Sekerková et al., 2004). This is because the thymidine analogue can be interpreted as a large level of DNA damage in the cell by various repair pathways (repair pathways of the mtDNA discussed in section 1.5.2).

Although the specific mechanism of toxicity by thymidine analogues remains unclear, a large amount of data is available on the toxicity caused by other thymidine analogues, such as azidothymidine (AZT) and stavudine (d4T) which are used in antiretroviral treatments of HIV/AIDS patients. These thymidine analogues exhibit a dose and time-dependent increase in mitochondrial dysfunction (including impaired membrane potential), mtDNA damage, ROS and autophagy (Kline et al., 2009, Stankov et al., 2013). For analogues such as AZT, the 3' 'OH' group is replaced by an ammonia group hence when this is incorporated into the DNA during synthesis, the chain extension is terminated due to the lack of an 'OH' group. This then inhibits the DNA polymerase and leads to mtDNA depletion (Scruggs and Naylor, 2008). Due to this reason, these analogues not used to study DNA replication.

3.1.3 *Significance of this study*

As mentioned in the introduction the formation of ΔmtDNA could be linked to mtDNA replication. Therefore, to further understand the impact of replication on deletion formation, it is important to discern its characteristics, specifically the level of replication in different neuronal populations. This may then also shed light on the reasons why different regions of the brain show varied levels of deletions, in both mice and humans (Perier et al., 2013, Dölle et al., 2016, Gu et al., 2002). This difference could prove beneficial in understanding the involvement of replication in deletion formation by looking at associations between the levels of replication and corresponding levels of ΔmtDNA within these regions. The primary objective of this study was to measure replication levels to see whether alterations in this process could be linked to the accumulation of the mtDNA deletions observed with age and disease. This

will be useful to develop hypotheses that may support or oppose current deletion formation theories. The mtDNA replication levels were also deduced in wildtype and *PolgA^{mut/mut}* mice to shed further light on how this correlates with defective replication or ageing. To deduce replication levels thymidine analogue labelling was used.

3.2   Aim and objectives

3.2.1   *Aims*

The aim of this chapter was to assess mtDNA replication levels in different regions of the mouse brain.

3.2.2   *Objectives*

The following objectives were fulfilled in this study;

- To compare mtDNA replication levels between different brain regions
- To compare mtDNA replication levels in neurons between young and aged mice
- To compare mtDNA replication levels in neurons between WT and *PolgA^{mut/mut}* mutator mice
- To compare the levels of mtDNA replication and ΔmtDNA in various neuronal types

3.3   Methods

3.3.1   *Double thymidine analogue labelling in vivo*

The methods utilised for this study are detailed extensively in section 2.2.2. Briefly, these mice were injected with 50mg/kg of CldU twice a day for 4 days at 10am and 6pm. On day 4, they were injected with CldU as normal at 10am, however at 6pm; they were injected with 50mg/kg of IdU and sacrificed after 14-16 hours (Table 2.6). Using this approach mtDNA which had replicated in the past 4.5 days would be labelled with CldU and the last 15 hours with IdU. The time-frame was optimised for another study, and as positive staining was observed, this was continued (Stamp, 2016). Details of the mice used in this study are provided in table 3.3.

	Sex	Genotype	Age when culled (months)	Mean age (months)
WT Young	F	Wild type	3.9	3.7
	F	Wild type	3.9	
	F	Wild type	3.9	
	F	Wild type	3.2	
POLG Young	F	PolgA$^{mut/mut}$	4	3.3
	F	PolgA$^{mut/mut}$	2.4	
	F	PolgA$^{mut/mut}$	3.3	
	F	PolgA$^{mut/mut}$	3.4	
WT Aged	F	Wild type	12.6	11.4
	F	Wild type	12.6	
	F	Wild type	10.9	
	F	Wild type	10.1	
	F	Wild type	10.9	
POLG Aged	F	PolgA$^{mut/mut}$	11	10.9
	F	PolgA$^{mut/mut}$	10.1	
	F	PolgA$^{mut/mut}$	12.1	
	F	PolgA$^{mut/mut}$	10.3	

Table 3.3 Mice used in this study. The table presents the gender, genotype and the ages of the mice used. The mean age for each group is also calculated. The highlighted grey cells represent littermates in each group.

3.3.2 *Immunohistochemistry to identify CldU/IdU labelling*

Details of all antibodies used in this chapter are provided in section 2.1.4. Serial sections were stained with anti-BrdU (to detect CldU), anti-IdU (discussed in section 3.4.1) and Tom20

antibodies to calculate the levels of replication in these brain regions. For analysis, four regions of the brain were selected, and within these, specific neurons were chosen. This was conducted to reduce variability between different neurons of the same region. Purkinje cells from the cerebellum, pyramidal cells from the cortex (layer 3/4) and hippocampus, and dopaminergic neurons from the SN were selected. Selection of these cell types was due to their abundance in these regions. The neurons per images were selected at random. These regions were chosen based on the differential levels of ∆mtDNA and the literature available on ∆mtDNA of these regions (see table 3.1 and 3.2).

3.3.3 *Immunohistochemistry to identify specific cells*

Immunohistochemistry was performed according to section 2.2.5. Initially the sections were stained using Tom20 as a mitochondrial marker, alongside CamKII which is a marker for pyramidal cells (hippocampus and cortex) and tyrosine hydroxylase (TH), a marker for dopaminergic neurons (SN). These neurons were chosen specifically due to the amount of literature available on them and their specificity within a region. Although the neurons of the cerebellum and hippocampus are easily identified, these neuronal markers were required to correctly identify the neurons of the SN and pyramidal cortical neurons. These markers were applied to sections to confirm the presence of the regions of interest, serial sections were then used for further CldU/IdU detection.

3.3.4 *Microscopy and analysis*

Images were initially obtained using the Axioimager M1 (Zeiss). Wide field fluorescent imaging did not provide adequate resolution to allow in depth study of CldU/IdU incorporation into mitochondria, therefore the Nikon A1R confocal system was used. To further analyse the images, various parameters were trialled in IMARIS and Image J (Fiji) (appendix 8.4). All of the parameters produced similar results which suggested the same pattern of thymidine analogue incorporation between the different groups. Therefore, based on the manufacturer's suggestion and the 2D nature of the images, 'number of voxels' was the parameter analysed using IMARIS (Bitplane) for all images. The thymidine analogue staining was expressed as a percentage of the total mitochondrial mass values in order to compensate for the differential cell sizes.

3.3.5 *Statistical analysis*

All statistical analysis are detailed in the appropriate sections with the results in order to explain the graphs. Briefly, due to variations between the mice, as confirmed by Kolmogorov-Smirnov testing ($p < 0.05$), one way-ANOVA was used to compare the different groups. Since the data is not normally distributed, quantile normalisation was used to account for the variation between the two replicates allowing them to be comparable (more details in appendix 8.6). The p-values obtained were then corrected using the 'false discovery rate' method. The statistical comparisons and normalisations were conducted by Dr Conor Lawless (Wellcome Centre for Mitochondrial Research).

3.4   Results

3.4.1 *Optimisation*

I) identifying an appropriate mitochondrial marker

Selection of an appropriate mitochondrial marker was crucial due to the nature of the experimental design. A mitochondrial marker was needed to normalise the levels and account for variation in cell size, to in order to more accurately assess replication levels. The different mitochondrial markers tried were Glucose-regulated protein 75 (GRP75) (Abcam), Voltage-dependent anion channel 1 (VDAC1) (Abcam), translocase of outer membrane (Tom20) (both Polyclonal rabbit and monoclonal mouse IgG2a) (Santa-Cruz). An anti-DNA (Merck Millipore) was also used to specificially mark the mtDNA. Neuronal markers were also used. All the mitochondrial antibodies and neuronal antibodies used are listed in table 3.4 which explains the use of certain combinations due to the IgG subtypes.

Mitochondrial markers	Subtype	Neuronal Markers	Subtype	mtDNA Replication	Subtype
anti-GRP75	Rabbit	anti-SMI-31	IgG1	anti-BrdU	Rat
anti-VDAC	IgG2b	anti-MAP2	Rabbit	anti-IdU	IgG1
anti-Tom20 (P)	Rabbit	anti-CamkII	IgG1		
anti-Tom20 (M)	IgG2a	anti-TH	Rabbit		
anti-DNA	IgG2a				

Table 3.4 Mitochondrial, neuronal and mtDNA replication antibodies used. This table presents all the antibodies and the subtypes used which explains the antibody cocktails trialled for this study. All suppliers are listed in section 2.14

The ideal mitochondrial marker would label all the mitochondria within the cell, have high specificity for mitochondria, produce punctate staining allowing the differentiation of individual mitochondria and have a low background allowing the use of low exposure values while imaging. The initial mitochondrial marker tried was VDAC1 alongside MAP2 (figure 3.2). MAP2 is a neuronal cytoskeleton specific marker that labels the microtubule assembly proteins (Shafit-Zagardo and Kalcheva, 1998). VDAC is protein that forms a channel through the outer mitochondrial membrane which allows small hydrophilic metabolites to pass through and the opening and closing of this channel is dependent on membrane potential (Shoshan-Barmatz et al., 2010, Yu et al., 1995). Staining for GRP75, in conjunction with SMI-31 was also trialled (figure 3.3). SMI-31 is a neuronal marker which stains for neurofilaments which contribute to the cytoskeleton of the neurons along with microtubules. GRP75 is a heat-shock precursor protein which mainly localises to the inner mitochondrial membrane. Low levels of this protein can also be found in the endoplasmic reticulum and cytoplasmic vesicles (Honrath et al., 2017, Pilzer and Fishelson, 2005). This protein has a role in the biogenesis of iron-sulphur clusters, protein translocation within mitochondria and general maintenance of the mitochondria (Ahmad et al., 2011, Shan and Cortopassi, 2016).

Both GRP75 and VDAC1 showed positive staining. VDAC1 did not give the same intensity of positively stained mitochondria as other markers. In terms of the GRP75, it was present mainly within the cell bodies with a low background. However, GRP75 has been suggested to localise

to ER and plasma membrane, hence this could skew the analysis. Following this, two Tom20 IgG subtypes were trialled and stained (figures 3.4 and 3.5). Tom20 is part of the TIM/TOM complex which is involved in translocation of proteins into the mitochondria. Tom20, as the name suggest is present within the outer membrane. This is an excellent marker due to its specificity. Of the two subtypes tried, the polyclonal rabbit performed better as the staining was more punctate.

Figure 3.6 presents the anti-DNA antibody. This was done to identify a mtDNA specific marker which would make the analysis more accurate. However, as seen in the figure, the mtDNA was not stained appropriately, due to large levels on non-specific staining. In addition to this, the nuclear DNA was also stained which would add additional steps to the analysis.

Due to specificity and co-localisation with the neuronal marker, Tom20 subtype rabbit was taken forward.
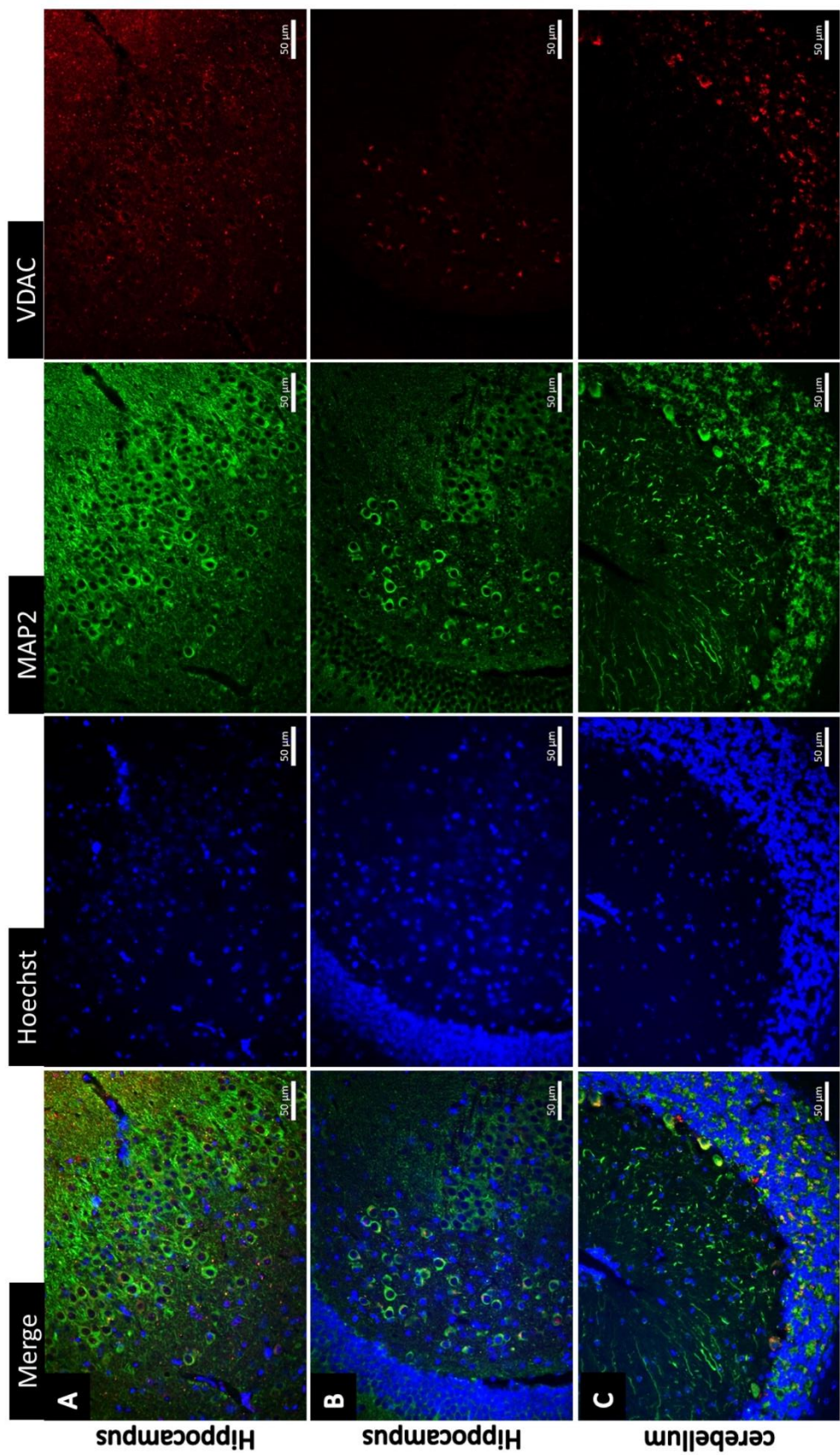
Figure 3.2 Optimisation of mitochondrial markers: VDAC - MAP2 was used to specify neurons. A and B presents regions of the hippocampus and C is the cerebellum. The mitochondrial marker is VDAC with the nucleus stained with Hoechst. The images were taken at x20 magnification. The scale bar represents 50 μm. Hoechst is present within wavelength 405 nm, MAP2 is imaged in 488 nm and VDAC in 546.
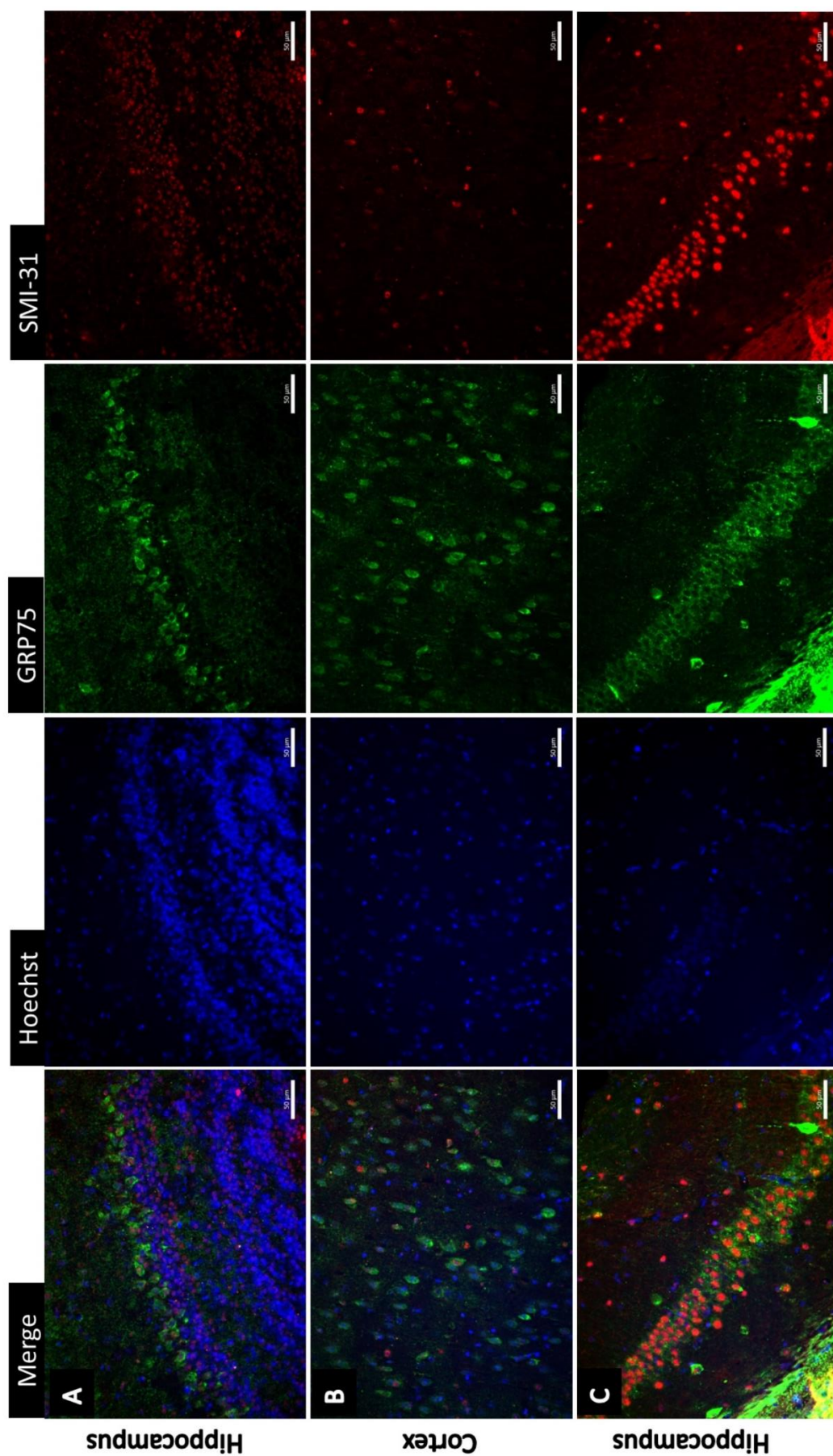
Figure 3.3 Optimisation of mitochondrial markers: GRP75 - SMI-32 is a neurofilament marker used to identify neurons. The brain region is Hippocampus in Image A, C and cortex in image B. The mitochondrial markers is GRP75 with the nucleus stained with Hoechst. The images were taken at x20 magnification. The scale bar represents 50 µm. Hoechst is present within wavelength 405 nm, GRP75 is imaged in 488 nm and SMI31 in 546.
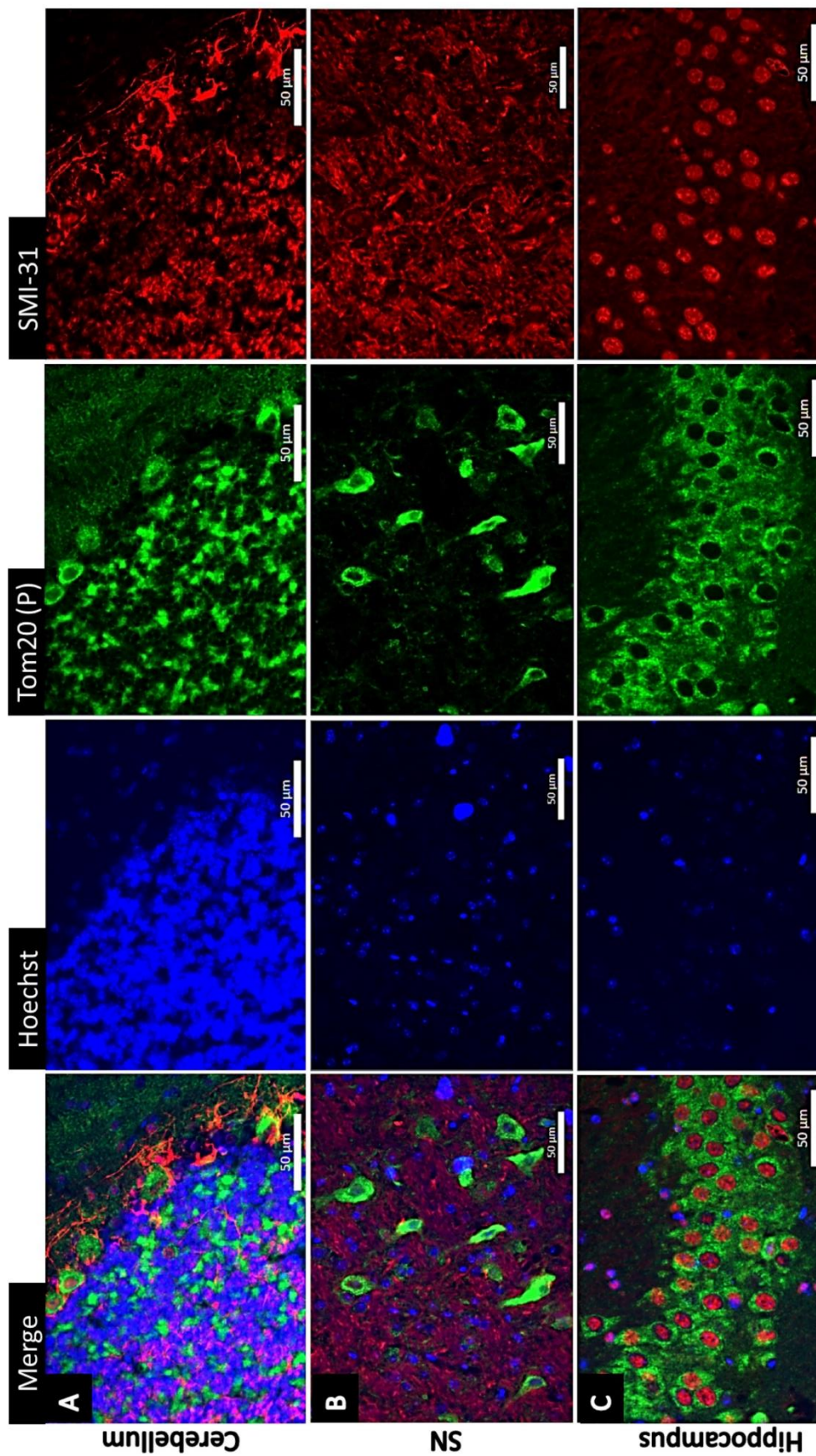
Figure 3.4 Optimisation of mitochondrial markers: TOM20 (P) - SMI-32 is a neurofilament marker used to identify neurons. The mitochondrial markers is Tom20, the P indicates polyclonal. Image A presents cerebellum, B presents the SN and C presents the hippocampus. The nucleus is stained with Hoechst. The images were taken at x40 magnification. The scale bar represents 50 µm. Hoechst is present within wavelength 405 nm, Tom20 is imaged in 488 nm and SMI31 in 546.

113
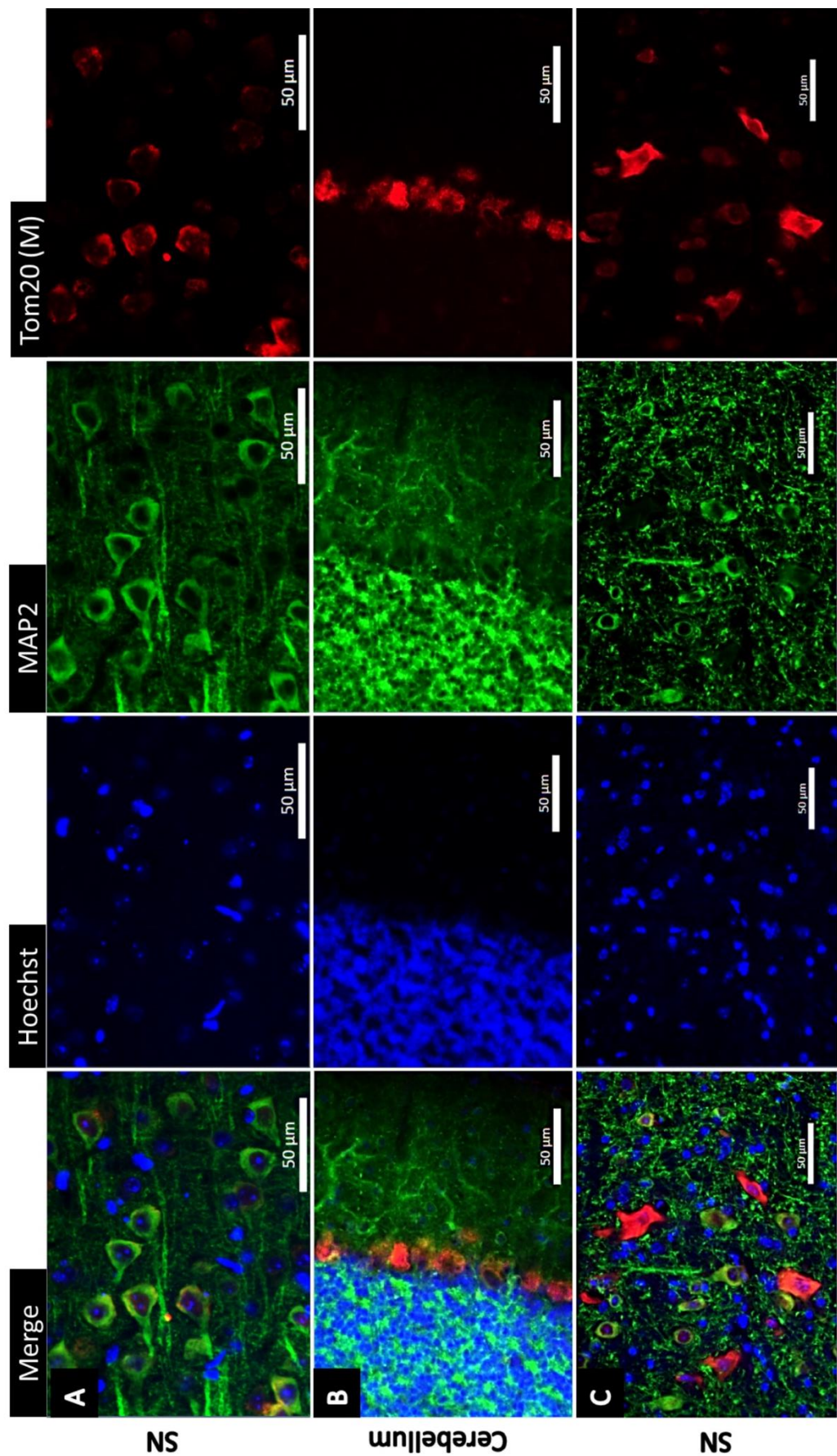
Figure 3.5 Optimisation of mitochondrial markers: TOM20 (M) – MAP2 is used to identify neurons. The mitochondrial markers is Tom20, The M indicated that this antibody is monoclonal. Image A is within the SN, B is in the cerebellum and C in the SN again.The nucleus stained with Hoechst. The images were taken at x20 magnification. The scale bar represents 50 μm. Hoechst is present within wavelength 405 nm, MAP2 is imaged in 488 nm and Tom20 in 546.
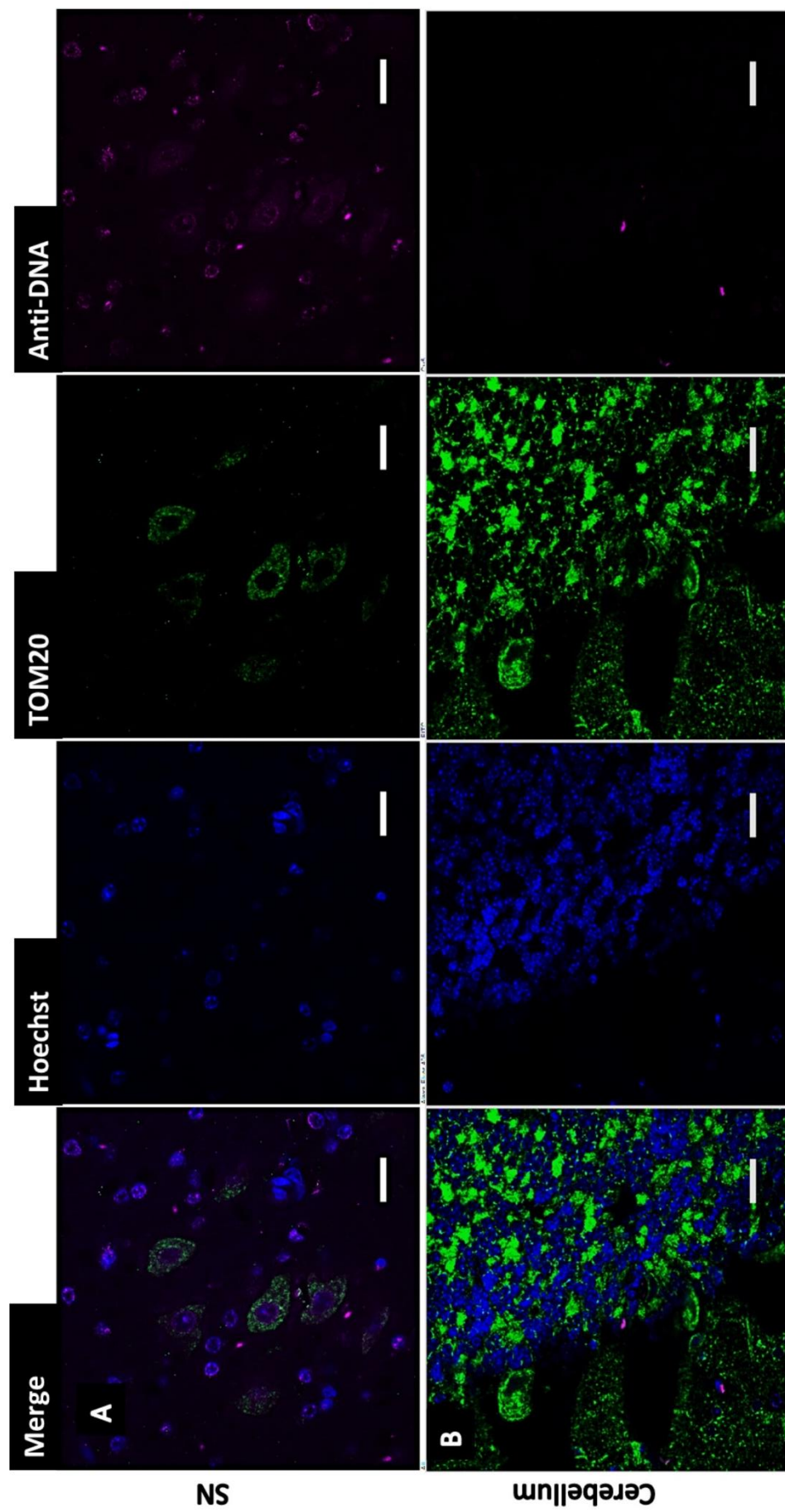
Figure 3.6 Optimisation of DNA marker: Anti-DNA antibody - Anti-DNA antibody was used in conjunction with the mitochondrial marker Tom20 (P) to highlight specifically mtDNA. The nucleus stained with Hoechst. The images were taken at x40 magnification. The scale bar represents 20 μm. Hoechst is present within wavelength 405 nm, Tom20 is imaged in 488 nm and anti-DNA antibody in 647.

115

II) Identifying specific neuronal populations

Another crucial factor was accurately identifying neuronal populations of interest within the selected brain regions. This study investigated the cerebellum, cortex, hippocampus and SN, and the major cell types in these regions are Purkinje cells, pyramidal cells (cortex and hippocampus) and dopaminergic cells, respectively. Based on their morphology and the organisation of the cerebellum, Purkinje cells could be easily and accurately identified. This is because they exist as large distinct cells within the border between the molecular and granule layers within the cerebellum (Gharravi, 2016). When labelled with Tom20 the Purkinje cells are clearly visible between the molecular and granular layer (Figure 3.7). However the pyramidal cells and dopaminergic cells required further labelling due to fewer architectural landmarks making them less easily identifiable, hence CamKII and TH were used.

CamKII is a kinase enzyme that functions to phosphorylate serine and threonine within a protein, is regulated by calcium and is involved in neurotransmitter release (He et al., 2000). CamKII is particularly abundant in the pyramidal cells of the hippocampus since it is involved in hippocampal long term potentiation which strengthens synaptic activity, important for learning and memory (Lisman et al., 2012, Wang et al., 2013). This has been used previously to target specifically the pyramidal cells of the hippocampus, and since pyramidal cells are present in the cortex, this can also be used to identify this region (Ding et al., 2013). However studies have also found that this marker is expressed in other non-pyramidal cells, but at lower levels (Jones et al., 1994, Tighilet et al., 1998). Hence, this is not a pyramidal cell specific marker per se, however due to its abundance in pyramidal cells; this can be used to label them in conjunction with anatomical landmarks.

In this study, CamKII was optimised for mouse brain tissue at dilution of 1:25 and 1:50 was tried based on the manufacturers' guidelines and previous experiments conducted on human brain in our research group (Lax, unpublished) (Figure 3.8). 1:50 dilution was chosen for all future work because both dilutions presented similar levels of staining which co-localised with Tom20. Figure 3.9 presents CamkII staining within the cerebellum, hippocampus and cortex. The cerebellum was used as a negative control since there are no pyramidal cells within this region. The images were background corrected using a no primary control and the positively

stained cerebellar section. It is important to highlight that not all cortical cells were positive for CamkII (Figure 3.9B). This is because there are other subtypes of neurons present within this area. This is another reason why structurally identifying the cells types is important. Hippocampal pyramidal cells were also robustly detected using this approach (Figure 3.9C).

To label dopaminergic neurons of the SN region, a TH antibody was used. This was previously optimised in our research group by Dr Amy Reeve and used at a dilution of 1 in 100. This antibody targets the tyrosine hydroxylase enzyme which converts the precursor tyrosine into dopamine, therefore, this is specific to dopaminergic neurons (Daubner et al., 2011). Since the anti-TH antibody has a polyclonal rabbit isotype, the monoclonal Tom20 (isotype IgG2a) was used to label the mitochondria.

The anti-TH antibody targets the tyrosine hydroxylase enzyme which converts the precursor tyrosine into dopamine, therefore, this is specific to dopaminergic neurons (Daubner et al., 2011). Since the anti-TH antibody has a polyclonal rabbit isotype, the monoclonal Tom20 (isotype IgG2a) was used to label the mitochondria. The TH population could be identified even at a low magnification using this approach (Figure 3.10A). Figure 3.10B presents positive staining within the dopaminergic neurons and Figure 3.10C presents the hippocampus, which was used as a negative control for this antibody and presents without any positive TH staining. In some sections, two sets of TH positive cells were observed. This is due to the presence of dopaminergic neurons in SN and the nearby ventral tegmental area (Margolis et al., 2006). In these cases, a mouse brain atlas was used to identify the correct population. This antibody had been previously optimised by Dr. Amy Reeve (Wellcome Centre for Mitochondrial Research) and was used at a dilution of 1:100.

The TH population could be identified at a low magnification using this approach (Figure 3.10A). Figure 3.10B presents positive staining within the dopaminergic neurons and Figure 3.10C presents the hippocampus, which was used as a negative control for the antibody and presents without any positive TH staining. In some sections, two sets of TH positive cells were observed. This is due to the presence of dopaminergic neurons in SN and the nearby ventral tegmental area (Margolis et al., 2006). In these cases, a mouse brain atlas was used to identify

the correct population. Positively stained dopaminergic and pyramidal cells are presented in figure 3.10
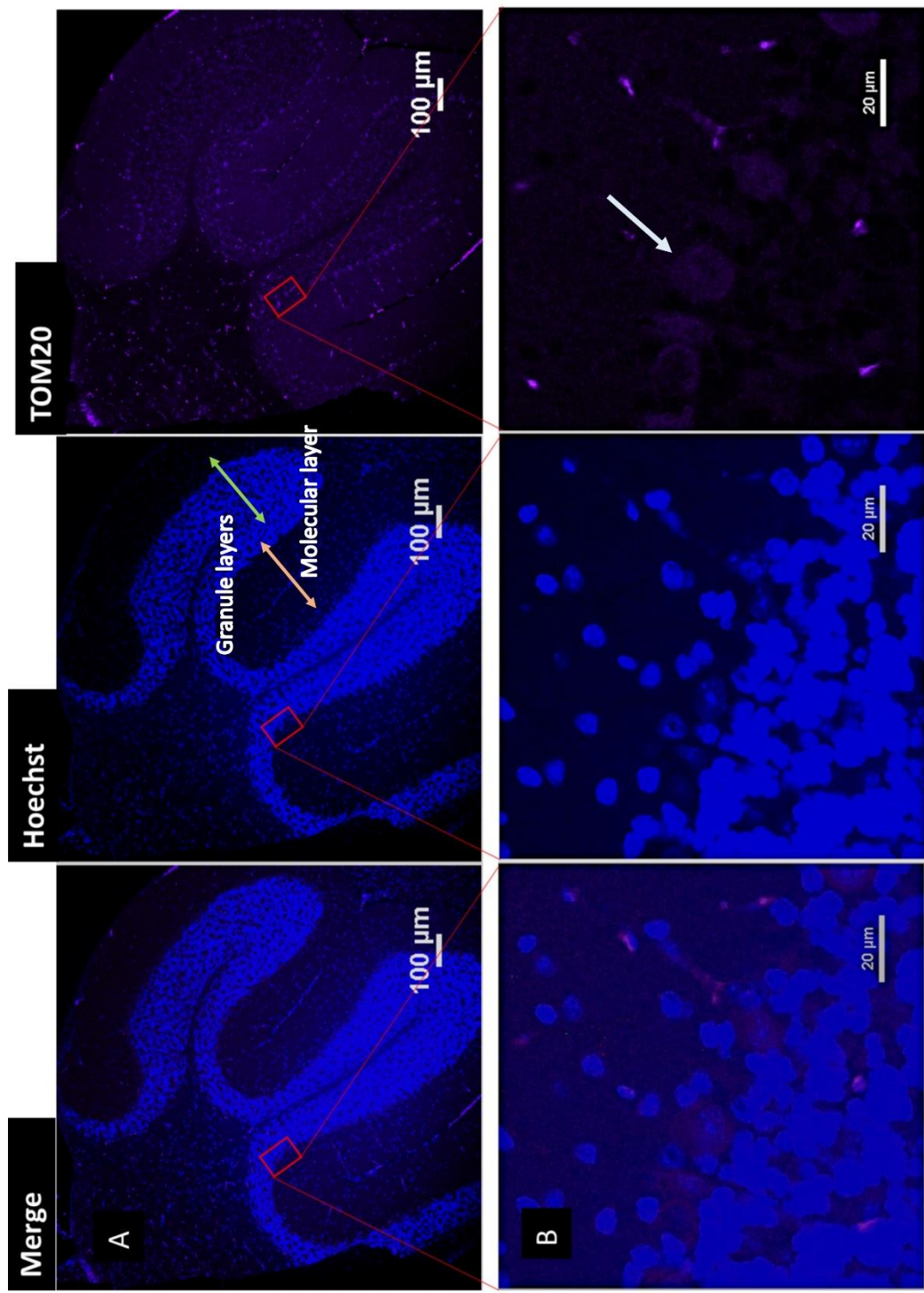
Figure 3.7 Morphological identification of cerebellum. The Purkinje cells are identified between the molecular and granular layer as highlighted in the image B by the white arrow within the Tom20 channel. The images were taken at x20 (A) and x40 (B) magnification using confocal microscopy. The scale bar represents 100 µm for image A and 20 µm for Image B. Hoechst is present within wavelength 405 nm and Tom20 in 647.

119
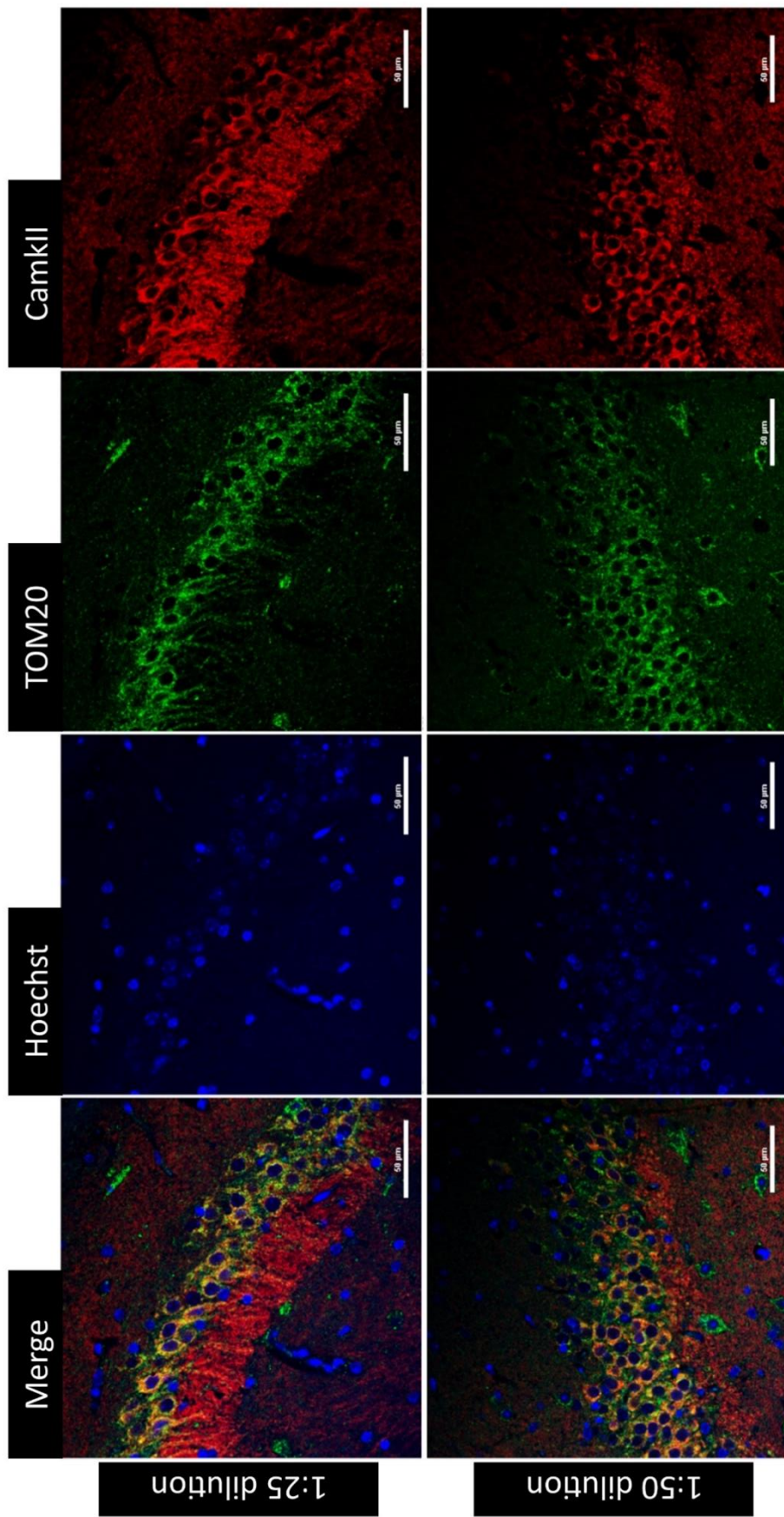
Figure 3.8 Optimisation of CamKII. This is a pyramidal cell marker and the tissue presented is the hippocampus. The dilutions tried are indicated in the Figure. The images were taken at x40 magnification using confocal microscopy. The scale bar represents 50µm. Hoechst is present within wavelength 405 nm, Tom20 in 488 and CamKII in 546.

Figure 3.9 Neuronal marker optimisation - CamKinase2 (CamKII) is a pyramidal cells marker. Image A presents cerebellum which contains Purkinje cells, and therefore was used as a negative control for CamKII antibody. Image B presents cortex and Image C presents Hippocampus, both of which are areas containing pyramidal cells and hence were stained positively with the antibody. This was used in conjunction with Tom20 as the mitochondrial marker and Hoechst is the nuclear staining. The images were taken at x40 magnification using confocal microscopy. The scale bar represents 20 μm. Hoechst is present within wavelength 405 nm, MAP2 is imaged in 488 nm and Tom20 in 546.

1
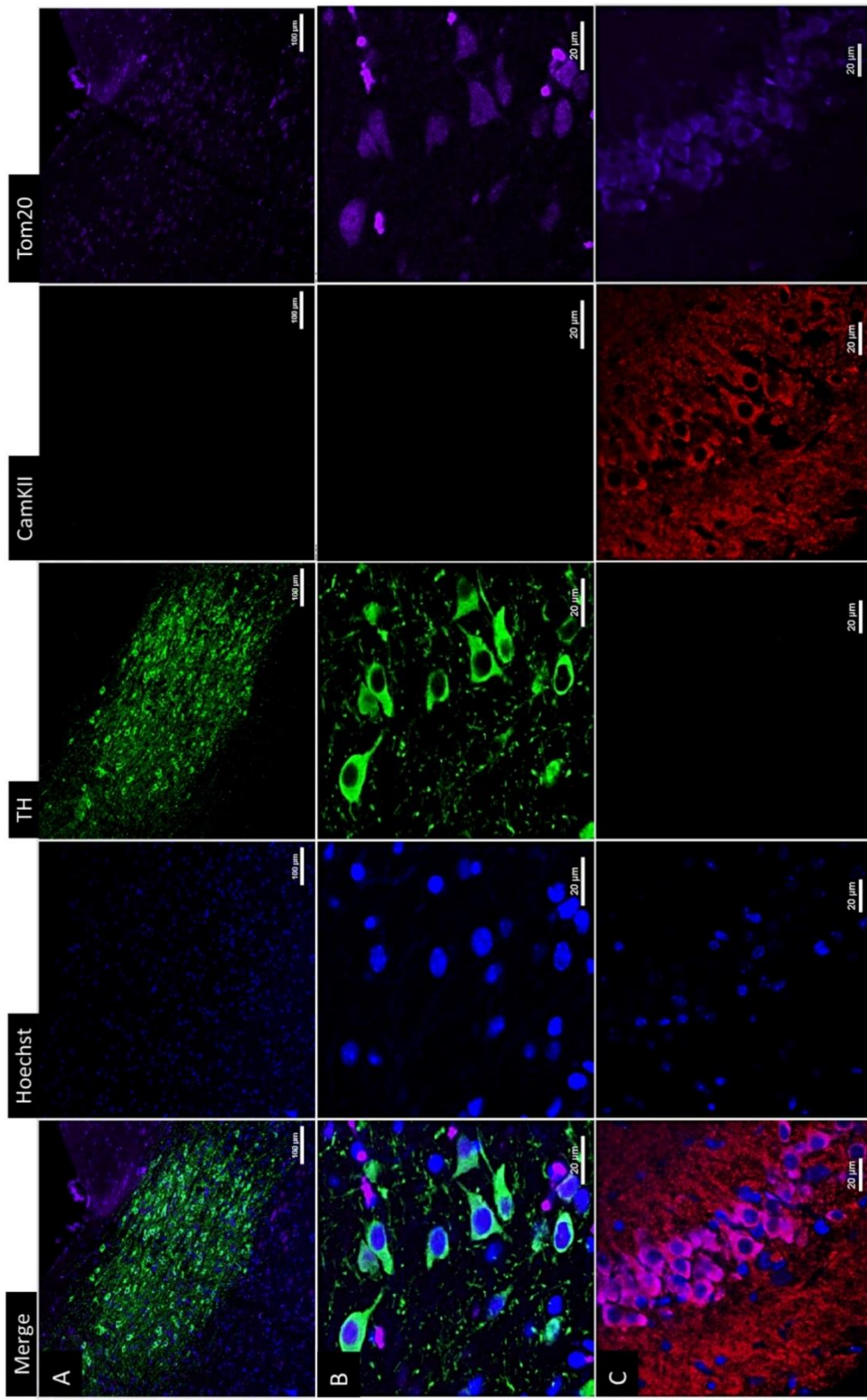
*Figure 3.10 Neuronal marker optimisation – Tyrosine hydroxylase (TH) antibody is a dopaminergic cell marker. This is used in conjunction with CamkII which is a pyramidal cells marker and Tom20 as the mitochondrial marker. Image A presents a lower magnification image to identify the TH positive population. Image B presents positive TH stained neurons. Image C presents the hippocampus as a negative control for TH. Hoechst is the nuclear staining. The images were taken at x10 for image A and x40 magnification for B and C, using confocal microscopy. The scale bar represents 100 μm for A and 20 μm for B and C. Hoechst is present within wavelength 405 nm, TH is imaged in 488 nm and camkII in 546nm and Tom20 in 647nm.*

III) CldU/IdU staining of mice brain

Following all the optimisation and validation, immunohistochemistry was conducted on all the mice from the four groups. Specific neurons were identified as described in 3.3.3 and sequential sections were histologically stained to confirm the specific regions and neurons. A representation of the CldU/IdU staining in the four regions of the brain is presented in Figure 3.11.
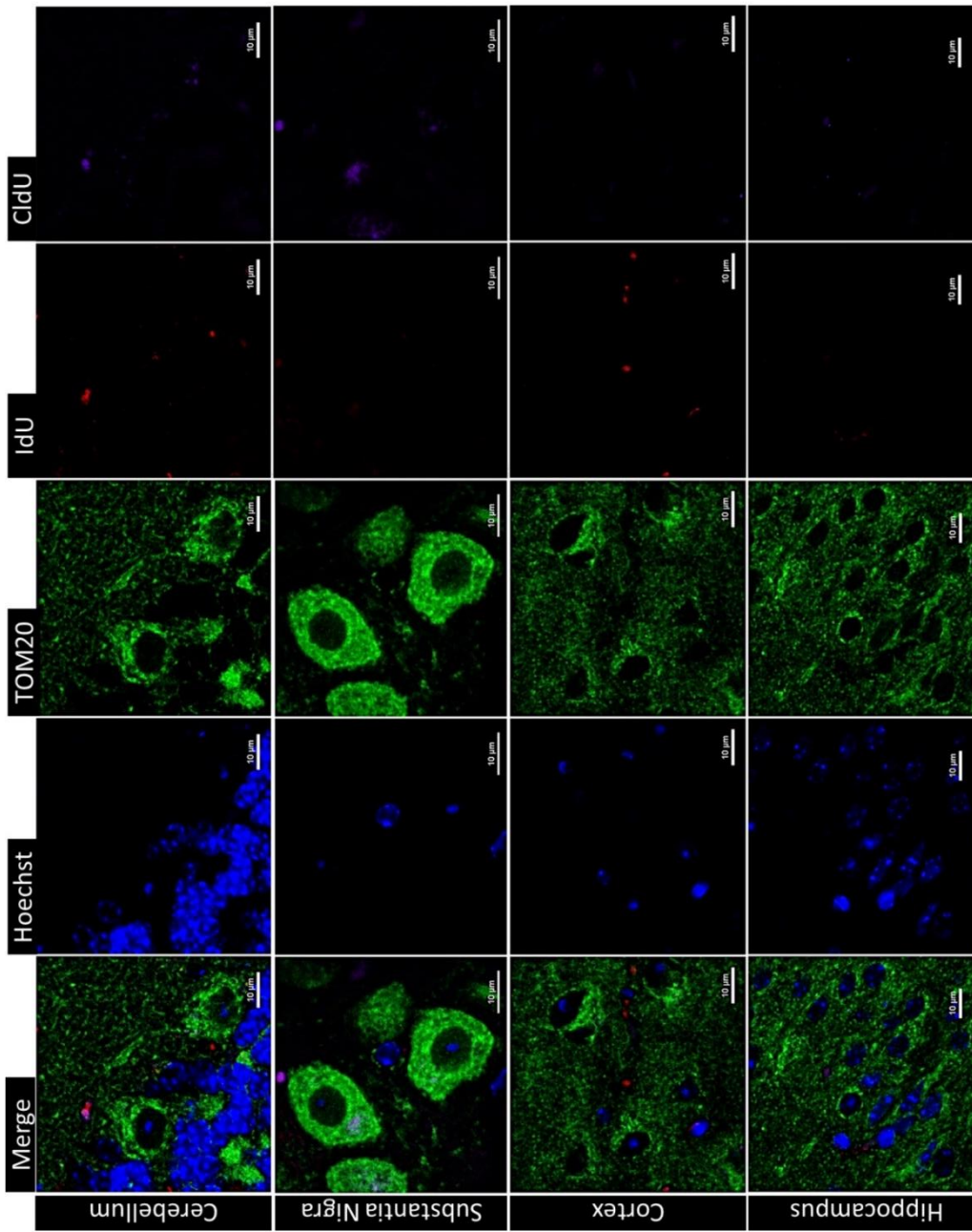
Figure 3.11 Thymidine analogue labelled mice brain regions. This image presents CldU and IdU co-localised with Tom20, the mitochondrial marker, was used to identify the cell boundary and mitochondria. The specific regions of the brain are indicated in the image. Any CldU and IdU not co-localised to the Tom20 is potentially the analogues present within blood vessels. The images were taken at x40 magnification using confocal microscopy. The scale bar represents 10μm for all images. Hoechst is present within wavelength 405 nm, Tom20 is imaged in 488 nm and IdU in 546 and CldU in 647nm.

3.4.2   *Data obtained*

I) MtDNA replication

Since various tissues, ages and genotypes of mice were used in this study, table 3.4 clarifies the subsequent abbreviations used for each tissue and mouse. The average level of CldU and IdU incorporation, as a percentage 'number of voxels' of the Tom20, is presented in table 3.5 alongside the standard deviation of the data. The values are the total number of voxels of the CldU and IdU relative to the total number of voxels of the tom20 channel. The average values, for all the neurons studied, are discussed relative to age, tissue type and genotype in the forthcoming section.

Abbreviation	Full form
Ce/Cer	Cerebellum
Co/Cor	Cortex
Hi/Hip	Hippocampus
SN	Substantia nigra
WY	wildtype young
WO	wildtype aged
PY	PolgA$^{mut/mut}$ young
PO	PolgA$^{mut/mut}$ aged

Table 3.5 List of abbreviations and their full forms used for the mice in this study

Age/Genotype	Region	% CldU	SD	% IdU	SD
WY	CER	31.05	17.68	8.90	10.17
WY	SN	11.27	8.26	7.85	11.43
WY	COR	20.42	14.24	2.04	3.86
WY	HIP	21.88	16.38	1.79	2.91
PY	CER	15.21	10.00	6.17	6.66
PY	SN	6.67	6.72	1.92	3.05
PY	COR	11.36	6.76	2.20	2.59
PY	HIP	8.55	4.21	0.20	0.43
WO	CER	18.99	16.37	7.33	7.70
WO	SN	10.63	8.23	3.75	5.42
WO	COR	7.43	10.24	1.78	3.30
WO	HIP	5.32	4.97	0.88	1.22
PO	CER	10.67	10.66	5.69	9.31
PO	SN	5.58	5.96	3.98	10.39
PO	COR	8.25	9.96	2.66	4.01
PO	HIP	1.94	1.85	3.71	4.41

Table 3.6 Average level of thymidine analogue incorporation into the mtDNA. For each neuron, a total of CldU and IdU was calculated as a percentage of the tom20. The average of this is present in this table. Definitions of abbreviations can be found in table 3.5.

As mentioned previously, CldU had been injected into these mice for 4 consecutive days and IdU had been injected into the mice ~15 hours prior to sacrifice. Therefore, CldU will label mtDNA which had replicated within the last 4 days and IdU, within the past 15 hours. Using both IdU and CldU would shed light on how mtDNA replication patterns change between the two time frames

II) MtDNA replication levels – variation between neuronal subtypes

When comparing the CldU incorporation between the neuronal subtypes, a significant difference ($p<0.05$) was observed between all regions except between the cortex and hippocampus of young wildtype mice (Figure 3.12A). CldU incorporation was highest in the cerebellum, followed by the cortex and hippocampus, with the lowest level in SN. This pattern was also observed in young *PolgA$^{mut/mut}$* mice (Figure 3.12B). For the wildtype aged mice (Figure 3.12C), the highest level of CldU incorporation was also within the cerebellum, however this was followed by the SN and then the cortex, with the lowest levels of incorporation in the hippocampus. For the aged *PolgA$^{mut/mut}$* mice, all the regions, except the cerebellum and cortex, were significantly different from each other (figure 3.12D). The pattern of CldU incorporation levels remained the same as for young *PolgA$^{mut/mut}$* mice, except the hippocampus which, like the wildtype aged animals, showed the lowest levels of incorporation.

IdU incorporation was highest in the cerebellum of young wildtype mice (figure 3.13), however, there was no significant difference between the cerebellum and SN. There was also no significant difference between the cortex and the hippocampus as with the CldU, however the cerebellum and SN both showed significantly increased levels of IdU incorporation compared to cortex and hippocampus. The young *PolgA$^{mut/mut}$* mice and the aged wildtype mice both presented with the same pattern of incorporation and significant differences between all the regions as the young wildtype mice (figure 3.13 B and C). Data from the aged *PolgA$^{mut/mut}$* mice shows the same pattern however none of the areas show significant differences except the cerebellum and cortex.
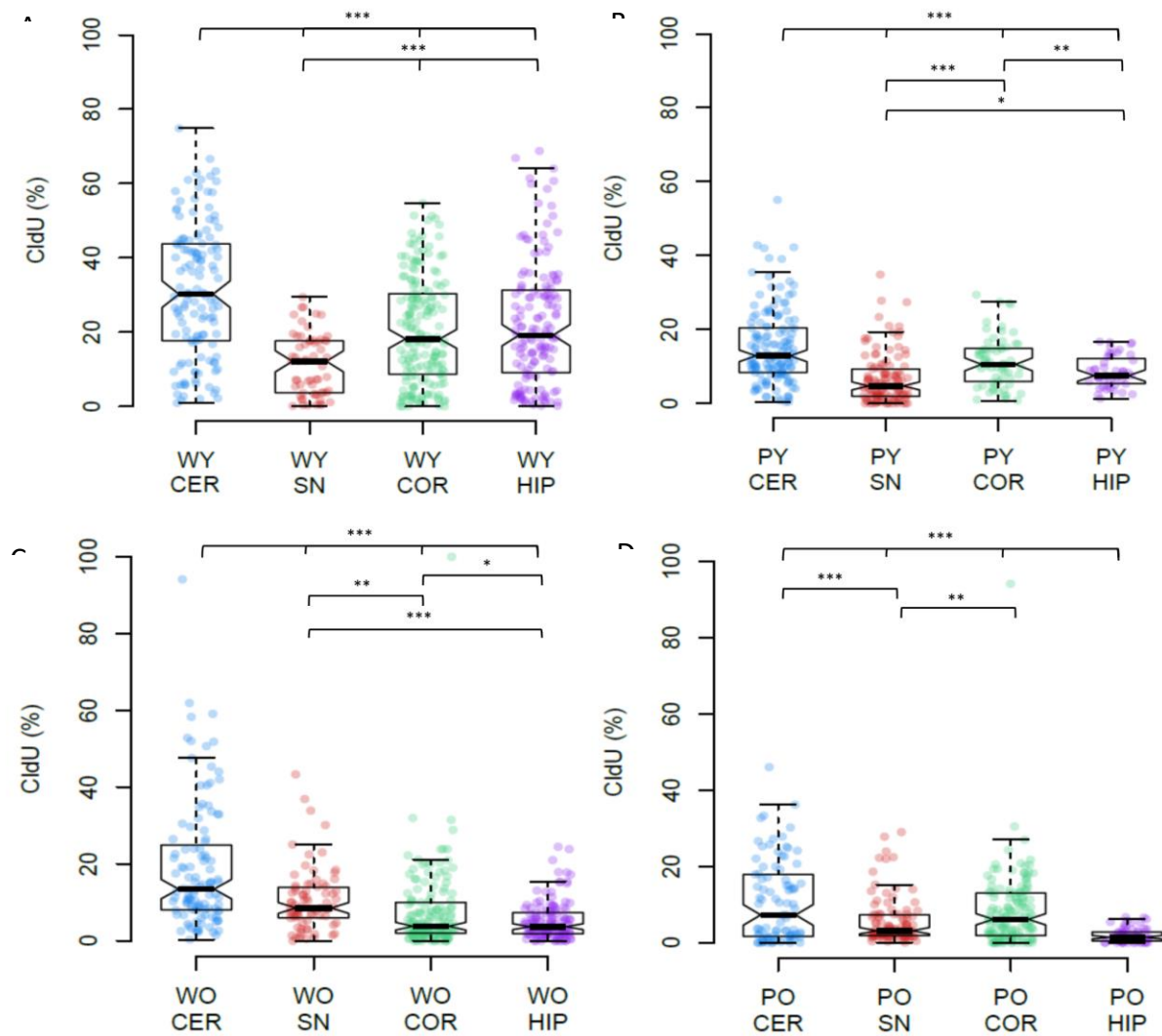
Figure 3.12 Regional variations in incorporation of CldU into mitochondria in mouse neurons – the abbreviations used in this graph are explained in table 3.5. The list of mice is present in table 3.3. Image A presents young wildtype mice, image B presents young PolgA$^{mut/mut}$ mice, image C presents aged wildtype mice and image D presents PolgA$^{mut/mut}$ mice. The error bars represent the +/-SD. n=4 mice per region. * indicates p < 0.05, ** indicates p < 0.01 and *** indicates p < 0.001 obtained using one way-ANOVA.
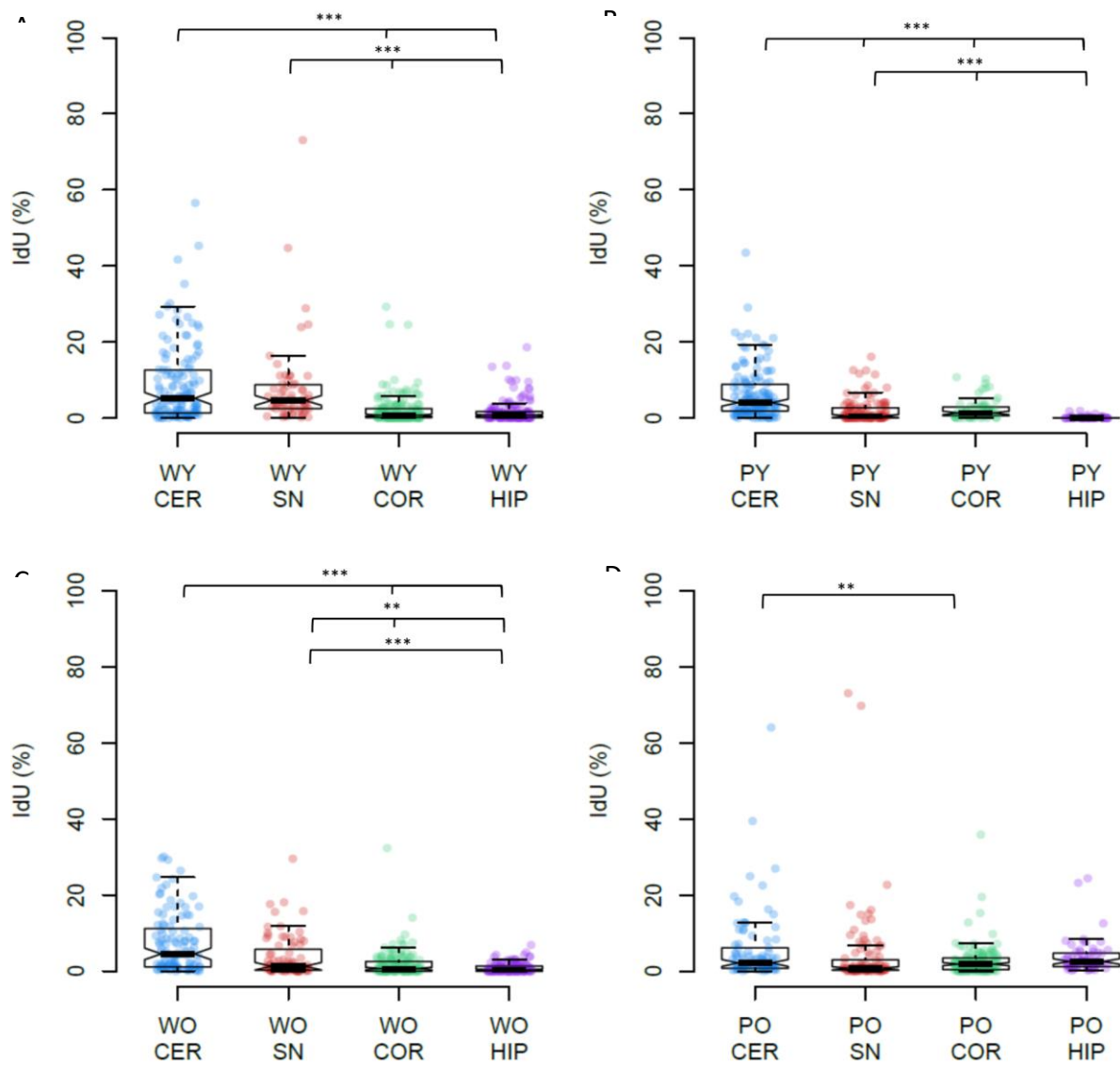
Figure 3.13 Regional variations in incorporation of IdU into mitochondria in mouse neurons –the abbreviations used in this graph are explained in table 3.5. The mice list is present in table 3.3. Image A presents young wildtype mice, image B presents young PolgA$^{mut/mut}$ mice, image C presents aged wildtype mice and image D presents PolgA$^{mut/mut}$ mice. The error bars represent the +/-SD. n=4 mice per region. * indicates p < 0.05, ** indicates p < 0.01 and *** indicates p < 0.001 obtained using one way-ANOVA.

II) MtDNA replication levels– Effect of ageing

The variations in CldU and IdU levels with ageing were also quantified. Figure 3.14 presents the variations in CldU incorporation in each brain region with ageing. All the brain regions, except the SN, in both genotypes, demonstrated a significant decrease (p<0.05) in CldU incorporation with age. The SN exhibited a low level of mtDNA replication, which remained similar with ageing.

The majority of brain regions did not show a significant effect of ageing on IdU incorporation (figure 3.15). However, *PolgA$^{mut/mut}$* and wildtype mice hippocampal neurons and wildtype SN neurons, where significantly different with age (p<0.05).
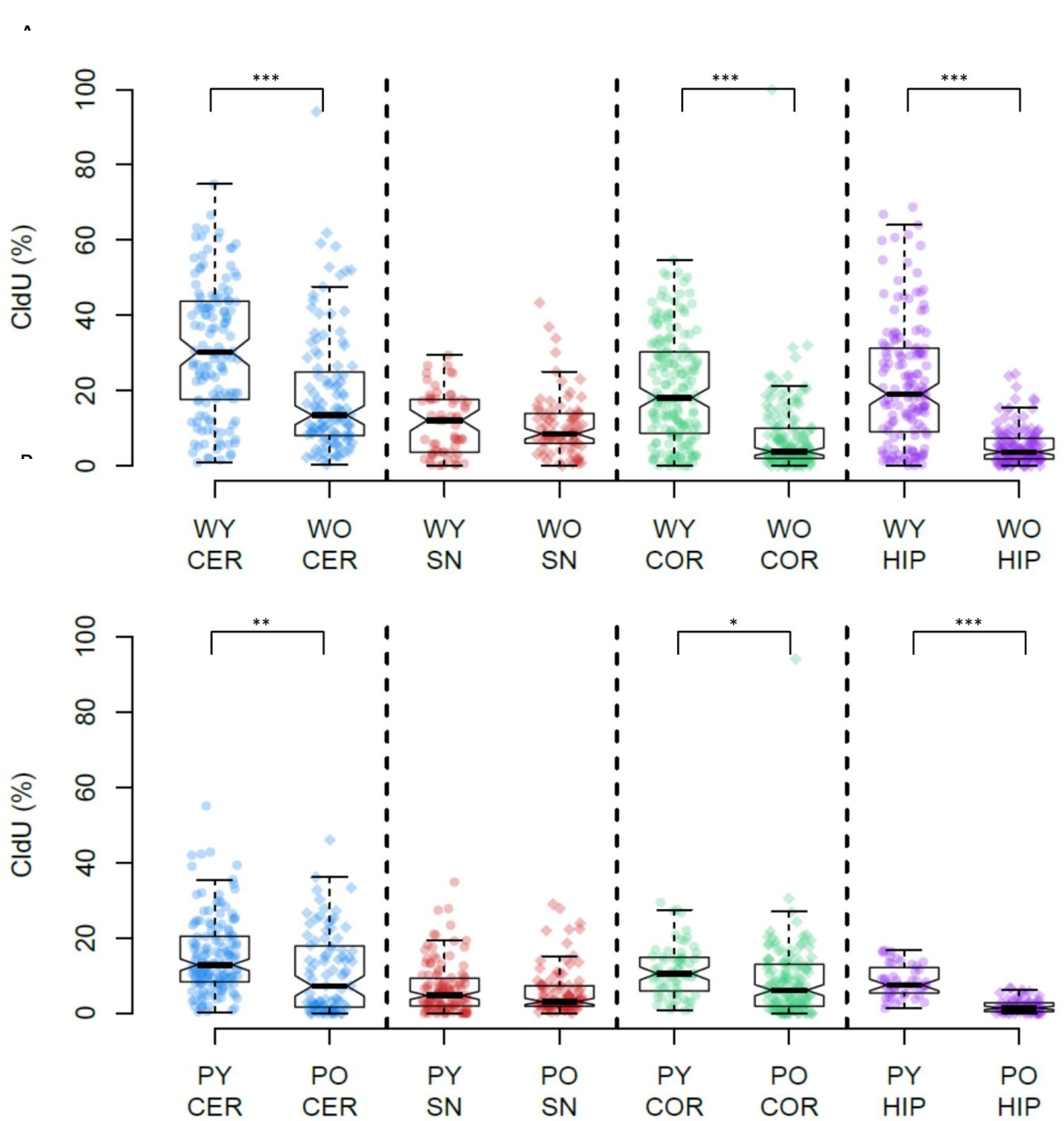
Figure 3.14 Variation with ageing in incorporation of CldU into mitochondria in mice neurons – the abbreviations used in this graph are explained in table 3.5. The list of mice is present in table 3.3. Image A presents wildtype mice and image B presents PolgA$^{mut/mut}$ mice. The error bars represent the +/-SD. n=4 mice per region. * indicates p < 0.05, ** indicates p < 0.01 and *** indicates p < 0.001, and dotted lines separate the regions obtained using one way-ANOVA.
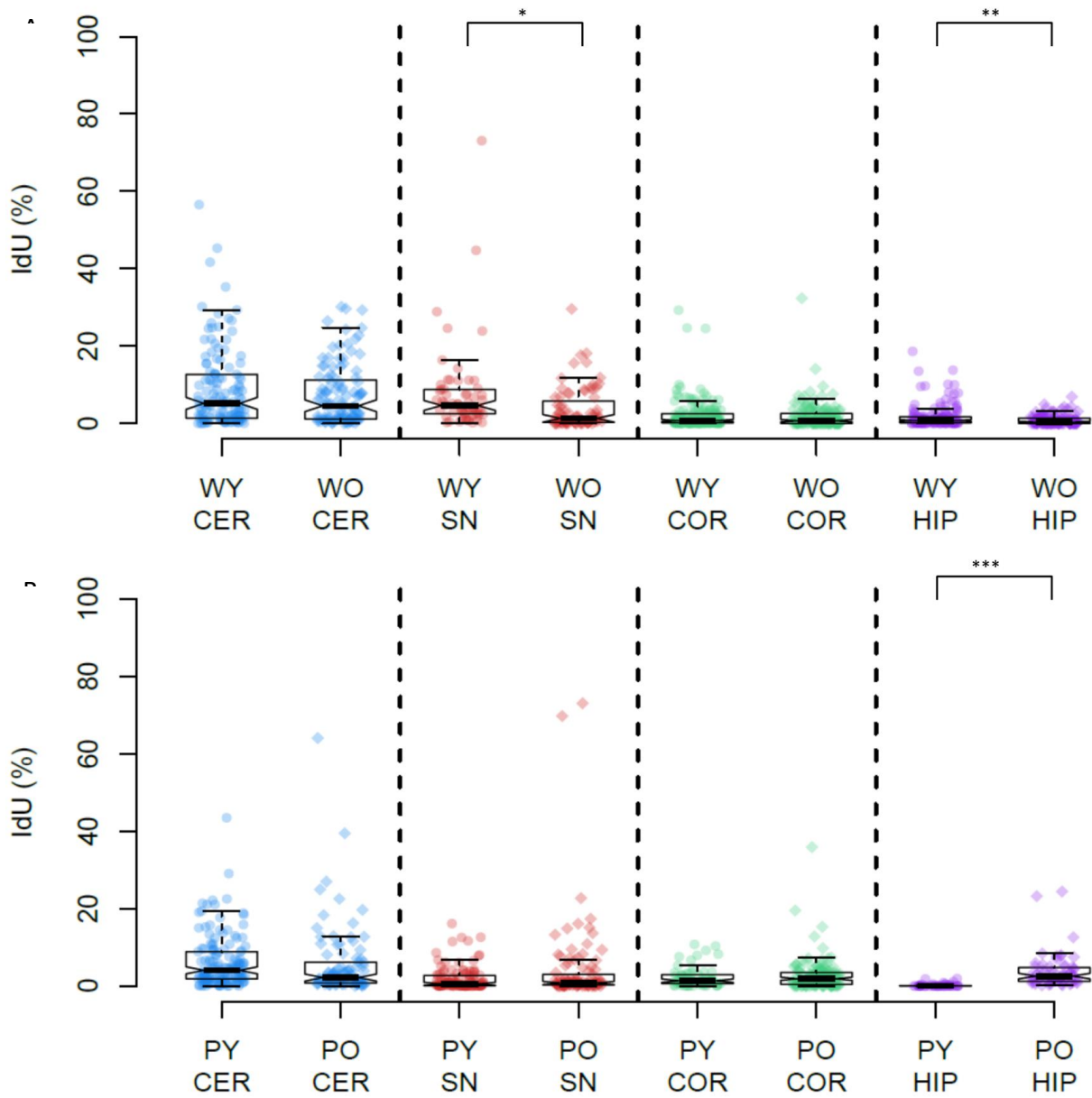
*Figure 3.15 Variation with ageing in incorporation of IdU into mitochondria in mice neurons – the abbreviations used in this graph are explained in table 3.5. The list of mice is presented in table 3.3. Image A presents wildtype mice and image B presents PolgA$^{mut/mut}$ mice. The error bars represent the +/-SD. n=4 mice per region. * indicates p < 0.05, ** indicates p < 0.01 and *** indicates p < 0.001, and dotted lines separate the regions obtained using one way-ANOVA.*

III) MtDNA replication – variation with disease

One of the aims of this study was to understand how mtDNA replication is altered in a model with defective replication. To study this, *PolgA^{mut/mut}* mice were compared to the wildtype mice cohort. For CldU incorporation (Figure 3.16), compared to wildtype mice, there was a significant decrease ($p < 0.05$) in incorporation observed in all brain regions in the *PolgA^{mut/mut}* mice, suggesting a decrease in mtDNA replication levels. In the case of IdU (Figure 3.17), a similar decrease in observed in the *PolgA^{mut/mut}* mice compared to the wildtype, however this is only significant in some regions as indicated in the graph.
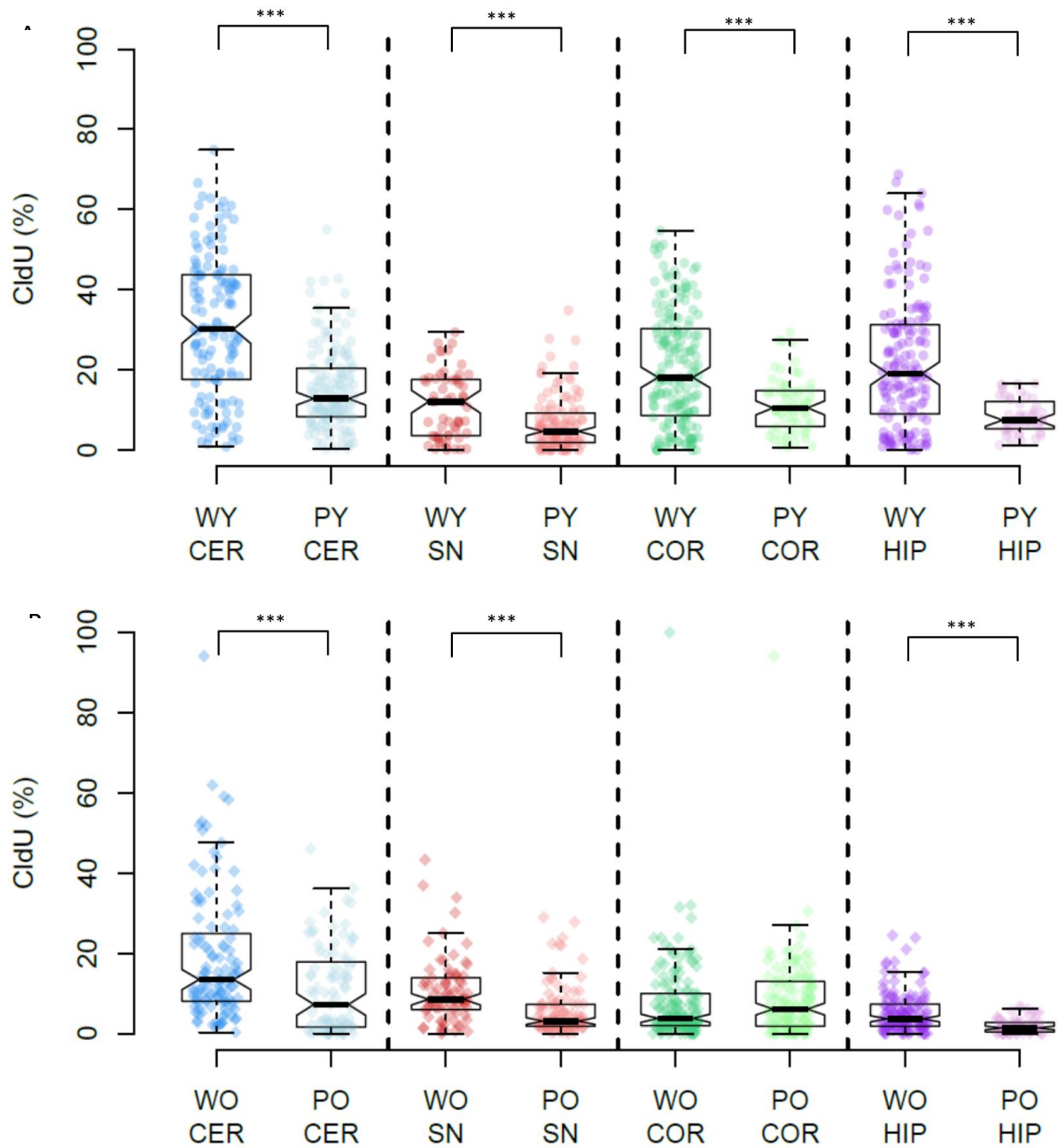
Figure 3.16 Variation with wildtype and PolgA^mut/mut^ model in incorporation of CldU into mitochondria in mice neurons – The abbreviations used in this graph are explained in table 3.5. The list of mice is present in table 3.3. Image A presents young mice and image B presents aged mice. The error bars represent the +/-SD.   n=4 mice per region. * indicates p < 0.05, ** indicates p < 0.01 and *** indicates p < 0.001 obtained using one way-ANOVA.
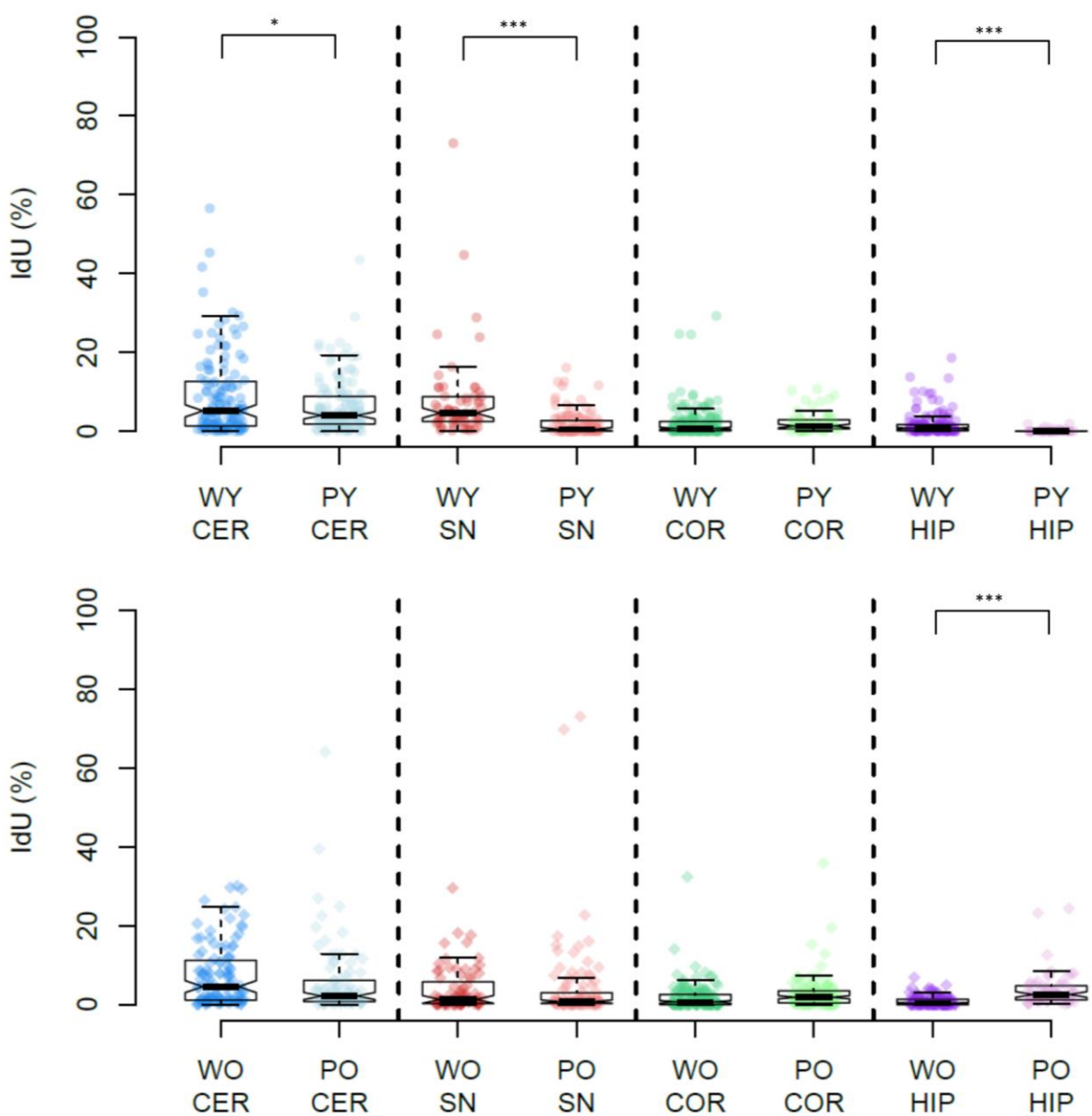
*Figure 3.17 Variation with wildtype and PolgA^mut/mut model in incorporation of CldU into mitochondria in mice neurons – the abbreviations used in this graph are explained in table 3.5. The list of mice is present in table 3.3. . Image A presents young mice and image B presents aged mice. The error bars represent the +/-SD. n=4 mice per region. * indicates p < 0.05, ** indicates p < 0.01 and *** indicates p < 0.001 obtained using one way-ANOVA.*

3.4.3 *MtDNA replication correlation analysis to previous literature*

I) Correlation to mtDNA deletion level

One of the aims of this study was to identify how the level of mtDNA replication correlates with the level of ΔmtDNA observed. In this study, this was also vital since a number of regions commonly associated with high ΔmtDNA demonstrated lower mtDNA replication levels. To identify, whether a correlation exists, it was important to investigate the relationship between CldU and IdU incorporation and ΔmtDNA.

Even though deletion level in the mice from this study has not been investigated, a large number of studies within the literature have investigated this (table 3.7). One of these studies, Perier *et al*, investigated the percentage of ΔmtDNA and copy number in different brain regions and similar to this study, also used wild type and *PolgA*$^{mut/mut}$ mice (Perier et al., 2013). The brain regions investigated in the study by Perier *et al* were cerebellum, cortex, hippocampus, striatum and midbrain. Although they did not look specifically at the SN, this region is present within the midbrain and should provide a representative measure of deletion within the SN, however it will be effected by other neuronal subtypes present in the midbrain. Alongside this, this thesis analysed single cells, while the Perier *et al.* study was conducted on homogenate tissue. However, all other parameters were consistent between the two studies. ΔmtDNA levels were measured using quantitative real-time PCR, and expressed as a percentage of the total mtDNA content. Details of the ΔmtDNA data from this study were kindly provided by Dr Celine Perier (Vall d'Hebron Institute of Research, Spain). The average percentage of ΔmtDNA and copy number per brain region per mouse, for both wild type and *PolgA*$^{mut/mut}$ animals were provided, however, comparative data between young and aged mice were not available. The average deletion levels are presented in table 3.6. As the raw values were not obtained, significant differences cannot be identified, however the original paper mentions significant differences (p<0.01) observed between different tissue types and between wild type and *PolgA*$^{mut/mut}$ mice.

		Wildtype	Polg[wt/mut]	PolgA[mut/mut]
Striatum	Deletions (%)	11.67	21.17	66.83
	SD	2.31	6.05	2.02
Midbrain	Deletions (%)	17.67	17.39	26.17
	SD	2.31	9.32	5.58
Cortex	Deletions (%)	19.83	22.83	57.17
	SD	1.53	9.09	7.42
Cerebellum	Deletions (%)	13.33	24.00	28.33
	SD	5.92	14.08	8.52
Hippocampus	Deletions (%)	23.80		45.50
	SD	7.16		11.90

Table 3.7 ΔmtDNAs in various brain regions. The difference in genotype is also highlighted in the table. The age of these mice range from 9-12 months. The deletions were calculated using quantitative real-time PCR and was expressed as a percentage of total mtDNA copy number. SD represents the standard deviation.

To determine whether an association between mtDNA replication levels (based on thymidine analogue incorporation) and ΔmtDNA levels exists, correlation analysis was conducted by Dr Conor Lawless (Wellcome Centre for Mitochondrial Research). For each tissue common to both datasets (assuming SN is represented by the midbrain), one replicate each was randomly selected from both the replication dataset and from the deletion dataset. By repeating this procedure 10,000 times, a distribution representing the uncertainty about the correlation was built, allowing comparison between the datasets. A Pearson's correlation coefficient was conducted to test for correlation between replication datasets and deletion datasets in these tissues (figure 3.18). To test if the observed correlations are significantly different from zero,

the 5th and 95th percentile range (vertical blue dashed lines) was calculated and checked to observe if this range included zero (vertical red dashed line). The spread of data (black line) demonstrates that in both the IdU and CldU a significant difference from zero could not be demonstrated, and therefore, there was no correlation between mtDNA replication and ΔmtDNA level detected.
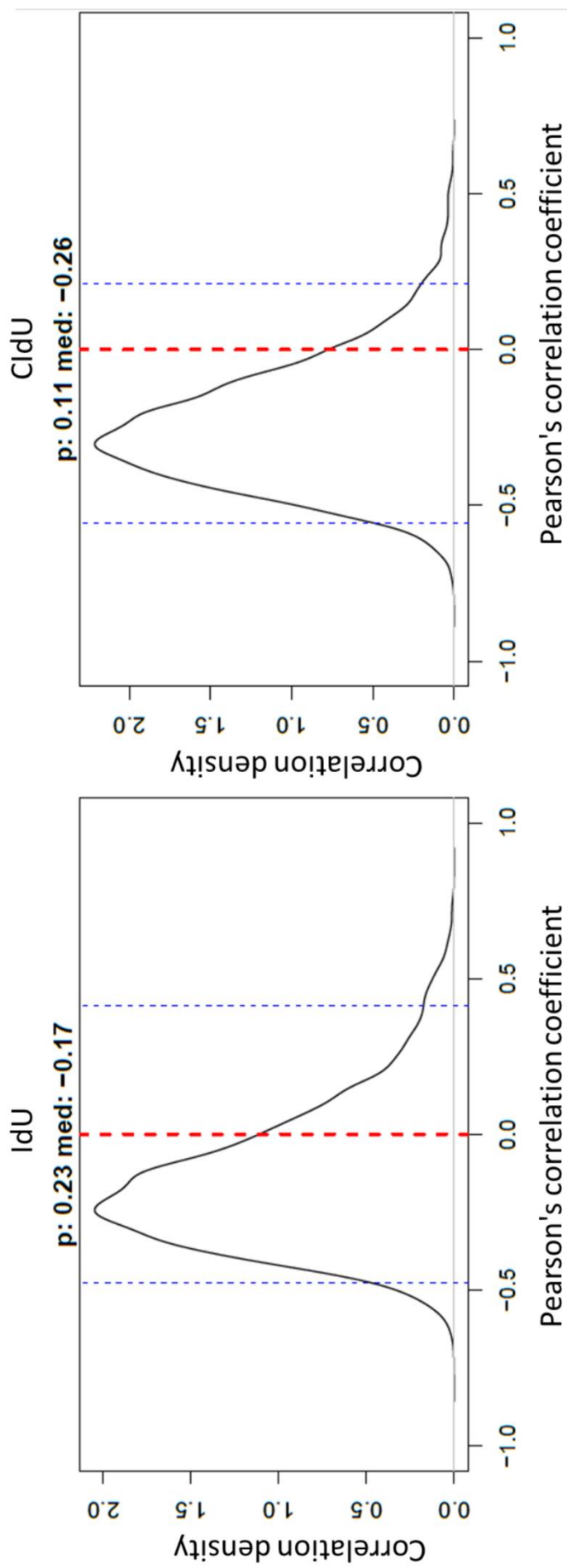
Figure 3.18 correlation between thymidine analogue incorporation and ΔmtDNA – The vertical blue dashed lines represents the 95%ile range and the vertical red dashed line checked is to identify if this range included zero. No significant difference from zero was noticed in this case.

II) MtDNA replication and correlation with mtDNA copy number.

As mentioned in the previous section, mtDNA copy number was also measured in the study by Perier *et al*. This is vital as an increase in mtDNA replication could lead to an increase in mtDNA copy number, and this has been suggested as a mechanism of protection against ΔmtDNA (Dölle et al., 2016). Therefore testing was performed to identify any association between mtDNA copy number and mtDNA replication level. Details of mtDNA copy number from their previously published study were kindly provided by Dr Celine Perier (Vall d'Hebron Institute of Research, Spain) and is presented in table 3.8 (Perier et al., 2013). To understand the relationship between mtDNA replication and copy number, correlation analysis, as mentioned in the previous section was performed. There was no significant correlation between mtDNA replication and mtDNA copy number detected (figure 3.19).

		Wildtype	Polg^{wt/mut}	PolgA^{mut/mut}

		Wildtype	$\text{Polg}^{wt/mut}$	$\text{PolgA}^{mut/mut}$
Striatum	copy number	9.92	8.70	19.33
	SD	2.35	1.26	2.43
Midbrain	copy number	9.53	10.17	13.49
	SD	0.72	2.14	0.94
Cortex	copy number	6.72	7.37	19.48
	SD	0.29	2.06	5.35
Cerebellum	copy number	1.58	1.78	2.24
	SD	0.13	0.23	0.82
Hippocampus	copy number	1.43		5.01
	SD	0.88		2.00

Table 3.8 MtDNA copy number in various brain regions. The difference in genotype is also highlighted in the table. The age of these mice range from 9-12 months. The copy number were calculated using quantitative real-time PCR.
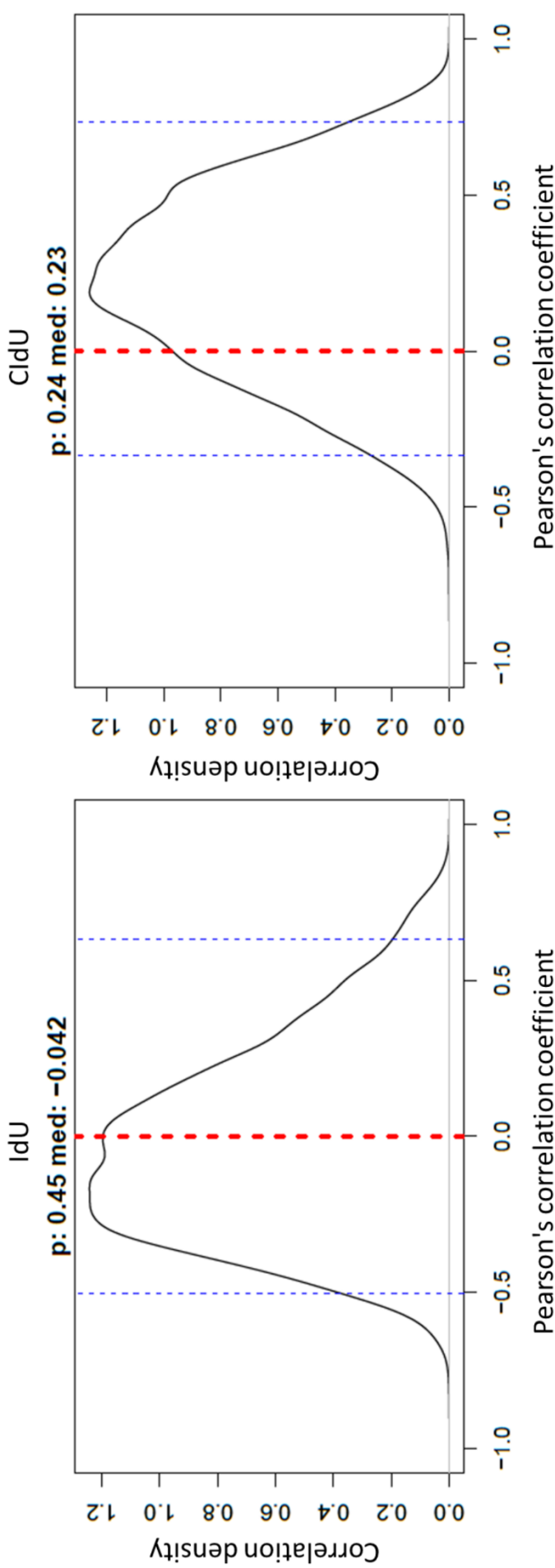
Figure 3.19 correlation between thymidine analogue incorporation and mtDNA copy number – The vertical blue dashed lines represents the 95%ile range and the vertical red dashed line checked is to identify if this range included zero. No significant difference from zero was notices in this case.

3.4.4 *Variability between individual mice*

Although the statistical testing identified significant differences between the groups, the variability between mice requires consideration. This is particularly important certain regions of the mice were not obtained due to technical difficulties. Alongside this, the numbers of neurons identified from each mice and region were also variable. The total number of regions and number of neurons in each region analysed is presented in table 3.9. In addition, as with humans, there are variations in other factors such as mtDNA deletions in individual mice which might also require consideration. Therefore, to further study this, individual mice were compared and presented in figure 3.20.

Even when comparing different regions within individual mice, the cerebellum still displayed the highest levels of CldU and IdU incorporation in most mice and SN generally produced the lowest incorporation. This is in further support of the results obtained. There are variation in some cases for examples young 3 in graph 3.10A and young 4 in graph 3.10B demonstrated a higher value for cortex and hippocampus than the cerebellum, however this is not common, and the SN is still the lowest.

Age/Genotype	Region	Number of mice	Number of neurons
WY	CER	4	163
WY	SN	2	106
WY	COR	4	186
WY	HIP	3	146
PY	CER	4	166
PY	SN	4	83
PY	COR	2	95
PY	HIP	1	60
WO	CER	4	169
WO	SN	3	117

WO	COR	4	145
WO	HIP	4	151
PO	CER	4	89
PO	SN	3	90
PO	COR	4	138
PO	HIP	1	49

Table 3.9 The total number of mice and neurons analysed per each age/genotype and region
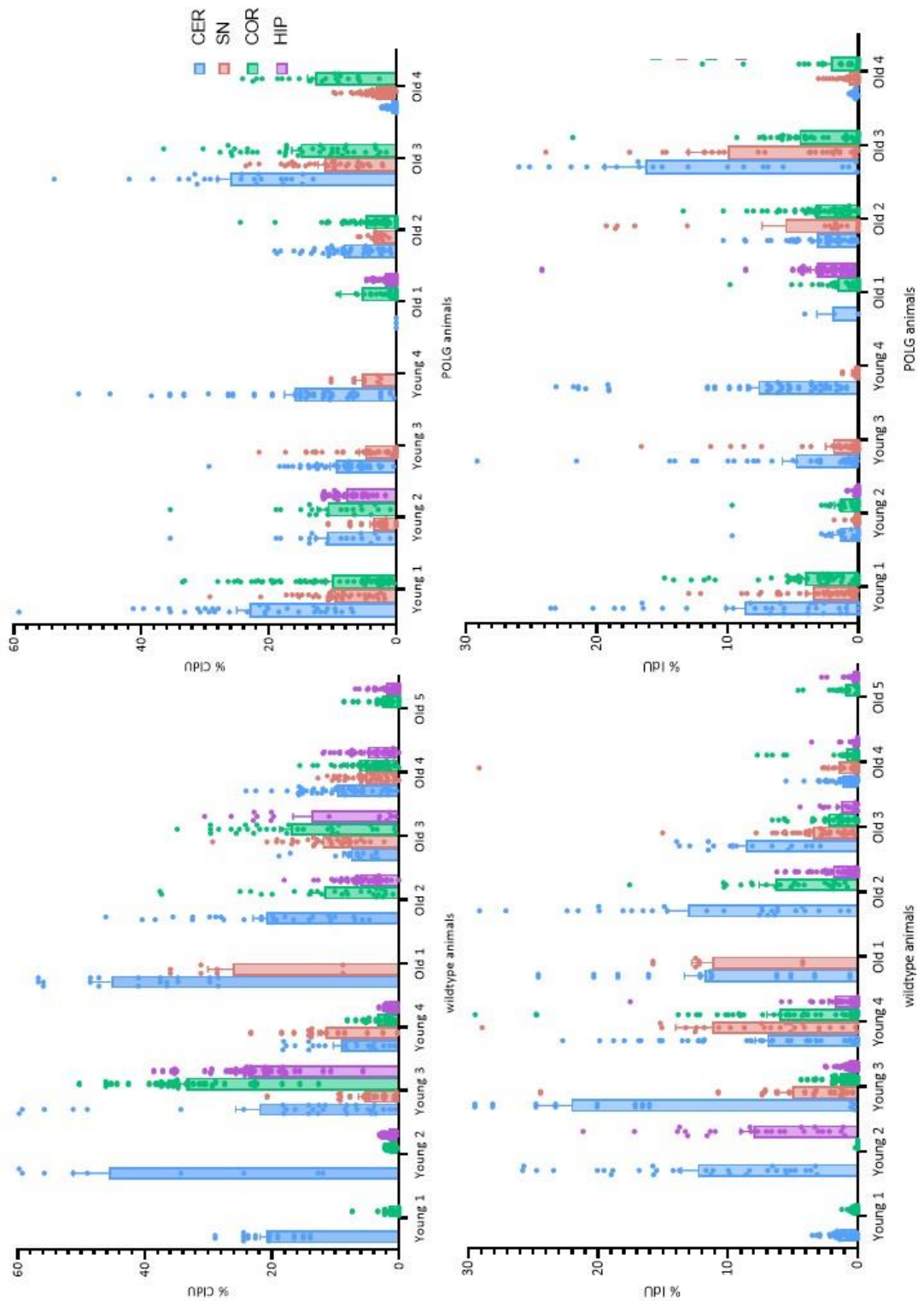
Figure 3.20 Variation between individual mice – These graphs highlight any variation present within the groups when comparing the individual mice. Some areas are absent from certain mice due to technical difficulties in obtaining them

3.4.5 *Mitophagy levels between cerebellum and SN*

Variations were observed between IdU (15 hours) and CldU (5 days) incorporation, and a suggested mechanism for these differences could be an increase in mtDNA degradation or transport of mitochondria to distal regions between the time points. MtDNA degradation could occur due to an increase in mitophagy, hence if a certain region has increased basel level of mitopgahy, this would effect the thymidine analogue levels observed in this regions. Therefore, to understand any effect mitophagy could be having in this regions, the levels of mitophagy in the cerebellum and the SN were used. For this, tissue from a mouse model allowing measurement of basal mitophagy was kindly donated by Dr Ian Ganley (University of Dundee) (McWilliams et al., 2016). Degradation of mitochondria via mitophagy would also lead to degradation of mtDNA therefore this could be studied relative to mitophagy. Briefly, these mice contain a construct comprising of both GFP and mCherry tags with the mitochondrial targeting sequence of FIS1, allowing expression to be targeted to the OMM of the mitochondria. Under normal circumstances both GFP and mCherry are expressed and therefore fluoresce. When a mitochondrion undergoes mitophagy, it is taken into a lysosome which contains an acidic environment that quenches the GFP, however the mCherry remains unaffected. Therefore, in the event of a mitophagic event, the only mitochondrial fluorescent signal comes from the mCherry tag. Therefore, this allows quantification of the levels of mitophagy within individual cells, based on the number of mCherry (red) puncta. These images were analysed using Colombus (PerkinElmer) by Dr Amy Reeve (Wellcome Centre for Mitochondrial Research). This analysis pathway detected the neuronal marker for each brain region, giving a measurement of neuronal area and then detected the bright mCherry spots specifically within this area for each neuron. The number of mCherry spots per unit area was then calculated, with each spot representing a mitochondria within a lysosome. As this was a preliminary study, only wildtype mice were used and images from a total of three mice were used for the SN and four for the cerebellum. These regions were chosen due to the variations observed within them in terms of mtDNA replication levels. The Purkinje cells from the cerebellum were identified by calbindin staining and SN dopaminergic neurons were stained with an anti-TH antibody (figure 3.21) (McWilliams et al., 2016).
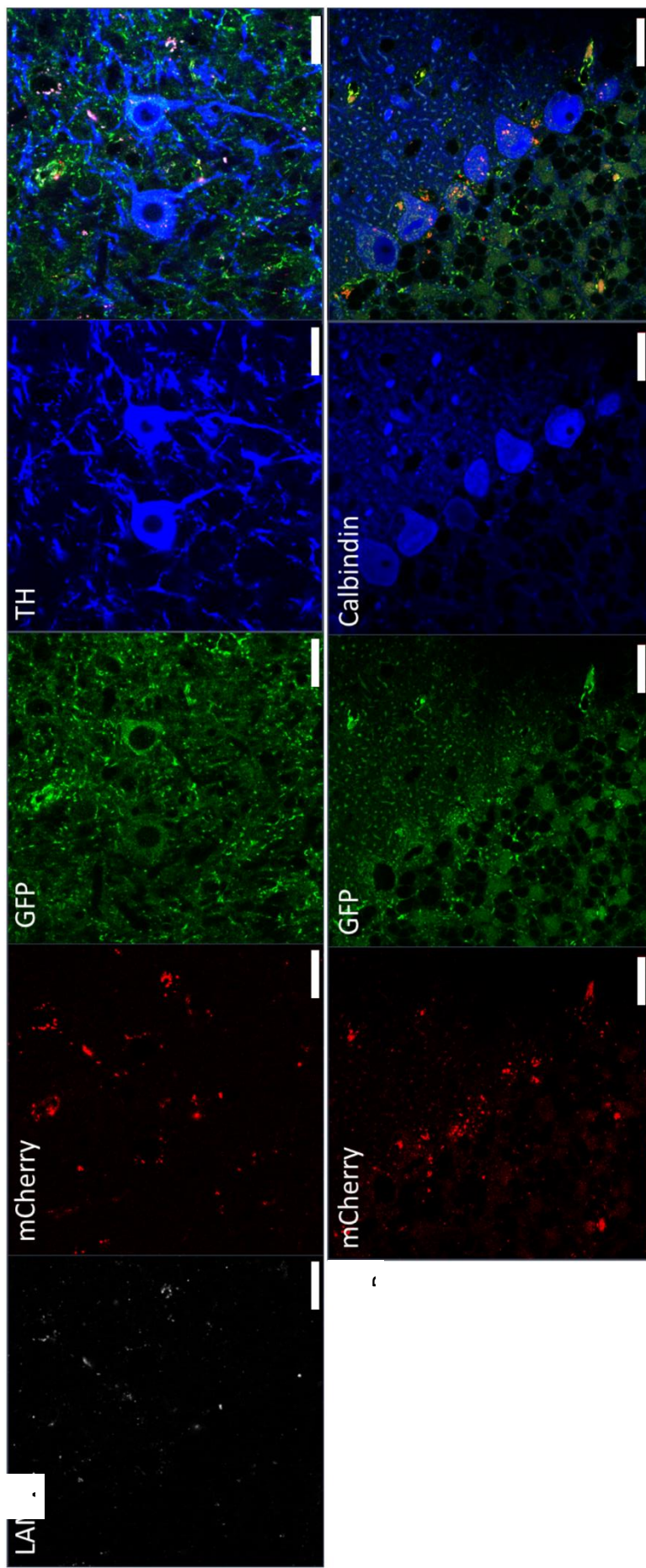
Figure 3.21 Staining of dopaminergic and Purkinje neurons from MitoQC mice. These images were were a kind gift from Dr Ian Gangley. This model has been imaged and described in the literature (McWilliams et al., 2016). The mitoQC mice allow identification of mitophagic events as bright red spots due to the quenching of GFP in these areas. The mCherry bright spots were also co-localised with LAMP1, the lysosome marker present in the dopaminergic neurons. TH was used to confirm the dopaminergic neurons (A) and calbindin for Purkinje cells (B). These sections were images at 63x magnification. The scale bar represents 20 µM.

Comparison of the two regions (figure 3.22) produced a significant difference ($p<0.001$) when compared via Mann-Whitney test as the data sets did not show a normal distribution (Kolmogorov-Smirnov test). A mean of 0.04 (SE +/- 0.002) mCherry puncta per cell was observed in the cerebellum, and higher levels of 0.06 (SE +/- 0.001) were observed in the SN. This suggests that there may be a significant upregulation of basal mitophagy in the SN compared to the cerebellum. However, this is a preliminary study, and further investigation, especially including the other brain regions, is required.
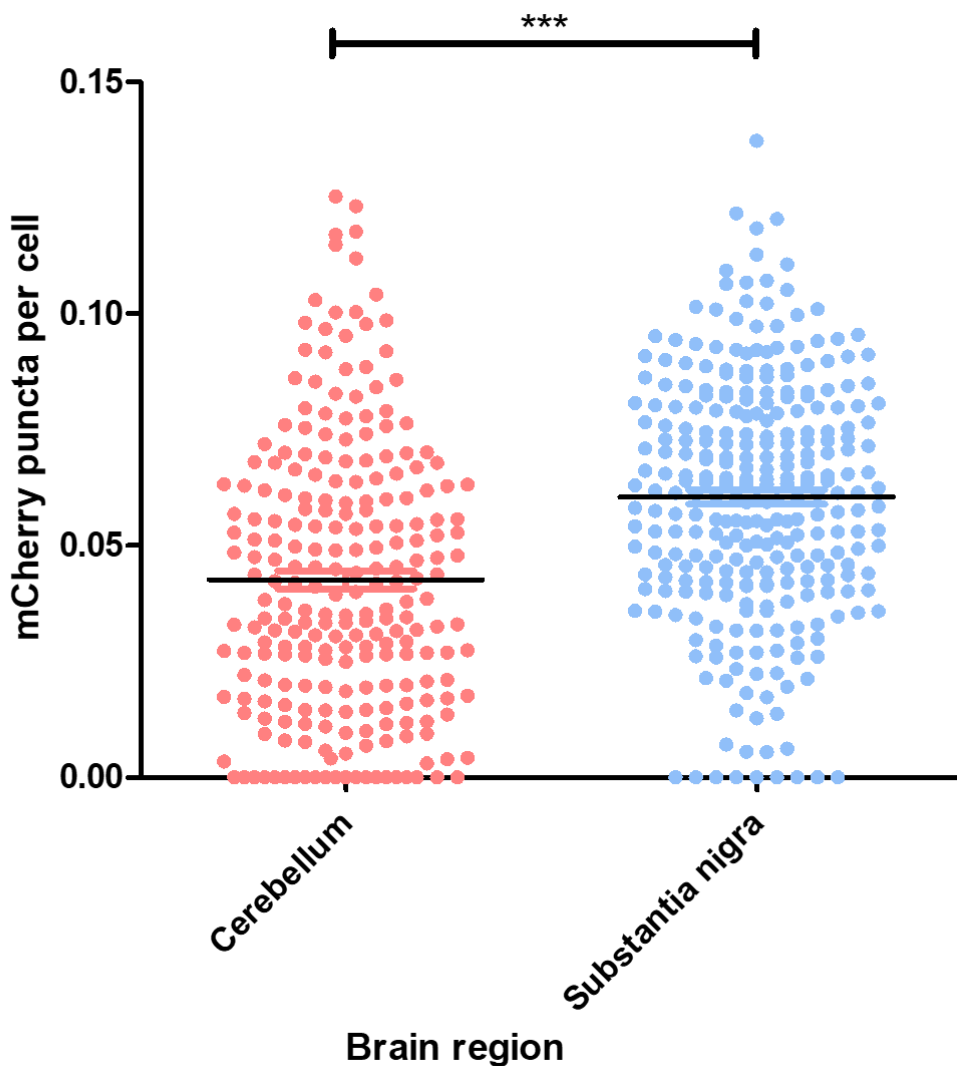
Figure 3.22 Mitophagy levels from the MitoQC mice – This graph presents the number of mCherry puncta in individual cells from the Purkinje neurons in the cerebellum and dopaminergic neurons from the SN. n=4 mice for the cerebellum and n=3 for the SN. **** indicates p < 0.001 obtained using t-test.

3.5   Discussion

The key outcomes from this chapter are as follows;

- MtDNA replication in individual cells from different regions of the brain was successfully identified, showing significant differences ($p<0.05$) in CldU and IdU incorporation between individual neuronal subtypes from the different brain regions.
- There were significant differences ($p<0.05$) between individual neuronal populations between the young and aged group.
- There were significant differences ($p<0.05$) between individual neuronal populations between wildtype and *PolgA^(mut/mut)* mice.
- Individual dopaminergic neurons from the SN show a significant increase ($p<0.05$) in the level of mitophagy compared to cerebellar Purkinje cells.

3.5.1   *Differentiating between mtDNA repair and replication*

One of the criticisms of using thymidine analogue labelling to study replication is the simultaneous incorporation of this analogue during repair. Theoretically, repair and replication, both involve incorporation of nucleotides and thus positive puncta could represent incorporation through repair. However as mentioned in section 1.5.2, the most common type of repair observed in mtDNA is BER. This, or other types of repair such as double strand break repair, involve a smaller length of mtDNA compared to replication which presents the opportunity to incorporate CldU and IdU into the full 16.5kbp of the mitochondrial genome. This is also suggested by other studies that have used BrdU for mtDNA replication labelling (Davis and Clayton, 1996, Van Laar et al., 2018). Therefore, CldU and IdU incorporated by replication would give higher signal intensity than repair within each mitochondrial surface, due to the presence of multiple thymidine analogues. Alongside this, the thymidine analogues will compete with endogenous thymidine, hence the proportion of opportunities for thymidine analogue incorporation is further decreased for both replication and repair. In addition to this, even though the nuclei in post-mitotic neurons do not divide, there will be DNA repair happening to a greater level in the nuclear genome than within the mitochondria, attributable to the size of nuclear genome and the various pathways of repair

available for the nuclear DNA as highlighted in section 1.8 (Magnusson et al., 2003, Alexeyev et al., 2013). Due to this, if thymidine analogue via repair is incorporated into the DNA, this should also be co-localised with the nuclear marker; Hoechst. However, as presented in Figure 3.9, in all the regions stained, IdU or CldU is not co-localised with Hoechst.

The intensity of each mitochondrial surface was measured in this study (appendix 8.5), as CldU/IdU incorporation via repair would have significantly lower intensity than replication. As 2 mitochondrial surfaces were noticed as having a significantly lower intensity than the other surfaces, this could potentially be identifying repair. This was also identified in 2 $PolgA^{mut/mut}$ mice. This may be due to the mutation in the proof reading domain of Polγ, leading to incorrect nucleotide incorporation, and therefore, repair is likely to be occurring at a higher level than in wildtype mice (Ponamarev et al., 2002, Trifunovic et al., 2004, Wanrooij et al., 2004). However, the low signal intensities of thymidine analogues thought to be due to repair could be non-specific signal. Either way due to the low frequency this would not affect the data, however the analysis was modified to remove these values.

3.5.2 *Is there variation in mtDNA replication levels between neuronal subtypes?*

As mentioned in Table 3.1 and 3.2, previous literature has demonstrated varying levels of ΔmtDNA within the four neuronal subtypes investigated in this thesis. One of the methods through which these deletions are thought to form is replication. This can be due to the 'slipped-strand' model or replication stalling (Section 1.1). Due to this suggested involvement of mtDNA replication in ΔmtDNA formation, and the differential levels of ΔmtDNA observed with different brain regions, the levels of mtDNA replication within four brain regions were investigated (SN, cortex, cerebellum and hippocampus). With ageing and in the $PolgA^{mut/mut}$ mouse model, the level of these ΔmtDNA are elevated, hence these were investigated to study how mtDNA replication is altered in ageing and in a disease model with an accelerated ageing phenotype.

First of all, when comparing the different regions of the brain there was a similar pattern of CldU incorporation in the young wildtype and $PolgA^{mut/mut}$ groups. The highest level of incorporation was observed in the Purkinje cells of the cerebellum, followed by the pyramidal cells of the cortex, pyramidal cells in the hippocampus and finally the lowest level in the

dopaminergic neurons of the SN. In some cases, a difference between cortex and hippocampus was not observed, this could be because although the regions are different, the neuronal subtype is pyramidal cells in both cases and hence they could be behaving in a similar manner. Where ΔmtDNA are concerned, the lowest levels are generally detected within the cerebellum and the highest levels within the SN, suggesting that a higher level of mtDNA replication could possibly correlates negatively with higher level of ΔmtDNA.

In the case of IdU, this pattern was mirrored, except in the SN. The cerebellum still presented the highest levels of IdU incorporation, however SN was the second highest. This suggests that time could have an impact on replication levels observed, and perhaps another process could be affecting the recently replicated mitochondria in the SN. This could be increased mitochondria transport, since SN neurons have long processes, mitochondria would be at high demand in distant regions of the cell and could have been transported there. Since the whole cell (including neurites) were not considered here, this could have an effect. Another process could be an increase in mitochondrial degradation through mitophagy, which was detected here as an increase in mCherry puncta per cell in the SN. However this requires further work to confirm.

3.5.3 *Is there variation in mtDNA replication with ageing and in replication defective model?*

With ageing, both wildtype and *PolgA$^{mut/mut}$* mice demonstrated a decrease in CldU and IdU incorporation (although this only reached significance (p<0.05) in 8 out 16 cases). This suggests that mtDNA replication declines with ageing, however, ΔmtDNA levels increase with ageing. This again suggests that a higher level of mtDNA replication does not lead to a higher level of ΔmtDNA. This data also suggests a possible negative relationship between the two factors, however this needs to be confirmed. Interestingly, no significant decrease in incorporation was seen in the SN. This again suggests, as in the previous section, another process that could be involved, especially due to the high ΔmtDNA levels observed in this region of humans.

3.5.4 *Correlative analysis of ΔmtDNA and copy number with mtDNA replication level*

As part of a collaborative study, previously published data (Perier et al., 2013) was obtained and correlated to the mtDNA replication levels observed in this study. This was done to identify any relationship between the levels of mtDNA replication and ΔmtDNA deletions. The Perier *et al* study was chosen as they used young and aged, wildtype and *PolgA^{mut/mut}* mutant mice. They also investigated various brain regions including cerebellum, cortex, hippocampus, striatum and midbrain. Although they did not look specifically at the SN, this region is present within the midbrain and should provide a representative measure of deletion within the SN. The average values were obtained and correlation analysis was conducted by Dr. Conor Lawless (Wellcome Centre for Mitochondrial Research).

The results obtained demonstrated no correlation between mtDNA replication and ΔmtDNA deletion levels within various brain regions, genotypes or in ageing. These data suggest that mtDNA replication may not have an impact on ΔmtDNA levels. However, this portion of the project does have a number of caveats. The Perrier *et al* study demonstrated the ΔmtDNA levels in homogenate tissue. Since different neuronal populations and glial cells are present within homogenate tissue samples, it could be suggested that the presence of other cells could affect the averages. Alongside this, an average of ΔmtDNA levels, rather than the raw values were used for each mouse. The statistical model was created by randomly associating ΔmtDNA and copy number with levels of mtDNA replication, therefore, the low number of values available could skew the data. Alongside ΔmtDNA levels, the Perrier *et al* study also provided the mtDNA copy number in these mice which also did not demonstrate a correlation with the mtDNA replication data. This is interesting as an increase in mtDNA replication could lead to an increase in mtDNA copy number. However, the copy number could also be affected by other processes such as mitophagy. In spite of these limitations, the data from this study suggests that mtDNA replication might not be the sole mechanism for deletion formation.

3.5.5 *Other mechanisms which may lead to mtDNA deletion formation*

If mtDNA replication is not causative of ΔmtDNA, another suggested mechanism is mtDNA repair (explained in section 1.6). The replication levels could be downregulated as the template strand of mtDNA is undergoing repair due to mtDNA damage. This is supported by

the general decrease in mtDNA replication in regions with the highest levels of ΔmtDNA, for example the SN. MtDNA repair activity could be increased, due to the high levels of ΔmtDNA levels in this region, potentially leading to the decrease in mtDNA replication. Previous literature has demonstrated that with age and disease, an increase in ROS production and mtDNA damage is observed. Studies in human skeletal muscle have demonstrated an age associated increase in DNA oxidisation using 8-Oxo-2'-deoxyguanosine (8-oxo-dG) (Short et al., 2005). An accumulation of 8-oxo-dG with ageing has also been observed in the cortex and cerebellum in humans (Hamilton et al., 2001). It might be suggested that, due to this age associated increase in mtDNA damage, the mitochondria is prioritising repair of an mtDNA molecule rather than replication of a damaged mtDNA molecule. This is also supported by a study that measured 8-oxo-dG glycosylase activity and demonstrated an age related increase in the activity of this enzyme on mouse liver mtDNA (de Souza-Pinto et al., 2001). This was significantly higher than the activity of this enzyme on the nuclear genome. However, this study, and others, also observed the activities of Uracil DNA glycosylase and endonuclease G both of which remains unchanged or decreased in ageing and AD disease model (Gredilla et al., 2010, Imam et al., 2006, Soltys et al., 2019). Therefore, this requires further experiments to validate.

Current literature has not studied mtDNA repair in different brain regions extensively, however a study has reported an age related decrease in DNA glycosylase activity in the mtDNA, but not in the nuclear DNA (Imam et al., 2006). They also demonstrated that this activity did not change with different brain regions suggesting that there is no difference in DNA repair between brain regions. Another study compared DNA glycosylase activities between hippocampus and cortex and observed lower levels in the hippocampus (Gredilla et al., 2010). Although this demonstrated difference between brain regions, based on this 'repair' theory, the data from this study demonstrates lower levels of mtDNA replication in the hippocampus than the cortex, and therefore is in opposition. However, these studies used homogenate cells and as SN was not studied. Alongside this, a recent paper demonstrated that a decrease in DNA glycosylase activity in AD patients was associated with a reduced mtDNA copy number, however there was no association with mtDNA mutations (Soltys et al., 2019). Therefore, maybe the theory requires modification to propose that a decrease in

mtDNA replication is associated with reduced mtDNA repair activity, and other mechanisms, such as mtDNA transcription increase to compensate for the biochemical defect. However, this requires further investigation as mentioned in the future work.

Alongside this, if ΔmtDNA formation is via replication stalling, it could be suggested that thymidine analogues could still be incorporated even though replication is stalled. With the analysis, this will be identified as a positively replicated mtDNA molecule even though replication in not complete to stalling. Therefore this is one of the limitations of this technique.

3.5.6 *Mechanisms that could affect the level of mtDNA replication observed*

I) MtDNA copy number

One of the mechanisms suggested in previous literature of coping with ΔmtDNA, is compensation via increased mtDNA copy number (Dölle et al., 2016). This might be beneficial since although it increases ΔmtDNA, the wildtype mtDNA will also increase and therefore any biochemical defect is compensated for by 'biochemical threshold effect' (Rossignol et al., 2003). This was also demonstrated in the case of a point mutation, whereby an abundance of wildtype mtDNA results in minimal COX deficiency and hence mitochondrial dysfunction, further suggesting that wildtype copy number is an important compensatory factor for mtDNA mutations (Durham et al., 2007). Increased copy number could potentially have an effect on mtDNA replication as this is required for synthesis of new mtDNA molecules, however this is not the sole mechanism that may affect mtDNA copy number.

When comparing the mtDNA replication levels detected in this study to copy number data, previous literature that used quantitative real-time PCR assay to determine mtDNA copy number in various regions of the mouse brain determined that SN neurons contained the highest level of mtDNA copy number (Fuke et al., 2011a). This study also highlighted that the lowest level of mtDNA copy number was present within the cerebellum. This suggests that an increase in mtDNA copy number is not associated with mtDNA replication, however as mentioned previously, this could be due to other processes such as mtDNA degradation or mitophagy. The mtDNA copy number recorded in other studies also demonstrates no

association with the differential mtDNA replication levels observed with this study (Dölle et al., 2016, Fuke et al., 2011a, Perier et al., 2013, Blokhin et al., 2008, Diaz et al., 2002).

The literature is inconsistent regarding mtDNA copy number changes with ageing. Most studies have demonstrated an age-related decrease or no change on skeletal muscle, which similar to the brain, consists of post mitotic cells (Welle et al., 2003, Miller et al., 2003, Barazzoni et al., 2000, Frahm et al., 2005). However studies have also presented an increase in mtDNA copy number in the skeletal muscle (Barrientos et al., 1997, Pesce et al., 2001). As mentioned before, this could be due to the methodology employed and using homogenate tissue instead of specific cell types or a possible effect of the species used. However, in individual neurons dissected from the cerebellum, cortex and SN, generally an age-related increase in mtDNA copy number was observed, however, this was not compared within the study (Dölle et al., 2016). They, and others, also investigated the effect of a disease model on mtDNA copy number, finding a lower level of mtDNA copy number in PD patients (Dölle et al., 2016, Pyle et al., 2015). This decrease in copy number was also observed in single neurons and glial cells from Multiple sclerosis (MS) patients (Blokhin et al., 2008). Therefore, although homogenate data is inconsistent, data from individual neurons demonstrates an age-related and disease-specific decrease in copy number which is in concurrent with the reduced mtDNA replication changes observed in these case for this study, though not demonstrating an association with the ΔmtDNA level observed.

II) MtDNA transcription

An increase in mtDNA mutations could also lead to mitochondrial dysfunction and biochemical defects (Stewart and Chinnery, 2015), due to this, there could be an increased requirement for mtDNA transcription to compensate for the biochemical defect. In situations such as these, a 'replication-transcription' switch has been suggested (Agaronyan et al., 2015). This is because both replication and transcription use the same mtDNA molecule as a template, therefore an increase in transcription could result in a decrease of mtDNA replication. Evidence against this comes from the observation that an increase in oxidative damage with age, leads not only to a decrease in mtDNA abundance but also a decrease in mRNA transcripts for COX3 and COX4 in the same individuals (Short et al., 2005). This suggests that transcription

is also down-regulated with an increase in mtDNA damage in these individuals. This is particularly relevant to the SN due to the high oxidative stress observed (section 3.1.3) which could result in the higher levels of mtDNA damage and decreased mtDNA replication observed via analogue incorporation.

III) MtDNA transport

Transport of mitochondria can also influence the mtDNA replication observed as recently replicated mtDNA molecules could be transported to other regions of the neurons not present within the focal plane, and hence the overall mtDNA replication levels could be effected. This could be particularly important in the SN, as between the IdU and CldU data, there are variations in the pattern of mtDNA replication (figure 3.20 and 3.21). This variation in mtDNA replication in SN was also observed with ageing, where all regions demonstrated a significant difference, however the SN displayed similar levels between young and aged (figure 3.22 and 3.13). This suggests that mtDNA replication could be increased in SN, but newly replicated mtDNA molecules are transported to distal regions at a faster rate and are hence, not available for interpretation. These variations are particularly interesting due to high mtDNA levels observed in this region, as these could lead to an increased demand for ATP in various regions of the neuron, hence transport could be increased to compensate for this demand. To further understand this process, the localisation of CldU and IdU incorporated molecules was also investigated (chapter 5).

IV) Mitophagy

The difference in the pattern of mtDNA replication in SN between the IdU (15 hours) and the CldU (5 days), and with ageing, could also suggest a variation in mitophagy. To model mtDNA degradation in this study, mitoQC mice were analysed (McWilliams et al., 2016). Preliminary data showed that SN neurons demonstrate higher levels of basal mitophagy compared to Purkinje neurons. Along with the previous finding of lower replication levels compared to Purkinje neurons, it could be suggested that in the SN, due to an increase in mitophagy, mtDNA are being degraded, and as a result mtDNA replication levels in the SN appear decreased, when measured using CldU incorporation compared to IdU. This could potentially suggest that mtDNA replication is high within the SN (as observed with the IdU data), but due

to increased mtDNA degradation over time, they appear to contain lower mtDNA replication. However, even with the IdU labelling, the cerebellum demonstrated higher IdU incorporation than the SN, therefore the mtDNA replication level is highest within the cerebellum at both times. Alongside this, it is important to consider that mtDNA molecules have been suggested to have a half-life of 6-31 days, which is particularly high in post-mitotic cells which fall into the longer values of the 6-31 range (Clayton, 1982, Gross and Rabinowitz, 1969, Korr et al., 1998). Recently analysis via stochastic computational models have suggested that the half-life is even higher (more than 31 days), when taking into account the levels of mtDNA mutation levels observed (Poovathingal et al., 2012). These suggest that the time point between the IdU and CldU is not sufficient to observe mtDNA degradation. Therefore, this would require further work.

3.5.7   *Future work*

Half of each brain from the mouse in this study was separated and frozen for molecular analysis. These can be used to laser-microdissect individual cells from different regions of the brain and analyse the level of total ΔmtDNA and copy number using quantitative real-time PCR Taqman assay (He et al., 2002, Russell et al., 2018). This would provide a better comparison of these parameters as this will be in individual cells, and also specifically correlated with CldU and IdU incorporation levels

As mtDNA replication is suggested to be not associated with ΔmtDNA from previous literature analysed in this study (figure 3.21), mtDNA repair needs to be analysed within different brain regions. Repair can be investigated in these tissues by transcriptomic or proteomic analysis to study the expression levels of various proteins involved in the repair pathway (table 1.1). The levels of these protein activity could also be vital to measure. This can be done by measuring mtDNA damage such as 8-oxo-dG in various regions of the brain. Transgenic mice with knockout of mtDNA repair genes such as OGG1 could also be utilised for this purpose (Yuzefovych et al., 2016).

A bigger sample set for the MitoQC mice including an ageing cohort would provide a more developed picture of how this process is effected in these tissue regions and ageing. This is

particularly important as this study observed a difference in mitophagy levels between the cerebellum and the SN.

Mitophagy, specifically in the mice brains used for this study, can be investigated. Protein expression could be measured by targeting for the lysosome markers such as anti-LC3II, anti-LAMP2A or anti-parkin. This, co-localised to a mitochondrial marker, could identify specific changes in the levels of mitophagy

Since it has been suggested that mtDNA has a half-life of 31 days, a longer time frame of labelling might produce results that are more representative. Since this has not been studied *in vivo*, this would require optimisation. Alongside this, previous literature has suggested that mtDNA replication only take ~75 minutes, hence this time frame is appropriate to study mtDNA replication.

Since transcription has been suggested to be one mechanism effecting the level of mtDNA replication, this required investigation. This could be done using transcriptomic studies to deduce the mRNA expression of various OXPHOS subunits in various tissues and deducing how this is altered in ageing.

3.5.8 *Final conclusion*

MtDNA replication as studied using thymidine analogue labelling shows significant differences between brain regions, with ageing and in the *PolgA$^{mut/mut}$* mice. Although variations were present, mtDNA replication generally demonstrated a decrease in regions associated with the highest levels of ΔmtDNA, suggesting that higher levels of mtDNA replication do not in fact correlate with high levels of ΔmtDNA. This was also demonstrated using data obtained from a previous study measuring ΔmtDNA in various regions of wildtype and *PolgA$^{mut/mut}$* mice. However, this could be due to the limitations as discussed. Alongside this, other factors such as mtDNA repair, transcription and mitophagy could also affect the overall process and would require further investigations.

Although no association between the mtDNA replication and mtDNA was observed, there were some reoccurring patterns that are important to consider.

Generally in regions with an increase in ΔmtDNA (such as SN compared to cerebellum, young mice compared to aged mice and wildtype compared to *PolgA*^{mut/mut} mouse), a decrease in CldU incorporation, and therefore mtDNA replication was observed. A number of alternative mechanisms have been suggested for this such as mtDNA repair, transcription, mtDNA turnover and transport into distal regions. These require further investigations.

As double thymidine analogue labelling was used, this allowed investigations of how mtDNA replication changed between two time points. This study demonstrated that there were difference in the pattern of mtDNA replication levels as notice with the CldU (4 days) and with IdU (~15 hours) particularly in the SN. SN was also differently effected with ageing compared to the other regions. Alongside this, quantification of mitophagy discovered increased levels within the SN neurons compared to cerebellum. All of these suggest a combination of effects that could result in the high levels of mtDNA observed in the SN, particularly in ageing.

Chapter 4: Optimising thymidine analogue labelling as a tool to assess the site of mtDNA replication in actively dividing cell lines

4.1 Introduction

4.1.1 *Thymidine analogues to study mtDNA replication*

Thymidine analogue labelling was a milestone in helping to understand the characteristics of mtDNA turnover. This technique was used initially on mitochondrial fractions *in vivo* to confirm that mtDNA does in fact replicate by incorporating nucleotides, similar to nuclear DNA (Karol and Simpson, 1968, Parsons and Simpson, 1967). BrdU was also used to initially determine that mtDNA replicates via a semi-conservative mechanism (Gross and Rabinowitz, 1969). Another study utilised buoyant density experiments to separate BrdU labelled mitochondria, which demonstrated the production of two species, one which represented unlabelled mtDNA (roughly 41.9mg/ml) and one which represented heavily labelled mtDNA (roughly 95.3 mg/ml). They also noticed a number of intermediate hybrids representing lightly labelled mtDNA. They thus concluded that mtDNA can be replicated multiple times or not at all at a specific time point (Flory Jr and Vinograd, 1973).

The time taken for mtDNA replication was studied using tritium thymidine and BrdU in a pulse chase manner (chase periods between 1.5-22h) on immortalised mouse cell lines (Bogenhagen and Clayton, 1977). They found incorporation of both analogues within the same mtDNA molecule at the shorter periods and concluded that mtDNA replication was 'quick' as mtDNA were labelled with both analogues after the first few chase time points. They also demonstrated that mtDNA replication occurs independently of the cell cycle since a constant fraction of mtDNA was labelled after each time point (Bogenhagen and Clayton, 1977). More recently, Davis and Clayton demonstrated BrdU incorporation into mtDNA in HeLa cells within 2 hours of adding the analogue (Davis and Clayton, 1996). This early incorporation of BrdU was due to thymidine-Kinase II (TK2) knock out, an enzyme responsible for thymidine synthesis specifically for the mitochondria (Johansson and Karlsson, 1997). They also agreed with the previous study that that mtDNA replication occurs independently of the nuclear

genome, since enucleated cells also showed BrdU incorporation into the mitochondria (Davis and Clayton, 1996).

Further experiments using post-mitotic myoblasts demonstrate that mtDNA replication did occur in post-mitotic cells, however this was suggested to be happening at a lower level as it took 16 hours to identify BrdU positive mtDNA in these cells, compared to 0.5-6 hours in HeLa cells (Magnusson et al., 2003). This was repeated by another study using embryonic chicken peripheral neurons (Amiri and Hollenbeck, 2008). They discovered that mtDNA replication occurred in both the cell body and axon of neurons. However, unlike (Magnusson et al., 2003), they noticed BrdU staining within the mtDNA from 3 hours. This was suggested to be due to more sensitive and robust techniques, such as an additional antigen retrieval step and HCl treatments to denature the mtDNA. A further study compared the level of BrdU incorporation (to investigate mitochondrial biogenesis) into mtDNA of primary neurons from wild type and amyloid beta precursor protein (AβPP) transgenic mice at two time points (4 and 20hours) (Calkins and Reddy, 2011). Their study demonstrated increased BrdU incorporation from 4 to 20 hours and interestingly the comparatively higher level of BrdU labelling occurred in the AβPP transgenic mice and when mitochondrial damage was induced in neurons with H_2O_2 and rotenone. This led them to conclude that the increase in BrdU labelling, and therefore mitochondrial biogenesis, was a compensatory mechanism in response to damage (Calkins and Reddy, 2011).

The studies mentioned in this section all used BrdU as a thymidine analogue; however, my study aimed to conduct pulse chase labelling to identify the turnover of mtDNA, hence double thymidine analogue labelling with CldU and IdU was used. BrdU antibodies have a lot of cross reactivity with CldU or IdU, because CldU and IdU are obtained from antiserum of rodents injected with BrdU. Hence, BrdU could never be used in conjunction with these analogues (Bianco et al., 2012, Asano et al., 2015). However, there is no cross reactivity between CldU and IdU, and both of these have been used in conjunction with each other in a number of studies (Tuttle et al., 2010, Schorl and Sedivy, 2007, Bulgar et al., 2013, Hirota et al., 2016). To further ensure a lack of cross reactivity between CldU and IdU in this study, the secondary antibodies were selected based on an additional purification step where they are subjected to a matrix containing potentially cross-reactive species that would bind any cross-reactive

antibodies. BrdU could be used in conjunction with EdU however, this would require two staining protocols using antibodies and a click reaction with fluorescence conjugated azide that could be detrimental to cell viability and multiple wash steps could affect the cell's adherence to the coverslips. Some studies have also highlighted cross reactivity between the BrdU antibody and EdU (Liboska et al., 2012).

Methods of thymidine analogue labelling have been used for many years, but more sensitive methodology development papers have been published very recently suggesting a need for better labelling techniques (Harris et al., 2018, Phillips et al., 2017). Combined with this, although many studies have used thymidine analogues to investigate mtDNA replication, none have attempted to quantify the site of mtDNA replication and the effect of mtDNA mutation on this.

This study aimed to optimise thymidine analogue labelling of cultured cells, including reprogrammed iPSCs and neurons with mtDNA deletions. This method will allow the site of mtDNA replication to be identified, as discussed in chapter 5. Initially optimisation will be conducted on HeLa cells. Although not post-mitotic, this would be a good model to use due to their quick doubling time and robustness. Since HeLa cells were used to optimise a method that can be modified for the iPSCs and neurons, this can be justified.

4.2 Aim and objectives

4.2.1 *Aim*

The aim of this chapter was to develop and optimise a method to label and visualise mtDNA replication and to use this to assess mtDNA replication levels in cells containing mtDNA deletions. This could be used to further shed light on deletion formation in various cell lines.

4.2.2 *Objectives*

The following objectives were fulfilled in this study;

- To develop a method of thymidine analogue labelling in HeLa cells

- To apply this method to reprogrammed iPSCs and differentiated neurons with mtDNA deletions

4.3 Methods

4.3.1 *CldU/IdU labelling*

Preparation of CldU and IdU working stocks is described in section 2.3.12. The cells were then subjected to IdU and CldU labelling (concentrations as optimised and mentioned in results (Section 4.4.2). After the initial addition of IdU and/or CldU, the cells were stored in an incubator at 37°C with 5% CO_2 allowing further growth and replication. The cells were fixed at various time points following the addition of the thymidine analogue labels. Cells were fixed using 4% paraformaldehyde (Santa-Cruz Biotechnology) for 20 minutes before washing with DPBS. Cells were immunofluorescently labelled as per the protocol described in section 2.3.6 to visualise the incorporated thymidine analogues. Anti-CldU (Novus biological) was produced using chemical BrdU as an immunogen. This antibody has a high affinity for CldU and no cross reactivity with thymidine or IdU according to the manufacture's protocol. Anti-IdU (BD Biosciences) was produced by using IdU as an immunogen, and therefore is not cross-reactive to CldU. Mitochondrial markers were also optimised along with their concentrations, details of this can be found in section 4.3.1. Images were acquired using a Zeiss axioimager M1 and Zen 2011 or Nikon confocal microscope and NIS elements at 40x magnification. The analysis of individual neurons and quantification of IdU levels are explained in detail in section 2.3.7.

4.4 Results

4.4.1 *Method optimisation – Mitochondrial markers*

Tom20, VDAC and anti-DNA antibodies have been previously discussed in section 3.4.2 as they were also optimised for use in the tissue study. Images of Tom20 and TFAM staining are presented in figure 4.1 and 4.2 respectively. TFAM has role in mtDNA maintenance, replication, transcription and packaging into the nucleoids, all of which is discussed in detail in chapter 1 (section 1.5). TFAM is found in abundance within nucleoids (Bogenhagen et al., 2008, Kaufman et al., 2007). Due to this location within nucleoids, it was selected as an

appropriate marker to normalise the thymidine analogue labels. Tom20 has also been described previously (section 3.4.2) and is a subunit within the TIM/TOM complex on the outer membrane of mitochondria and is involved in transport of proteins into the mitochondria.

For tom20, dilutions from 1 in 200 to 1 in 1000 were tried based on manufacturer's instruction and previous tissue study (section 3.4). 1 in 400 was identified as the optimal dilution and was carried forward and presented in all further figures. The tom20 staining (figure 4.1 and 4.2) was reliable with punctate staining around the nucleus, similar to that seen within tissue. For TFAM, dilutions of 1 in 100 and 1 in 200 were tried and the images from 1 in 100 are presented in figure 4.2. This antibody was punctate but the staining was not uniformly present within the cell co-localising with tom20 suggesting that a number of mitochondrion were not labelled. This could be an issue with the antibody, and only one type of TFAM antibody was used. A lower dilution might have also provided an increased region of positive staining, but could have also increased background staining. A reassuring factor is that most of the TFAM staining co-localised with Tom20.
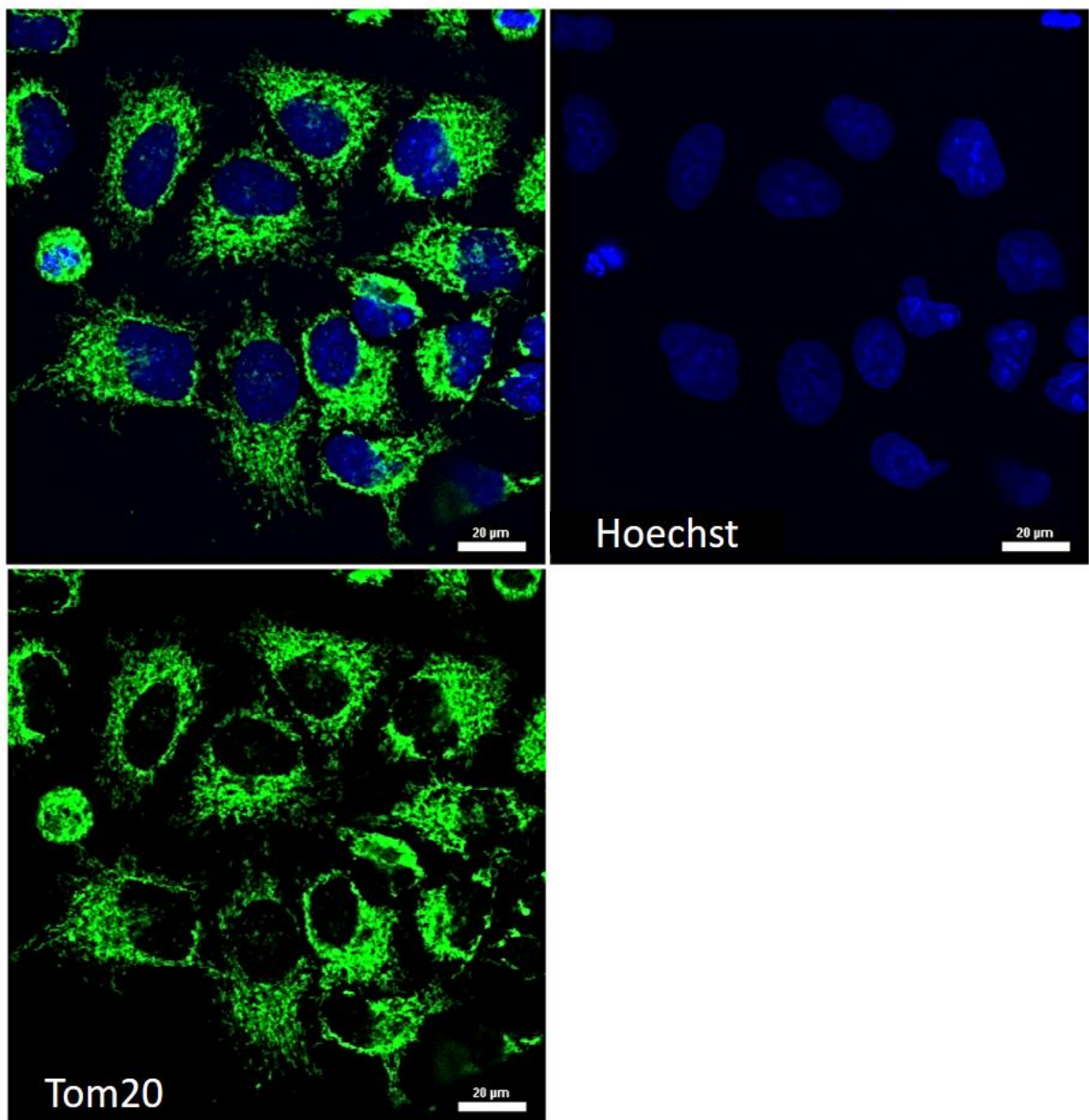
Figure 4.1 Optimisation of mitochondrial marker staining. This image displays staining with TOM20 with Hoechst staining nuclear DNA as observed in HeLa cells. The scale bar represents 20μM. The images were obtained at 40x magnification using Nikon A1R confocal microscope. Hoechst was imaged at 405nm and tom20 in 488nm.
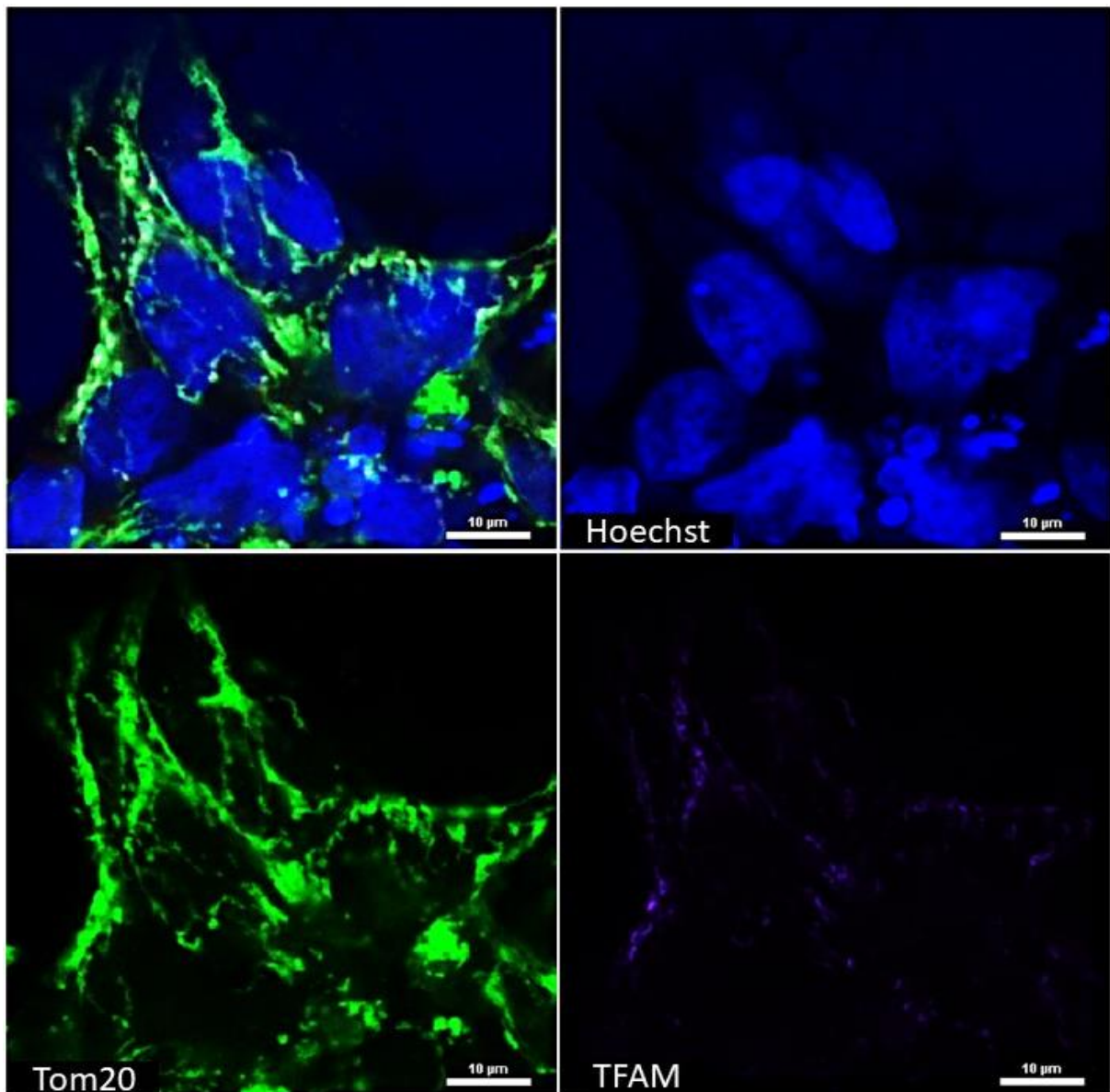
Figure 4.2 Optimisation of mitochondrial marker staining. This image displays staining of the mitochondria with tom20 and TFAM in iPSC stem cells. The Hoechst stains the nucleus. The scale bar represents 10μM. The images were obtained at 40x magnification using Nikon A1R confocal microscope and zoomed in to clearly visualise TFAM. Hoechst was imaged at 405nm, tom20 in 488nm and TFAM in 647nm.

The anti-DNA antibody (Merck Millipore) binds to double stranded DNA (dsDNA) with a very low affinity for single stranded DNA (ssDNA). It was initially produced using synthetic base pairs and calf thymus DNA as antigens (Ballard and Voss, 1985). This study also mentioned how the affinity for ssDNA was minimised by purifying using an ssDNA binding agarose, however according to the manufacturer's guidelines, there is still a 28% reactivity with ssDNA, making it less specific as it can also bind to mRNA within the cytoplasm. PicoGreen is a

fluorescent synthetic dye which is capable of binding to nucleic acids resulting in an increased fluorescent signal (Haugland et al., 1995). When compared to Hoechst, PicoGreen bound with same sensitivity to all the nucleic acids and is 400 fold more sensitive (Singer et al., 1997). This study also demonstrated that PicoGreen could detect small concentrations of DNA as little as 25pg/ml. It has also been used to label mtDNA in previously reported studies (Ashley et al., 2005, Ashley and Poulton, 2009, Tyynismaa et al., 2004).

The anti-DNA antibody (figure 4.3) and PicoGreen (figure 4.4) show similar nuclear staining as they both stain the same substrate. However, the PicoGreen did not produce any staining co-localised with the mitochondrial marker. The PicoGreen concentration was already optimised at 3µl of stock per ml (Ashley et al., 2005). The anti-DNA antibody was trialled at 1 in 100 and 1 in 200 dilutions. This was lower than previous studies as this was commonly used to detect nuclear DNA, and this study required mtDNA staining (Henault et al., 2012).

The anti-DNA antibody staining is saturated within the nucleus as the exposure time was set based upon the positive identification of any mtDNA signal which resulted in the nuclear DNA fluorescent signal often being more intense. One of the obvious problems with the two methods of detection was the nuclear labelling. The method of analysis developed at this point required a specific mitochondrial marker, and the nuclear staining could have effected that. However, this could have been overcome by setting a threshold and subtracting the nuclear staining based on the Hoechst staining. Alongside this, the nuclear staining was too saturated, especially for PicoGreen, which could result in a scattered light around the nucleus that might produce false positive mtDNA staining.
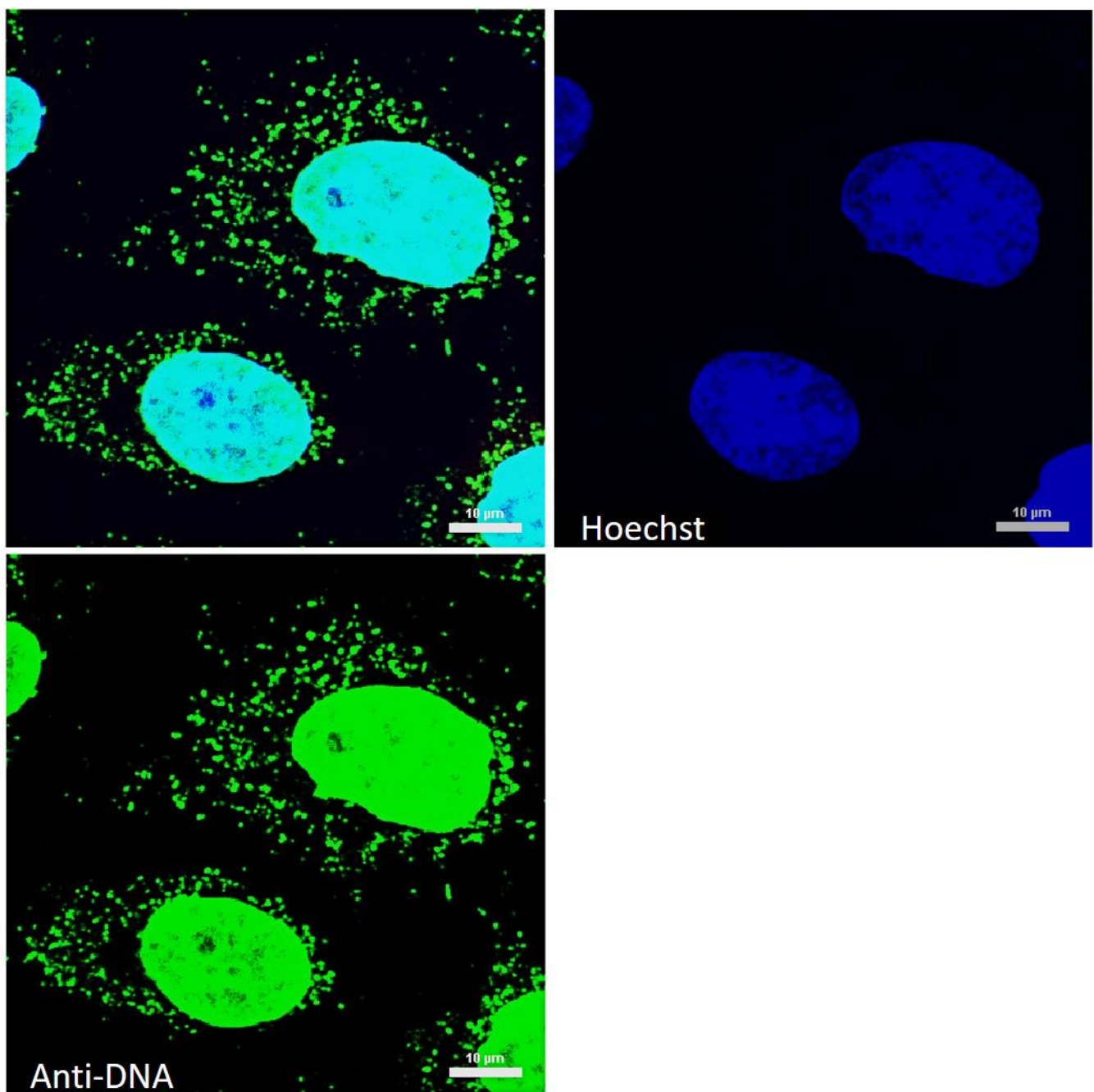
Figure 4.3 Optimisation of mitochondrial marker staining. This image displays staining of the nuclear and mtDNA with anti-DNA antibody in HeLa cells. Hoechst stains nucleus. The scale bar represents 10 µM. The images were obtained at 40x magnification using Nikon A1R confocal microscope. Hoechst was imaged at 405nm and anti-DNA in 488nm.
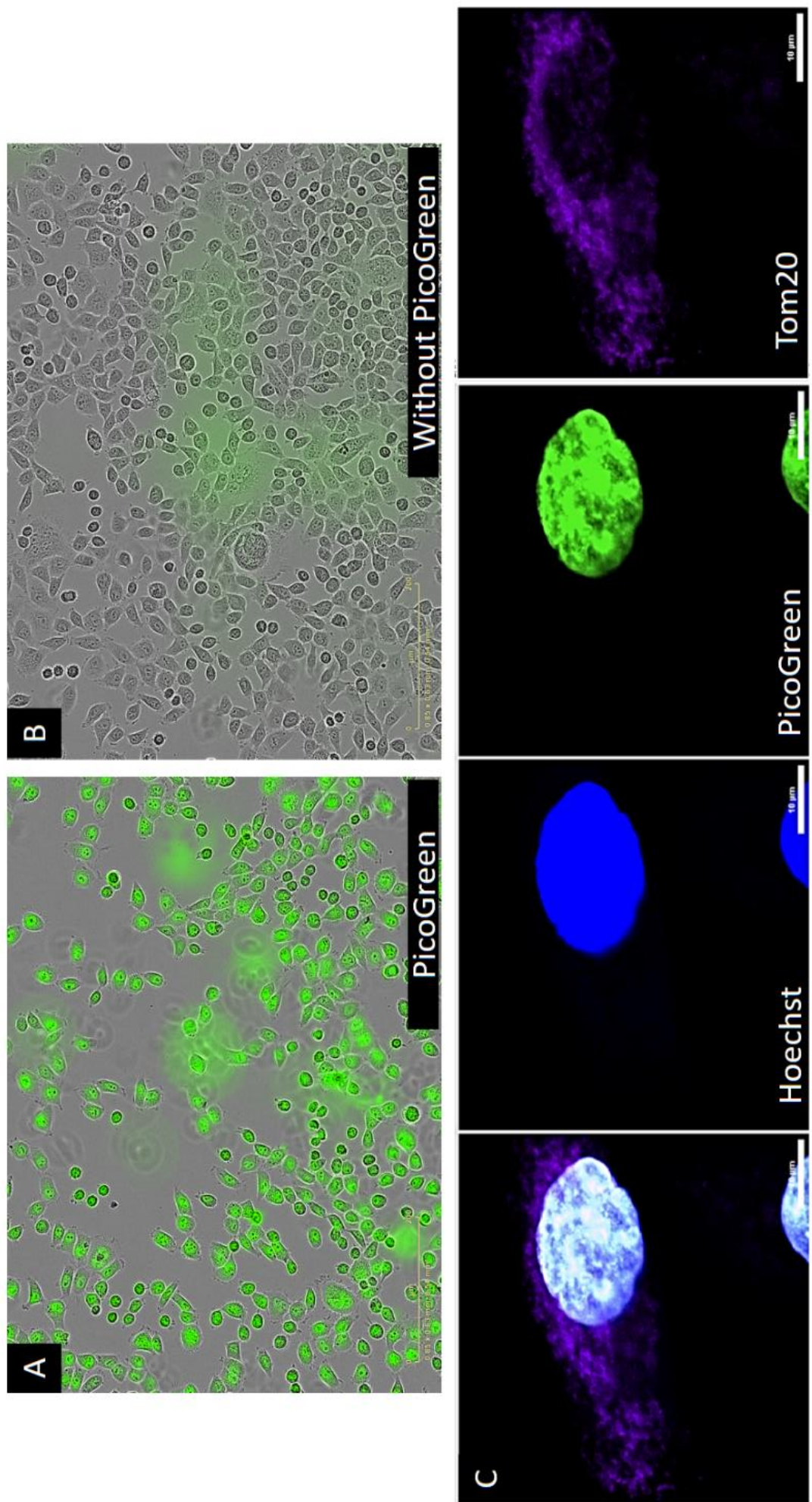
Figure 4.4 Optimisation of mitochondrial marker staining. This image displays staining of the nuclear and mtDNA with anti-DNA antibody in HeLa cells. Hoechst stains nucleus. The scale bar represents 10 µM. The images were obtained at 40x magnification using Nikon A1R confocal microscope. Hoechst was imaged at 405nm and anti-DNA in 488nm.

59

The next markers trialled were Twinkle and VDAC (figure 4.5). Twinkle is a mitochondrial helicase causing the mtDNA to unwind for replication (Korhonen et al., 2003). Although the protein has been identified as localising to the mitochondrial matrix and nucleoids, in this study, this marker appeared more nuclear, with limited punctate staining within the mitochondria (Spelbrink et al., 2001, Korhonen et al., 2004). Therefore, this was not considered an appropriate marker. The nuclear staining could be because the TWNK gene that codes for this protein in encoded in the nuclear genome, hence translated, and transcribed in the nuclear region before being transported to the mitochondria. The nuclear staining is present in abundance therefore this could also be due to any bleed through occurring from the other channels. However, a reassuring factor was that in areas within the cytoplasm that had positive staining for Twinkle, these foci co-localised nicely with the IdU suggesting that IdU was being incorporated into the mtDNA and that the staining was positive, as highlighted in the figure 4.5.

VDAC is also encoded by the nuclear genome however, it is specifically localised to the mitochondria. It is present on the outer mitochondrial membrane as is involved in the transport of proteins and other metabolites (section 1.2) (Shoshan-Barmatz et al., 2010). Two dilutions of this antibody were used; 1 in 200 and 1 in 500 were trialled based on previous work in our lab (Ahmed et al., 2017, Rocha et al., 2015). VDAC, similar to the *in vivo* staining (figure 4.1), produced very faint staining without any specific punctate foci. This antibody was also imaged in the 647 wavelength at which the laser-blocking filter in the Nikon A1R confocal system is not as efficient hence, some reflection is possible and since it is a higher wavelength, the theoretical resolution is also decreased according to the manufacturer. Alongside this, since the antibody has successfully stained mitochondria previously in our lab, the problem might lie with the protocol (Ahmed et al., 2017, Rocha et al., 2015). However, these studies were *in vivo* and this might require optimisation *in vitro*. Tom20 produced punctate staining therefore VDAC was not further optimised.

NDUFB8 (figure 4.6) was also considered as a mitochondrial marker. NDUFB8 is a subunit of NADH dehydrogenase (complex I), present within the inner mitochondrial membrane. This antibody has been previously used in our lab at a dilution of 1 in 100 (Ahmed et al., 2017, Rocha et al., 2015). NDUFB8 was a good marker since the staining was punctate and was visibly

specific. However, tom20 was still preferred due to a lower dilution and exposure time. The lower exposure time could be beneficial in reducing photo bleaching.

Mitotracker (figure 4.7) was the final mitochondrial marker trialled. This is a dye that is added to live cells, is taken up by mitochondria as a function of their membrane potential where it then accumulates. The concentration used was 50nM which was previously used for live cell imaging (Buckman et al., 2001, Dickinson and Chang, 2008). Mito tracker Red CMXRos was used specifically since the dye is stable upon fixation of cells. The Mito tracker stain was weak resulting in the requirement for a high exposure time. The staining also looks very perinuclear. There could abundance of mitochondria in the perinuclear region due to the presence of a number of nuclear factors required for mitochondrial functions, which could lead to the abundant staining in this area (Geisler et al., 2010, Psarra and Sekeris, 2008, Leigh-Brown et al., 2010). However this was not observed when other mitochondrial markers were utilised, hence could be false positive or nonspecific. Alongside this, staining was not punctate and was not considered further.

Since Tom20 showed punctate staining which was specific and accurately detected mitochondria, this was selected for further immunofluorescence experiments.
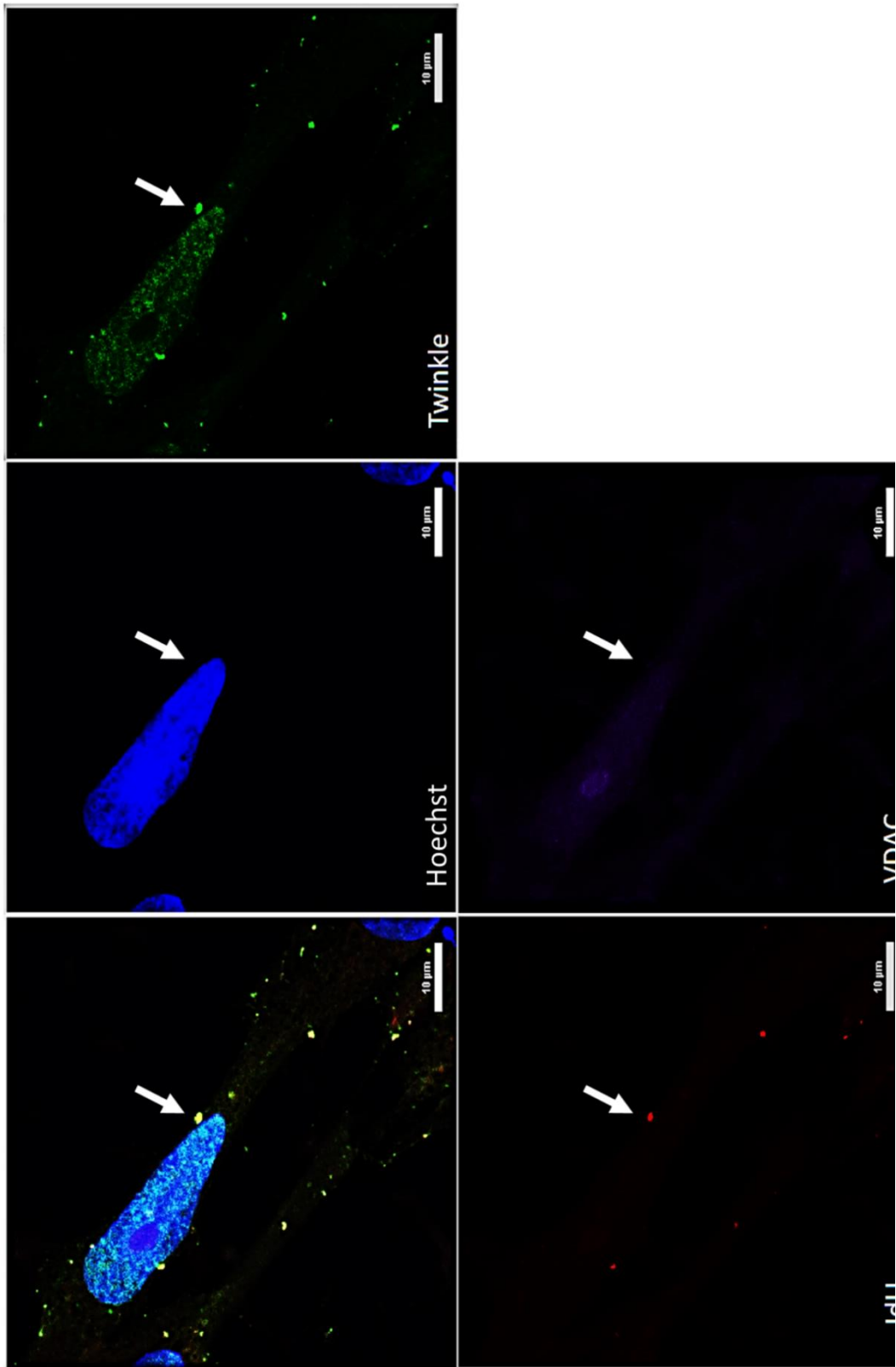
Figure 4.5 Optimisation of mitochondrial marker staining. This image shows Twinkle and VDAC staining alongside IdU staining in iPSC stem cells. Scale bar represents 10 µM. The punctate foci within the IdU channel also co-localised with the twinkle as highlighted by the white arrows. The images were obtained at 40x magnification using Nikon A1R confocal microscope. Hoechst was imaged at 405nm, twinkle in 488nm, IdU in 546nm and VDAC in 647nm.
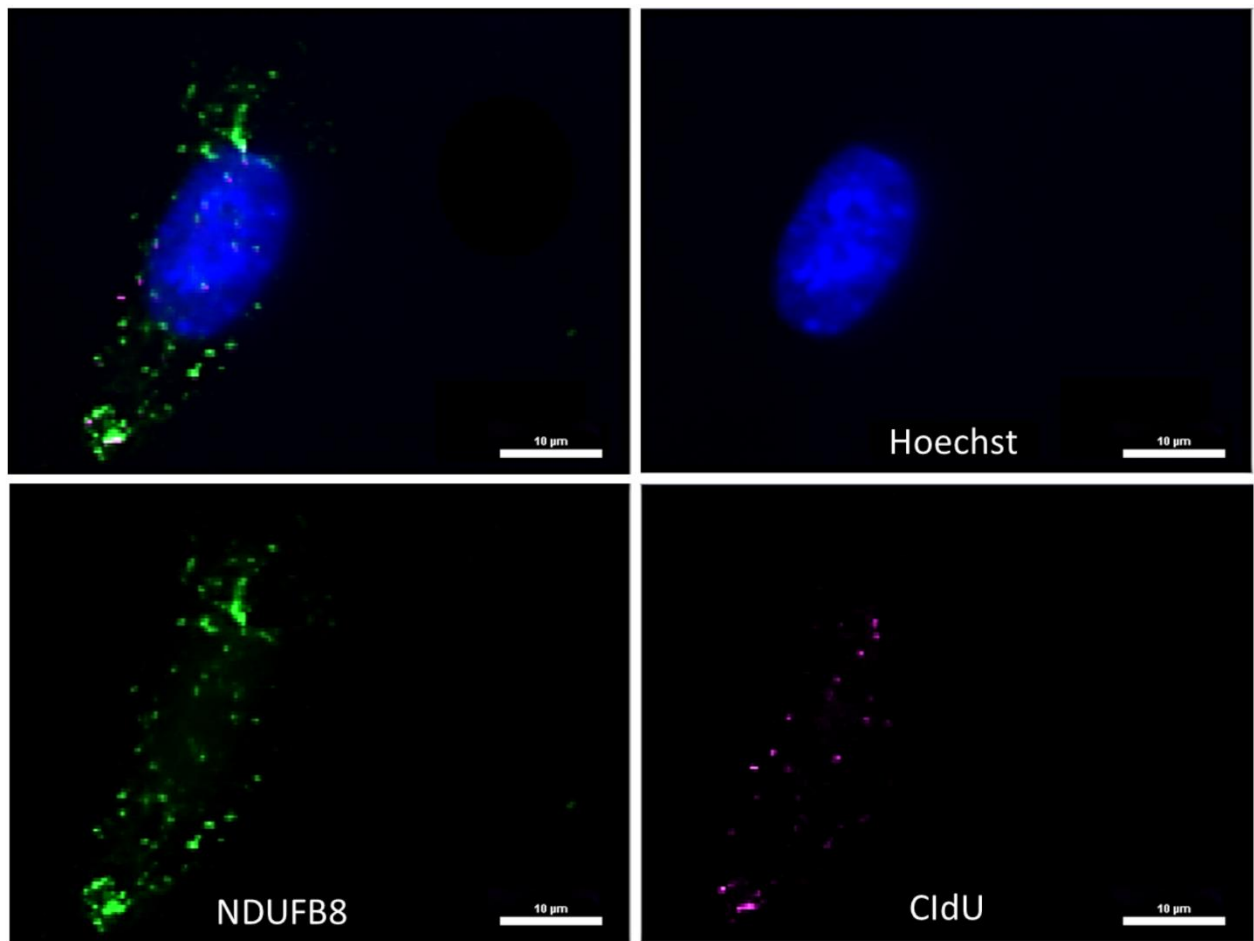
Figure 4.6 Optimisation of mitochondrial marker staining. This image shows NDUFB8 staining alongside CldU staining in iPSC stem cells. Scale bar represents 10 μM. The images were obtained at 40x magnification using Zeiss microscope. Hoechst was imaged at 405nm, NDUFB8 in 488nm and CldU in 647nm.
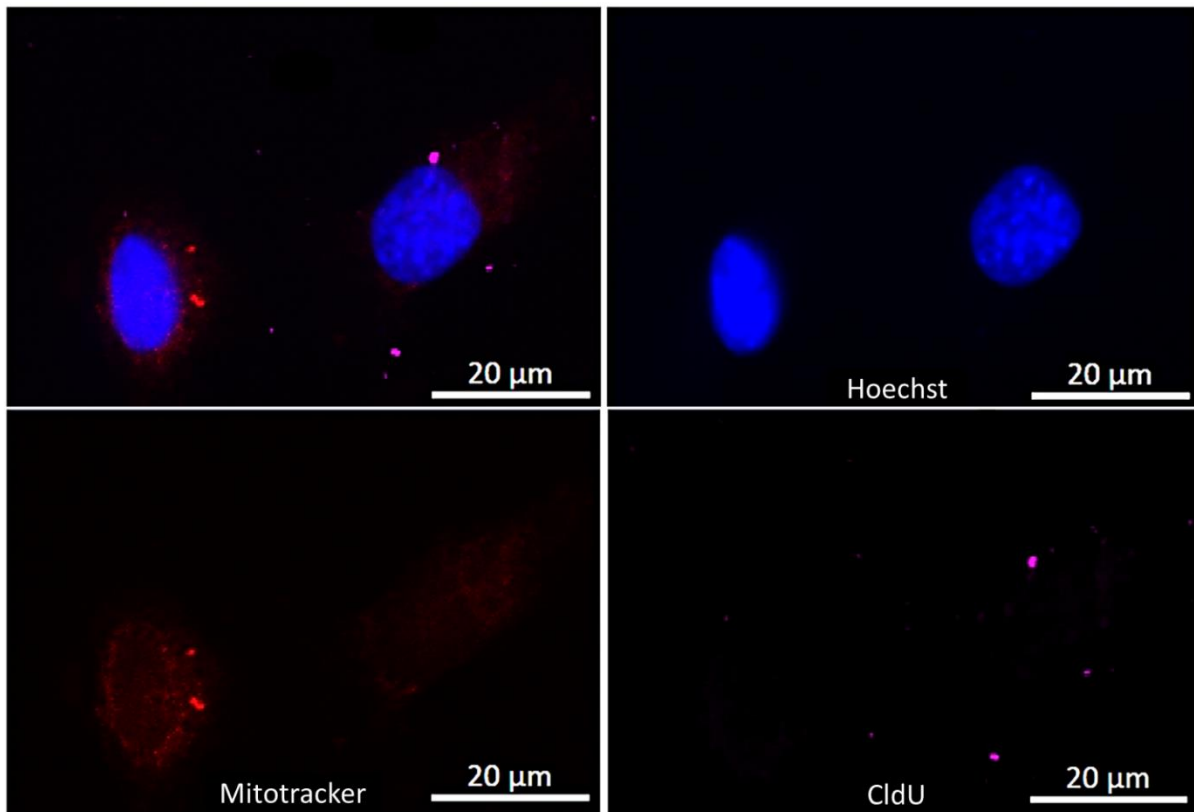
Figure 4.7 Optimisation of mitochondrial marker staining. This image shows Mitotracker staining alongside CldU staining in iPSC stem cells. Scale bar represents 20 µM. The images were obtained at 40x magnification using Zeiss microscope. Hoechst was imaged at 405nm, Mitotracker in 546nm and CldU in 647nm

Tom20 was selected due to uniform and punctate staining within cells (figure 4.1 and 4.2).

4.4.2 *Thymidine analogue concentration optimisation*

Previously, the combination of CldU and IdU for labelling has been used *in vivo* but their use *in vitro* is a very recent development where these analogues have been utilised to study the formation of the 'common' 4977bp mtDNA deletion (Phillips et al., 2017). However, the use of these analogues in the specific cell lines included in this study is novel. Due to this, further optimisation was required.

Initially, the concentration of the thymidine analogues used was based on previous *in vivo* experiments in this thesis (section 2.2.2) and previous literature that used BrdU labelling *in vitro* to study both nuclear and mitochondrial replication (Amiri and Hollenbeck, 2008, Calkins and Reddy, 2011, Davis and Clayton, 1996, Dimitrova and Gilbert, 1999, Magnusson et al.,

174

2003). All of these previous studies used 10-30µM to detect mtDNA replication. A concentration of 15µM was used initially for the optimisation of this study. This equates to 5.311µg/ml of IdU based on its molecular weight (354.10g/mol) and 3.94µg/ml of CIdU (molecular weight 262.65g/mol). Both thymidine analogues were added to the cells for 2-48 hours at time points 2-3 hours apart. Initially this lead to a high level of cell death in the HeLa cells, which was the most robust cell line used in this study (further details in appendix 8.1). Due to this, the concentration of the thymidine analogues required further optimisation. A concentration range from 3-60µg/ml was tested for each thymidine analogue however, a large amount of cell death (morphologically identified in figure 4.8) was observed with IdU labelling even at 3µg/ml (figure 4.9), and hence the concentration was reduced further to trial a range between 1-6µg/ml. The cells were labelled for 24 or 48 hours. Although the cell death was quantified, this was not representative of the images as many dead cells are removed during wash steps in IF, hence the total number of cells was used to quantify cell survival.
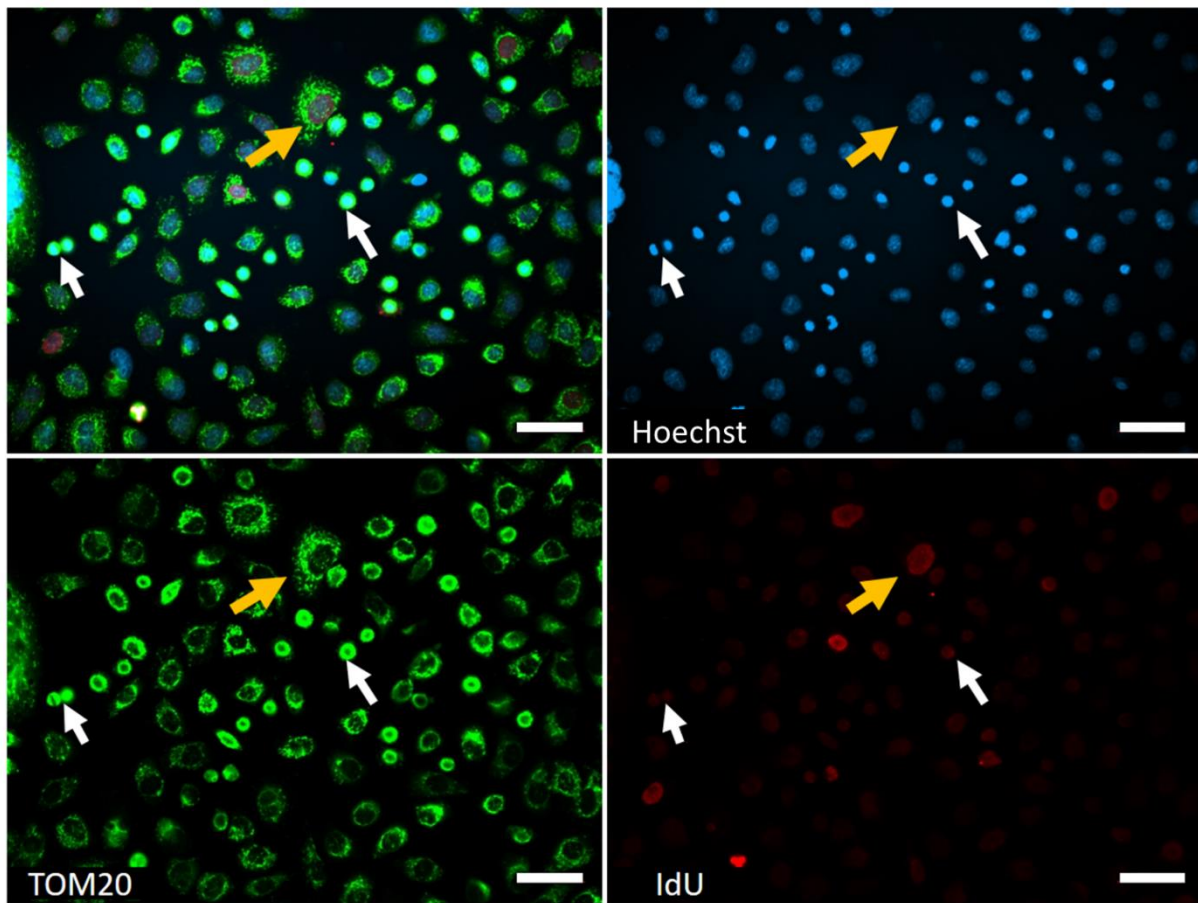
Figure 4.8 IdU staining of HeLa cells. Cell death was observed in most of the images with the treatment. The images above were taken of cells following dosing with IdU at a concentration of 2.5µg/ml. The white arrows highlight dead cells. These cells are identified based on their morphology and increased saturation compared to dividing cells due to perinuclear clustering as a response to damage. They also have a condensed nuclei and cell body and as a result, they appear round in shape at a much smaller size than a surviving cell highlighted by the yellow arrow. Actively dividing cells are identified via the incorporation the IdU into the nucleus. Scale bar is 50 µM. The images were obtained at 20x magnification using the Zeiss microscope. Hoechst was imaged at 405nm, Tom20 at 488nm and IdU at 546nm.

CldU and IdU labelling at various concentrations is presented in figure 4.9 and 4.10. The parameters analysed to identify optimum concentration were total number of cells and total number of cells with mtDNA incorporation of thymidine analogue (figure 4.11). In figure 4.9, the IdU labelling in HeLa cells is displayed at various concentrations. This shows that both nuclear DNA and mtDNA signal was faint at 2µg/ml, though the highest level of mitochondrial IdU signal was noticed at 2.5µg/ml. At high concentrations such as 6µg/ml, the majority of the IdU was incorporated into the nuclear genome. The higher concentrations were expected to have a higher level of mtDNA incorporation of the analogues since more analogue was available for incorporation; however, this was not the case. This could be because at higher

176

concentrations, despite an increased level of thymidine analogue incorporation into mtDNA, these concentrations had caused an increase in cell death (figure 4.8). The nuclear incorporation of CldU remained similar at all the concentrations trialled, however noticeable differences were observed in the number of cells incorporating CldU that co-localised with Tom20 (figure 4.10). An increase in the number of cells with mitochondrial incorporation was observed as concentration increased (figure4.11B).
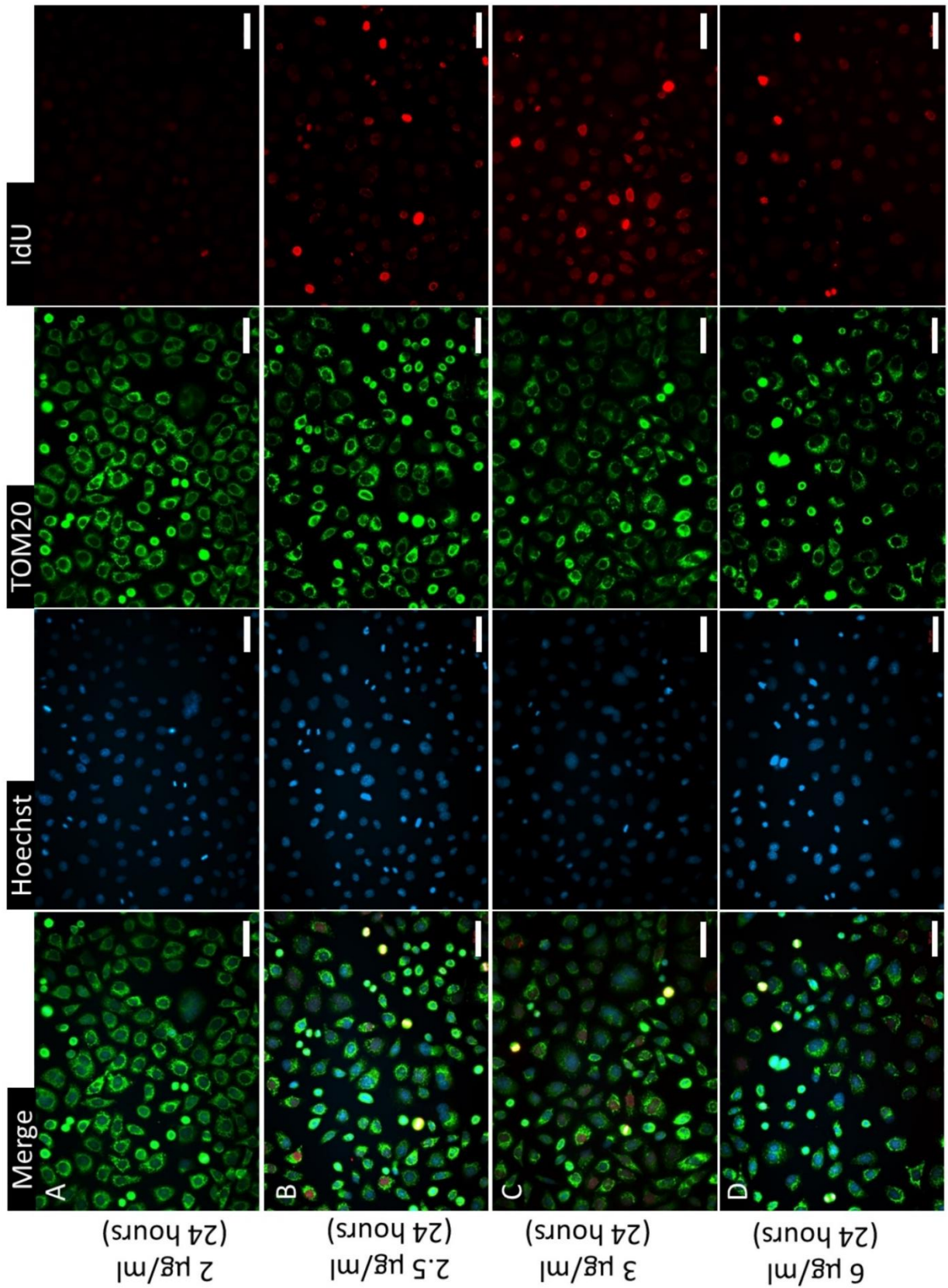
Figure 4.9 Optimisation of various IdU concentrations in HeLa cells. This image represents the level of IdU incorporated into the nuclear and mtDNA of the cells. The cells were subjected to 2µg/ml (A), 2.5µg/ml (B), 3µg/ml (C) and 6µg/ml (D). All of these were subjected for 24 hours. Scale bar is 50 µM. The images were obtained at 20x magnification using Zeiss microscope. Hoechst was imaged at 405nm, Tom20 at 488nm and IdU at 546nm.

Column headers (top to bottom): CldU, TOM20, Hoechst, Merge

Row labels: 3 µg/ml (24 hours), 6 µg/ml (24 hours), 30 µg/ml (24 hours), 60 µg/ml (24 hours)
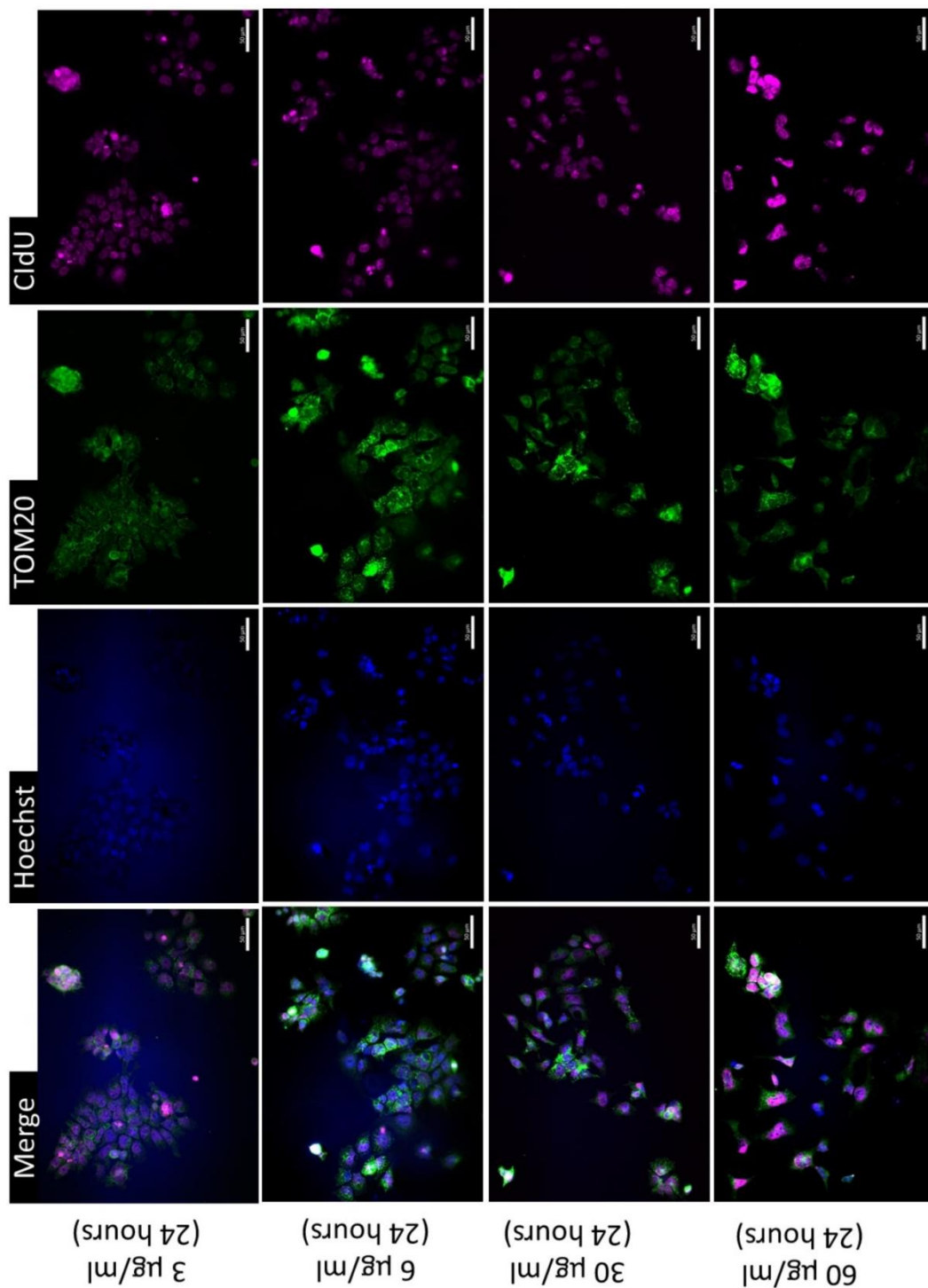
Figure 4.10 Optimisation of various CldU concentrations in HeLa cells. This image represents the level of CldU incorporated into the nuclear and mtDNA of the cells. The cells were subjected to four concentrations ranging from 2µg/ml to 60µg/ml as labelled in the images. All of these were subjected for 24 hours. Scale bar is 50 µM. The images were obtained at 20x magnification using Zeiss microscope. Hoechst was imaged at 405nm, Tom20 at 488nm and CldU at 647nm.

179

The effect of IdU and CldU concentration on thymidine analogues incorporation into the mitochondria for 24 and 48 hours is shown in figure 4.11. Graphs A and C in the figure represent the total cell count for IdU and CldU labelled HeLa cells. This was based on the total number of individual Hoechst stained nuclei in each image, as it includes all nuclei, this also accounts for the dead cells. The total number of labelled cells were higher in the IdU labelled group compared to the CldU. For the IdU labelled cells, there was a decrease in cell count after 48 hours incubation compared to a 24 hour incubation period. All the 24 hour concentrations were compared to the untreated control as the untreated was also fixed after 24 hours. For the CldU labelled cells, even the low concentrations had an effect on cell survival suggesting that the toxicity was high and maybe a lower concentration might be required. However, this would compromise the mtDNA incorporation of the thymidine analogue.

Figures 4.11B and 4.11D present the total number of cells at each concentration and time point that showed positive mitochondrial thymidine analogue staining which co-localised with the mitochondrial marker (Tom20, quantified using Image J (Fiji)). This did not include the dead cells due to difficulties in identifying nuclear or mitochondrial incorporated analogue as morphologically the cells appear condensed and hence were difficult to distinguish.

For CldU the maximum incorporation of the analogue, occurred at 3μg/ml and for the IdU, the maximum incorporation was equal at both 2.5μg/ml and 6μg/ml. For the CldU, the time points of 24 and 48 hours produced similar number of cells with incorporation into the mitochondria, except for the lower concentrations of 3μg/ml and 6μg/ml. There is an increase in mitochondrial incorporation of CldU at 48 hours because the CldU was available in the media for a longer time. This increase is not imitated at higher concentrations potentially due to toxicity as demonstrated by the decreased total number of cells. Similarly, at higher concentrations the level of IdU incorporation was much lower following 48 hours incubation compared to 24. Correspondingly, the total number of cells is also lower compared to 24hours suggesting a toxic effect over a longer incubation period. At concentrations lower than 2.5μg/ml, there were no cells showing positive staining for IdU within the mitochondria demonstrating this concentration was not adequate for mitochondrial staining.
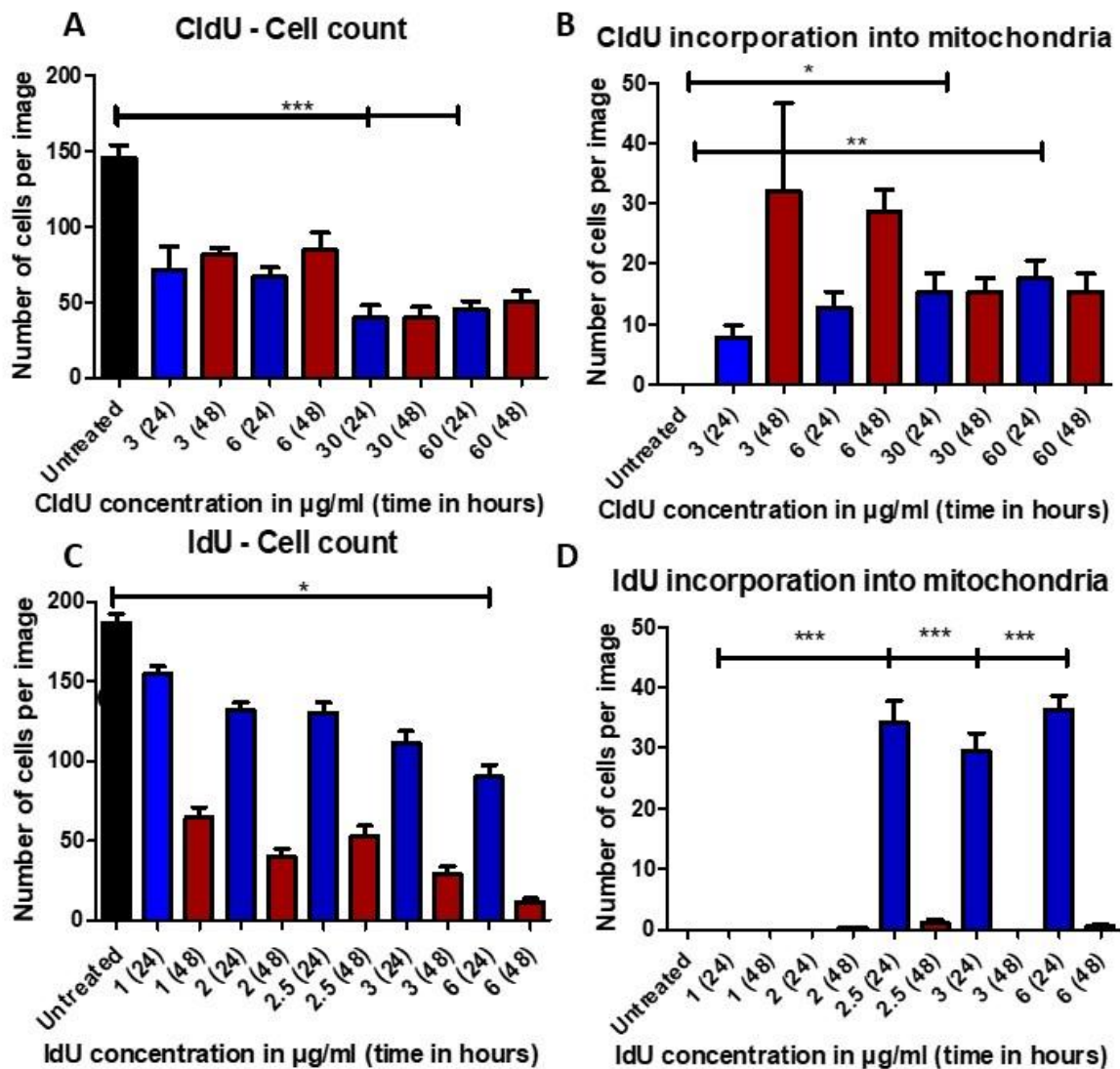
*Figure 4.11 Optimisation of CldU and IdU labelling in HeLa cells. Images A and B presents the total cell count per image for CldU and IdU respectively. Images C and D presents the total number of cells that incorporated each of the label into the mitochondria (co-localised with mitochondrial marker; Tom20). N=10 images for each thymidine analogue label. Significant differences were determined between the untreated cells and those cells incubated with CldU and IdU, * indicates p < 0.05, ** indicates p < 0.01 and *** indicates p < 0.001 obtained using one way-ANOVA.. As the untreated cells were fixed after 24 hours, the data from 48*

The optimal concentration was chosen as the concentration at which there was the highest amount of mtDNA incorporation of the analogue with maximum total number of cells (suggesting cell viability) compared to the untreated cells. For CldU labelling, an optimal concentration of 6µg/ml was chosen due to the increased mitochondrial incorporation and

181

without compromising the total number of cells. For IdU 2.5μg/ml was chosen for similar reasons. Since visualisation of the staining needed high resolution imaging to be able to distinguish mitochondrial structure and analogue incorporation, confocal microscopy was used for all future imaging (figures 4.12).

4.4.3 *Dual thymidine analogue toxicity*

After optimising the concentration of thymidine analogues, HeLa cells were labelled with IdU (pulse) for 24 hours followed by CldU for a variety of times ranging from 1-48 hours (chase) (figure 4.12). The combination of CldU and IdU labelling produced punctate staining at 40x magnification that co-localised with Tom20. A noticeable factor was that the level of cell death was still high. This was particularly visible when the thymidine analogues were incubated with cells for a longer time (figure 4.12B). Compared to row A, the cells appear to have a more condensed nucleus and cell body, with saturated staining suggesting high levels of cell death which was quantified (figure 4.13). Due to this, for all future analysis a single thymidine analogue label was used to minimise toxicity and cell death. IdU was chosen as the thymidine analogue to carry forward. This was because it showed a higher level of incorporation into the mtDNA compared to CldU (figure 4.12 and 4.13). The lower levels of CldU incorporation into mtDNA could be because of the toxicity. As seen in figure 4.11, the total cell count is increased in IdU labelled cells in comparison to CldU. Therefore, in the CldU experiments, the cells that have incorporated CldU could have detached from the surface, decreasing the total number of cells with CldU labelled mtDNA. This further favoured the use of IdU as it is better for cell viability.

182
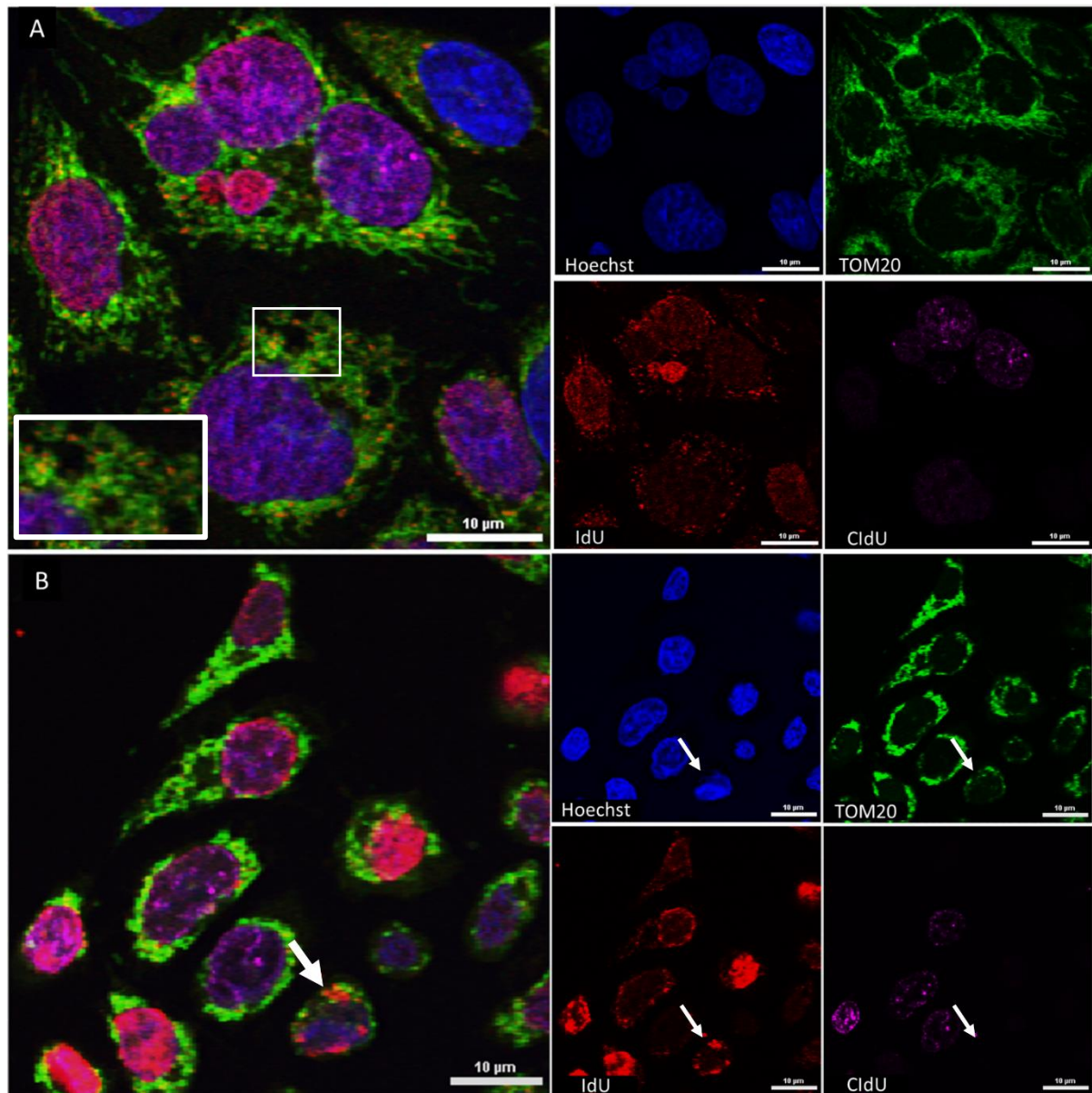
Figure 4.12 Images of CldU and IdU labelled HeLa cells obtained with confocal imaging. In image A the IdU was added and left for 24 hours, the cells were washed and CldU was added and left for 1 hour. In Image B, the same process as before, but the CldU was left for 24 hours. Dead cells are highlighted in image B with white arrows. Scale bar represents 10 μM. The images were obtained at 40x magnification using Nikon A1R confocal microscope. Hoechst was imaged at 405nm, Tom20 at 488nm, IdU at 546nm and CldU at 647nm.
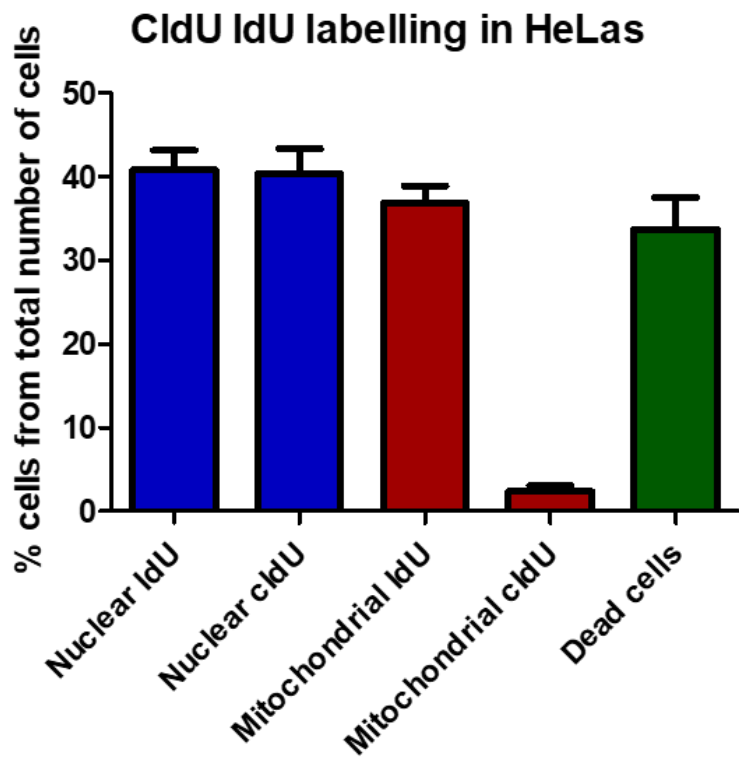
Figure 4.13 Graphical representation of the percentage of cells with nuclear and mitochondrial incorporation of thymidine analogues. The y axis represents the percentage of the total cells within an image that have incorporate the analogue in to the nuclear genome and the mtDNA, calculated from the total number of cells based on the Hoechst foci. The cells were labelled with IdU and left for 24 hours, the cells were washed and CldU was added and left for 24 hours. The differences are not statistically significant. N =73 cells.

4.4.4 *Reduction of IdU nuclear staining*

Following optimisation of the working concentration, IdU was added and the cells were fixed at various time points from 0.25-8 hours. One of the main issues of this experiment was the abundance of thymidine analogue incorporation into the nucleus (figure 4.11, 4.12 and 4.13). Since the nuclear DNA is much larger, when it is actively replicating, the majority of the IdU will be incorporated here limiting the IdU available for mtDNA, and increasing the concentration is not a viable option due to toxicity. Therefore, to halt nuclear genome

replication, aphidicolin (Sigma) was used. This is an antibiotic, isolated from *Nigrospora sphaerica*, that has been used in previous studies that utilised thymidine analogue labelling (Rodriguez-Acebes et al., 2018, Speit et al., 2016). Aphidicolin blocks nuclear DNA replication and repair, by inhibiting eukaryotic nuclear DNA polymerases of the B-family; Polα, Polδ, Polε and Polζ (Hanaoka et al., 1979). This is achieved by causing conformational changes to their active site by rotating the template guanine, which then blocks cytosine base pairs from binding (Baranovskiy et al., 2014). Aphidicolin does not inhibit mtDNA polymerase γ (Polγ), therefore although nuclear DNA replication is halted, mtDNA replication can continue. This inhibition of nuclear incorporation of thymidine analogues, allows their incorporation into mtDNA to be more easily visualised.

Based on previous literature, a stock of aphidicolin was made up in DMSO and used at a final concentration of 7μg/ml (Davis and Clayton, 1996). This study also found complete arrest of nuclear DNA replication occurred within 1-2 hours, therefore aphidicolin was added 3 hours prior to IdU labelling in this study, and was left in the media for the duration of the experiment until the cells were fixed (figure 4.14). In the cells untreated with aphidicolin, the majority of the IdU has been incorporate into the nucleus with a scarce amount of incorporation to the mtDNA. With aphidicolin treatment, there was no nuclear staining at all and an increased amount of IdU was incorporated into the mtDNA. Therefore, this step was added to the protocol. Following this, the cells were stained with IdU and fixed at 1 hour intervals until 48 hours. An preliminary analysis pipeline was also developed and presented in appendix 8.2.
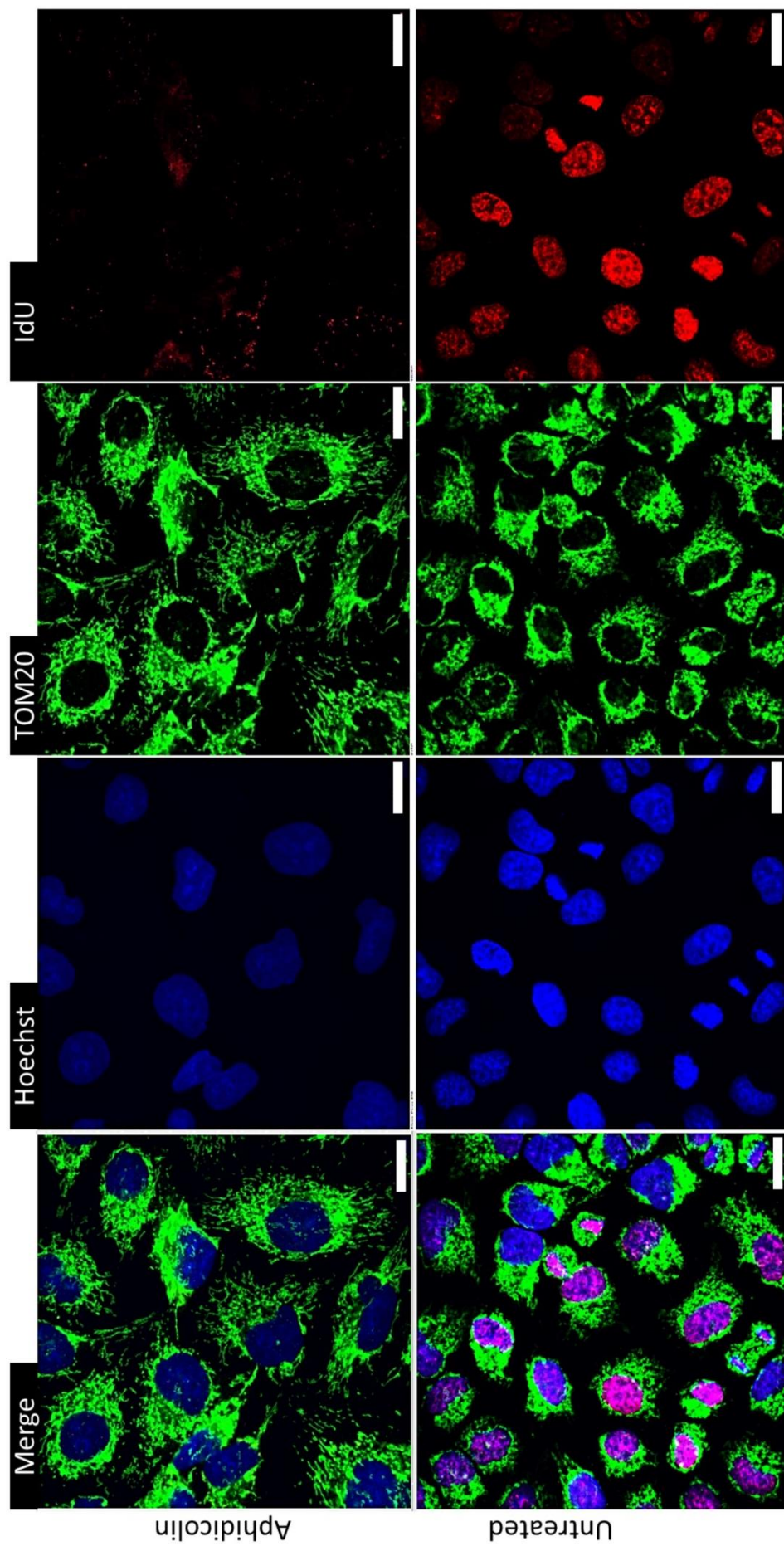
Figure 4.14 IdU incorporation into nucleus and mitochondria of HeLa cells with aphidicolin (7μg/ml) added cells and untreated cells as labelled. Aphidicolin blocks nuclear DNA replication allowing increased IdU incorporation within the mtDNA. The images were obtained at 40x magnification using Zeiss microscope. Hoechst was in wavelength 405, mitochondria is stained for with Tom20 and imaged at 488. IdU was imaged at wavelength 546. Scale bar represents 20 μM

4.4.5 *Thymidine analogue labelling in iPSCs and derived neurons*

Thymidine analogue labelling was also trialled on iPSCs and neurons reprogrammed from patient fibroblasts (Russell et al., 2018). This is because the overall aim of this thesis was to study mtDNA replication and how it is related to the high levels of mtDNA deletion that are detected in some neuronal populations with advancing age. During reprogramming into iPSCs, clones with varying levels of heteroplasmy were produced. This allowed the use of isogenic cell lines with varying levels of mtDNA deletion load. In this study, the cell line with high deletion (~40% deletion load) was used as a disease model and compared to a low deletion cell line (>10% deletion load) which acted as an isogenic control. These iPSCs were also differentiated into neurons to provide a model to investigate the correlation between mtDNA replication location and mtDNA deletion load within neurons in an *in vitro* setting.

The differentiation of the stem cells into neurons is described in section 2.3.7. A seeding density of $3x10^5$ was optimised for the stem cells and $5x10^5$ for the neurons per well. This was based on the cell viability within the time taken for this experiment. This seeding density is higher than the HeLa cells since iPSCs have a longer doubling time of 44 hours compared to 24.67 hours for HeLa cells (Boisvert et al., 2011, Takahashi et al., 2007). Both the stem cells and the neurons could potentially be more sensitive to thymidine analogue toxicity compared to the HeLa cells. This is because HeLa cells are able to tolerate mechanical disruption more and are also more adherent to the growing surface; hence, a higher seeding density was used to compensate for this. After labelling, IdU was successfully incorporated into the mtDNA of iPSCs (figure 4.15) and neurons (figure 4.16). The cells were fixed at intervals of 2 hour for 20 hours, and cell viability was noticed as being reduced at longer time points of incubation with the analogue. Figure 4.15 has cell lines from two different time points (8 and 10 hours), as this produced the high intensity staining with minimal cell death.
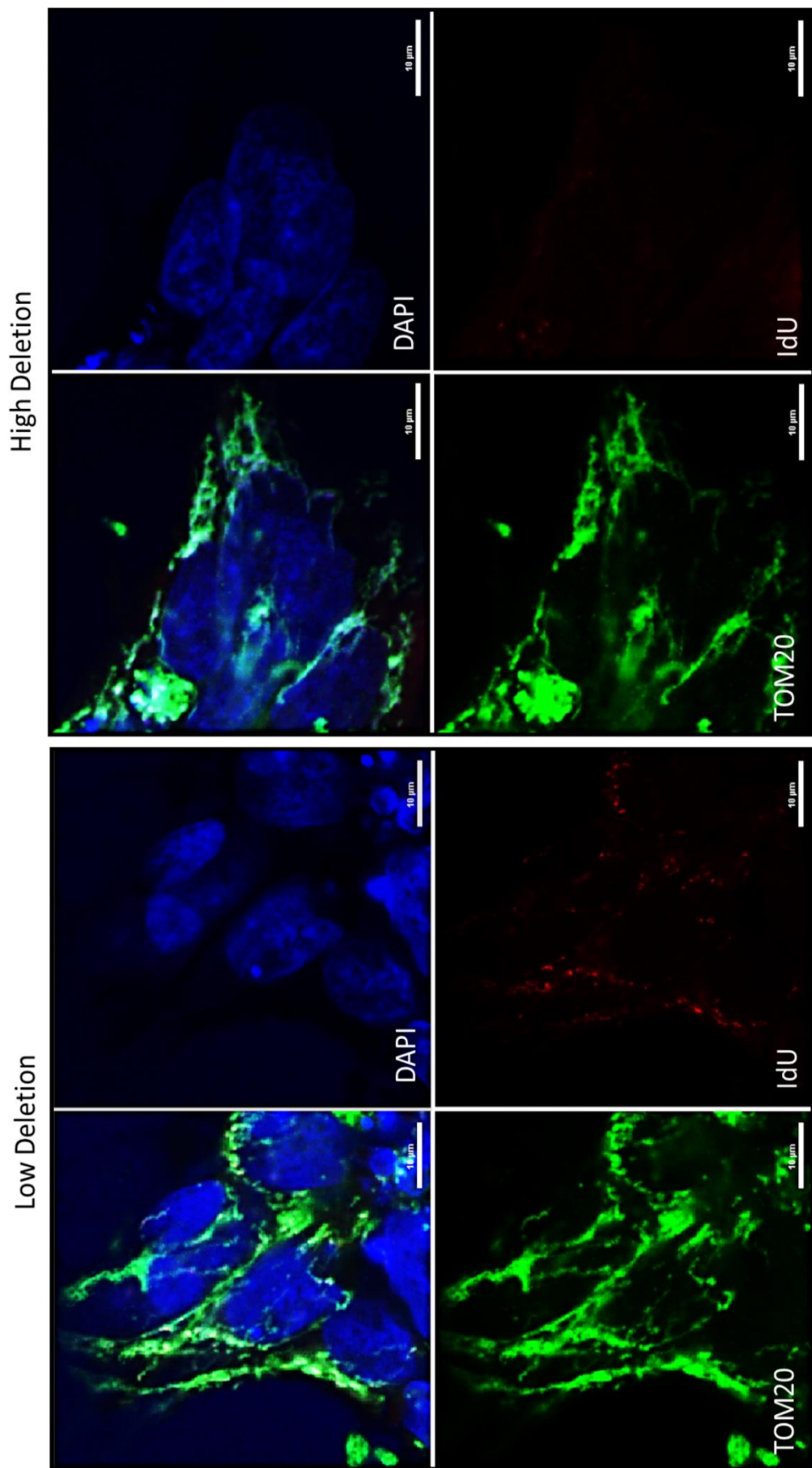
Figure 4.15 IdU labelled iPSC stem cells. The image presents the set of cells with a high deletion load at labelling time 8 of hours and the low deletion line at 10 hours. The images were obtained at 40x magnification using Zeiss microscope. Hoechst was in wavelength 405, mitochondria are stained for with Tom20 and imaged at 488 and IdU was imaged at wavelength 546. Scale bar represents 10 μM.
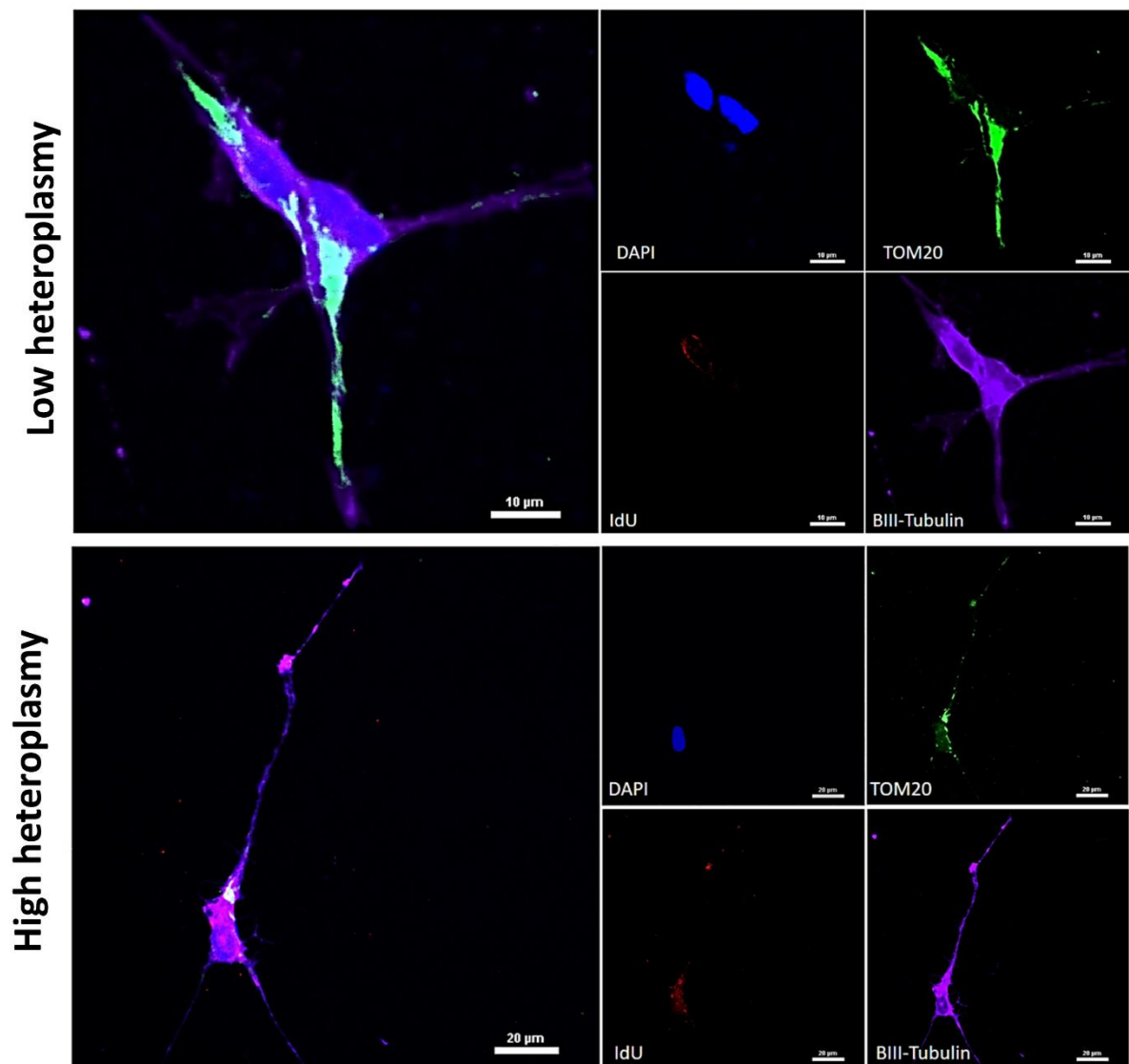
Figure 4.16 IdU labelled neurons. The image presents the set of cells with a high and low deletion load at labelling time 8 of hours. The images were obtained at 40x magnification using Zeiss microscope. Hoechst was in wavelength 405, mitochondria are stained for with Tom20 and imaged at 488 and IdU was imaged at wavelength 546, and the neuronal marker βIII-Tubulin in 647. Scale bar represents 20 μM.

4.5 Discussion

The key outcomes from this chapter are as follows;

- A model to label mtDNA replication *in vitro* and suitable analysis method for quantification of results were successfully optimised
- iPSCs and neurons were successfully labelled with IdU, which is novel

4.5.1 *Thymidine analogue labelling methodology*

The aim of this study was to develop a methodology to label mtDNA replication *in vitro*, which was successfully developed in the HeLa cells and carried forward to iPSCs and neurons. This was beneficial to deduce the location of mtDNA replication as reported in chapter 5.

One of the limitations of the technique is that the thymidine analogue competes with endogenous thymidine. TK2 is responsible for thymidine synthesis for mtDNA and knock out of this gene has been used in previous studies to halt thymidine production and ensure that endogenous thymidine is not available for mtDNA replication, ensuring complete incorporation of the thymidine analogues (Davis and Clayton, 1996). However, in this study, since this methodology was developed for use in various cell lines, genetic TK2 ablation was not feasible. Alongside this, TK2 mutations in humans have led to mitochondrial disease and mtDNA depletion, therefore this could affect the reliability of the result (Saada et al., 2001). Another option would be to use siRNA knockdown for TK2 which would give similar results to genetic knockout, however it is not as reliable either.

Another limitation is the use of single analogue. Initially a double thymidine analogue labelling with a pulse chase method was used, however due to reduced low cell viability, an individual analogue was used. A pulse chase method would have been beneficial in normalising any variation between cell lines or the different passages used to create a baseline of mtDNA replication. A methodology for mtDNA labelling with IdU and CldU *in vitro* was developed recently and the name 'mito-SMARD' (single-molecule analysis of replicating DNA) was coined (Phillips et al., 2017), however this requires further downstream processes and is not feasible for single cell. The combination of analogues in this study could have been optimised again

following addition of aphidicolin. In this case, a lower concentration of CldU and IdU could have been used and the combination of both of these might not have been toxic for the cells. This is a consideration for future work.

In addition, the thymidine analogue and the antibodies used could be additional limiting factors. In terms of the thymidine analogue chosen, the initial reason for using CldU and IdU instead of BrdU was because of its cross reactivity with the other analogues in terms of the antibodies, due to the structural similarities in the thymidine analogues. Another reasoning for the use of these specific analogues was because they were used in the *in vivo* study of this thesis (chapter 3); hence, this would offer continuity, allowing comparison between the projects. BrdU and EdU could also have been used in conjunction with each other, however this requires a more elaborate methodology as one analogues relies on antibodies for visualisation and the other on fluorescence conjugated azide (Liboska et al., 2012). However, since single thymidine analogue labelling was used, other analogues could have been trialled. EdU could have been optimised for visualising mtDNA replication as this protocol does not require the use of harsh chemicals and temperature for antigen retrieval (Haines et al., 2010a, Lentz et al., 2010). However, the HeLa cells in this study remained unaffected by the harsh chemicals, such as HCl, and the temperature used, further supporting the use of this analogue.

4.5.2 *IdU incorporation into iPSCs and neurons*

The use of a thymidine analogues on iPSCs and neurons reprogrammed from a patient fibroblast was novel. Previous studies that have looked at mtDNA replication in neurons *in vitro* have used primary cultured neurons from animals (Magnusson et al., 2003, Haines et al., 2010b, Calkins and Reddy, 2011).

As high cell death was also observed in the iPSCs and neurons, the methodology could be improved. Since the concentration was optimised in HeLa, they could potentially tolerate the mechanical disruption more, and are more adherent to the surface compared to the iPSCs and neurons. Hence, the concentration of the IdU used might need to be further optimised for the iPSCs and neurons. This is one of the steps for future work. All the previous studies *in vitro* that have used thymidine analogues have used HeLa cells or primary cell cultures and for a shorter length of labelling time (Amiri and Hollenbeck, 2008, Bogenhagen and Clayton, 1977,

Calkins and Reddy, 2011, Davis and Clayton, 1996, Magnusson et al., 2003, Phillips et al., 2017). Therefore, in these cases, the thymidine analogue might be tolerated due to this.

Another limitation is the longer doubling time of the iPSCs compared to HeLa cells (Boisvert et al., 2011, Takahashi et al., 2007). Even during culture, HeLa cells would reach 70% confluency by 2 days whereas iPSCs take about 4 days. This longer doubling time could indicate that the mtDNA turnover is happening slower and hence the time point studies might also require further optimisation. Alongside this, differentiated neurons are not dividing; hence, this turnover could be even slower in neurons. This is supported by *in vivo* data that studied the half-life of mtDNA in various tissues of rat using isotope thymidine (Gross et al., 1969). It was discovered that mtDNA has a half-life of 31 days within the brain compared to 6.7 days in the heart and 9.4 days in the liver. This is also supported by an *in vitro* study looking at an undifferentiated embryonic carcinoma cell line (Wang et al., 1997). They demonstrated that ethidium bromide at concentrations that induced damage in the undifferentiated cells, could not damage the neuronal cells differentiated from the same cell line. They concluded that this is due to the slow turnover rate of mtDNA in neurons, which results in the ethidium bromide not being incorporated into the mtDNA. Such evidence suggests that the technique is still sensitive but the timing needs optimisation.

4.5.3 *Future work*

The methods described in this chapter were carried forward to successfully label mtDNA replication and to examine the mtDNA replication levels and loci in multiple cell lines, however there are still ways in which this method could be improved. A few examples are listed below.

- Signal enhancers such as biotin and streptavidin, tyramine signal amplification or Image-It FX could be used to enhance the weak mtDNA signals. This could also result in using a reduced concentration of IdU that might increase the cell viability in iPSCs.
- Use digitonin prior to fixing cells. This is a detergent that solubilises the cell membrane as it binds to cholesterol and other β-hydroxysterols which are present in the plasma membrane, hence any non-specific incorporation into the cytoplasm will be removed with this was step (Smale, 2009).

- Optimise combined concentration of CldU and IdU after addition of aphidicolin.

- Optimisation of IdU concentration on iPSCs and neurons.

- To further test the methodology, cells with knock out Polγ could be used to observe if thymidine analogue is incorporated. Since is Polγ involved in both replication and repair, it should block total thymidine analogue incorporation.

- TK2 knock out HeLa cells could be used to identify if the pattern of labelling is similar.

- The cells could also be labelled with a different thymidine analogue such as BrdU or EdU to confirm the pattern of mtDNA labelling.

4.5.4 *Final conclusion*

Although the methodology has been developed to study mtDNA replication *in vitro*, this requires further improvements as suggested in the above sections. Use of this methodology on iPSCs and neurons were novel. The staining technique optimised here was used in experiments to study the localisation of replication in chapter 5.

Chapter 5:   Chapter 5: Investigating the localisation of mtDNA replication in neurons: Implications for mtDNA deletion formation and accumulation.

5.1   Introduction

5.1.1   *Is there a preferential location for mtDNA replication in neurons?*

While studies observing mtDNA replication have shown this process can occur in axons, the majority of mtDNA replication has been suggested to occur within the cell body (Amadoro et al., 2014, Amiri and Hollenbeck, 2008, Calkins and Reddy, 2011). Since the metabolic needs of the neuron are not uniform (Wong-Riley, 1989), mtDNA replication occurs in the perinuclear region of the cell, with mitochondria then transported into various regions, as and when required (Davis and Clayton, 1996, Chang and Reynolds, 2006). Initially studies on HeLa cells showed increased mtDNA replication in the perinuclear region using BrdU staining, which with time became present within the cytoplasm (Davis and Clayton, 1996), suggesting that mtDNA is replicated near the nucleus, and mitochondria containing these mtDNA molecules are then transported to peripheral regions. Studies have also visualised mtDNA replication in the axons of cultured primary neurons, however, this occurred at lower levels compared to the cell body (Amiri and Hollenbeck, 2008, Lentz et al., 2010, Calkins and Reddy, 2011). In fact 32.92% of cell body mitochondria showed BrdU incorporation, compared to only 0.22% of neuritic mitochondria (Calkins and Reddy, 2011). This perinuclear hotspot for replication is further supported by the fact that mtDNA replication depends on a number of proteins transcribed from the nucleus such as twinkle and Polγ (Young and Copeland, 2016). This is particularly important for neurons due to axon and dendrite length being a limiting factor for the interaction of nuclear encoded factors with distal mitochondria. Although studies have observed thymidine analogue labelling 2 hours after enucleation. Incorporation was possible since a full complement of nuclear encoded proteins would remain, as mRNA or protein turnover would take longer than 2 hours (Blomstrand and Hamberger, 1969, Koenig, 1958, Enríquez et al., 1996). Furthermore, PolγB has been found to be uniformly distributed within the cell body and neurites of differentiated SHSY-5Y cells (Magnusson et al., 2003). However, studies in SA15q-3 cells containing duplication of chromosome 15 (which encodes the catalytic subunit of Polγ) found that, despite an increase in Polγ protein expression, there was no

difference in mtDNA abundance. This demonstrated that the expression of Polγ is not associated with mtDNA abundance and suggests that it is not the rate-limiting factor in mtDNA replication (Schultz et al., 1998). This study also noted an abundance of mtSSB in the perinuclear region, supporting this as the location of mtDNA replication. MtSSB binds to the single strand template DNA during replication (section 1.5.1). Given the uniform localisation of PolγB (Magnusson et al., 2003) it could also be suggested that mtDNA replication may occur at multiple sites in the cell, although this does not oppose the cell body as a primary loci for mtDNA replication. However, PolγB is also required for the repair of mtDNA (section 1.5.1), hence the uniform localisation may reflect the repair of mtDNA in distal neurites and axons (Graziewicz et al., 2006). Studies have also shown the presence of ER within axons, which has the potential to translate proteins for mitochondrial biogenesis (Luarte et al., 2018). Alongside this, gene expression data has demonstrated that nuclear encoded mRNAs that target mitochondria were detected within the axons suggesting that mitochondrial proteins can be translated in distal axons (Willis et al., 2011, Spillane et al., 2013, Minis et al., 2014, Aschrafi et al., 2016, Shigeoka et al., 2018).

The detection of thymidine analogues within axons, suggests perinuclear mtDNA replication followed by transport to distal regions of the neuron (Davis and Clayton, 1996, Calkins and Reddy, 2011). Thus, it is important to differentiate between mtDNA replication occurring at these two regions. While this is technically difficult to do, Amiri and Hollenbeck (Amiri and Hollenbeck, 2008) attempted to study this by separating the cell body from the axon via axotomy and suspension of transport in dorsal root ganglia neurons. This study showed that following both axotomy and transport suspension (via vinblastine treatment), mtDNA could be detected in distal axons in intact cells, 12% of axonal mitochondria showed BrdU incorporation which dropped to 4% of mitochondria in separated axons. In vinblastine treated cells, 25% of axonal mitochondria showed BrdU incorporation compared to 43% in untreated cells. This suggests that mtDNA biogenesis and replication was not limited to the cell body. However as mentioned before, this suggests that mtDNA replication can occur in distal regions, but not that this is the primary location for it, as it occurs at lower rate compared to the cell body.

195

5.1.2 *How is mtDNA replication affected by mtDNA damage?*

It is important to understand how the localisation of mtDNA replication and biogenesis changes in response to mtDNA damage and mutations, as neurons are post-mitotic and acquire these with age and in various diseases (section 1.6.5). Increased distal mtDNA replication was observed after 1 week of exposure to rotenone (1nM), however after 2 weeks, this increase was also present in cell bodies (Van Laar et al., 2018, Arnold et al., 2011). Conversely, damage induced by rotenone and H_2O_2 (25nM of both), was found to increase BrdU incorporation in the cell body, which was decreased in neurites compared to untreated controls (Calkins and Reddy, 2011). They also compared wild type mice to AβPP mice (model for AD by overexpressing the Aβ protein), which further demonstrated an increase in BrdU incorporation within the cell body of neurons, although there was a decrease in BrdU incorporation within neurites. This seemed to suggest that in the presence of stressors, there was a decrease in mtDNA replication in distal regions. This is contrary to the studies mentioned above. However it could be suggested that this is because the BrdU treatment lasted a maximum of 20 hours in the Calkins and Reddy study and lasted for up to 2 weeks in the previous study (Van Laar et al., 2018), therefore transport of mitochondria over time could affect the results.

5.1.3 *Significance of this study*

Although still inconclusive, the majority of the studies mentioned above suggest that mtDNA replication within a neuron occurs perinuclearly or in the cell body, with data showing a decrease in BrdU incorporation with increasing distance from the nucleus (Calkins and Reddy, 2011). This is also the same situation for mitochondria targeted for mitophagy, where data shows that such mitochondria are transported in a retrograde direction back into the cell body to be degraded (Sheng and Cai, 2012). Both replication and mitophagy could occur here due to the reliance of both of these processes on nuclear encoded factors. Based on this evidence, it could be suggested that the cell body is the primary location for mtDNA biogenesis and quality control of damaged mitochondria, suggesting that they both happen simultaneously and in close proximity to each other which could be beneficial in understanding mtDNA deletion formation. Due to this, it could be hypothesised that this increases the probability of

a damaged mtDNA potentially being replicated, and as a result, an increase in ΔmtDNA levels (figure 5.1).
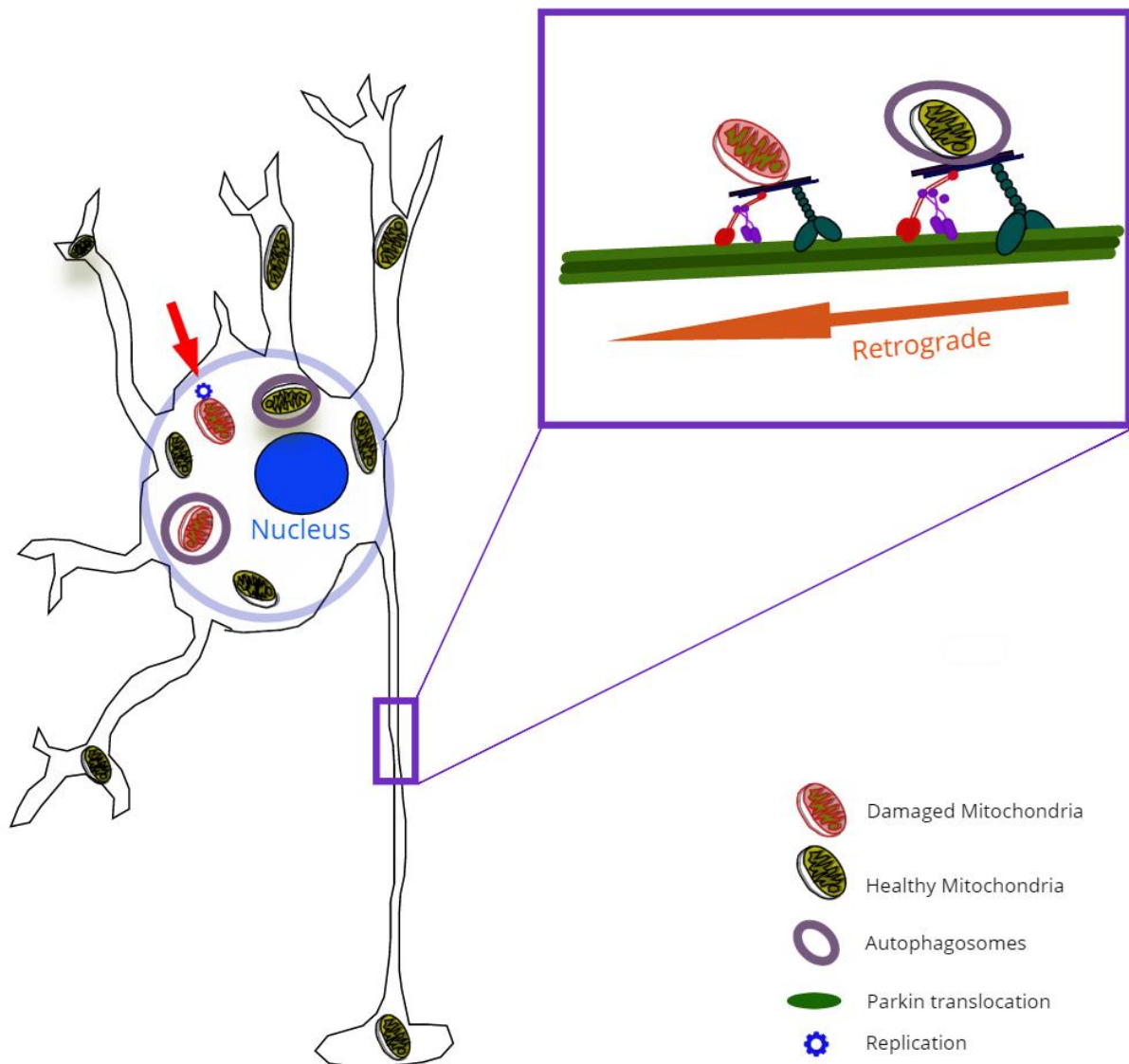
Figure 5.1 This figure presents the prime loci of mtDNA replication and mitochondrial degradation via mitophagy based on the current literature. Damaged mitochondria are targeted and transported in a retrograde direction back towards the nucleus, and cell body has been identified as the prime location of mtDNA replication suggesting that both processes happen in close proximity to each other. The transparent blue circle suggests the 'hotspot' where mtDNA replication and mitophagy is occurring. The red arrow points to a damaged mitochondria-undergoing replication.

As discussed previously (section 1.6.5), neurons have a high energy demand and with ageing also show an increase in ΔmtDNA load. Since the formation of these deletions and their accumulation to high levels is still debated, it is important to identify any alterations in mtDNA replication that could explain the high levels of deletion observed. Subsequently different regions of the brain have varying levels of ΔmtDNAs (table 3.1 and 3.2), therefore it is important to understand how this perinuclear 'hotspot' could differ between different regions to investigate any relationship with ΔmtDNA. The study of mtDNA replication localisation in various regions of the brain is novel.

This study aimed to understand the location of mtDNA replication in terms of distance from the nucleus. This would corroborate previous findings that suggest that the cell body is the primary loci for mtDNA replication, with minimal replication occurring in the distal regions of the neuron. CldU and IdU incorporation was used to quantify mtDNA replication in a transgenic mouse model with a mutation in Polγ (section 2.2.1) (Kujoth et al., 2005). Therefore, this model is an adequate model for studying the effect of mtDNA mutation on the location and rate of mtDNA replication. Using these four groups of mice; wildtype young, wildtype aged, $PolgA^{mut/mut}$ young and $PolgA^{mut/mut}$ aged provided information on how mtDNA replication loci change might change with advancing age and replication defects.

5.2 Aim and objectives

5.2.1 *Aim*

To identify the primary loci for mtDNA replication in neurons, in various brain regions, and to deduce how this is altered in the presence of mtDNA mutations and ageing.

5.2.2 *Objectives*

The objectives of this study were;

- To optimise analysis to identify mtDNA replication loci within a single cell
- To compare mtDNA replication loci in different neuronal subtypes
- To compare mtDNA replication loci between young and aged mice

- To compare mtDNA replication loci in neurons between WT and *PolgA^mut/mut* 'mutator' mice

5.3   Methods

5.3.1   *In vivo analysis of mtDNA replication*

For details regarding the mice used, regions selected, confirmation of brain regions, identification of a specific subset of neurons via immunofluorescence, antibodies used, CldU/ IdU labelling in mice and visualisation via immunofluorescence and microscopy, refer to chapter 2 (section 2.2) and chapter 3 (section 3.2 and 3.3, table 3.3 and 3.5).

5.3.2   *In vitro analysis of mtDNA replication*

For details regarding the cell line used, cell culture techniques, differentiation of stem cells into neurons, IdU labelling and visualisation via immunofluorescence and microscopy, refer to chapter 2 (section 2.3) and chapter 4 (section 4.2 and 4.3).

5.3.3   *Analysis of mtDNA replication loci*

Confocal images were analysed in Image J (Fiji). The images were converted to a TIF format with a different image for each channel. The cell boundary based on the mitochondrial marker channel (tom20) was used to represent the cell area. The 'straight' line tool was used to draw a straight line through the cell (figure 5.2). If a straight line did not follow the trajectory of the neuron, multiple straight lines were drawn and presented as a single line. The spread of intensity for tom20 along each pixel of the line is produced as a histogram using the 'plot profile' function within the analyse option. The line drawn on the tom20 channel is then saved using the 'ROI manager' function in the 'tools' option of the 'analyse' option. This line is then added to the image for the Hoechst channel (nuclear marker) and IdU channel (mtDNA replication marker), and a spread of the intensity for each channel is produced using the 'plot profile' function. The values from the histogram are exported into Excel (Microsoft). The highest point of Hoechst intensity is then identified and this point is set as the middle of the cell or '0' on the X axis (graph in Figure 5.2), which measures distance from the nucleus in pixels. This is because the highest point of Hoechst often produces a precise estimate of the

middle of the nucleus. In addition to this, the average diameter of the nucleus was obtained from these images and the final graphs were adjusted for this.

The values of CldU and IdU are expressed as a ratio of the tom20 sign al to normalise the quantification of thymidine analogue incorporation. The spread of CldU or IdU values along the X axis or distance in pixel, in relation to the perinuclear region can then be identified. Multiple plot profiles were obtained from a total of at least 10 images from all the different mouse groups. The total number of neurons per region is presented in table 5. The number of neurons are different to chapter 3, as this study required identification of axons and dendrites which were not always visible in each analysed image.

Age/Genotype	Region	Number of mice	Number of neurons
WY	CER	4	12
WY	SN	2	11
WY	COR	4	31
WY	HIP	3	21
PY	CER	4	22
PY	SN	4	27
PY	COR	2	26
PY	HIP	1	21
WO	CER	4	14
WO	SN	3	27

WO	COR	4	26
WO	HIP	4	21
PO	CER	4	16
PO	SN	3	27
PO	COR	4	28
PO	HIP	1	11

Table 5.1 The total number of mice and neurons analysed per each age/genotype and region.

5.3.4 *Classification of perinuclear and distal regions.*

Since the aim of this study was to understand the location of replication, it was important to classify the perinuclear and distal regions in order to quantitatively compare them. For this purpose, the radius of the nucleus for each group was measured and used to create a perinuclear region that starts from the value '0', following on from this, any values 2 standard deviations from this was classified as distal (Figure 5.3). This was done to avoid any overlap between the regions and to truly make sure we were classifying two separate regions. Due to its length, the full extent of the neuronal processes are generally not present within the same section as the cell body, therefore the 'distal regions' usually describes the initial lengths of the processes. However, this region is still 2 standard deviations from the perinuclear region.
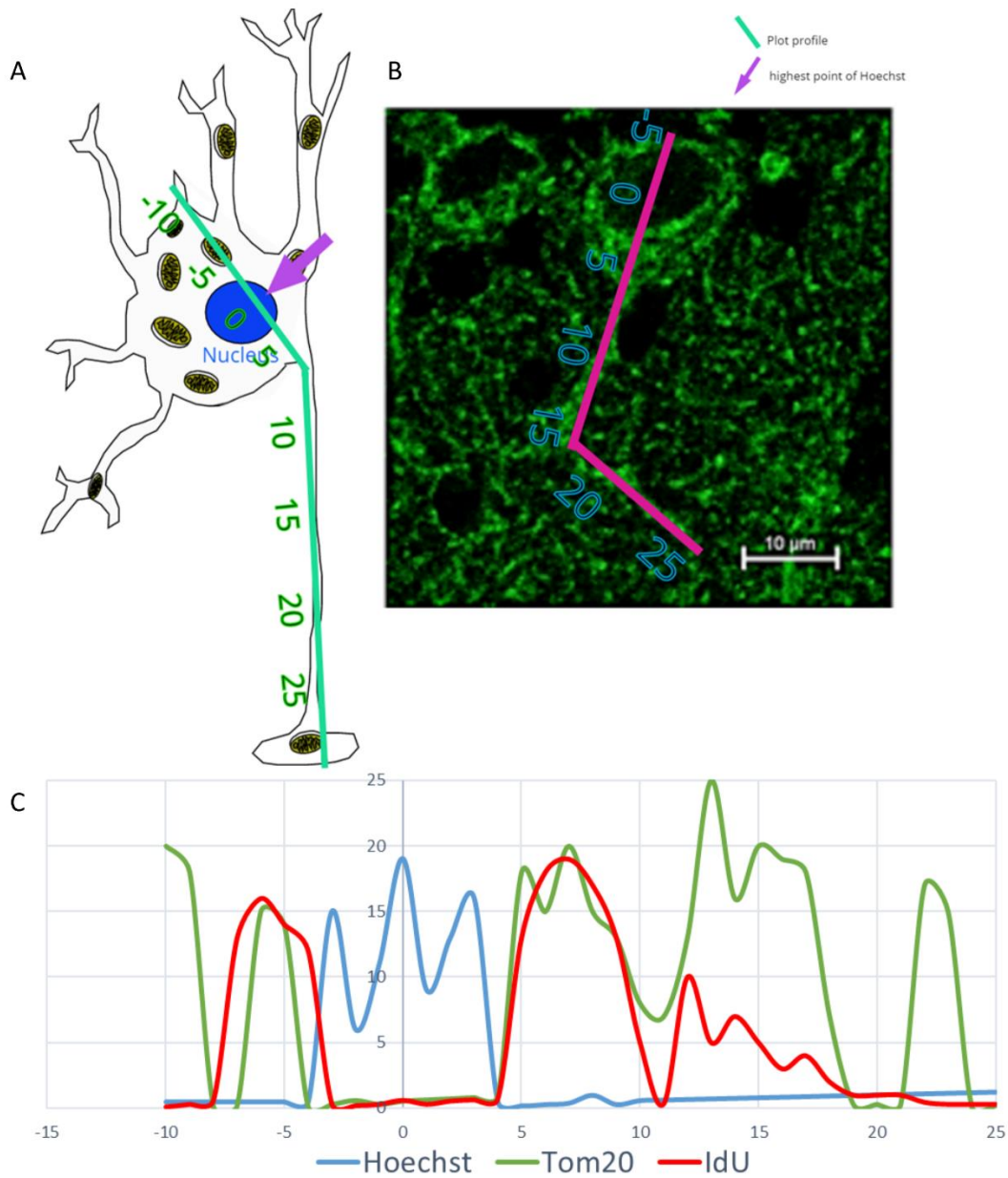
Figure 5.2 Simplified cartoon of the analysis pipeline. A) This image presents a neuron, and as mentioned in section 5.2.3, a straight line is drawn through the cell (green line in cartoon, pink line in image). Using the plot profile function, this intensity of each pixel along this line, from each channel can be measure. The highest intensity of Hoechst is identified and set as the middle of the cell by setting that value as '0' on the x axis which measures distance in pixels. The distance to the left side of the cell is identified with values from '-1' onwards till the end of the line which is '-10' in this case and vice versa, the right side of the cell is also identified with a value from '1' until the end of the cell which is 25 in this case. B) Presents the method described in A but on one of the Purkinje cells used in this study. C) The graph produced from the histogram is represented on the X axis of the graph in the image. The tom20 and IdU intensity can also be measured along this line and is plotted on the included representative graph.
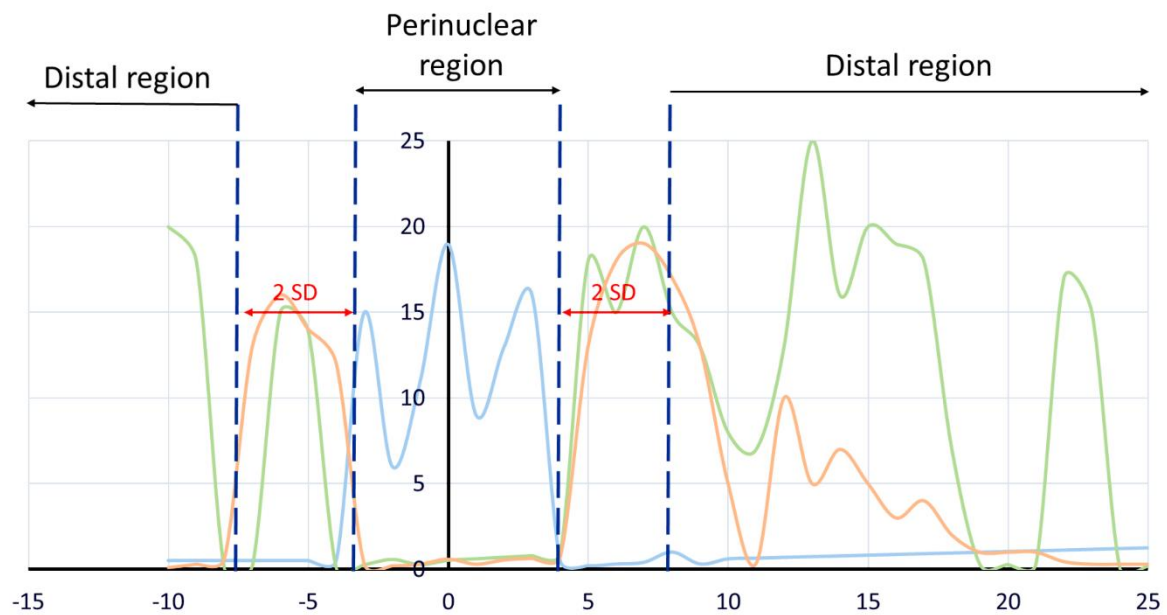
Figure 5.3 Visual representation of the classification of the perinuclear and distal regions. This line presents a histogram as described in the previous figure. The nuclear radius is obtained and used to calculate a perinuclear region. 2 standard deviations (SD) away from this region is then calculated to give the area that will classified as distal. In doing so, this allowed quantification and comparison of the two regions.

5.3.5 *Statistical analysis*

Dr Conor Lawless (Wellcome Centre for Mitochondrial Research) undertook the statistical analysis. The perinuclear replication *in vivo* data was subjected to Loess smoothing (Jacoby, 2000). This is because analysis yields a larger number of values for multiple profiles, hence a large amount of noise is produced, this smoothing function is used to reduce this noise. To analyse differences between the perinuclear and distal regions, the significant effects within the groups were analysed via ANOVA. This identifies any differences for a group, for example differences in CldU between the perinuclear and distal regions within each brain region. For each of the groups, a delta value was calculated by subtracting the median of the distal intensity of thymidine analogue values from their perinuclear counterpart for each neuron. This was performed for both CldU and IdU staining. Therefore the delta value measures the difference in perinuclear and distal cytoplasmic values for each genotype, age and brain region group. An equation for delta is presented in equation 5.1. Figure 5.4 presents an example of delta values calculated from four scenarios of CldU incorporation. The median was used as it

203

correctly represents the range by catering for the high number of 0% in regions with a lack of thymidine analogue labelling.
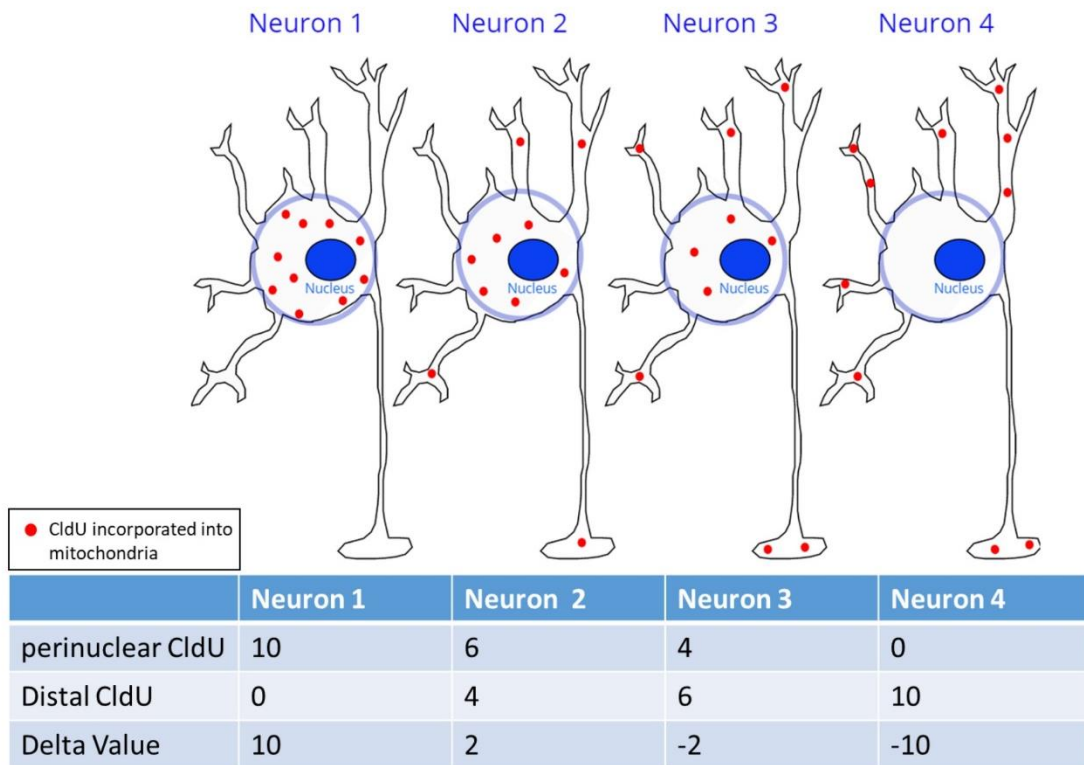
Figure 5.4 Mock representation of delta calculation. This image presents four different scenarios of CldU incorporation, the perinuclear value, distal value and the calculation of delta from this is also presented.

Significant effects between the groups (genotype, age and brain regions) were then determined using a Wilcoxon test, which compares data between the groups. This generated P-values that compared the median delta between the groups. These P-values were corrected using multiple testing to produce 'Q-values' which ultimately determined any significant differences between groups.

Delta = (Average of perinuclear analogue signal)-(Average of distal analogue signal)

Equation 5.1 Calculation of delta values

5.4 Results

5.4.1 *Distribution of thymidine analogues within single neurons*

Confocal images were obtained from four distinct brain regions, examining 3 specific neuronal types, namely Purkinje cells from the cerebellum, pyramidal cells from the frontal cortex and the CA1/CA2 region of the hippocampus, and dopaminergic neurons from the SN. After identification of neurons, the levels of CldU and IdU incorporation were measured following immunofluorescence (figure 5.5). The thymidine analogue staining was punctate and co-localised with the mitochondrial marker, tom20. Detailed information on the choice of neurons is explained in section 3.4.1.

At least 10 images containing multiple neurons (approximately 2-4) were analysed each brain region (figure 5.6 and 5.7 (including the number of neurons analysed), from the four experimental mouse groups which varied by age and genotype. The distribution of CldU and IdU labelling within these neurons is presented in Figure 5.6 (CldU) and 5.7 (IdU). The blue dotted lines differentiate the nuclear region from the distal regions based on the nuclear radius. CldU staining (figure 5.6) highlights that in the majority of the cases, there is an increased signal in the perinuclear region that reduces with distance from the nucleus. However, in the case of IdU (figure 5.7), no such pattern was observed. This could be due to low levels of incorporation of this analogue, into a small proportion of the neuronal populations, due to the shorter period of labelling (15 hours). It is also important to note that none of the CldU or IdU staining was noticed as being co-localised with the nucleus; hence the higher signal in the perinuclear region is not due to this. To statistically compare between the perinuclear and distal regions, the raw data from figures 5.6 and 5.7 was reclassified as described in section 5.3.4. This was necessary to account for any variation due to difference in sizes of the neurons. Therefore, classification of the cell into perinuclear and distal regions is vital and allows the values to be averaged to find a median value, allowing quantification and comparison of the perinuclear region to the distal regions. To further analyse the replication pattern between brain regions, ages and genotypes, using a single value for each cell, a delta value was calculated.

205
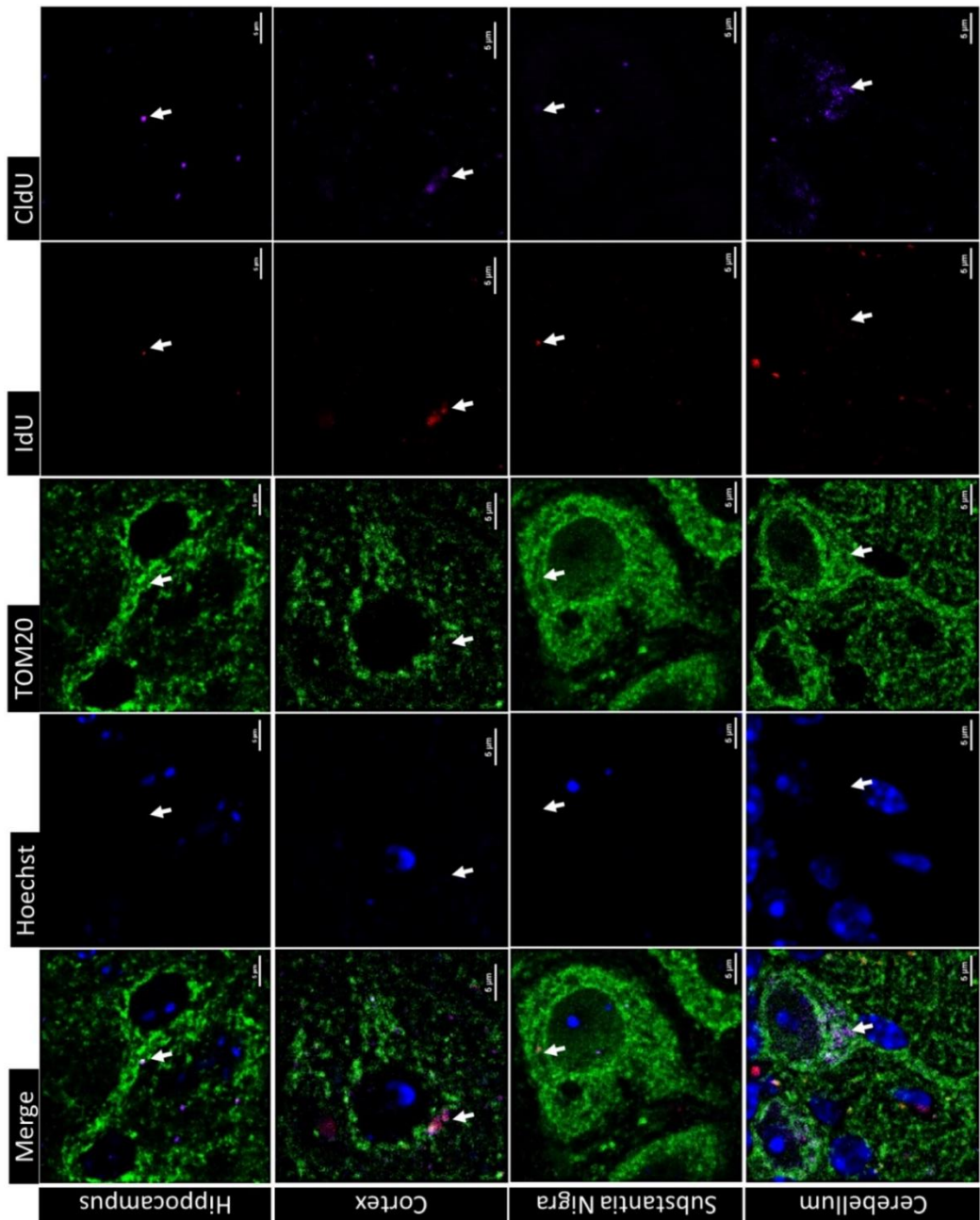
Figure 5.5 Tom20, the mitochondrial marker, was used to identify the cell boundary and mitochondria. Co-localised IdU and CldU are indicated using the white arrows. The images were taken at x40 magnification using confocal microscopy, but the images were zoomed in for the purpose of visualising. The scale bar represents 5μm for Hippocampus and Cortex and 10μm for SN and cerebellum. Hoechst is present within wavelength 405 nm, tom20 is imaged in 488 nm and IdU in 546 and CldU in 647nm.

207
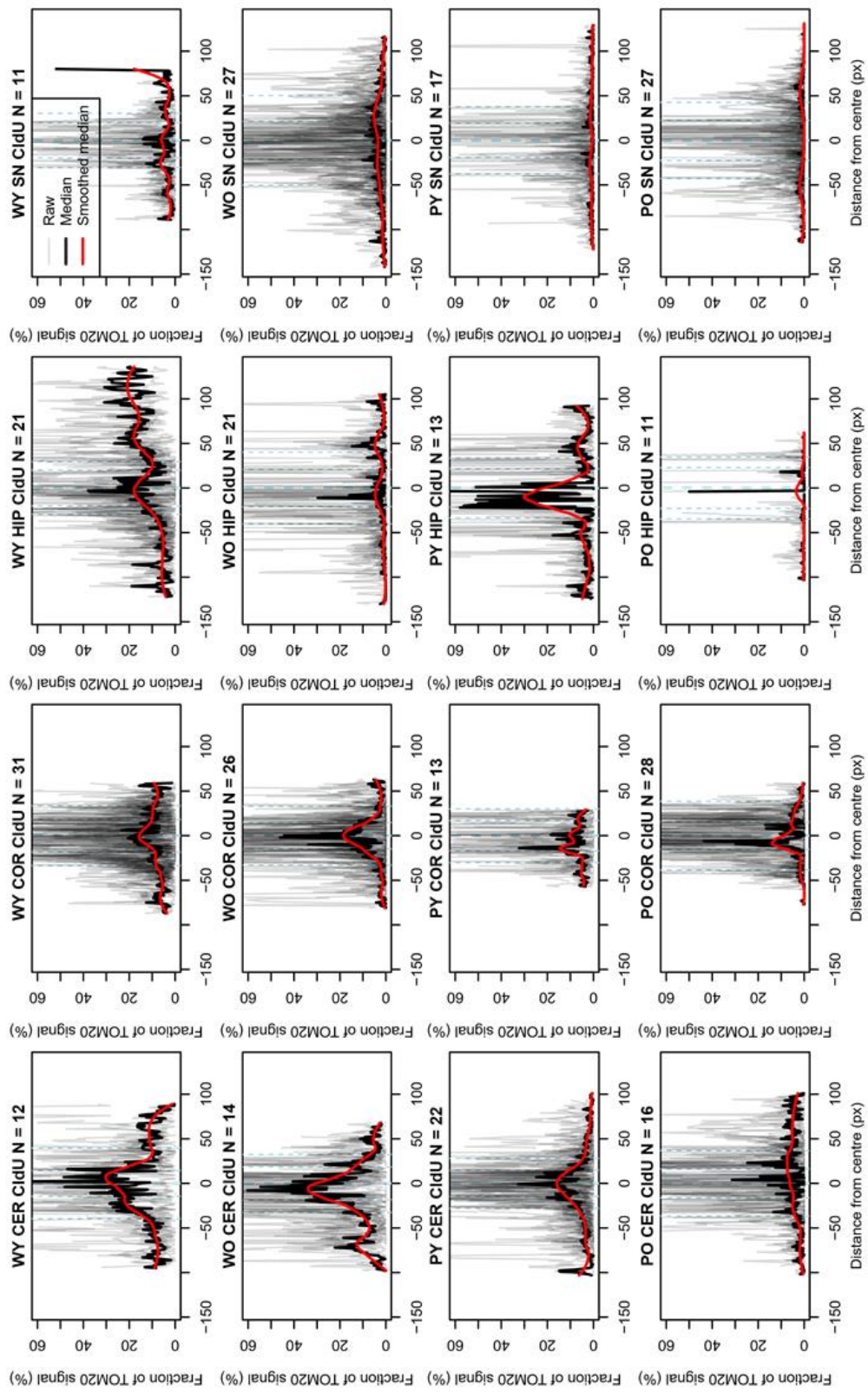
Figure 5.6 Variations in CldU incorporation with distance from the nucleus in vivo. The centre of the graph, at 'O' is the nucleus. This graph is to show the spread of the raw data in grey, the median in black and the smoothed median in red. This is to observe changes in the pattern of mtDNA replication localisation in various tissue. The blue vertical lines represent the perinuclear and distal regions. CER represents cerebellum, COR represents cortex, HIP represents hippocampus, SN represents Substantia nigra, PO represents PolgA$^{mut/mut}$ old, PY represents PolgA$^{mut/mut}$ young, WO represents wild type old, WY represents wild type young. The N number of neurons is also present above each graph.
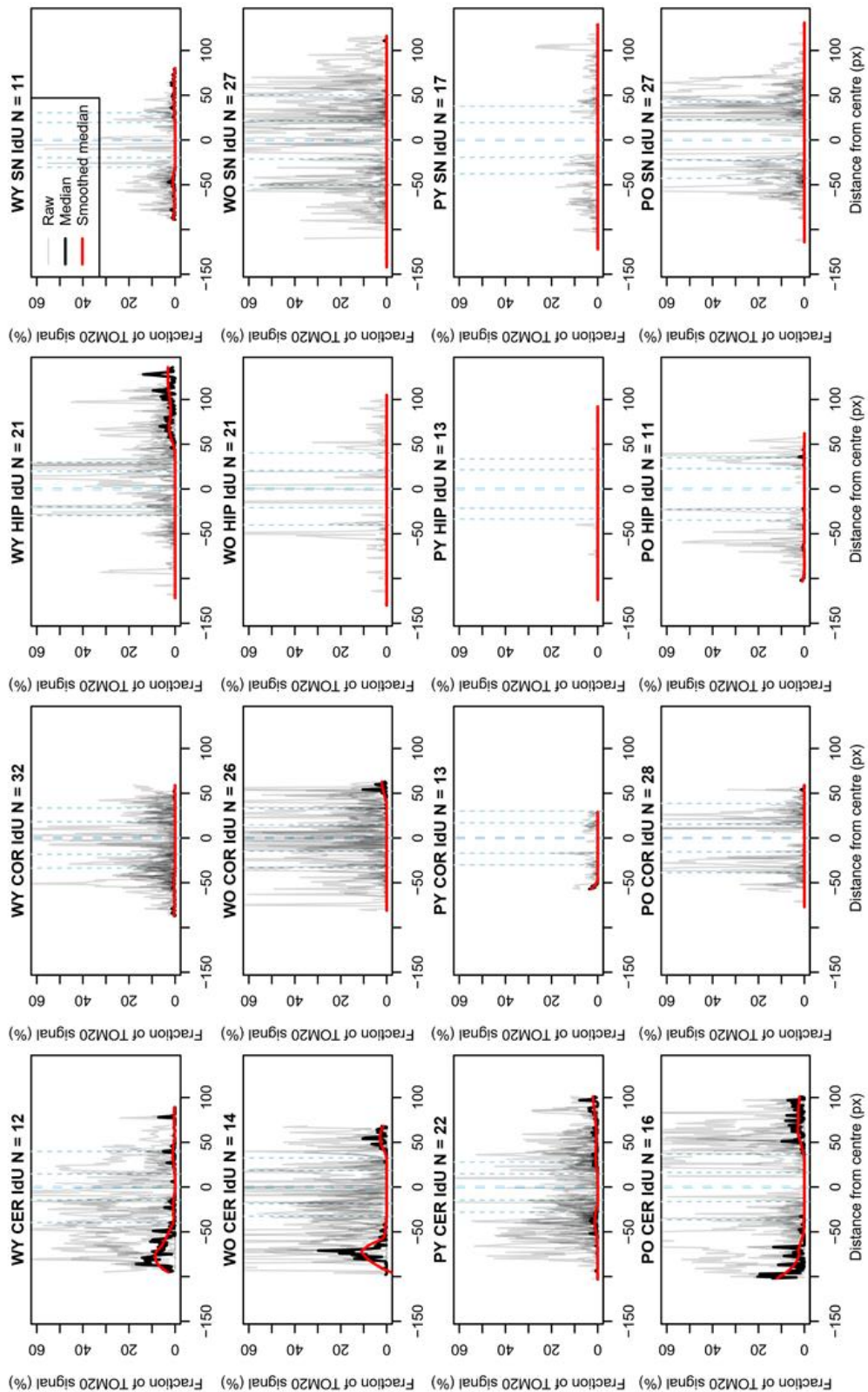
Figure 5.7 Variations in IdU incorporation with distance from the nucleus in vivo. The centre of the graph, at 'O' is the nucleus. This graph is to show the spread of the raw data in grey, the median in black and the smoothed median in red. This is to observe the changes in pattern of mtDNA replication localisation in various tissue. The blue vertical lines represent the perinuclear and distal regions. CER represents cerebellum, COR represents cortex, HIP represents hippocampus, SN represents Substantia nigra, PO represents PolgA^mut/mut old, PY represents PolgA^mut/mut young, WO represents wild type old, WY represents wild type young. The N number of neurons is also present above each graph.

5.4.2 *Site of mtDNA replication within single neurons*

A median value was calculated for each neuron from the perinuclear and distal regions to compare mtDNA replication between the brain regions for each mouse group studied (figure 5.8). This demonstrated a significant increase in perinuclear incorporation of CldU, compared to the distal regions, in most cases (p<0.05), with the exception of wildtype young cerebellum and *PolgA^{mut/mut}* old hippocampus. The lack of significance in these regions could be due to the low number of neurons studied (figure 5.6) due to lack of neurons and neurites visible in a section.

In the case of IdU, the pattern of results showed more variability. A general pattern of a decrease in IdU signal within the perinuclear region was observed for the majority of regions when compared to the distal region. However this did not reach significance (p<0.05) in wildtype young cerebellum and hippocampus, wildtype aged cortex and hippocampus, *PolgA^{mut/mut}* young cortex and *PolgA^{mut/mut}* old cortex and SN. The only case with a significant decrease (p<0.05) in IdU levels in the distal regions compared to the perinuclear region was wildtype aged SN. This is interesting due to the high levels of deletion observed in this region in humans (tables.3.2 and 3.3)

These differences in CldU and IdU pattern could be due to the labelling times used. CldU had been injected into the mice for 4 days, hence it represents total mtDNA CldU incorporation over this time. However IdU injection is conducted ~15 hours prior to death and hence, represent only the mtDNA incorporation that has occurred within this much shorter period. Although the timing is different, this is in concurrence with previous literature that demonstrated an increase in distal mtDNA replication one week after induced damaged, however, after two weeks, mtDNA replication was determined to have increased in the perinuclear region (Van Laar et al., 2018).
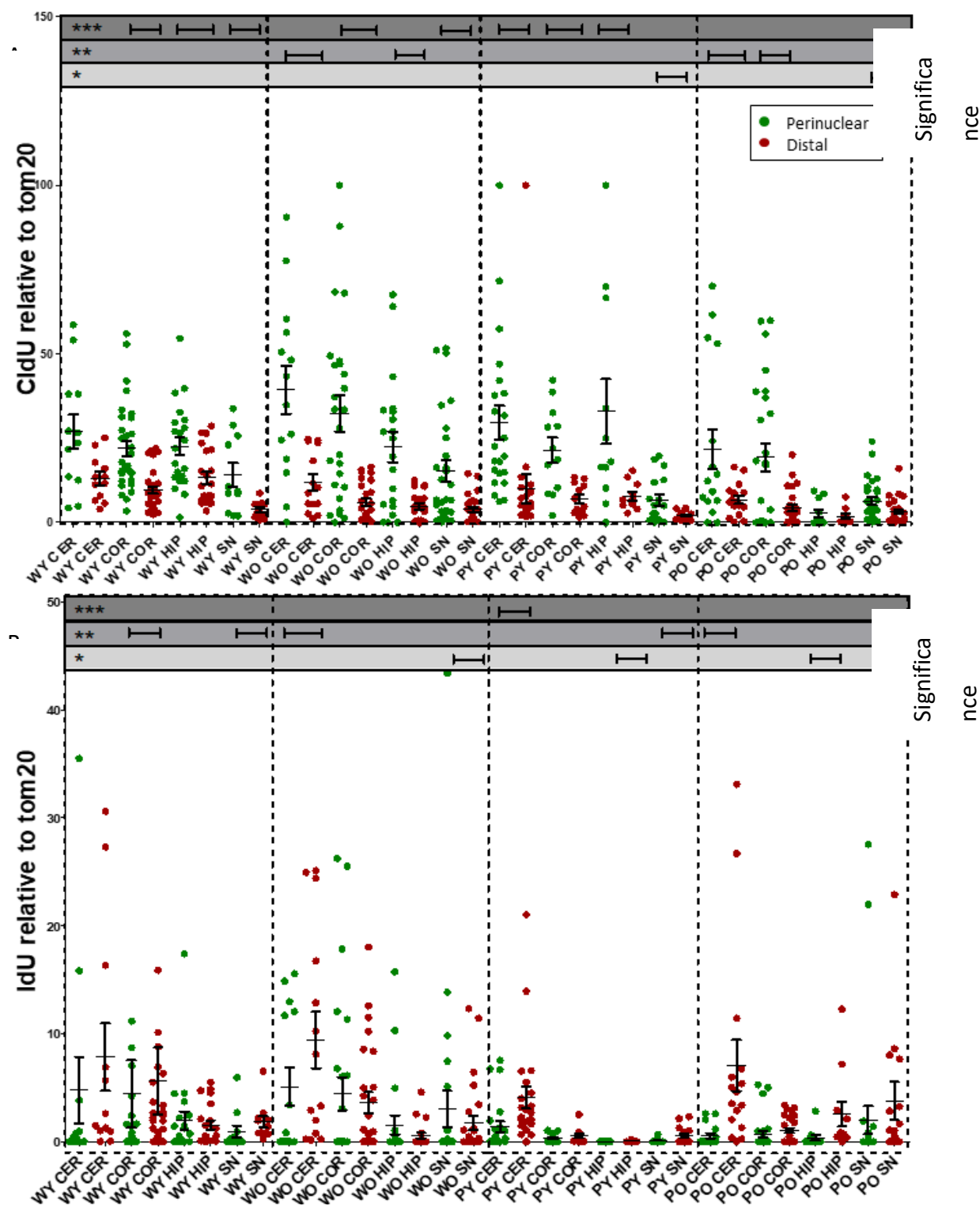
Figure 5.8 Differences between CldU and IdU incorporation into perinuclear and distal regions in vivo. Image A presents CldU and B presents IdU. The histograms were split into perinuclear and distal regions based on the nuclear radius. CER represents cerebellum, COR represents cortex, HIP represents hippocampus, SN represents Substantia nigra, PO represents PolgA^{mut/mut} old, PY represents PolgA^{mut/mut} young, WO represents wild type old, WY represents wild type young. The N is at least 10 neurons for case and the median plotted +/- SD. Wilcoxon test was used to identify significant differences stated on the graph. * indicates p < 0.05, ** indicates p < 0.01 and *** indicates p < 0.001 obtained using one way-ANOVA.

210

5.4.3 *Variations in delta values between neuronal subtypes*

To compare the various brain regions, ages and genotypes, delta values were calculated giving a single value for each cell that could be analysed statistically (section 5.2.5, figure 5.3). Delta values calculate the difference between perinuclear and distal thymidine analogue signal, with a higher delta highlighting increased perinuclear incorporation. When comparing between the different neuronal subtypes, a general pattern observed for the CldU data (figure 5.9A) was increased delta values in the cerebellum with the lowest value for the SN. This pattern was consistent between all the mice groups used, although there were no significant differences ($p<0.05$) detected between brain regions, except between the cerebellum and the SN in the young $PolgA^{mut/mut}$ cohort. Therefore it can be suggested that the location of CldU incorporation does not differ between neuronal subtypes. However, the data suggests that in the cerebellum of young $PolgA^{mut/mut}$ mice, there is more perinuclear mtDNA replication than in the SN. Although not, significantly different, this pattern is also observed in the other mice groups, however to confirm, further investigations are required.

In the case of IdU (figure 5.9B), the general pattern was that the lowest delta value was detected in the cerebellum and the highest in the SN, the opposite pattern to the CldU data. The majority of the cases were not significant, however the cerebellum had significantly decreased delta values compared to the other regions ($p<0.05$) in aged wildtype mice, young $PolgA^{mut/mut}$ mice and aged $PolgA^{mut/mut}$ mice. This suggests that the delta difference in the cerebellum is affected by ageing or replication defects, which will be discussed in the following section (section 5.4.4). This suggests that, due to the lower delta values, that the cerebellum, compared to the other regions, has an increased level of IdU signal in the distal mtDNA. This is particularly interesting when considering the previous literature, where a number of studies have identified the lowest number of ΔmtDNAs in the cerebellum compared to the other regions in mice and humans (refer to table 3.1 and 3.2).

5.4.4 *Variations in delta values, the effect of age and a replication defect*

As significant differences were not detected, it could be concluded that age and replication defect do not affect mtDNA replication localisation, however patterns in the data could be observed between groups. With ageing and a replication defect, increased ΔmtDNA levels are

211

generally observed (table 3.1 and 3.2), the site of mtDNA replication between these groups were also compared (figure 5.9). With age, a pattern of increase in CldU and IdU delta was observed for all brain regions studied in the wild type mice (not significant). This suggests that with ageing, the site of mtDNA replication could shifts to the perinuclear region. However, these changes were not significantly different.

When a replication defect is considered, an overall increase in CldU and IdU delta was also observed in the $PolgA^{mut/mut}$ mice compared to the wildtype. This also suggests that in $PolgA^{mut/mut}$ mice compared to the wildtype, there is an shift to perinuclear mtDNA replication. However, when $PolgA^{mut/mut}$ young mice are compared to $PolgA^{mut/mut}$ aged mice, there was a observed decrease in CldU and IdU delta in aged mice compared to young. This could suggest altered mtDNA replication localisation between healthy ageing and the $PolgA^{mut/mut}$ mice, However, these patterns are not statistically significant ($p<0.05$), therefore no firm conclusions can be drawn, although, a significant decrease ($p<0.05$) in delta was observed between the aged and young hippocampus tissue in $PolgA^{mut/mut}$ mice.
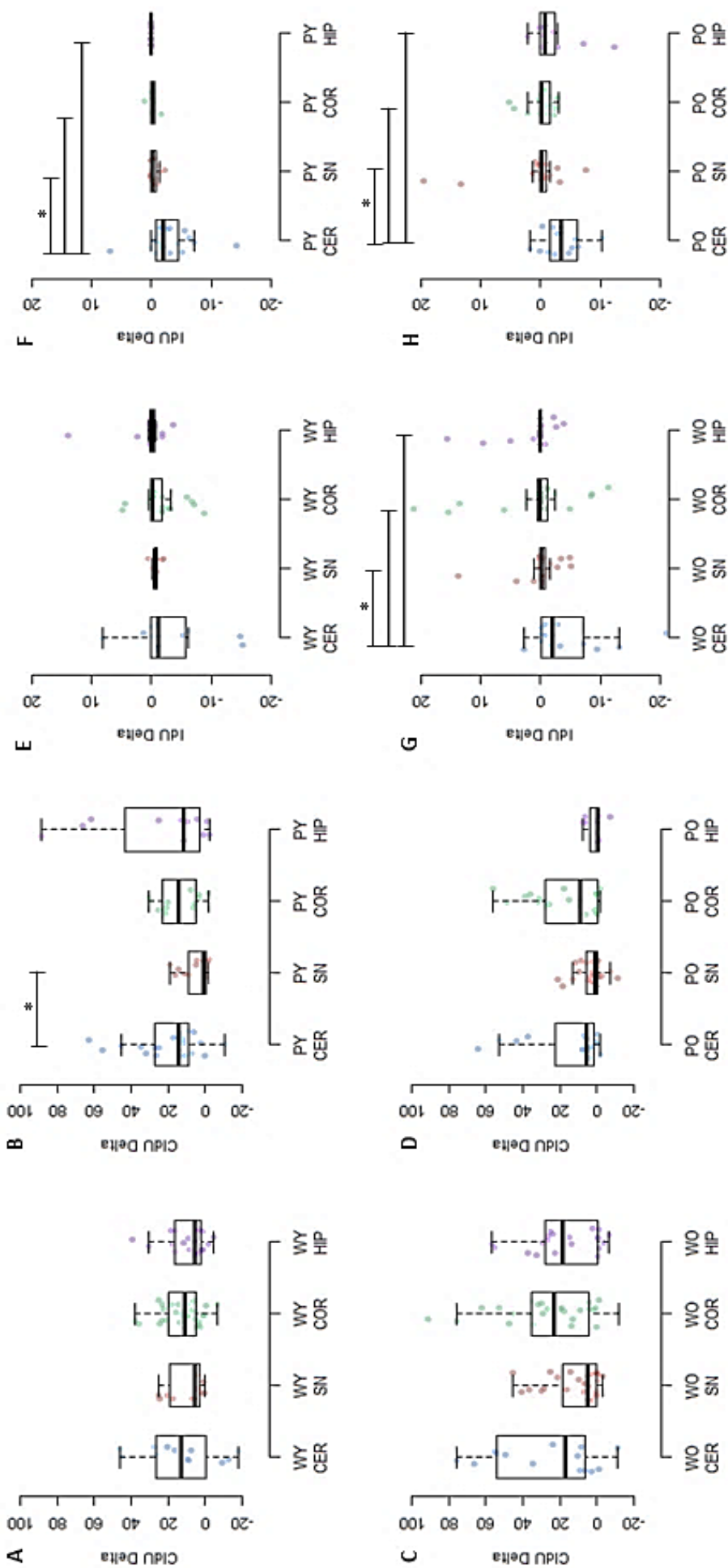
Figure 5.9 Delta values to compare the effect of age, genotype and brain regions on CldU nd IdU incorporation into perinuclear and distal regions. Graph A–D presents the CldU data and E–H presents IdU data. The delta values were calculated from the equation in equation 5.1. CER represents cerebellum, COR represents cortex, HIP represents hippocampus, SN represents Substantia nigra, PO represents PolgA$^{mut/mut}$ old, PY represents PolgA$^{mut/mut}$ young, WO represents wild type old, WY represents wild type young. The N is at least 10 neurons for case. The significant differences were compared between age, genotype and tissue. * indicates p < 0.05, ** indicates p < 0.01 and *** indicates p < 0.001 obtained using one way-ANOVA.

5.4.5 *Preliminary data – mtDNA replication site within neurons in vitro*

To further understand the influence of ΔmtDNA levels on the site of mtDNA replication, preliminary work was undertaken in cultured cells. The thymidine analogue labelling was optimised for cultured cells (as described in chapter 4), and differentiated neurons containing varying levels of heteroplasmy was used. Using cultured cells is also beneficial in identifying distal neurites further away from the cell soma, which are not necessarily observable in tissue. This allowed more accuracy regarding the distal region. As with the CldU data *in vivo*, a significant increase ($p<0.05$) in thymidine analogue incorporation was observed between the perinuclear region compared to the distal region (figure 5.10A).

Since a high and low heteroplasmy cell lines were used the influence of ΔmtDNA on the site of mtDNA replication could be understood. Since these cell lines are isogenic controls, any differences are less likely to be due to other variables. The delta values demonstrated that there was no difference between the delta values with varying ΔmtDNA levels (figure 5.10B). This imitates the *in vivo* data suggesting that ΔmtDNA does not influence the site of mtDNA replication.
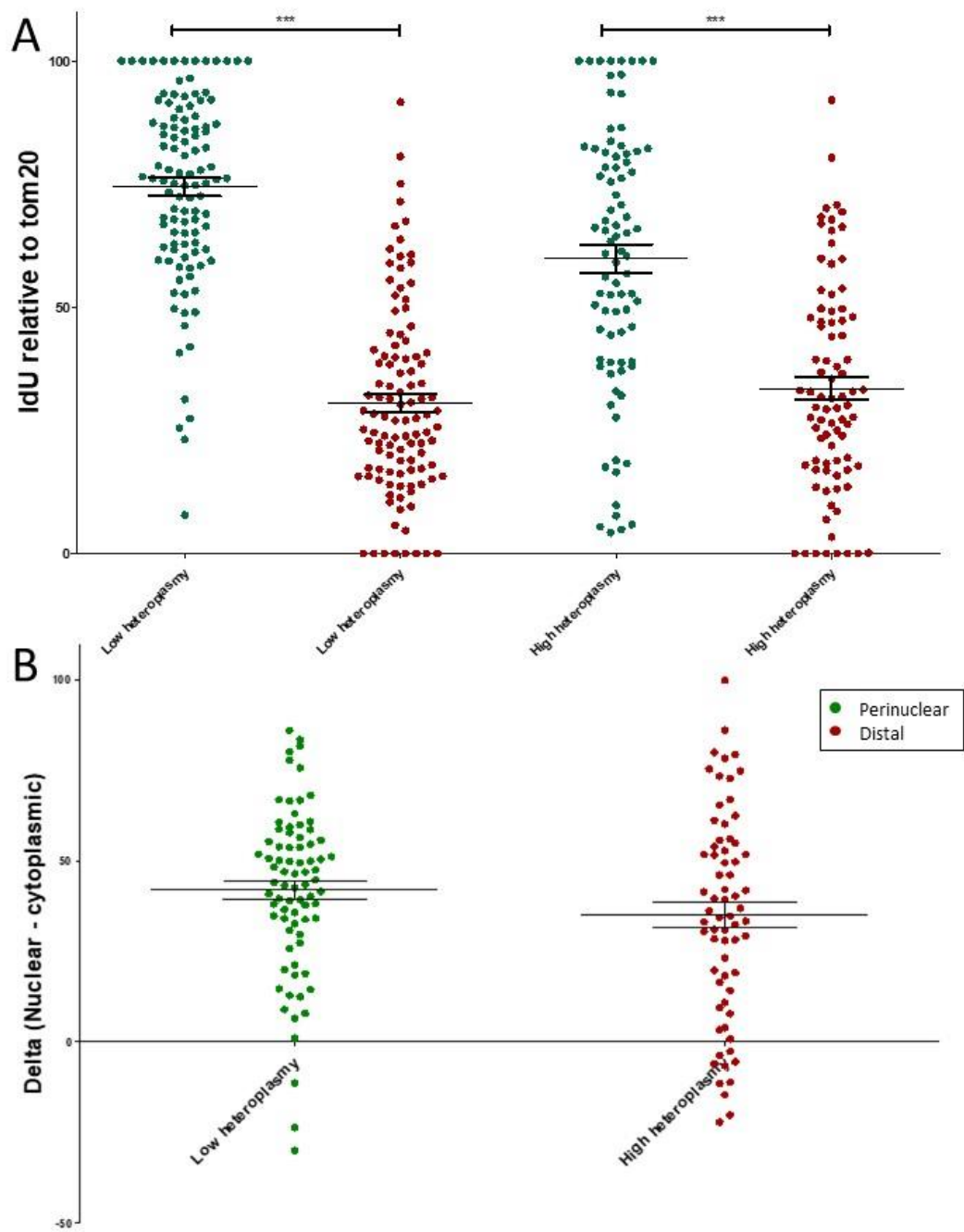
Figure 5.10 IdU incorporation in vitro. The data was split into perinuclear and distal regions based on the nuclear radius in the low and high heteroplasmy neurons. Image A demonstrates the difference between the perinuclear and distal regions and image B demonstrated the delta values to compared the cell lines. The N is 107 for low heteroplasmy cells and 83 for high heteroplasmy cells *** indicates p < 0.001 obtained using t-test..

215

5.4.6 *Preliminary data – Detection of the site of mitophagy*

Since variation in delta values was observed between the different brain regions, suggesting variations in the location of mtDNA replication, it was important to study where mitophagy occurred. This would be beneficial in understanding not only the loci of mitophagy but also if this is related to the loci of mtDNA replication. Therefore, as a preliminary step, this study aimed to develop a method to analyse the location of mitophagy in images from brain regions in the mitoQC mice (McWilliams et al., 2016). The images were a kind gift from Dr Ian Ganley (University of Dundee). The images (Figure 5.11) were analysed using Image J as described in section 5.2.3. Since the obtained images did not contain a nuclear marker, the analysis had to be modified. The nuclear region was identified by the region that lacked the anti-TH antibody and since the highest intensity was not visible, this anti-TH region was considered the perinuclear region. Data from an average of 33 cells from dopaminergic neurons of 2 wild type mice was collected and the difference in perinuclear and distal region calculated (figure 5.12). In concordance with the previous literature, although mitophagy did occur in distal regions, the perinuclear region had an increased level of mitophagy as observed via mCherry intensity. Since this was a preliminary study, there was no other region for accurate comparison, which could be conducted as part of the future study.
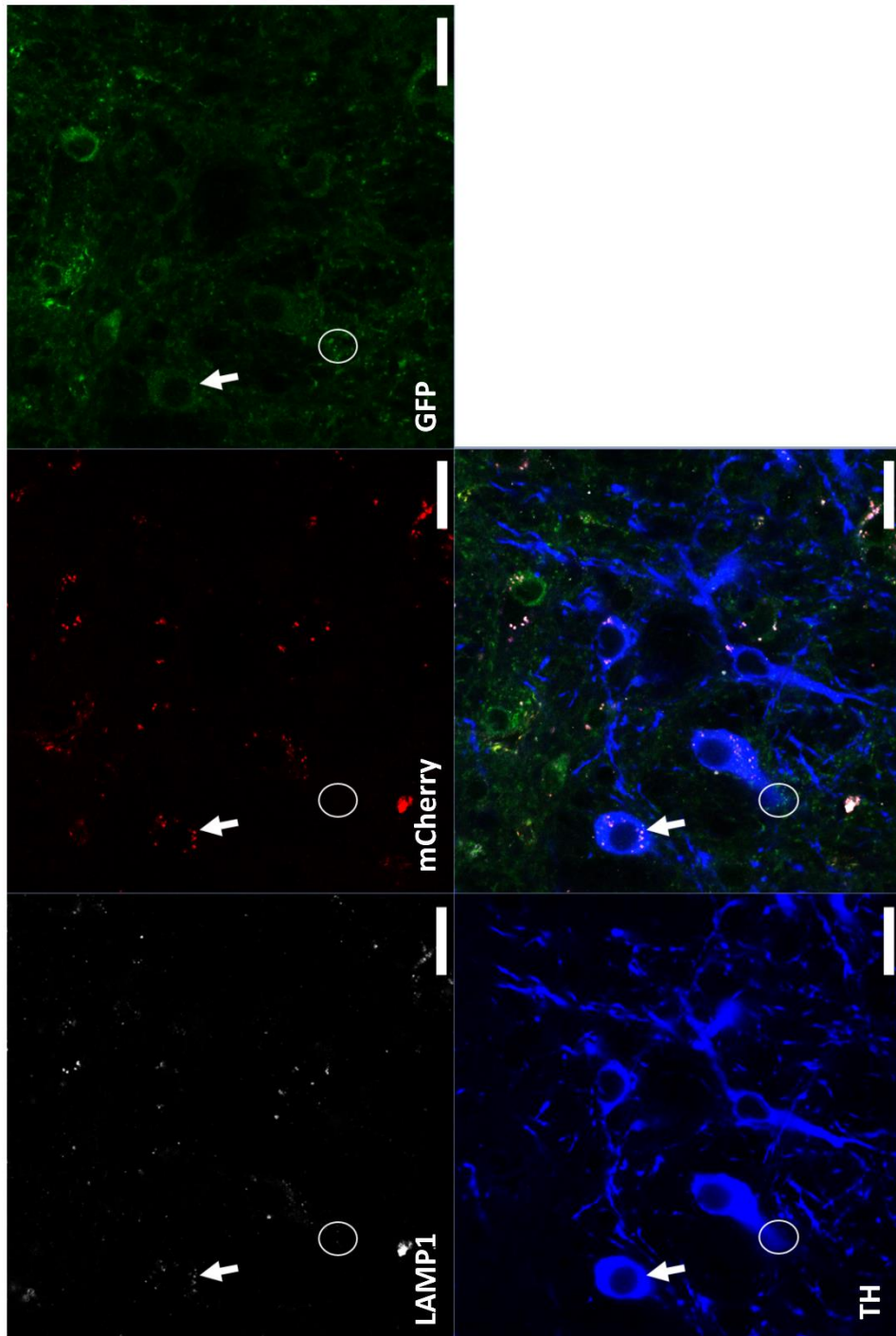
Figure 5.11 Staining of dopaminergic neurons from MitoQC mice. These images were a kind gift by Dr Ian Gangley. This model has been imaged and described in the literature. The mitoQC mice highlights regions of mitophagy as bright red spots due to the quenching of GFP in these areas. The mCherry bright spots were also co-localised with LAMP1, the lysosome marker. TH was used to confirm the dopaminergic neurons. The white circle highights a region displaying no mCherry spots within the cells and the white arrow points to a positive mCherry puncta co-localised to LAMP1. These sections were images at 63x magnification.
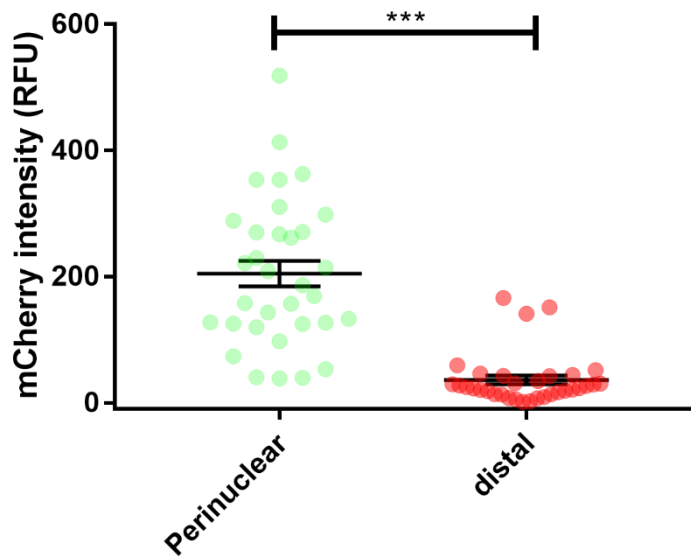
Figure 5.12 Localisation of mitophagic events in dopaminergic neurons from MitoQC mice. The spread of the bright mCherry spots were measured along the distance from the nucleus, and based on the nuclear radius, the values were separated into perinuclear and distal regions and the averages are presented here. N=33 neurons from 2 mice. *** indicates p < 0.001 based on t-test.

5.5 Discussion

5.5.1 *Key results*

- *In vivo* CldU (4 days) shows increased perinuclear replication; however, IdU labelling (~15 hours) demonstrated variations.
- No significant differences were noticed in delta values between brain regions for CldU in most groups, however significant differences were noticed in delta values between the cerebellum and the other regions for IdU.
- Neither ageing nor the presence of a defective mtDNA polymerase altered the location of mtDNA replication, as measured with either CldU or IdU incorporation.
- Preliminary *in vitro* study demonstrated no significant difference in delta between cell lines with high and low ΔmtDNA levels.
- Preliminary mitophagy study demonstrated an increased signal intensity in the perinuclear region in dopaminergic neurons.

5.5.2 *MtDNA replication occurs primarily in the perinuclear region*

In the *in vivo* study, with CldU, a significant increase in analogue signal and therefore mtDNA replication was observed in the perinuclear regions of neurons. This could suggest that, mtDNA replication is more abundant within the perinuclear region compared to the distal, when analogue presence is maintained over a long time frame (4 days). As mentioned in the introduction (section 5.1.1), distal regions did contain positive signals for mtDNA replication, however perinuclear regions had a significantly higher signal. This is in concordance with the previous literature (Amiri and Hollenbeck, 2008, Calkins and Reddy, 2011, Davis and Clayton, 1996, Magnusson et al., 2003). For IdU, there was either no difference between the regions or a significant increase of IdU signal, and therefore mtDNA replication within the distal regions. This significant increase is only present in 8 out of the 16 cases trialled. These 8 cases were in different regions in different cohorts, therefore there appeared to be no pattern to these data. Although IdU produced different data to the CldU, this was also observed in previous literature when comparing between two time points. The study by Van Laar used two separate time points similar to this study. They also induced damage via rotenone and

219

noticed that at the shorted time point, the thymidine analogue was increased in the distal region compared to control, however with the longer time point, this was increased in the perinuclear region (Van Laar et al., 2018). They suggested that the rotenone damage led to axonal loss and therefore the mtDNA replication in distal regions was subsequently effected. However, in this study, no such difference was observed. Alongside this, another study using primary neuronal cultures demonstrated that between two time points of 4 hours and 20 hours, there was no difference in mtDNA replication localisation (Calkins and Reddy, 2011). At both time points, mtDNA replication was higher in the cell body compared to the neurites. These differences could be due to the variable time points studied.

The difference between CldU and IdU could suggest a time dependent variation in location, it could be considered that initially mtDNA replication occurs equally in the perinuclear and distal regions or in the distal region in some cases, however with time, these replicated mtDNA accumulate within the perinuclear region.

Although the IdU data demonstrated inconsistencies, the CldU data demonstrated a significant increase in the perinuclear region. Therefore, to identify whether mitophagy also occurs in the same vicinity, mitoQC mice were used as part of a preliminary study (further detailed in section 5.4.5). After analysing dopaminergic neurons from three mice, the data demonstrated a significant increase ($p < 0.05$) in basal mitophagy in the perinuclear region compared to the distal. This suggests that mtDNA replication and mitophagy could occur in the vicinity of each other further increasing the chances of a damaged mtDNA molecule being replicated. This has implications for ΔmtDNA formation and clonal expansion. Therefore, this preliminary study needs to be expanded to further study mitophagy in different regions of the brain. It is also important to consider the selection process of the template mtDNA for replication. Previous studies have demonstrated that the mtDNA template for replication is chosen randomly (Davis and Clayton, 1996). To study this, co-staining of damaged mitochondria and replicating mitochondria could be conducted, which would identify whether the two factors would co-localise. This could also be part of the future work of this study.

5.5.3   *The site of MtDNA replication does not alter with variations in ΔmtDNA levels*

Although the CldU and IdU data displayed variations between the perinuclear and distal regions, it was important to compare how the site of mtDNA replication is related to ΔmtDNA levels, to understand how mtDNA replication might be involved in this process. Therefore, the site of mtDNA replication was compared between different brain regions in aged, and *PolgA^{mut/mut}* mice compared to the wildtype, as these generally present with varying levels of ΔmtDNA (table 3.1 and 3.2). In order to accurately compare the site of replication, delta values were calculated. These values provide a value based on the direction of change and the degree of change. By doing this, I successfully developed a method that allows comparison of how the site of replication changes in different cases.

The results demonstrated no significant difference between the different regions of the brain or between aged and *PolgA^{mut/mut}* mice compared to the wildtype. This suggests that mtDNA replication location does not have a correlation with the levels of ΔmtDNA. This is not in agreement with previous literature as a previous study using wildtype and AD mouse models (Calkins and Reddy, 2011), demonstrated that the site of mtDNA did alter between these mice. The location of mtDNA was also measured after damage induced by H_2O_2 and rotenone. This demonstrated that in cases with potentially higher mtDNA mutations mtDNA replication in distal regions is decreased, and increased in the perinuclear region. If delta values were calculated in these studies, I would predict that the group with mitochondrial damage would have significantly higher delta values than the wildtype mice. Although in this study, no significant differences were observed; the pattern of the data suggested an increase of delta values in regions typically associated with higher ΔmtDNA. For example, in both CldU and IdU, there is a slight increase in the delta value in the wildtype aged mice compared to the wildtype young which suggests more perinuclear and less distal mtDNA replication with ageing. This increase in delta was also observed in *PolgA^{mut/mut}* mice compared to wildtype, and when comparing between the different brain regions. This pattern was not observed when comparing CldU in the different brain regions of *PolgA^{mut/mut}* aged mice compared to *PolgA^{mut/mut}* young mice (figure 5.9A). Both these groups demonstrated the highest delta value in the cerebellum, which is associated with the lowest levels of ΔmtDNA.

The preliminary data from the *in vitro* study using cell lines of varying ΔmtDNA levels also demonstrated no significant difference in the delta values further supporting the *in vivo* data. A benefit to using *in vitro* neurons was the identification of neurites. This is particularly visible when considering the difference in X-axis values between the *in vivo* data where the distance in nucleus ranged from -150 to 100 while for the *in vitro* data, this ranges from -400 to 400. Since they were both imaged at the same magnification, and since the size of the cell body is not extensively variable, this suggests that the *in vitro* study was successful in capturing distal axonal regions. Therefore, the lack of significant difference in the delta values might be more reliable. However, this is preliminary and more replicates at various time points would further support these data.

5.5.4 *Limitations of the study*

One limitation of this study is the definition of perinuclear and distal regions. As mentioned in section 5.4.2, within the *in vivo* tissue, distal regions of the cells are technically difficult to identify. Therefore the distal regions are more appropriately the distal regions of the cell body and the start of the axons and dendrites rather than distal axons, this would benefit from further modifications to the technique and analysis. Other techniques such as CLARITY could be used, where staining of sections with thickness of 200µm can be conducted (Morawski et al., 2018). This would allow identification of soma and axons appropriately and produce accurate results.

Another limitation is the use of a line in image J to access the change in mtDNA replication with distance. Since mtDNA replication can occur in any loci of the cell, possible CldU or idU positive puncta might be neglected, as it does not fall in the trajectory of the line manually drawn. Introduction of an area larger than a line, e.g. a rectangle along the trajectory of the cell, would introduce another variable, the area of the rectangle. Alongside this, image J does not have the function to calculate distance along a rectangle. Previous studies have opted to measure the spread of thymidine analogue labelling by classifying into categories based on the distance (Amiri and Hollenbeck, 2008, Magnusson et al., 2003).However this was done in *in-vitro* cells, and tissue contains more background which would decrease the reliability.

A further suggestion is that the thymidine analogue signal could be recognised as damage by the cells, and hence mtDNA molecules harbouring these analogues are transported to the perinuclear region over time for degradation or repair. This might suggest that replication occurs in all regions of the cell and the CldU data is due to thymidine analogue toxicity. As mentioned in section 4.1.1 (chapter 4), thymidine analogues could be considered as toxic at high levels. Other thymidine analogues, although structurally different to CldU and IdU, are used for antiretroviral treatment of HIV/AIDS patients and have been noticed to increase ROS production and mtDNA mutations (Kline et al., 2009, Stankov et al., 2013). Therefore further investigation would need to consider the effect of these analogues on mitochondrial dysfunction and mtDNA mutations. This also links to the previous theory of increased mtDNA repair in the perinuclear region, but these mtDNA molecules could also be targeted for mitophagy, which occurs predominantly in the perinuclear region, as suggested in section 5.1.2.

5.5.5 *Future work*

- One of the limitations of the analysis *in vivo* was the lack of axons identified. This could be repeated using Z-stacks of the sections captured by confocal microscopy. If this technique is not sufficient to identify axons, CLARITY could be used which can label sections up to 500µm in thickness and has been optimised with the Wellcome Centre (Phillips et al., 2016).

- The *in vitro* work (section 5.4.5) would requires repeating. In addition to this, since high and low heteroplasmy neurons dependent on glycolysis for ATP production (Russell et al., 2018), substituting glucose with galactose, would force the cells to rely on the OXPHOS system, which might more accurately predict any effect on mtDNA replication. Other methods of inducing mitochondrial dysfunction such as treatments with H_2O_2 or rotenone could also be useful for this purpose (Calkins and Reddy, 2011, Van Laar et al., 2018).

- An increased number of time points, and longer time periods could be used to identify any differences in delta *in vitro*.

- Study mitochondrial motility between the different brain regions to consolidate the theory of increased transport. This is due to the differences in replication localisation pattern observed between the 15 hours (IdU) and 4 days (CldU).

- Obtain mitophagy localisation data from the hippocampus, cerebellum and cortex of the mitoQC mice, stain for a nuclear marker and analyse in comparison to different brain regions to study how mitophagy could effevt this process.

5.5.6 *Final conclusion*

Initially in the introduction (section 5.1.5), a theory of a replication 'hotspot' was discussed where the perinuclear region was identified as a region with high levels of mtDNA replication and mitophagy. By using CldU labelling (over 4 days), the majority of mtDNA replication was identified as being perinuclear. Studies on dopaminergic neurons from the MitoQC mice also observed higher levels of mitophagy in this region. Even though both data sets warrant further investigation, this is in support of a 'hotspot' region. This suggests that localisation of damaged mitochondria, mitophagy and mtDNA replication, are all present or occurring in close proximity to each other due to their dependence on nuclear factors. Therefore, it could be suggest that ΔmtDNA, present within damaged mitochondria, has an increased probability of being replicated, leading to the accumulation of ΔmtDNA with age. However the IdU data did not correspond to this. A variation from this 'hotspot', with more distal mtDNA replication was also observed suggesting that this is not involved in progression of mitochondrial dysfunction or mtDNA damage. Other process that could be involved in this such as mtDNA transport needs to be analysed to further understand this difference.

The delta calculation was developed to analyse between datasets as differences in mtDNA is observed between the brain regions and groups. There were significant differences noticed between the cerebellum and the other brain regions, and could possible suggest a compensatory mechanism in this region that leads to the lower ΔmtDNA. However, this requires further investigations. Alongside, there are no significant differences between the other regions, ageing or genotype, therefore it could be suggested that mtDNA replication localisation is not associated with the ΔmtDNA levels observed. However, patterns of variation were noticed between brain regions, ages and genotype, therefore a higher n number of

neurons and mice might increase the statistical power and highlight further significant differences. Variations between the two time points used in the *in vivo* study also suggests that maybe replication localisation could differ with time, however the *in vitro* data produced contradictory data. However, both sets have limitation and require optimisation of the time points.

Chapter 6: Proof of concept study investigating the ultrastructure of mitochondria in dopaminergic neurons; implications for neurodegeneration

6.1 Introduction

6.1.1 *Electron microscopy advances*

Initially, electron microscopy (EM) was used to understand the basic structure of mitochondria (Palade, 1953). Due to the high resolution providing significant detail, this technique remains unparalleled for understanding mitochondrial structure. Initial techniques such as transmission electron microscopy (TEM) and scanning electron microscopy (SEM) can be used to analyse morphology and ultra-structures in a 2D format. However, since mitochondria are not isolated entities, but form complex reticular networks that are impossible to image in 2D, better techniques are required for studying mitochondria as 3D structures. Due to this, a number of studies transitioned to using other technologies such as confocal microscopy with Z-stacking (Glancy et al., 2015, de Brito and Scorrano, 2008, Song et al., 2008). Although this does not provide the resolution offered by EM to study nanoscale structures, this in fact did allow the study of mitochondria in a 3D format.

However, recent advances in EM have enabled 3D visualisation of minuscule structures, which allows the study of mitochondrial structure in a more dynamic way, taking into account their 3D structure. Initially, these studies were performed using a technique called serial section transmission electron microscopy (ssTEM) where ultra-thin sections were manually sliced and imaged individually using TEM (Bang and Bang, 1957). Another technique employed was focused ion beam milling scanning electron microscopy (FIM-SEM) (Escovitz et al., 1975). This is a type of Focused ion beam-SEM (FIB-EM) and although this paper developed a method of high resolution image capturing, it was not used for 3D image analysis until later (Uchic et al., 2006). Compared to the ssSEM, this is a more automated process. This uses two types of focused ion beam; low beam and high beam. Low beam is used to image the samples via the SEM, and high beam is then used to slices the section, which is them imaged again at the low beam. Both ssTEM and FIB-SEM are currently used and the studies using these techniques will be discussed in the forthcoming section (Rodriguez-Moreno et al., 2017, Fischer et al., 2018).

226

A disadvantage of these techniques is that with ssTEM, there is the lack of automation and FIB-SEM can only use smaller volumes of samples for imaging. However, over the years, better techniques requiring less manual work and time, alongside with the ability to analyse large samples, have been developed (McEwen and Marko, 2001).

The technique employed for this thesis is called serial block-face SEM (SBF-SEM) (Denk and Horstmann, 2004). SBF-SEM is described in detail in section 2.4.3 of this thesis. Briefly, this technique utilises a scanning electron microscope and a microtome. Initially, the sample is placed on the microtome, and an electron beam is used to scan the section and the backscatter is collected by a detector to produce an image. The microtome contains a diamond knife, which can be used to slice ultrathin sections of down to 25nm in thickness (Pfeifer et al., 2015). When the section is removed, the electron beam is illuminated again to produce a second image before the tissue is sectioned and imaged again. This process can continue sequentially and essentially produces a Z-stack of the images at a high resolution not offered by other microscopes. This will allow reconstruction of miniscule nanoscale structures including mitochondria, offering analysis of parameters such as mitochondrial volume, complexity or surface area that is not possible by 2D TEM (Eustaquio et al., 2018). This ability makes this technique vital for research investigating mitochondrial structural changes in response to various factors including age or neurodegeneration.

6.1.2 *Significance of this study*

Understanding the 3D structure of mitochondria is very beneficial for the progression of research. A recent study conducted using SBF-SEM has demonstrated that there are variations in the mitochondrial network in the skeletal muscle fibres, which were not noticed before in the previous literature using 2D (Vincent et al., 2018). This highlights the importance of studying the ultrastructure of mitochondria in a 3D format, and identifying any difference in ageing and neurodegeneration.

As discussed in the previous chapters, brain, similar to skeletal muscle, contains post mitotic cells which have been shown to have high levels of ΔmtDNA which are particularly prominent in the SN (Bender et al., 2006c, Kraytsberg et al., 2006b). Previous chapter in this thesis also discusses the formation and accumulation of these ΔmtDNA. The condition of the 3D

mitochondrial network could be a major factor in the accumulation of ΔmtDNA. This is because the fusion of mitochondria could lead to sharing of the contents between mitochondria. Therefore, a highly connected network could potentially present with an advantage in sharing these ΔmtDNA molecules which could beneficial for the accumulation of a mutated mtDNA species or for compensating for the mutation and therefore, cell survival. Due to this, it is vital to study the mitochondrial network *in vivo*.

It is also important to understand if the ultrastructure of mitochondria changes under disease conditions, and if yes, how it is altered. Interrogation of these changes will provide more clarity with regards to the formation and accumulation of mtDNA deletions. In the previously mentioned study on human skeletal muscle study, mitochondria from three related individuals with the same m.8344A>G mutation presented differences in mitochondrial complexities based on the heteroplasmy of their mutation (Vincent, 2017). In a patient with low levels of heteroplasmy (~40%), increased mitochondrial connectivity was observed compared to control. When heteroplasmy was increased to ~63% and 97% in 2 other patients, the mitochondrial network appeared more fragmented than in controls. This suggested that in patients with the same mutation, mitochondrial complexity could potentially influence heteroplasmy, or vice versa, further suggesting a role in mtDNA mutation accumulation. Since, similar to skeletal muscle, neurons are also post-mitotic cells, and an accumulation in mtDNA deletions is observed in substantia nigra neurons (refer to table 3.1 and 3.2 for more details), the ability to study mitochondrial connectivity in the neurons may provide crucial information.

This is a new area of research with a limited number of studies attributed to it (Park et al., 2013, Tamada et al., 2017), and none of them have been conducted on human brain tissue. However, ssTEM has been performed in human brain tissue from control and individuals with Alzheimer's disease (AD), which led to the model of 'mitochondria on a string' (MOAS) (Zhang et al., 2016). This model will be discussed in more detail in section 6.4.7.

Another study has utilised FIB-SEM to study neuronal mitochondria (Tamada et al., 2017). This study used a DRP1 (mitochondrial fission protein) KO mouse, which demonstrated an increase in 'enlarged' mitochondria. Mitochondrion that have increased in size were also observed in a *Drosophila melanogaster* model of AD using FIM-SEM (Park et al., 2013).

The only study that has utilised SBF-SEM to study neuronal mitochondria was conducted in rats (Eustaquio et al., 2018). This study aimed to understand overall mitochondrial morphology in untreated control neurons and neurons treated with Ketamine, an inducer of apoptosis at high concentrations. This study also used TEM, which demonstrated 'swelling' of the mitochondria. This was also confirmed by SBF-SEM; however, this technique was also beneficial in identifying an increase in mitochondrial fragmentation, suggested to be due to mitochondrial fission, which could not be deduced from TEM.

Due to the lack of available literature and the variation in the mitochondrial network observed in skeletal muscle between control and patients, it is necessary to understand how this feature of the mitochondria is effected in another post-mitotic tissue, which also shows increased mtDNA deletion load. By gathering data on the characteristics of the mitochondrial network in these cells inferences may be made (in a similar way to those in the muscle) as to how mitochondrial connectivity may lead to the accumulation of these mutations. In chapter 3, I have described how mitochondrial replication changes between different neuronal populations and the impact of these changes on the mutations we detect in the SN and so the study described here will add further information to complement these studies.

Another novelty of the study detailed here is the comparison between perinuclear and distal region mitochondria in human dopaminergic neurons. A similar study in ground squirrels and rats, have identified that mitochondria in the perinuclear region appear more connected, compared to axonal mitochondria that are fragmented and <3µM in length (Popov et al., 2005). This can be looked in relation to the previous chapter of this thesis, which studied the mtDNA replication using thymidine analogue labelling in perinuclear and distal regions of the neuron.

Although previous chapters focused SN with ageing and PD, in this chapter the focus is more on AD and DLB. This is due to the availability of fresh tissue. However, this is justified as AD and DLB are also age related neurodegenerative diseases and this thesis concentrates on mtDNA deletions, which is also found in patients with AD and DLB (Chinnery et al., 2001, Krishnan et al., 2012, Mawrin et al., 2004, Phillips et al., 2014).

6.2 Aim and objectives

6.2.1 *Aim*

To provide a proof of concept study to understand whether SBF-SEM can be utilised to study mitochondrial complexity in 3D in single human substantia nigra neurons, and to understand if this changes in disease.

6.2.2 *Objectives*

The following objectives were fulfilled in this study;

- Identify a suitable methodology to image and analyse mitochondrial parameters
- Provide proof of principle data on how the mitochondrial network is altered in disease conditions.
- Provide proof of principle data to identify any alterations in mitochondrial morphology and connectivity in perinuclear and distal regions in dopaminergic neurons.

6.3 Methods

6.3.1 *Patient Cohort*

The list of patients used and their details are provided in table 6.1.

Age (years)	Gender	Pathology	PM delay (hours)	pH upon dissection	Case
54	F	Cognitively normal control - metastatic breast cancer	19	6.87	C1A, C1B
99	F	Frailty of old age, bronchopneumonia	21	6.53	C2

92	F	Bronchopneumonia secondary to COPD	16	6.43	C3
81	F	Metastatic liver cancer	19	6.09	NA
87	F	AD	21	6.35	NA
70	F	AD	24	6.46	P1
77	M	DLB (neocortical alpha-synuclein)	15	6.17	P2a, P2b
79	M	DLB	12	6.57	P3

Table 6.1 List and details of individuals used for this study. The pathology section describes the disease conditions present within the patient and for the controls the cause of death. AD indicates Alzheimer's disease, DLB indicates Dementia with Lewy bodies. The PM delay is the time taken to remove the Substantia Nigra following the death of the patient. The pH of the sample before fixing is indicated. The case number given to the individual for the purpose of this study is indicated in the column 'case'. NA in this column indicates that this sample was unavailable for analysis due to its quality. Certain individuals have two cases number because two different neurons were processed and analysed from the same individual, which were compared separately. The length of fixation represents the amount of time the tissue was present in the fixative.

6.3.2 *Sample collection and preparation*

Substantia Nigra samples from human brain were collected and fixed by Dr Chris Morris (Medical Toxicology Centre, Newcastle University). The list of cases used, age, gender, any associated pathology, and the pH of the buffer are all detailed out in table 6.1. The tissue was fixed in 4% PFA +2.5% EM grade glutaraldehyde in sodium cacodylate buffer at 4°C until processed for electron microscopy. The post mortem (PM) delay for each sample is listed alongside the sample list in chapter 6. This indicates the time after death where the tissue was removed and fixed. The processing of the samples, imaging using transmission electron microscopy (TEM) and serial block face sectioning/ scanning electron microscopy (SBF-SEM) was done by Dr Kathryn White and Tracey Davey at Electron Microscopy Research Services (EMRS) at Newcastle University.

6.3.3 *Transmission electron microscopy (TEM)*

TEM was conducted to identify dopaminergic neurons prior to SBF-SEM and was performed by Dr Kathryn White and Tracey Davey at Electron Microscopy Research Services (EMRS) at Newcastle University.

Initially, the quality of the samples were visualised prior to SBF-SEM using TEM. The quality is referring to the heavy metal staining, the morphology of the samples and the amount of artefacts in the samples. In some cases there were areas of the tissue missing within the neuron which would skew the analysis. This also allowed identification of dopaminergic neurons present within the tissue. Dopaminergic neurons were selected with the presence of neuromelanin, which is a dark pigment found within these neurons in humans. If the quality was not up to standard or if dopaminergic neurons are not found within the sections, a new section was taken from the sample and analysed using TEM again.

For TEM, the samples were post-fixed in 1% osmium. This is for useful for preservation of the cell membrane as it reacts with the lipid bilayer and also provides contrast for EM imaging. The tissue was subjected to heavy metal staining protocol as described (Wernitznig et al., 2016, Wilke et al., 2013, Cocks et al., 2018). The protocol involves penetration of the samples with a number of heavy metals as SBF-SEM imaging requires backscattered electrons, which can only occur if the tissue is electron dense. After the final heavy metal solution, the tissue is dehydrated using increasing concentration of acetone from 25% to 100%. The acetone was then replaced with increasing concentrations of 812 epoxy resin. The embedding was done in 100% resin at 60^OC for 48 hours. The sections were cut using an ultra-microtome at a thickness of 1 μM and stained with toluidine blue, which is a basic dye and stains acidic components such as nucleotides which can be visualised under a light microscope. This was used to identify the relevant areas and then ultrathin sections (70nm for this study) were cut using a diamond knife on a Leica EM UC7 ultra-microtome. Following this, the compression in the tissue is removed by stretching in chloroform and the section was picked up on Pioloform-filmed copper grids. The sections were imaged using the Philips CM100 TEM and images obtained using AMT CCD camera.

The region of interest was identified at a magnification of 1400x. The magnification is relatively low due to the size of dopaminergic neurons being around 20-25 µM within the samples. More detailed images were captured at 13500x. If the tissue was adequate, the tissue was then imaged using SBF-SEM technique.

6.3.4 *Serial block face scanning electron microscopy (SBFSEM)*

This was conducted to obtain the 3D structure of mitochondria in individual neurons and again, was performed by Dr Kathryn White and Tracey Davey at Electron Microscopy Research Services (EMRS) at Newcastle University.

The serial block face /scanning electron microscopy (SBF-SEM) technique has been described previously in the literature (Denk and Horstmann, 2004, Peddie and Collinson, 2014). The resin-embedded samples were glued onto a metal pin, trimmed to approximately 0.5 x 0.5mm and coated with gold.

This technique provides a 3D model of the tissue using a Z-stack. This uses a Zeiss Sigma Scanning Electron Microscope incorporating the Gatan 3view, which is a microtome and a diamond knife inside the SEM chamber. An image is taken using an electron beam that scans the tissue block surface and the backscattered electrons are detected to produce the image. An ultrathin section (of 50nm for this study) is cut using the diamond knife, and another image is taken. The resolution of the images was 3000x3000 pixels or 3500x3500 pixels. These variations are due to the variations in size of individual neurons. This process of section, image, section, and image is repeated until the necessary depth is acquired to produce the Z-stack required. For the purpose of this study, stacks of 150-300 images were collected. A specific region of interest can be chosen, and based on the number of cells within a section, a maximum of 4 regions of interest were selected per section.

6.3.5 *Analysis of the 3D structures*

The stack of tiff images were manually reconstructed in microscopy imaging browser (MIB) (Belevich et al., 2016). A guide to using this software has been published (Cocks et al., 2018). The resolution that was optimised and used allows visualisation of the cristae, through which

233

mitochondria are identified. Mitochondria were randomly chosen from a single slice based on the proximity to nucleus. The Z-stack was then analysed to see if the mitochondrion is fully included within the stack. If it is not the case, the mitochondrion is discarded and another is chosen at random so that its structure is entirely contained within the Z-stack. The chosen mitochondrion is then manually traced on consecutive slices and reconstructed based on the 3D slices in MIB. A total of 32 mitochondria from the perinuclear region and 32 from the distal regions were reconstructed producing a total of 64 mitochondria from an individual neuron. A larger number of mitochondria was available but was not analysed as this is a preliminary study. The definition of perinuclear and distal regions are as described in the previous chapter section 5.3.4. To identify these regions based on the distance from nucleus, the nucleus was also reconstructed. The images were exported to IMARIS 9 and AMIRA and the parameters of surface area and volume were obtain from both software allowing comparison between them. Using IMARIS to obtain these parameters has been described previously in this thesis (section 2.2.7) and using AMIRA has been presented in the above mentioned study (Cocks et al., 2018). An additional parameter used to quantify mitochondria branching and connectivity was the mitochondrial complexity index (MCI). This parameter allows in depth analysis of the mitochondrial network. The equation used for this is presented in equation 6.1 and is has been previously developed and validated by Dr Amy Vincent (Wellcome centre for mitochondrial research, Newcastle University) (Vincent, 2017).

$$MCI = \left(\frac{SA^{3/2}}{4\pi V} \right)^2$$

Equation 6.1 The MCI equation used to calculate mitochondrial branching. The SA refers to the area of the surface and V refers to the volume of the surface.

6.4   Result

6.4.1   *Optimising methodology*

Due to the novelty of this study, optimisation of certain parameters were required. Small regions of the substantia nigra (SN) were collected from individuals and fixed by Dr Christopher Morris (Newcastle Brain Tissue Resource). These specific neurons were targeted due to the large levels of ΔmtDNA deletions observed in this region, data I had collected in previous studies and their importance for Parkinson's disease (Kraytsberg et al., 2006b, Bender et al., 2006c). A comparison of the levels of ΔmtDNA within different regions of the brain is also provided in tables 3.1 and 3.2.   Within the SN, dopaminergic neurons were distinguished from other neuronal populations by their size and the due to the presence of neuromelanin. Figure 6.1 presents an image of a neuron with and without neuromelanin.

Since Dr Kathryn White and Tracey Davey at Electron Microscopy Research Services (EMRS) at Newcastle University, provided expert knowledge and vast amounts of experience in processing and imaging samples, the technique of SBF-SEM did not require any additional steps of optimisation.

235
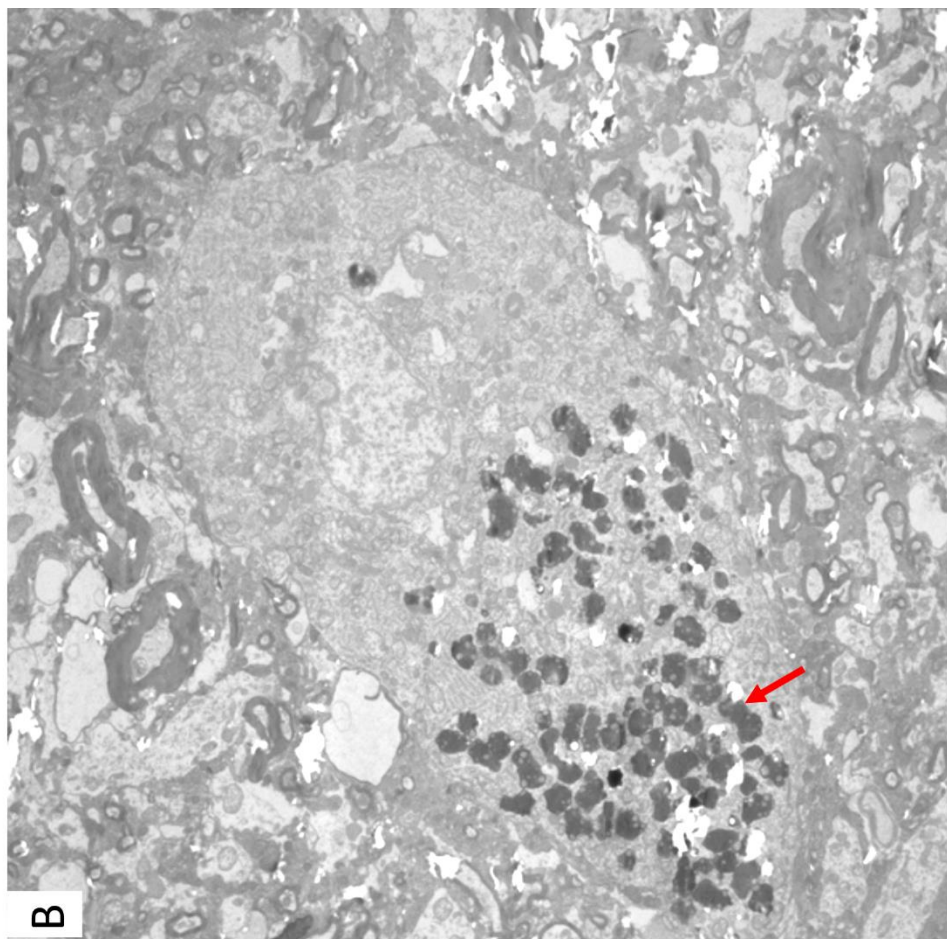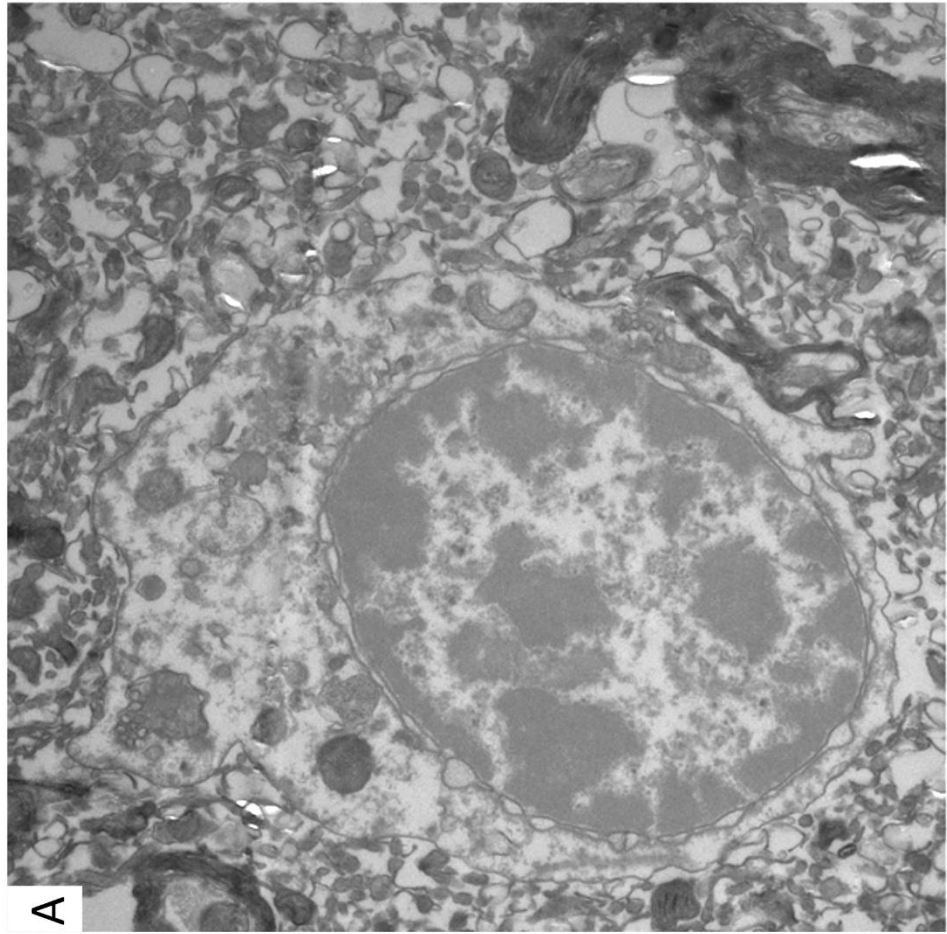
Figure 6.1 Dopaminergic neurons are distinguished from other neuronal population by the presence on neuromelanin, the type of cell is unknown. Image A presents a neuron without neuromelanin. Image B presents a dopaminergic neuron due to the presence of neuromelanin as highlighted by the red arrow. The scale bar for image A is 2µM and for B is 10µM, which further highlights the increased size of dopaminergic neurons. The images were obtained using TEM, at a magnification of 10500x for image A and 2600x for image B.

Following successful identification of dopaminergic neurons, the resolution had to be adjusted to correctly identify the whole neuron without compromising this resolution. This is because a higher resolution would require higher magnification, which would render the already big dataset, even bigger. This could cause computational problems. This study aimed to investigate the connectivity of the mitochondrial population within dopaminergic neurons, there was a need to be able to confirm the neuronal membrane to ensure analysed mitochondria were within this. Furthermore, as highlighted in figure 6.1, the dopaminergic neurons are large cells. A few different magnifications were trialled and a magnification of 3000-3500x was set as the standard as it allowed visualization of the cristae within the mitochondria allowing appropriate identification of mitochondria, however, other smaller structures such as nucleoids could not be properly distinguished at this magnification. However, it did allow representation of the whole neuron. A range of 3000-3500x was used as a standard and the magnification was set individually for each case based on the size of the dopaminergic neurons.

Previous studies on skeletal muscle identified a section thickness of 30-50nm (Cocks et al., 2018, Vincent, 2017). Due to issues with the section variations at 30nm, the thickness of the section in this study was trialled at 50nm as it appropriately identified the same mitochondria in sequential stacks, and the end of a mitochondrial network was identified more accurately. SBF-SEM has the capacity to reduce section thickness to 25nM, however, a lower thickness is also associated with other technical difficulties such as the section not being properly sliced or removed by the microtome or sectional variation.

The number of sections (depth of dataset) was then optimised for SBF-SEM. This feature also depended on the individual case and the size of the neuron. For this study, at least 100 sections were used to identify the whole mitochondria. In this case, none of the stacks had a complete dopaminergic neuron cell body, again due to the size of this cell. Therefore a minimum of at least 100 sections are required for appropriate identification of the mitochondrial population. A range of sections from 100-200 per neuron was collected in this pilot study.

6.4.2 *Comparison between IMARIS 9 and AMIRA*

IMARIS was initially considered for use in this study for continuity reasons following on from previous chapters. However, a number of computational problems were encountered due to the size of the dataset. This could be a computational processor problem rather than the actual software. When this occurred, Amira was chosen due to in-house experience by Ross Laws (EMRS) and previously optimised techniques to analyse SBF-SEM data in this software (Cocks et al., 2018). IMARIS was preferred for analysis due to the added parameter of distance between each surface created. This allows quantification of the distance between the nucleus and each surface. This measurement was calculated as the distance between the midpoints of both surfaces. In Amira, this requires manually drawing a line and measuring it on the software, and in a large-scale study, such as this which aimed to examine a large number of mitochondria, this is not feasible to do. However, due to the processing problems in IMARIS, AMIRA was chosen for this study. The distance from nucleus was compared manually, as presented in figure 6.2.

The parameters of surface area and volume were obtained from Amira. This was also compared to the few of the cases that successfully worked on IMARIS 9. One-way ANOVA showed no significant differences in both these parameters in an individual case between both these software, further validating the data obtained. The graph comparing IMARIS 9 and AMIRA data is presented in figure 6.3.
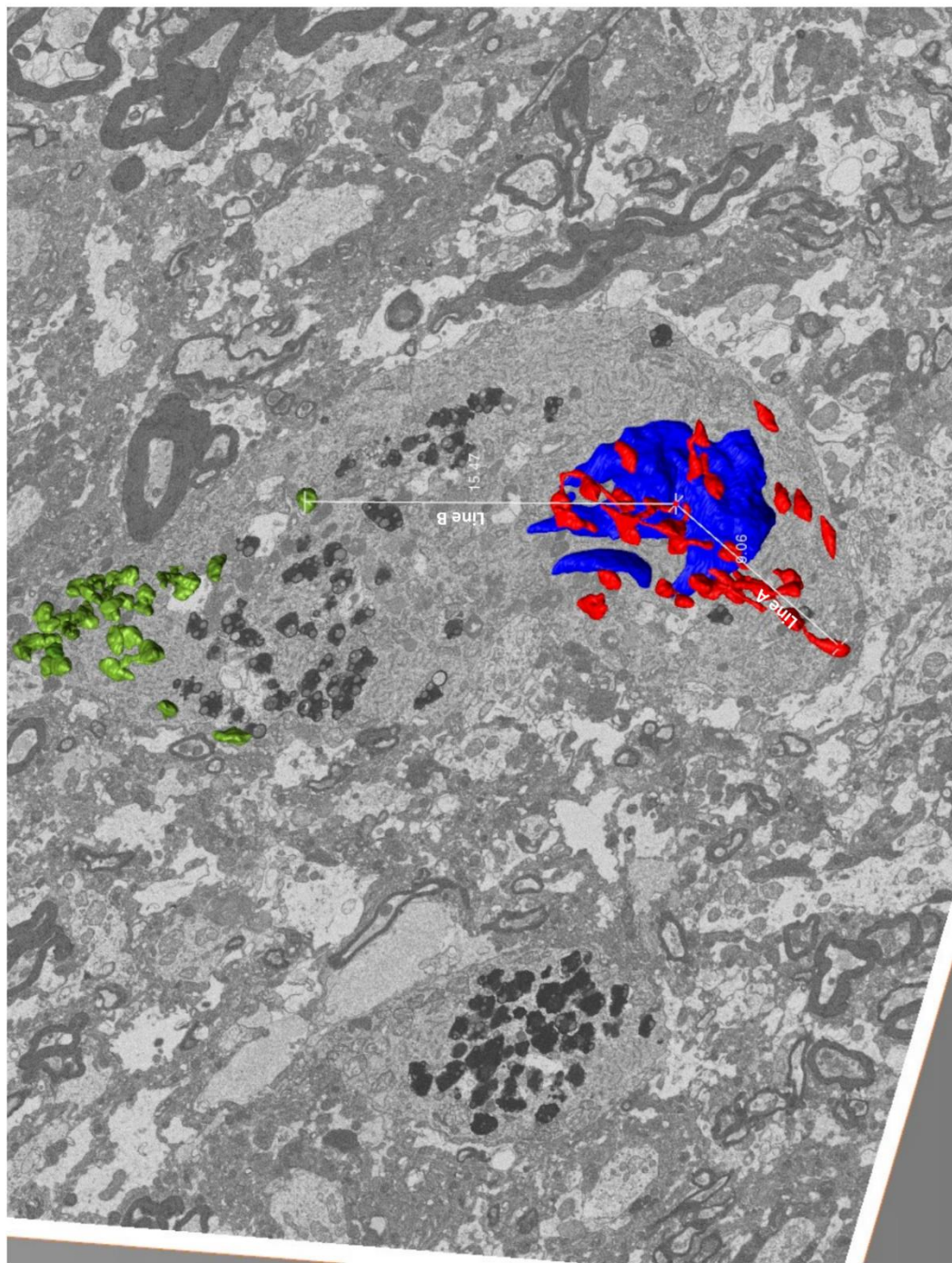
Figure 6.2 Manually measuring the distance from nucleus in AMIRA. This image presents a 3D reconstruction with two lines drawn from the centre of the nucleus to the furthest mitochondria in the region considered perinuclear and to the closest mitochondria in the region considered 'distal'. Line A has a length of 9.06nM and Line B is 15.47 nM. The images were obtained using SEM, at a magnification of 3500x. The blue surface highlights the nucleus, red highlights perinuclear mitochondria and the yellow highlights distal mitochondria.
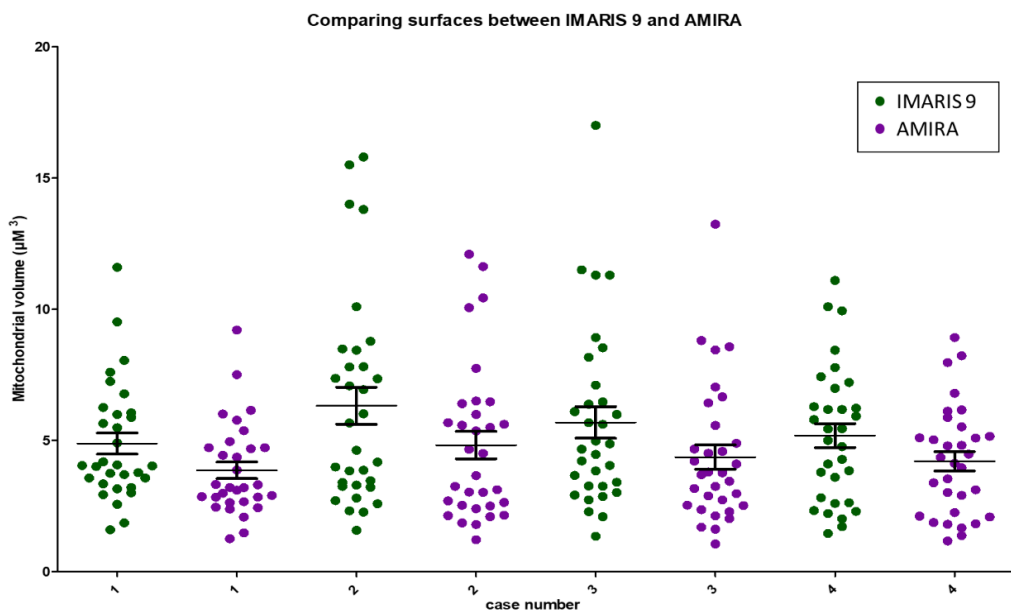
Figure 6.3 Comparing mitochondrial volumes obtained from IMARIS 9 and AMIRA. This was conducted to validate the data between the two software suggesting that the data is reliable as there were no significant differences observed from two independent software. The data was tested using a one-way ANOVA and with p>0.05.

6.4.3 *Comparing variability between controls*

All the controls were compared to analyse any variability between each other in each of the parameter tested, which were mitochondrial surface area, mitochondrial volume and MCI. Previously in the literature, a 'form factor' was calculated from 2D images of mitochondria, which provided the degree of branching (Mortiboys et al., 2008, Koopman et al., 2005). This was calculated based on the length and aspect ratio of the mitochondria. This equation was modified for use in 3D structures and is presented in equation 6.1. This equation took into account the 3D nature of these structures by using the surface area and volume of each mitochondrial surface. This equation has been systematically evaluated and validated to study mitochondrial branching (Vincent, 2017).

One-way ANOVA was used to test any significant differences between the cases. No significant differences were observed between the controls, except in the case of MCI. This is presented

in the graphs in figure 6.4. Significant differences in the MCI between C3 and some of the other cases could potentially be due to biological variation, which could be confirmed by increasing the sample size.
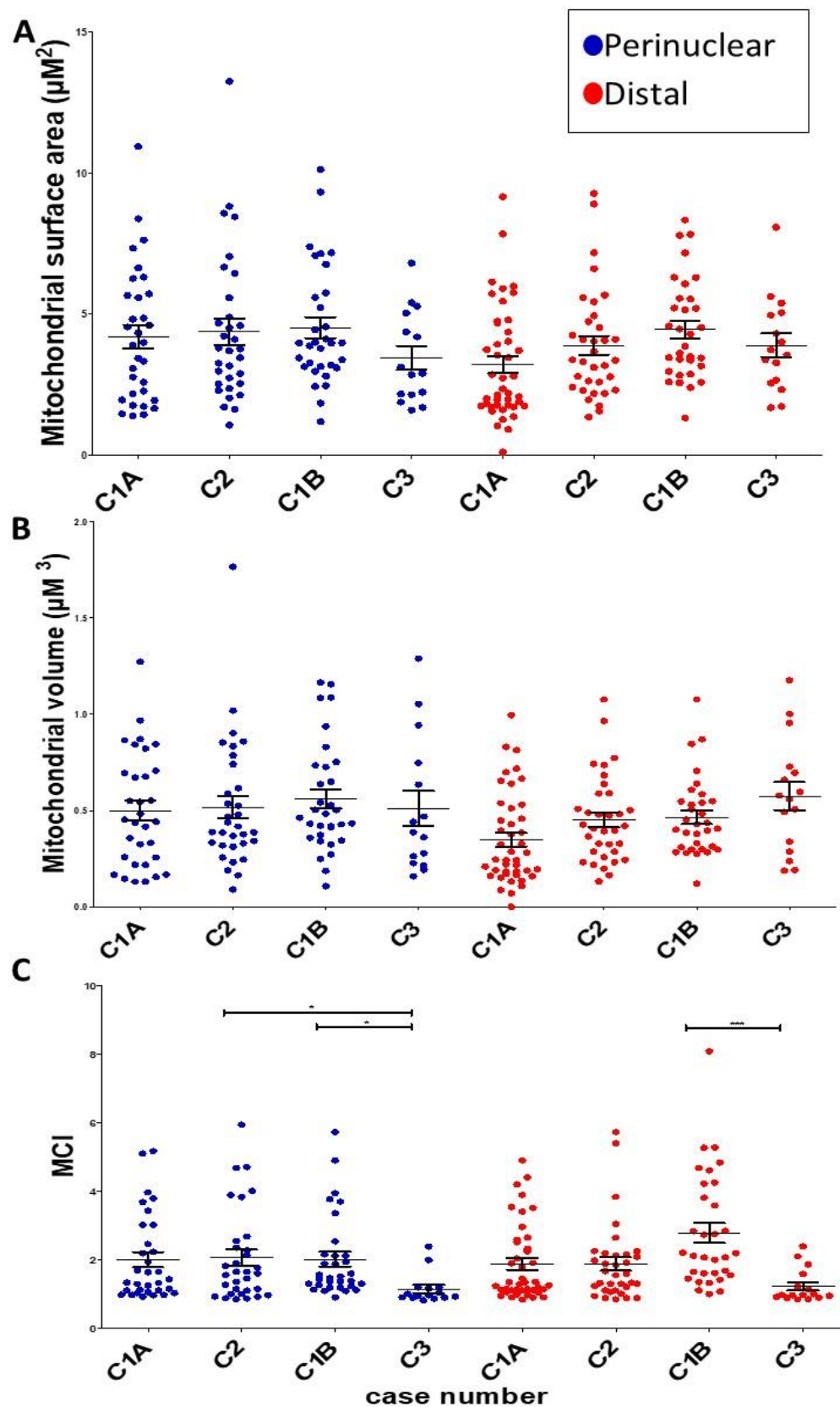
Figure 6.4 Testing the variability between controls. This was conducted to validate that the controls were in fact controls. The details of the cases are highlighted in table 6.1. The data was tested using a one-way ANOVA and * indicates p>0.05 and *** indicates p>0.001.

6.4.4 *Comparing mitochondrial parameters with healthy ageing and disease conditions*

Mitochondrial surface area, volume and MCI was also compared between healthy ageing and patient tissue. The controls were pooled together and compared to the patient tissue. The graphs are presented in figure 6.5.

In the case of mitochondrial surface area and volume, there is no significant difference between the control neurons and the patients, in both the perinuclear and distal group.

The MCI data showed significant differences ($p < 0.001$), however, all these differences were between the case P3 and all the other data. All the other cases did not show any significant differences from the control. In the distal region, P2A was also not significantly different from the P3 region. An image of P3 compared to one of the control, C1A, is presented in figure 6.6. This highlights the clear difference in the mitochondrial branching.

The significant differences observed in MCI that was not present in the mitochondrial surface area and volume highlights the importance of studying mitochondrial connectivity in 3D.
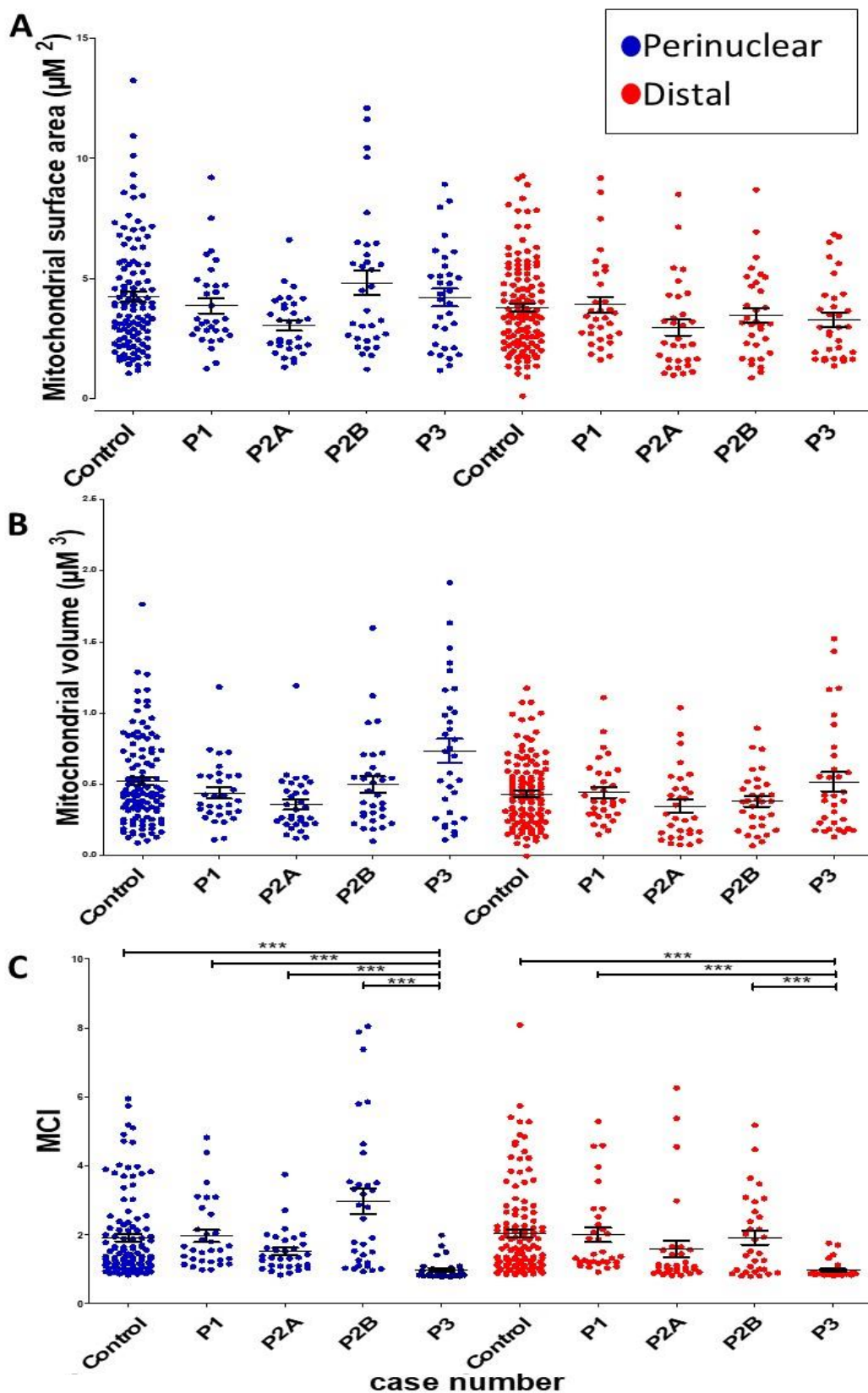
*Figure 6.5 Comparing mitochondrial parameters between healthy ageing and disease conditions. This figure presents the mitochondria surface Area (A), mitochondrial volume (B) and MCI (C). The data was tested using a one-way ANOVA and ** indicates p>0.01 and *** indicates p>0.001.*
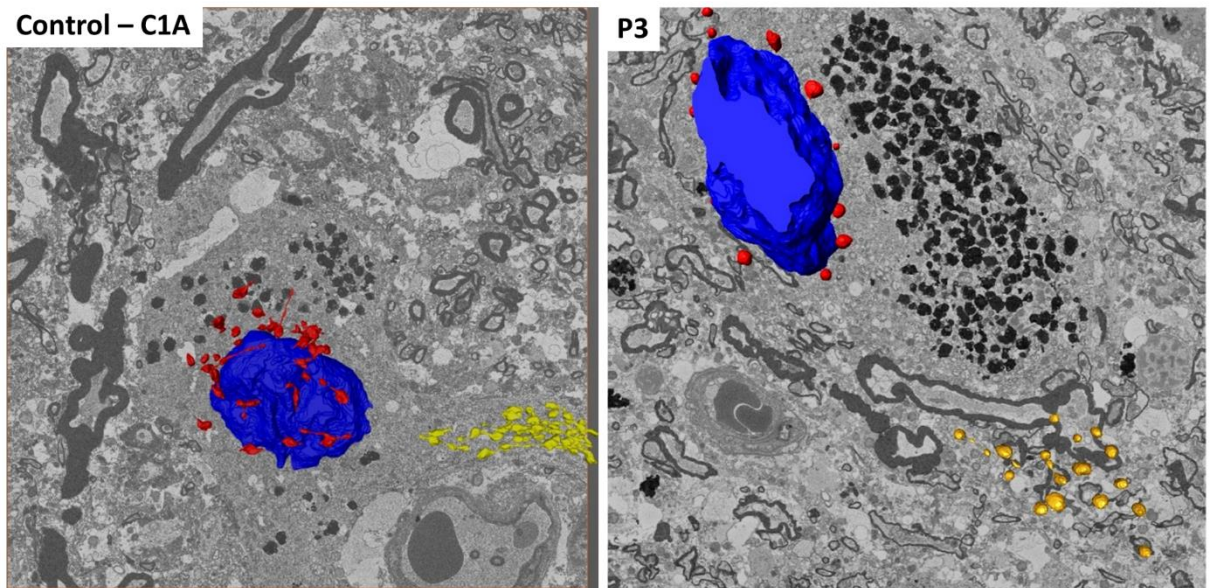
Figure 6.6 Comparing mitochondrial MCI (degree of branching) between healthy ageing and DLB. This figure presents the 3D reconstructions of the mitochondria in in a control case C1A and in the DLB case P3. P3 has significantly different (p<0.001) MCI values from most of the controls and other disease individuals used. The blue surface highlights the nucleus, red highlights perinuclear mitochondria and the yellow highlights distal mitochondria.

6.4.5 *Comparing mitochondrial parameters in neurons with Lewy bodies*

As mentioned above, in some cases, multiple neurons from the patient were reconstructed. In one of the DLB patients, two separate dopaminergic neurons from the same patient were analysed: P2A and P2B. One of these neurons presented with Lewy bodies, however the other did not show evidence of a Lewy body within the stack analysed. An image of both the neurons, along with the 3D reconstructions is presented in figure 6.7. Although significant differences (p<0.05) were not noticed when the datasets were compared, there are observable differences. In the neuron without the Lewy bodies (P2B), the mitochondria appeared elongated and branched and in the neuron with the Lewy bodies, the mitochondria appeared more fragmented. However, an increased number of mitochondria will need to be analysed to study this in more detail.

245
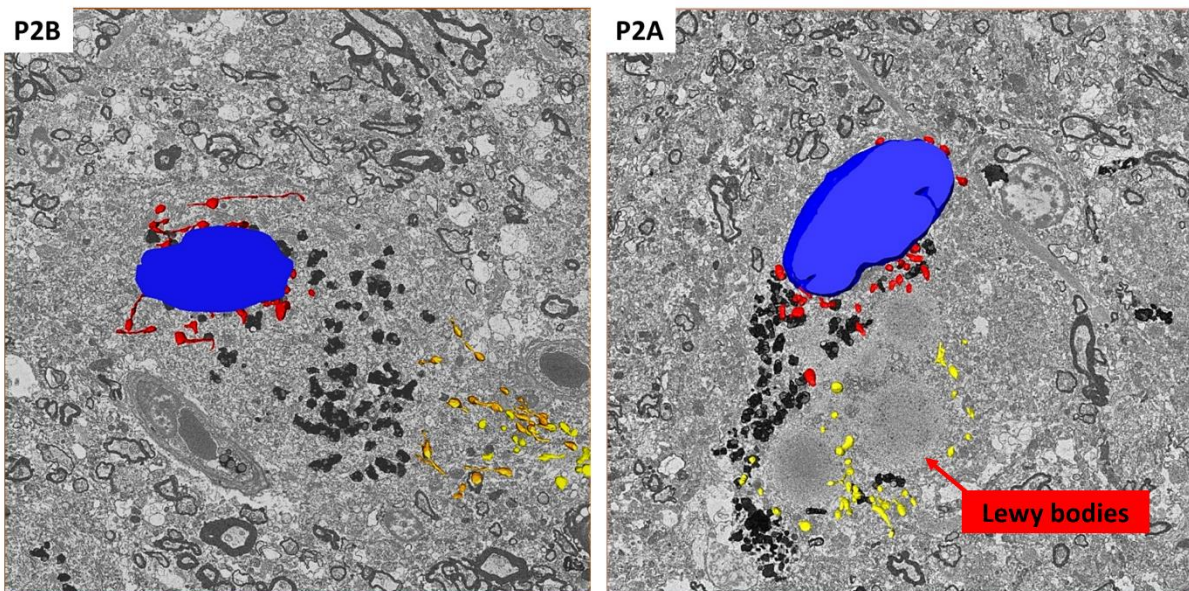
Figure 6.7 Comparing cells with and without Lewy bodies from the same patient. This figure presents the D reconstructions of the mitochondria in two neurons from the same DLB patient. One cell contained lewy body heighted by the red arrow, and the otherdid not. The blue surface highlights the nucleus, red highlights perinuclear mitochondria and the yellow highlights distal mitochondria.

### 6.4.6 *Comparing mitochondrial parameters with perinuclear and distal mitochondria*

There were no significant differences (tested for $p < 0.05$) between the perinuclear and distal regions in all the three mitochondrial parameters tested. This is presented in figure 6.8. This could be due to two main factors, one of which is the number of mitochondria studied. A total of 32 mitochondria per region could not be a large enough 'n' number to see any significant differences. A high total number of neurons analysed could be beneficial. Alongside this, due to the technique, there were difficulties in establishing a perinuclear or distal region. In the majority of the neurons studied, axonal regions were not visible. This could suggest that all the mitochondria studied in these cases were actually perinuclear. This will have to be improved in further studies.
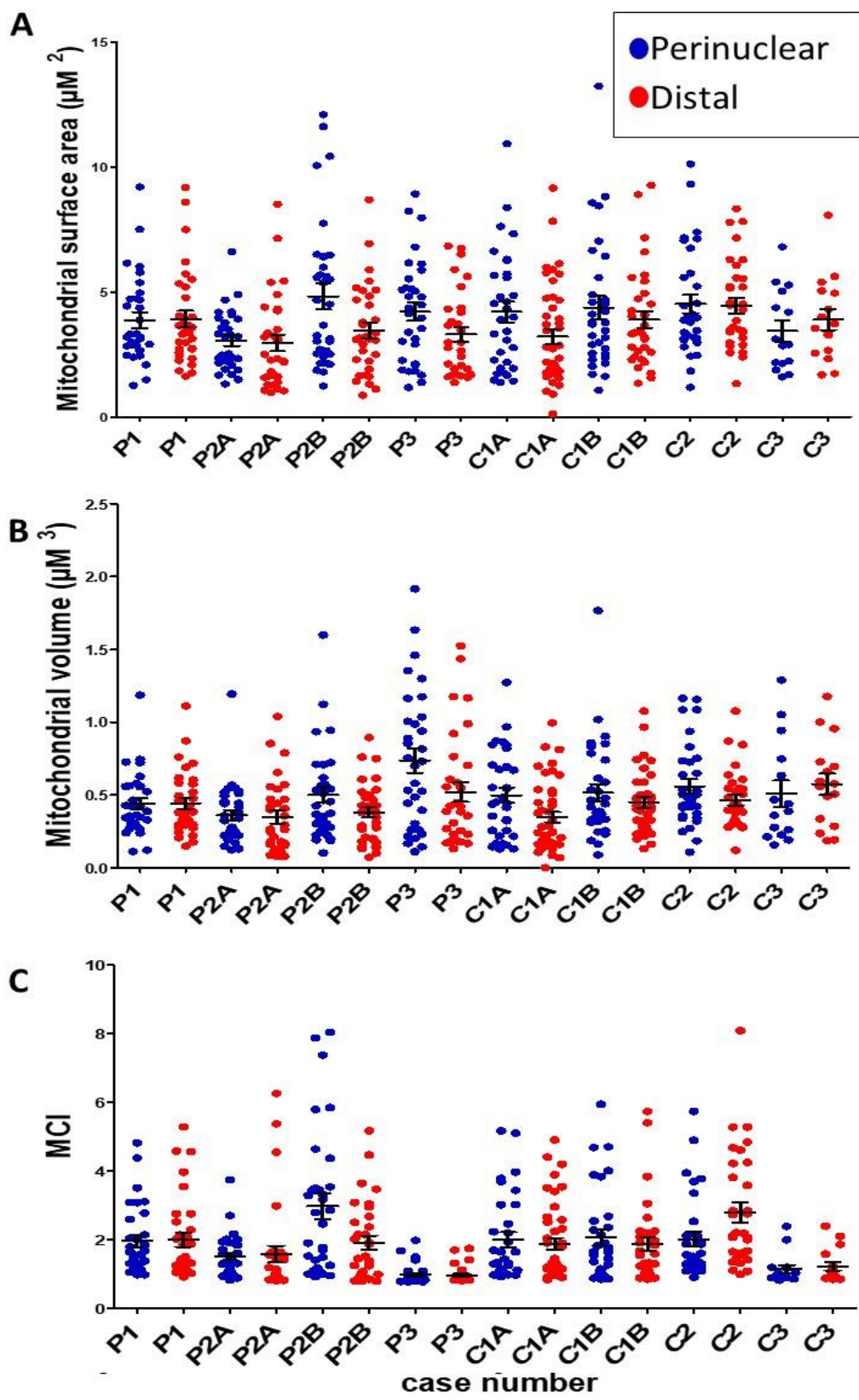
Figure 6.8 Comparing mitochondrial parameters between perinuclear and distal mitochondria. This figure presents the mitochondria surface Area (A), mitochondrial volume (B) and MCI (C). The data was tested using a one-way ANOVA and no significance was observed at p>0.05.

247

6.4.7 *Nanotunnels or Mitochondria on a string (MOAS)*

Two of the studies mentioned in the introduction have noticed certain structures of mitochondria where two bodies of mitochondria are connected by a long tubular structure (Zhang et al., 2016, Vincent et al., 2017). Initially, these structures were identified in studies in cardiomyocytes and kidney cell with Confocal imaging and TEM respectively (Huang et al., 2013, Gupta et al., 2008). In the study on kidney cells, these thin microtubular structures were termed 'mitochondrial extensions'. The study on cardiomyocytes coined the term 'nanotunneling' and suggested this to be a mechanism of communication between static mitochondria to exchange contents or signals between the network (Huang et al., 2013). Following this, a study on skeletal muscle identified these structures using SBF-SEM (Vincent et al., 2017). They identified a number of features of these structures including the presence of a double membrane, a diameter of 40-200nM and a length of up to 30μM. This study also suggested these structures to aid the sharing of contents between mitochondria. Following this, nanotunnels were also found to be at an increased frequency in patient tissue compared to controls (Vincent, 2017). These nanotunnels are consistent with the bacterial origin of mitochondria as nanotubes are used by bacteria for the purpose of communication (Dubey and Ben-Yehuda, 2011).

However, a similar structure has also been identified from the brain of Alzheimer's patients using ssTEM (Zhang et al., 2016). They termed this structure 'mitochondria on a string' (MOAS) due to its appearance. They suggested that this structure was due to arrested fission of the mitochondria in a damaged tissue, developed as a compensatory mechanism to counteract the biochemical defect and protect from mitophagy. They also found this structure in wild type mice when damage was induced by hypoxia or in an ageing cohort. Following this study, ssTEM was also used on rhesus macaques where this structure was also observed with ageing (Morozov et al., 2017). They suggested this could be a result of a malfunction in dynamics with ageing.

Another study in mice using FIB-SEM also recognised tubular mitochondria. In this case, these mice were transgenic with an inducible Drp1 ablation, specific for neurons (Tamada et al.,

248

2017). Drp1 is involved in fission of the mitochondria. This study discovered that, when the Drp1 mutation was induced, after one week it lead to various tubular mitochondria, however after two weeks, these resulted in enlarged mitochondria. It has been suggested that, due to the lack of Drp1, the mitochondria fused together. In this scenario, the fission arrest lasted for a week and lead to enlarged mitochondria. If MOAS theory is true, a large number of enlarged mitochondria would be observed in the cases presenting a large number of nanotunnels. However, this cannot be confirmed since the mice used in this study specifically had a *DRP1* knockout. However, in patients, fission arrest could be temporary, hence it does not lead to enlarged mitochondria.

These structures were identified in this study in single substantia nigra neurons and images of them are present in figure 6.9. The sequential images (A-N) presents the reconstruction of two mitochondria which are connected via a nanotunnel highlighted in red. Due to the number of stacks through which this extends, a few sections were omitted in the figure, and thus a representative reconstruction is presented in this figure. Another mitochondrion with a nanotunnel is presented in figure 6.10, which also contains the measurement of its diameter. Both of these were from case P2B (DLB), where a large number of tunnels were observed. Nanotunnels were also observed in both patient and control tissue, however, none compared to the number in the case P2B. These nanotunnel structures were also observed frequently in P1 which is a patient with AD. This is in concordance with the paper stating the MOAS theory (Zhang et al., 2016). The presence of nanotunnels were cell dependent as they were noticed in some disease and control cases, and were also equally absent from other disease and control cases. This is presented in figure 6.11. However, as mentioned before, this could be the effect of using aged controls, however this is a pilot study with a small sample size and requires extending to a larger number of neurons.
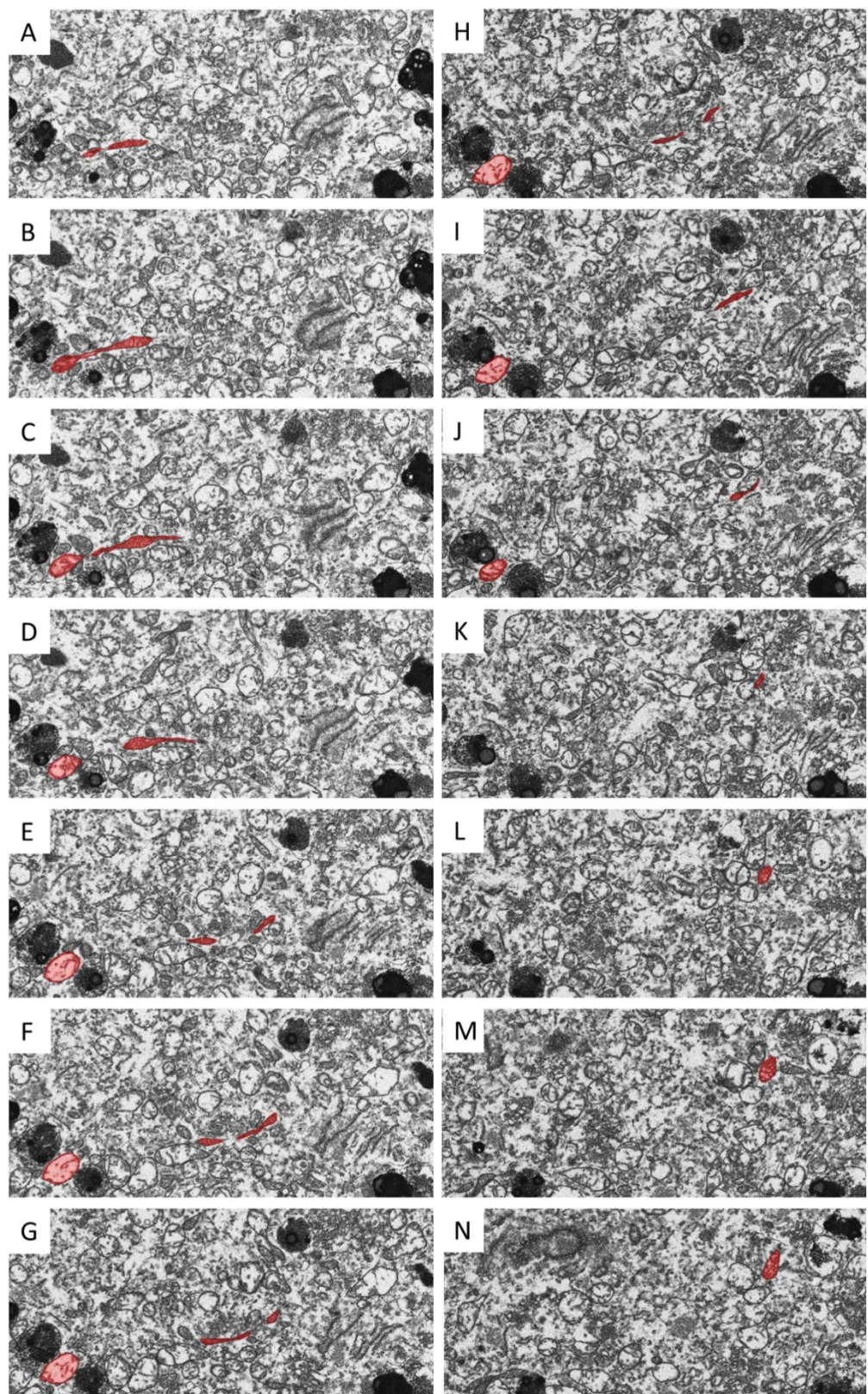
Figure 6.9 sequential sections highlighting the tubular structure. This image presents a 3D reconstruction of the nanotunnels. The images were obtained using SBF-SEM, at a magnification of 3500x.
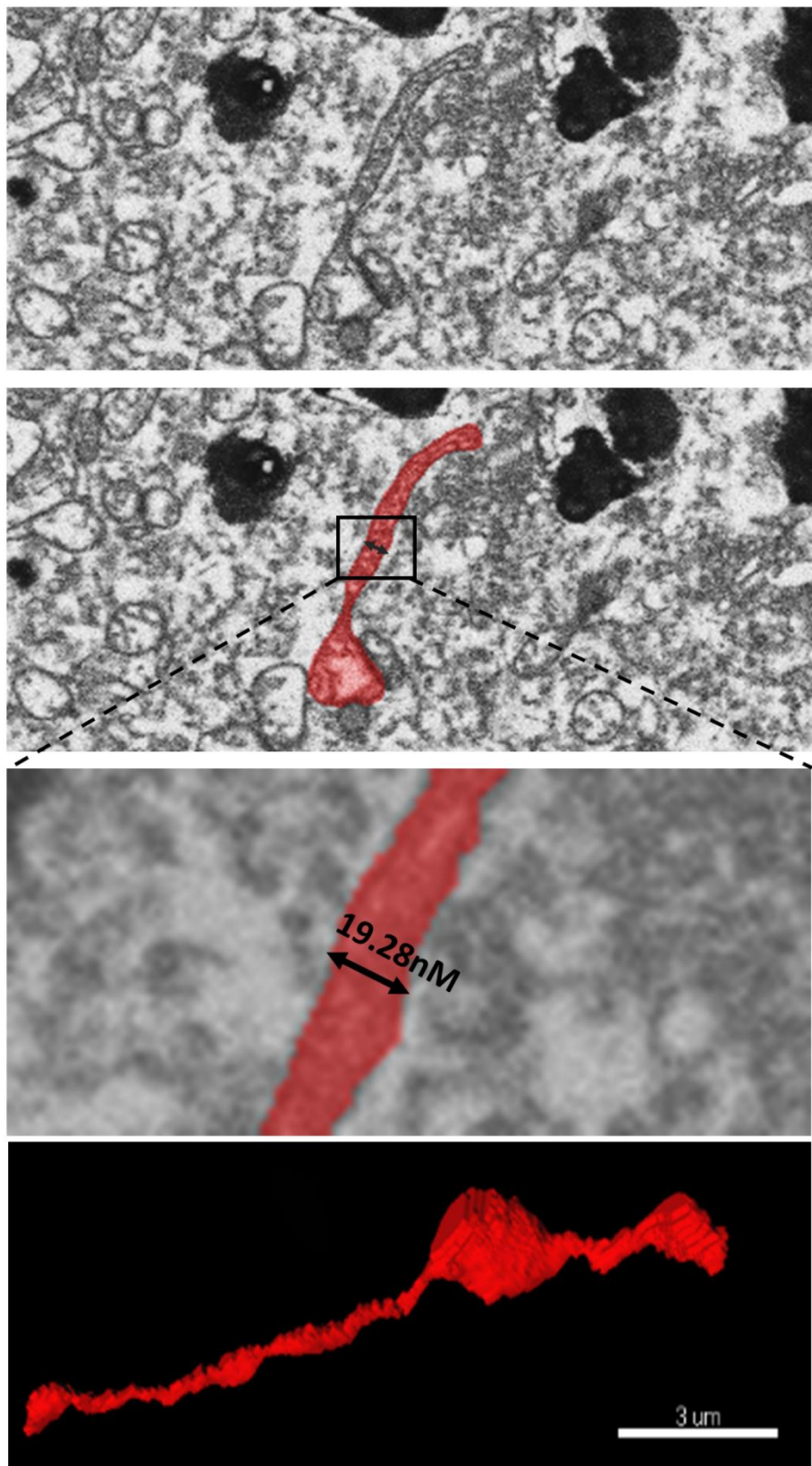
Figure 6.10 Mitochondrial nanotunnel. The diameter of this structure is presented in the image. A 3D reconstruction of this mitochondrion with the nanotunnels is also presented in this image. The images were obtained using SBF-SEM, at a magnification of 3500x.
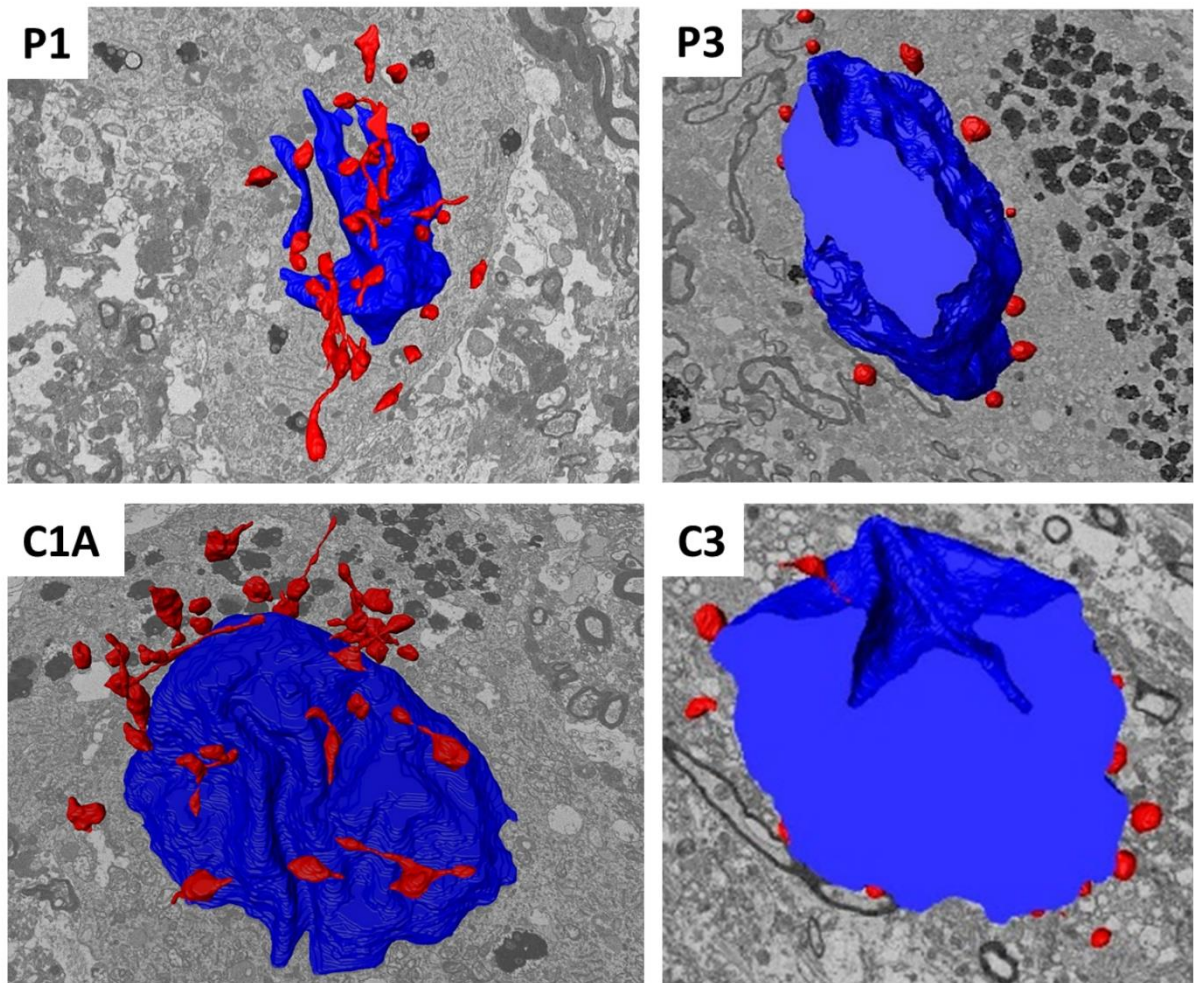
Figure 6.11 Mitochondrial nanotunnels in patient and control cells. This figure presents the 3D reconstructions of the mitochondria with nanotunnels in the cases P1 and C1A and mitochondria without nanotunnels from the cases P3 and C3. The details of each case are highlighted in table 6.1. The blue surface highlights the nucleus and the red highlights perinuclear mitochondria. The cytoplasmic mitochondria are not presented in these cases.

6.5   Discussion

6.5.1   *Comparing mitochondrial parameters between healthy ageing and patients*

In this study, I successfully used the SBF-SEM to reconstruct mitochondria from single dopaminergic neurons from human tissue in healthy aged controls and a small cohort of patients with neurodegenerative diseases including AD and DLB. We also undertook the first assessment of the mitochondrial 3D network in this tissue in humans. The technique needed optimisation, which was undertaken and is detailed in the results section. A fully optimised

method to study mitochondria in human dopaminergic neurons has been developed in this study.

Four neurons from patients with neurodegenerative diseases and four controls were used in this study. The controls were tested for variability. No significant differences ($p < 0.05$) were noticed between the control in the mitochondria surface area and volume, however, there were a few significant differences ($p < 0.05$) in the MCI values. This could be due to biological variation or due to the age of this control. This is potentially the effect of a small sample size, as it renders the statistical power weak. Since this is a pilot study, it was useful to investigate any statistical differences. A larger number of neurons would of course have to be studied to validate this and statistical power.

When these parameters were compared between patients and between patients and the controls, significant differences ($p < 0.05$) were noticed in mitochondrial surface area and MCI, but not in volume. This suggests that mitochondrial volume remains same in healthy ageing and in neurodegenerative conditions, however, the surface area and MCI changes suggests that the mitochondria may become more tubular and branched, but the overall volume remains the same. This might suggest that the mitochondria are altering their shape, but not their volume. In support of this is work that suggests that fission and fusion proteins such as drp1, mfn1 and mfn2 are altered in AD models (Westermann, 2010, Manczak et al., 2011, Wang et al., 2009). Changes in the shape of mitochondria are also linked to neurodegeneration as it affects cell physiology and signalling (Campello and Scorrano, 2010). However, as mentioned before, detailed analysis need to be performed here due to the small sample size and in order to make firm conclusions more cases and neurons require analysis

6.5.2 *Comparing mitochondrial parameters between perinuclear and distal mitochondria*

Unlike the previous chapter and previous literature using ground squirrels and rats (Popov et al., 2005), all of the mitochondrial parameters tested were not significantly different between the perinuclear and distal mitochondrial populations. This could be due to three main reasons. Since the controls used were aged individuals, maybe ageing could influence this similarly in control and disease models. Previous studies on brain tissue from healthy ageing and PD patients have demonstrated that the levels of mtDNA deletions and COX-deficiency were

similar in PD and age-matched controls, which were significantly different from a younger group (Bender et al., 2006c, Kraytsberg et al., 2006b). However, the result from the previous chapter highlight no significant differences in thymidine analogue incorporation and therefore mtDNA replication between these regions in a young and aged cohort.

Another reason for the lack of any significant difference could be due to the regions in this study that were termed perinuclear and distal. Since the Z-stacks were based on the cell body, the majority of the neurons did not produce an axon. Due to this, the mitochondria termed 'distal' could in fact be perinuclear. A number of the Z-stacks, along with the cell body of a dopaminergic neuron, also contains axons from nearing cells. These are myelinated and easily identified, Therefore, to combat this, mitochondria within nearby axons could be studied. However, this presents another problem that the mitochondria studied will be from different cells and as noticed before, there could be cell to cell differences (figure 6.7). Alongside this, the sample size is too small and hence, the statistical power is weak. Therefore, this required a higher number of neurons analysed.

6.5.3 *Variability between cells from the same patient*

This study also noticed variability in two different neurons from a patient with DLB. These were observational and not significantly different for the parameters tested. From this patient I investigated a neuron which contained a Lewy body and one which did not. In the neuron without the Lewy body, the mitochondria appeared highly tubular and elongated, whereas in the presence of Lewy body, mitochondria appeared fragmented (figure 6.7).

GBA1 is a gene which is highly variant in individuals with PD, which is a disease that presents with Lewy bodies. Mutations leading to loss of functions in this GBA1 gene in a mouse model demonstrated accumulation of α-synuclein which is the main component of Lewy bodies (Osellame et al., 2013). This study also demonstrated an increase of fragmented mitochondria in this case. Increased fragmentation of mitochondria has also been demonstrated in vitro upon the over-expression of α-synuclein (Nakamura et al., 2011). This suggests that the fragmented mitochondria could be the result of the Lewy bodies. However, mitochondria have also been suggested to influence α-synuclein accumulation as they can release a protease enzyme called neurosin that can cleave the α-synuclein aggregation or the Lewy body, but can

also release cytochrome C which is suggested to be involved in the accumulation of α-synuclein (Iwata et al., 2003).

However, this requires further work, since the neuron without Lewy body could actually in fact contain Lewy bodies, which were not present in the Z-stack taken. In addition to this, the lack of significant differences could be due to the parameters tested or due to the small sample size.

6.5.4 *Nanotunnels*

As mentioned before, although the presence of these long tubular structures were observed in AD from neurons in the hippocampus, cortex and cerebellum, this study is the first to observe this within dopaminergic neurons from patients with AD, DLB or in healthy ageing. A number of the reconstructed mitochondria were presented with these nanotunnels. These structures were frequent in P1 and P2B. P1 is a patient tissue affected by AD and these structures were observed on the case of AD tissue previously and was suggested to be due to fission arrest (Zhang et al., 2016). This is a novel discovery in the case of a neurons affected by DLB. However another neuron from the same tissue was presented with no nanotunnels, although this neurons contained Lewy bodies (refer to figure 6.7), therefore the nanotunnel could potentially be a compensatory mechanism present at low levels of cellular stress. However, neurons from control also demonstrated an absence of nanotunnels which could be due to the specific control used. Nanotunnels were observed in C1A where the age of the patient was 54, but absent from C3 where the patient was 94 years old. This is preliminary and the differences were observed but not quantified, therefore, the study needs to be extended to a larger dataset in order to test for a relationship between these nanotunnels and ageing and disease state.

6.5.5 *Accumulation of ΔmtDNA*

This pilot study has identified a technique through which variations within the ultrastructure of the mitochondria could be observed from the SN, which also possess high levels of ΔmtDNA. Since the sample size is small, these variations are not significant between healthy ageing and individuals with AD and DLB. Alongside this, variations between the perinuclear and distal

mitochondria were also not observed as discussed above. However there were observational differences in both groups which could potentially be significant with a larger sample size.

In addition to this, nanotunnels were noticed in some cases. If the mitochondria, due to these nanotunnels, are more connected within the mitochondrial network, this could potentially provide a route for the accumulation of ΔmtDNA. However, unpublished data from our group suggests that nanotunnels are unlikely to transport nucleoids since only 4% of nanotunnels are actually wide enough in muscle. Therefore, this would also require further analysis by measuring the lumen diameter of these structures in neurons.

6.5.6 *Future work*

The aim of this chapter was to provide a proof of concept data in studying mitochondrial network and connectivity in a 3D format in human dopaminergic neurons. A large amount of future work remains.

- One of the criticisms against this technique could be the post-mortem (PM) delay variation highlighted in table 6.1. The PM delay is unavoidable as this study was conducted in human tissue. Although no specific association of post-mortem delay was observed in this study, and the quality of the samples was not affected with a higher length of PM delay, this would still require validation. These can be conducted *in vivo* potentially using mice models. The same mice can be used for this purpose. The brain could be sliced down the midline. The SN can be extracted from one half and fixed immediately, and the SN from the other half can be fixed with a stimulated delay. Conducting SBF-SEM on these two sections would allow comparison for any differences associated with the PM delay.

- Since this study is on human, brain tissue from young controls would be more difficult to obtain. Therefore, in order to study an effect on ageing on mitochondrial network and connectivity, *in vivo* studies on mice could be conducted.

- The analysis for this technique is time consuming as the reconstruction is conducted manually. Therefore, 32 mitochondria was selected from each region. However, when expanding, all the mitochondria within a neuron could be studied for an increased N

number. These could be classified based on distance after the reconstructions by obtaining the distance from IMARIS for each mitochondria from the nucleus. With further optimisations and machine learning, this time consuming process could also be automated.

- Since axons are myelinated, SEM easily identifies them. Therefore, this analysis could be extended to axons rather than solely to the cell body. This would be a better representative of the distal mitochondria. However, this might not be reliable due to the different population of neurons present, which would suggest that the axon does not belong to a dopaminergic neuron.

- The previously mentioned study using FIB-SEM has defined and described various structures of mitochondria (Tamada et al., 2017). Classifying mitochondria based on their structure would provide a good comparison between disease and patients and will provide an extra parameter to compare, which could take into account the nanotunnels; however this will be observational and could lead to bias.

6.5.7 *Final conclusion*

This technique is feasible in human SN neurons. This technique is also sensitive enough to notice ultrastructure variations within the mitochondria. Manual reconstruction of the mitochondria is time-consuming, however this ensures the accuracy of this technique as each mitochondrion is studied. Since variations were noticed in this small sample set, this should be repeated to a higher sample size to provide an increased statistical power for analysis.

Chapter 7:   Final discussion

7.1   Introduction

Mitochondrial DNA deletions (ΔmtDNA) have been implicated to be important for ageing as well as a number of disease conditions, including Parkinson's disease and mitochondrial disease. Although they lead to mitochondrial dysfunction and COX-deficiency, the mechanisms by which these deletions form and accumulate to high levels remains unknown. The suggested pathways for deletion formation are through error prone replication or inadequate repair (section 1.6). This study aimed to investigate the role of alterations in mtDNA replication in this process. Although many post mitotic cells present with high levels of ΔmtDNA, the brain was studied in this thesis since it is a vital tissue affected in both mitochondrial disease and PD, and the highest levels of ΔmtDNA reported in the literature are found within this tissue (Cortopassi et al., 1992, Meissner et al., 2008).

7.2   Major findings and further work

7.2.1   *Variations in mtDNA replication with neuronal type, age and genotype.*

Using thymidine analogue labelling, mtDNA replication levels in various brain regions, ages and genotypes were successfully compared in mice. Double thymidine analogue labelling was used, with CldU labelling mtDNA for 4 days and IdU for 15 hours. These timings were optimised as part of another study (Stamp, 2016). Four specific neuronal subtypes and regions were chosen: Purkinje neurons (from cerebellum), Pyramidal neurons (cortex and hippocampus) and dopaminergic neurons (SN). These regions were studied in four groups of mice; wildtype young, *PolgA$^{mut/mut}$* young, wildtype aged and *PolgA$^{mut/mut}$* aged.

The original hypothesis of the study was that if the mechanism of ΔmtDNA formation was through mtDNA replication as suggested (section 1.6), then an increase in mtDNA replication would be associated with an increased level of ΔmtDNA. However, this was not observed, when replication levels from this study was correlated with a previous study in the literature (Perrier *et al*). This would suggest that ΔmtDNA could potentially be forming via another mechanism, for example, mtDNA repair. However, evidence supporting an association of

mtDNA replication with ΔmtDNA was also uncovered, in that there is an inverse relationship between mtDNA replication levels and ΔmtDNA in different brain regions, ages and genotypes. For example, mtDNA replication was found to be increased in the cerebellum and decreased in the SN, whereas levels of ΔmtDNA is comparably lower in cerebellum and highest in SN (table 3.1 and 3.2). Similarly, aged *PolgA$^{mut/mut}$* mice also demonstrated lower levels of mtDNA replication, but high levels of ΔmtDNA (table 3.1 and 3.2). This suggests that in regions with high levels of ΔmtDNA, there are lower levels of mtDNA replication.

My data suggests a general pattern of an increase in mtDNA replication in regions associated with a decrease in ΔmtDNA. Therefore, it could be suggested that increased mtDNA replication results in increased mtDNA copy number, which could function as a compensatory mechanism, whereby the levels and biochemical defect produced by ΔmtDNA appear minimal in these situations. This increased copy number acting as a compensatory mechanism against ΔmtDNA has been suggested previously in the literature (Dölle et al., 2016). On the contrary, some studies have found comparably lower mtDNA copy number in the cerebellum, which is a region with high mtDNA replication and low ΔmtDNA (Fuke et al., 2011b). Other factors which might have an on mtDNA replication levels in association with ΔmtDNA are mtDNA transcription, transport of mitochondria and mitophagy as discussed in chapter 3.

However, there are exceptions to this idea of 'increased ΔmtDNA in regions showing lower mtDNA replication'. For example, the SN generally presents with a higher level of ΔmtDNA with advancing age (table 3.1 and 3.2), however, there was no age associated decrease in mtDNA replication either in the aged wild type or aged *PolgA$^{mut/mut}$* mice. It could be suggested that since the mtDNA replication levels were low to begin with in these neurons, further reduction was not observed with ageing. However, since the mtDNA replication levels are low to begin with, this increase in ΔmtDNA could also be explained by clonal expansion of mutations over time. As suggested in the previous paragraph, due to a lack of compensatory effect by wildtype mtDNA, the ΔmtDNA have an increased chance of replicating and clonally expanding (Dölle et al., 2016).

When considering IdU incorporation, the pattern of replication was as demonstrated with the CldU, however not all the cases are significantly different to each other. There were also a few

differences, notably within the SN. With CldU, the total mtDNA replication level was the lowest in SN, however with IdU, the SN had the second highest mtDNA replication levels after cerebellum. This suggests that mtDNA replication occurs at a higher level compared to hippocampus and cortex in the short term (15 hours), which reduces to the lowest level of all the brain regions within the 4 days. This implies that the CldU incorporation over the 4 days could be effected by other mechanisms, such as mitophagy. Therefore, to test this theory, MitoQC mice, donated by Dr Ian Ganley (University of Dundee), were used to analyse the levels of mCherry positive puncta (mitophagic events) in a cell. Images of dopaminergic neurons (SN) and Purkinje neurons (cerebellum) were obtained and compared to each other. A significantly higher level of mitophagy was observed in the SN compared to the cerebellum. However, validation would require further investigation, such as the study of more brain regions.

7.2.2 *Relationship between ΔmtDNA and mtDNA replication*

Since an association between regions and groups with high levels of ΔmtDNA and low levels of mtDNA replication was noticed, it was vital to study the correlation between these two cases. Published data regarding ΔmtDNA and mtDNA copy number in different brain regions was kindly shared by Dr Celine Perier (Vall d'Hebron Institute of Research, Spain)(Perier et al., 2013). Their study was similar to this study as several regions of the brain were investigated in wild type and $PolgA^{mut/mut}$ mice. No association was observed between the mtDNA replication levels and corresponding ΔmtDNA levels in the various brain regions studied or in $PolgA^{mut/mut}$ mice. There was also no association between the mtDNA replication levels and the mtDNA copy number in these regions, suggesting that ΔmtDNA are not caused by replication, rather, by other mechanisms, such as repair.

Although the studies were similar, there are a number of limitations between the two. This study analysed individual cells from these regions, however Perier *et al.* studied homogenate tissue samples. The use of homogenate data could be contaminated by other cell types (for example astrocytes or interneurons) which could skew the data. Variations in mtDNA copy number have been demonstrated in studies investigating the same tissue but in homogenate and individual neurons (Coxhead et al., 2016, Dölle et al., 2016, Pyle et al., 2015). Furthermore,

since an average value per mouse was obtained, and not the raw values per replicate, this saturates the statistical power. In addition to this, Perier *et al.* reported that the cerebellum contained a higher ΔmtDNA load than the midbrain (where SN is located) which contradicts other studies in the literature (refer to Table 3.1 and 3.2 in Chapter 3). Due to the differences between the two studies, further investigations are required. To accommodate future work in this area, half of each mouse brain used in this study was snap frozen. Individual neurons could be isolated via laser-microdissection, and molecular analysis could be conducted using quantitative real-time PCR to study the total levels of ΔmtDNA as described previously (He et al., 2002).

7.2.3 *Developing thymidine analogue labelling for use in vitro*

Thymidine analogue labelling has been used previously to study mtDNA replication *in vitro*, however single analogues were commonly used (Section 4.1.1). Until very recently, double thymidine analogue labelling had not been used *in vitro* to study mtDNA, likely due to the technical optimisation required (Phillips et al., 2017). The initial idea was to develop a pulse chase experiment to study the turnover of mtDNA replication, and for this reason the methodology was developed on HeLa cells. The optimum concentration of both analogues was deduced separately, based on cell viability and level of mtDNA incorporation of each analogue. Although the concentration was optimised for each individual analogue, the combination of analogues was toxic, and therefore a single analogue was selected. IdU was chosen due to the higher level of incorporation within the mtDNA. Since nuclear genome replication was also incorporating IdU, aphidicolin was used to block this to ensure that only mtDNA replication was being labelled. Following this, appropriate analysis was also developed for future use.

Following optimisations in HeLa cells, this methodology was successfully employed in iPS cells and differentiated neurons generated from fibroblasts containing a single, large-scale mtDNA deletion. This technique can successfully label mtDNA replication and was then used to obtain preliminary data for chapter 5.

7.2.4 *Localisation of mtDNA replication within neurons in vivo*

Thymidine analogue labelling was also used to study the localisation of mtDNA replication. Successful analysis was optimised to study this, and compared between each cohort of mice using delta values produced by Dr. Conor Lawless (Wellcome Centre for Mitochondrial Research). This was achieved by identifying perinuclear and distal mtDNA replication based on the nuclear radius, allowing comparison of mtDNA replication localisation between groups (in depth explanation in chapter 5).

Differences were noted between the time points of IdU (15 hours) and CldU (four days) *in vivo*. At 15 hours, a large number of data sets from the mouse cohorts demonstrated increased mtDNA replication in the distal regions. However after four days, the majority of the mtDNA replication was present within the perinuclear region. This pattern of increased mtDNA replication in the distal region at the shorter time frame and increase in the perinuclear region at the longer time frame was previously observed (Van Laar et al., 2018). This shift from the distal to the perinuclear region of mtDNA replication localisation could be to aid quality control or due to increased anterograde transport. However, this requires further investigation. When the delta values were compared, significant differences were only observed between the cerebellum and other regions when analysed for IdU incorporation. The cerebellum had significantly lower delta values compared to the other regions, suggesting an increase in distal replication compared to the other regions. Since damaged mitochondria are targeted and transported anterograde into the perinuclear region, this could be a compensatory mechanism to avoid replicating ΔmtDNA. Localisation of mitophagy was also analysed in dopaminergic neurons of MitoQC mice, donated by Dr Ian Ganley (University of Dundee) as part of a preliminary study to identify localisation of mitophagy. These data suggest an increased perinuclear localisation of mitophagy within the SN. However, other regions of the brain would require analysis to make firm conclusions.

7.2.5 *Could mitochondrial structure affect the clonal expansion of mtDNA deletions?*

As differences in mtDNA replication localisation were observed, it was important to study the ultrastructure of mitochondria to investigate mitochondrial network and interconnectivity, which would shed more light on spread of ΔmtDNA. This was performed via SBF-SEM as it

reveals the mitochondrial structure and connectivity in a 3D format without compromising the resolution. This was a 'proof-of-concept' study on dopaminergic neurons from both human healthy aged controls and patients with Alzheimer's disease (AD) or dementia with Lewy bodies (DLB). Imaging was conducted to obtain a 3D model allowing measurements of parameters not available from a 2D image. This allowed identification of alterations to the 3D structure such as volume and variations in the structural connectivity of the mitochondrial network.

Although variations between the perinuclear and distal mitochondria were not observed, this was mainly due to the limitations discussed in chapter 6 and were likely due to the small sample size included in this study. Variation was observed between the healthy ageing controls and the patients in terms of mitochondrial surface area. Variations between patients, concerning mitochondrial branching were also observed. Since a small number of neurons was analysed, a greater number will need to be analysed to statistically compare between patients affected by neurodegenerative diseases and those who are unaffected.

An interesting observation from this study was the identification of two neurons from the same DLB patient, one with Lewy bodies and one without. Variations were noticed between the two neurons from the same patient. The mitochondria within the neuron containing Lewy bodies appeared more fragmented, with reduced mitochondrial branching. Alongside this, elongated tubular structures were noticed (highlighted in figure 6.9 and 6.10). Previous literature has suggested that these could be nanotunnels between mitochondria that will allow communal sharing of contents between mitochondria (Vincent et al., 2017). Nanotunnels might be forming to compensate for the limited movement of mitochondria, which might be blocked by Lewy bodies in this case. This is the first time nanotunnels have been noticed within neurons and could be functioning as a compensatory mechanism as this was noticed in both patients (DLB and AD) and healthy ageing. On the other hand, it could also aid in the accumulation of ΔmtDNA, as these molecules could be shared throughout the network. However, measurements of these nanotunnels in muscle suggest that only 4% of the nanotunnels have sufficient diameter to allow transport of nucleoids (Vincent et al., 2019). Alternatively, these structures could be 'mitochondria on a string' (MOAS) as described by another study which suggested that they occur due to fission arrest (Zhang et al., 2016). In the

study by Zhang *et al*, these structures were noticed in AD patient, which was also the case with this study. However, these structures were also noticed in a healthy ageing individual in this study. Therefore further steps to confirm these structures and their function could provide the required information on disease progression and ΔmtDNA accumulation.

7.2.6 *Role of ΔmtDNA replication in mtDNA formation and accumulation*

An increase in mtDNA replication was not observed in brain regions with an increase in ΔmtDNA, suggesting that mtDNA replication does alone not directly lead to formation of ΔmtDNA. However, a pattern of association, specifically a decrease in mtDNA replication in regions of high ΔmtDNA was observed, suggesting a relationship between these two processes. In addition to this, variations were also noticed in the location of mtDNA replication with respect to neurons both *in vivo* and *in vitro*. This was particularly noticeable between the two time points of 15 hours and 4 days *in vivo*, suggesting that another mechanism could function to effect both mtDNA replication and ΔmtDNA. This could be altered transport, mitophagy, transcription or mtDNA repair.

7.3 Final conclusion

The aim of this study was to further our understanding of the role of mtDNA replication in deletion formation and accumulation within the brain. The main findings were as follows;

- This study was the first to identify variation in mtDNA replication levels within different neuronal populations *in vivo* and found associations with ΔmtDNA levels, however this requires further work to successfully establish a relationship.
- A methodology was developed to study mtDNA replication turnover *in vitro*.
- The location of mtDNA replication localisation was identified as being increased in the perinuclear region. The localisation of mtDNA deletions did not alter between neuronal subtypes, or in ageing or replication defect.
- The feasibility of using SBF-SEM on human post mortem brain tissue, to understand mitochondrial ultrastructural changes in disease was proven.

This study has uncovered potential compensatory mechanisms present within different brain regions to protection against ΔmtDNA. Analysis of ΔmtDNA levels in single laser micro-dissected neurons could be used to correlate with these findings as most studies in the literature uses homogenate data.

8.1   Thymidine analogue incorporation – cell death

Figure 4.8 displays images of IdU labelled HeLa cells at 2.5µg/ml and also highlights the cell death that was observed and the morphology of the dead cells. Cell death was noticed in these cases; however, they were not as elevated as in the previous tries with the combination of the thymidine analogues (data not presented). The cell death was quantified using Image J and is presented in supplementary figure 8.1 for each of the concentrations and times trialled. These were identified based on the morphology as indicated in figure 4.8. An untreated control was used to compare the level of cell death. Since this control was only left for 24 hours, statistically this was not compared to the concentrations at 48 hours, as the cell death could have increased naturally at 48 hours.
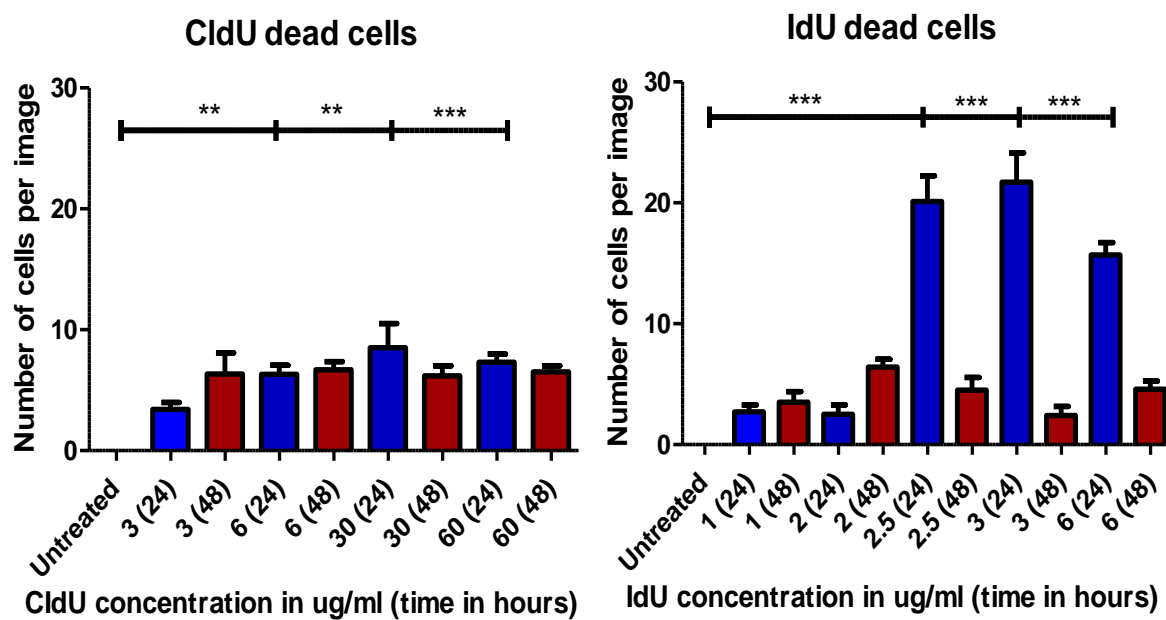
*Supplementary figure 8.1 The effect of CldU and IdU labelling on cell survival in HeLa cells. The cells were treated for either 24 or 48 hours with concentrations ranging from 3-6µg/ml for the CldU and 1µg/ml for the IdU. A control was used which was an untreated well which was fixed after 24 hours. Since this was fixed with the concentrations at 24 hours, these were compared to each other statistically. The N=10 images for each thymidine analogue label. Each 24 hour concentration was compared to the untreated cells ** indicates p < 0.01 and *** indicates p < 0.001*

With the CldU, the number of dead cells were similar for all the concentrations and time points that were all significantly different from the untreated (p < 0.01 and p < 0.001). These were also decreased compared to the IdU cells but this could be due to the dead cells detaching and being removed during washing. This is reflected in the fact that the total cell count is reduced. For the IdU labelled cells, the lower concentrations showed reduced cell death compared to 2.5μg/ml and above. At 6μg/ml, the number of dead cells appear reduced compared to the lower concentrations; however, this was due to the detachment of dead cells, which could potentially have been removed along with the media prior to fixation. A limitation of attempting to measure toxicity is the detachment of the cells following steps during immunofluorescence. Due to this, the number of dead cells not be accurately represented since these are not accounted for and hence may not correctly measure toxicity.

8.2   Analysis of thymidine analogue labelling in vitro using IMARIS 9

The correct quantification and analysis of IdU incorporation into cells was vital for the success of this project. Analytical approaches used the mitochondrial marker to normalise the IdU incorporated into mtDNA since each cell is different in terms of size and abundance of mitochondria. Two methods of analysis were considered. The first method of analysis used ImageJ (Fiji). In this case, the images were exported as TIFFs exporting each individual channel as a separate file. The images were then opened in ImageJ (Fiji). The 'Freehand selection' function was used to draw around the cell region based on the Tom20 channel to create a ROI. This was then duplicated on to the IdU channel using the 'ROI manager' function, which can pick up this exact region based on the loci in multiple images. The mean intensity for each ROI in each channel was then produced by the 'measure' function. The intensity of the IdU channel is then expressed as a percentage of the Tom20 channel.

Since this method produces the mean intensity per unit area, this is not completely accurate, as the range of intensities within the cell cannot be obtained from the software. If individual mitochondrion in a cell had a very high incorporation of IdU into the mtDNA, this might produce a similar mean intensity as another cell with multiple mitochondria with IdU incorporation but with a lower intensity. In this way, the data may not accurately reflect the total number of mtDNA molecules that have replicated in a single cell. For this reason, another

analysis method using Image J was also considered, such as choosing multiple ROI's within a single cell based on the Tom20 channel. This was randomized and identified multiple mitochondrial regions within a single cell allowing calculation of the sum of total intensity and range, however this also had the problem of not including every mitochondria.

To overcome this problem, IMARIS (bitplane) was used. In IMARIS, a surface is created by manually drawing around the cell boundary in the Tom20 image to produce an ROI. This is then masked on to the Tom20 channel to produce a surface only within the area where there is positive staining for Tom20. The Tom20 mask was then used to select a new channel that detects only the IdU staining within the Tom20 surface created (i.e. only IdU incorporated into mitochondria). This allows the creation of a surface that accurately represents the total number of IdU positive areas within the Tom20 positive population. The sum of the volumes for the Tom20 and IdU channel are then obtained from the software. The total IdU values are then expressed as a percentage of the total Tom20 values. This way, all the individual IdU positive puncta are considered individually unlike the previous analysis. The systematic guide to conduct this analysis is presented in Supplementary figure 8.2. With the surface creation, background subtraction was a function that was used to choose positive staining for mitochondria based on their size. Since IMARIS provided was the most accurate method, this was carried forward for future experiments.

A Image is opened in IMARIS

B Manually draw around the cell for ROI

C Surface is created for the ROI

D The Surface is masked on to tom20 channel

E Surface is created for the new tom20 channel created in D

F This is then masked on to the IdU channel

G Surface is created for the new IdU channel created in F

H Sum of both surface is obtained from the channel
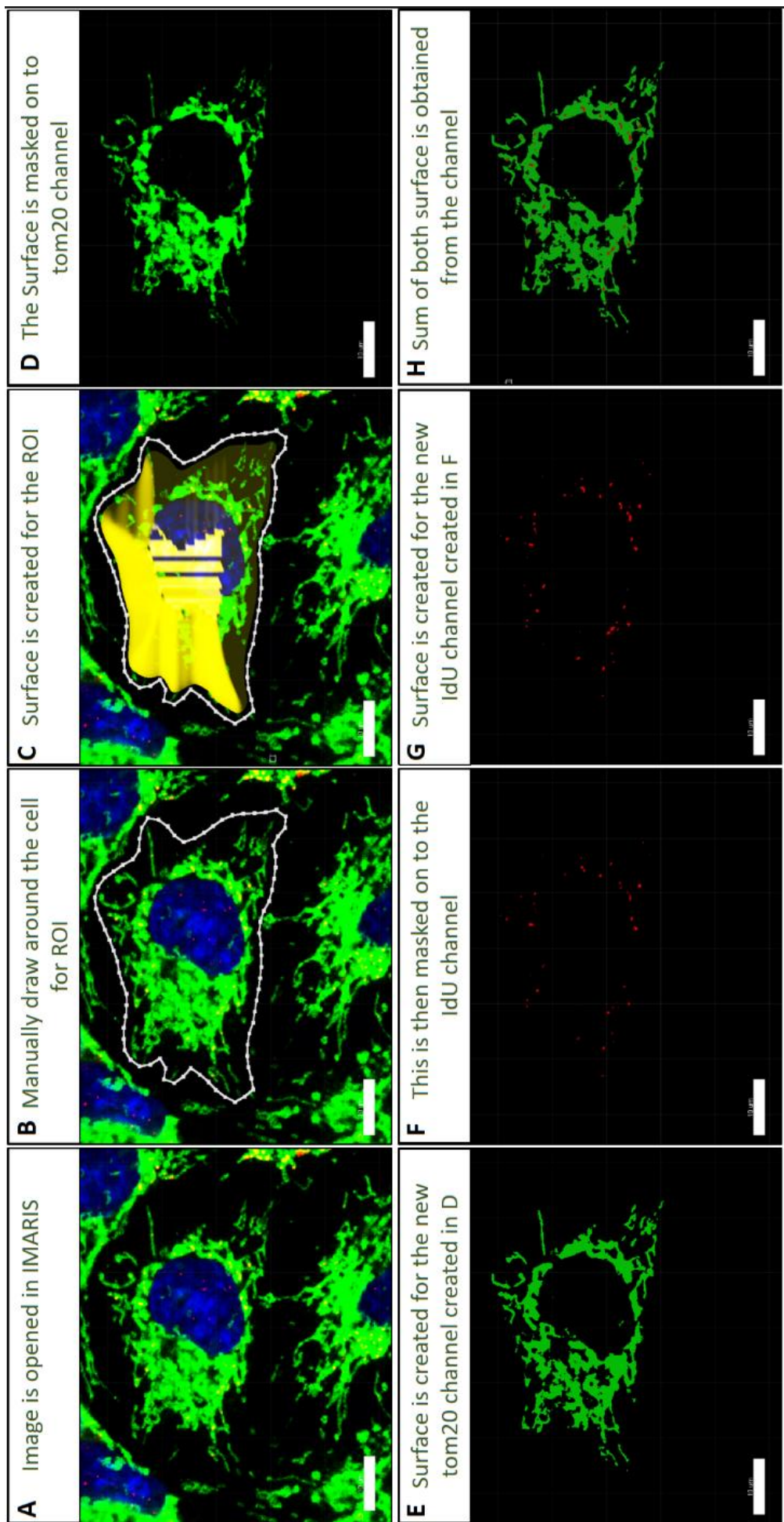
Supplementary figure 8.2 The steps to analysing the IdU labelled cells using IMARIS (bitplane). Scale bar represents 10 µM.

8.3   Determination of nuclear size

The CldU and IdU labelled mouse brains were stained and imaged using the Nikon A1R confocal system. Initially it was determined to identify the diameter of nucleus based on the intensity of the Hoechst channel. This can be identified using a threshold value for positive staining within this channel an d any values above this value would determine the presence of nucleus and any values below, an absence of a nucleus. However due to the high level of noise and saturated pixels in this channel, it was difficult to accurately determine the nuclear membrane as suggested by a threshold value. Therefore, this led to development of other techniques to identify the perinuclear and distal cytoplasmic regions.

When the data was obtained, since the highest point of Hoechst was designated as the centre of the cell, the perinuclear region differed between cells, especially since the neurons have varying sizes. However, since a large number of cells from at least 10 images (per region/per genotype/per age) were analysed (at least 160 images), this should average out the intensities in the perinuclear region. To increase the accuracy of this calculation, the diameter of the nucleus in pixels was also measured manually using image J, and the radius calculated. This was conducted for a minimum of 10 neurons per region per group. The nuclear radii for each region from each group is plotted in supplementary figure 8.3. When comparing between regions, there are significant differences ($p<0.05$) in nuclear radius between all the neuronal types. This was expected due to the differences in neuronal size. When comparing between ages and genotype, there were no significant differences detected ($p<0.05$) except in the case of *PolgA$^{mut/mut}$* old, which was significantly increased to the other cohorts. The reason for this in unknown. However, since this method was developed for classifying the regions of the cell, and this was conducted successfully and this method was carried forward for further experiments. This step of validation was also conducted for the *in vitro* study as well, with no significant differences detected in nuclear radius between the low and high heteroplasmy lines (data not presented).

270
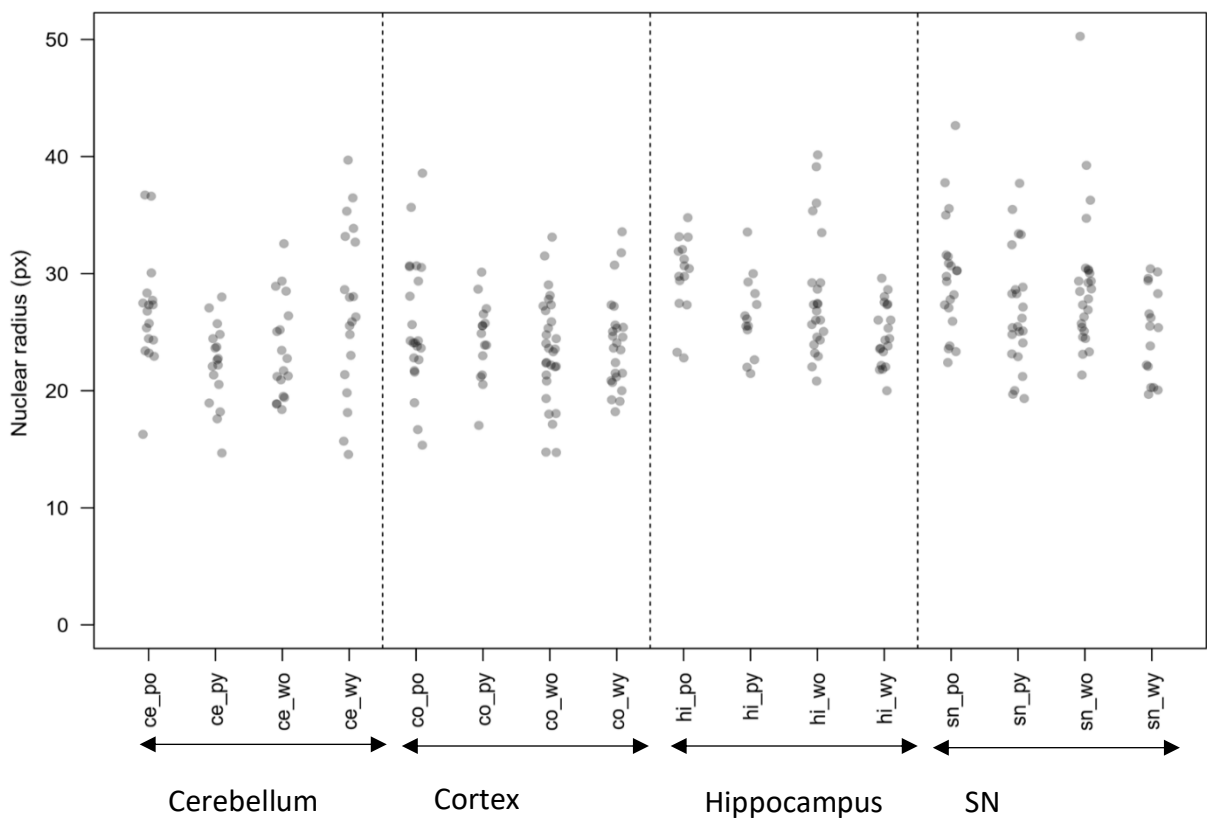
Supplementary figure 8.3 Variations in nuclear radius diameter (in pixels). The graph presents the spread of nuclear radii from which the average nuclear radius is calculated to separate the perinuclear region from the distal regions of the cell. Ce represents cerebellum, co represents cortex, hi represents hippocampus, sn represents substantia nigra, PO represents PolgA$^{mut/mut}$ old, PY represents PolgA$^{mut/mut}$ young, WO represents wild type old, WY represents wild type young and px represents pixels.

8.4   Immunofluorescent image analysis optimisation

Since IMARIS provides analysis of various parameters, four parameters were selected and compared. These included area, volume, fluorescent intensity and number of voxels. IMARIS surfaces are constructed by triangular shaped objects called voxels which are the equivalent of a pixel in an image, therefore, 'number of voxels' gives the number of said voxels used to construct the image. All of the different parameters produced similar results with no significant differences (at a p value of 0.05) in terms of the level and pattern of replication. Since there were no significant differences, the number of voxels was carried forward for the future analysis. This was suggested by the manufacturer due to the 2D nature of the images.

Other studies have also analysed thymidine analogue labelling using Fiji (Image J) (Van Laar et al., 2018, Schindelin et al., 2012). A subset of the data from this study was also analysed this way to test for any differences to IMARIS to allow the selection of the most appropriate technique. This analysis was undertaken on at least five images from the young wild type and young *PolgA$^{mut/mut}$* groups (Supplementary figure 8.4). The approach using Fiji revealed differences to previously obtained results from IMARIS in terms of the levels of CldU and IdU within each region. In these graphs, there was a significant difference between the four different brain regions in terms of CldU and IdU labelling as highlighted in the graph (Supplementary figure 8.4A and B). However, there were also differences in the number of puncta of the Tom20 and area, which demonstrated an increase in the cerebellum compared to the other areas for both the wild type and the *PolgA$^{mut/mut}$* mice (Supplementary figure 8.4C and 8.4D). This highlights a flaw with this analysis when used to compare different cell types, as it does not take into consideration the size of the cell. Cell size can account for the increase in puncta per cell and per area within the cerebellum and SN, since the Purkinje cells and dopaminergic cells are morphologically larger than pyramidal cells.
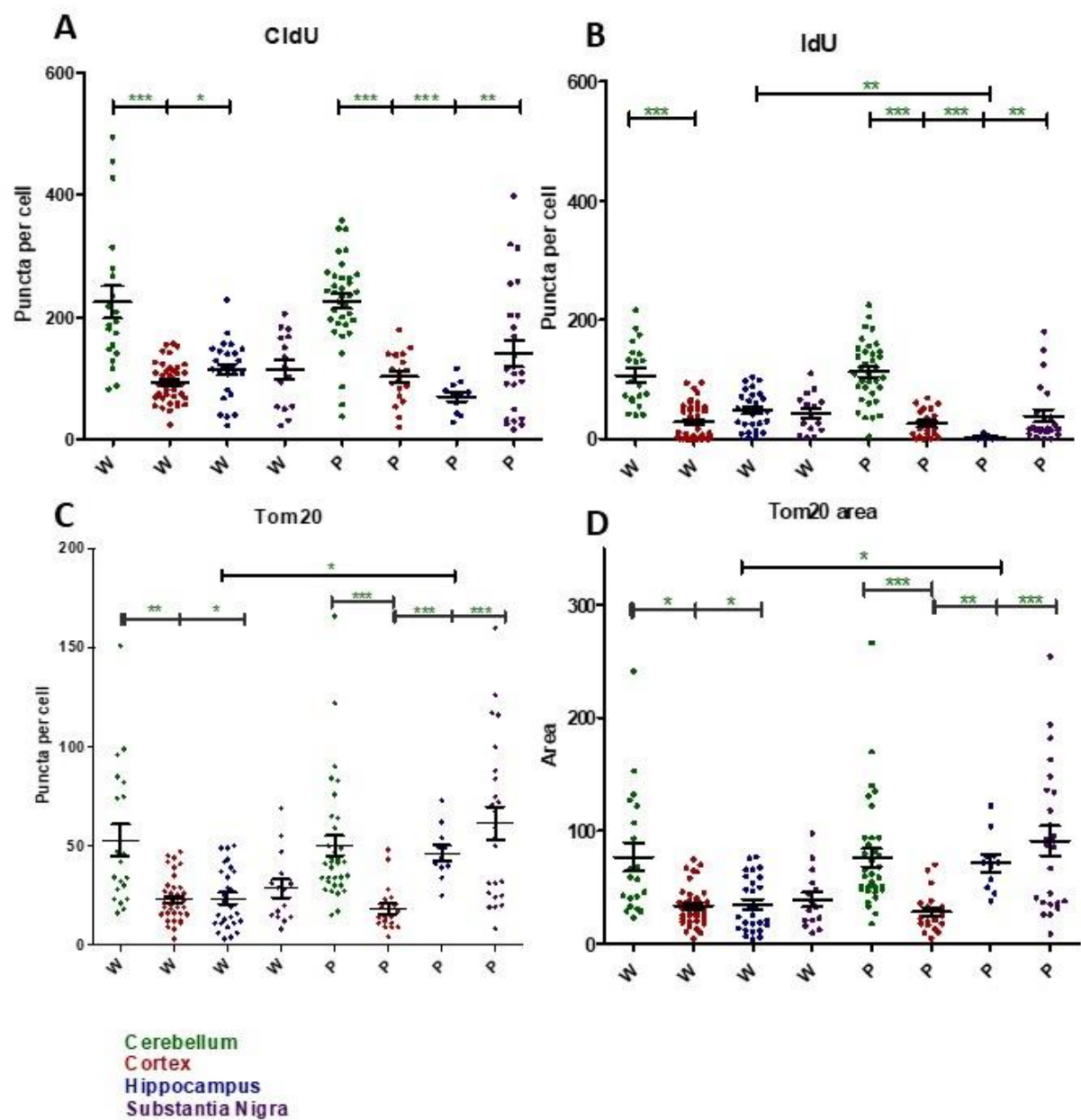
Supplementary figure 8.4 Analysis optimisations: IMARIS vs Image J – The puncta per cell values are obtained from Image J. Images A and B presents the puncta per cell values for the CldU and the IdU channel. Images C and D presents the variation in the Tom20 channel for the puncta for cell values and the area of cell within each tissue type. The tissue type is indicated by colour with the key. All these mice were from the young group, W indicates wild type mouse and P indicates PolgA$^{mut/mut}$ mice. The N is at least 5 images for each area. * indicates p < 0.05, ** indicates p < 0.01 and *** indicates p < 0.001.

Due to these variations, to normalise the data, the Tom20 puncta per cell was divided by the area of the cell (Supplementary figure 8.5A), this generated similar patterns between the regions for all cell types suggesting normalisation to area as a valid step in this analysis. The values from CldU and IdU in the young group of wild type and *PolgA^{mut/mut}* mice were normalised to the area of the cell and produced a similar pattern to the IMARIS analysed data. Image J and IMARIS analysis of CldU (Supplementary figure 8.5B and D) and IdU signal (Supplementary figure 8.5C and E) were then compared. The range of values are different from the two image analysis packages: 0-30 for Image J and 0-100 for IMARIS. This was because, in Image J, the values are divided by the area of the Tom20 puncta and in IMARIS, the values are expressed as a percentage of the Tom20 values.

There are still notable variations, for example between the wild type cerebellum CldU signal compared to the hippocampal data from the same group. This could be due to the number of values for each group. In the image J group, the maximum number of cells analysed was 40 and for the IMARIS, this was 106. This is because, only a subset of 5 images were selected for analysis via Image J. It is however, reassuring that all the significant differences identified by the Image J values were also identified by IMARIS values. However, again potentially due to the higher number of cells, IMARIS identified more significant differences and was therefore selected for further analysis
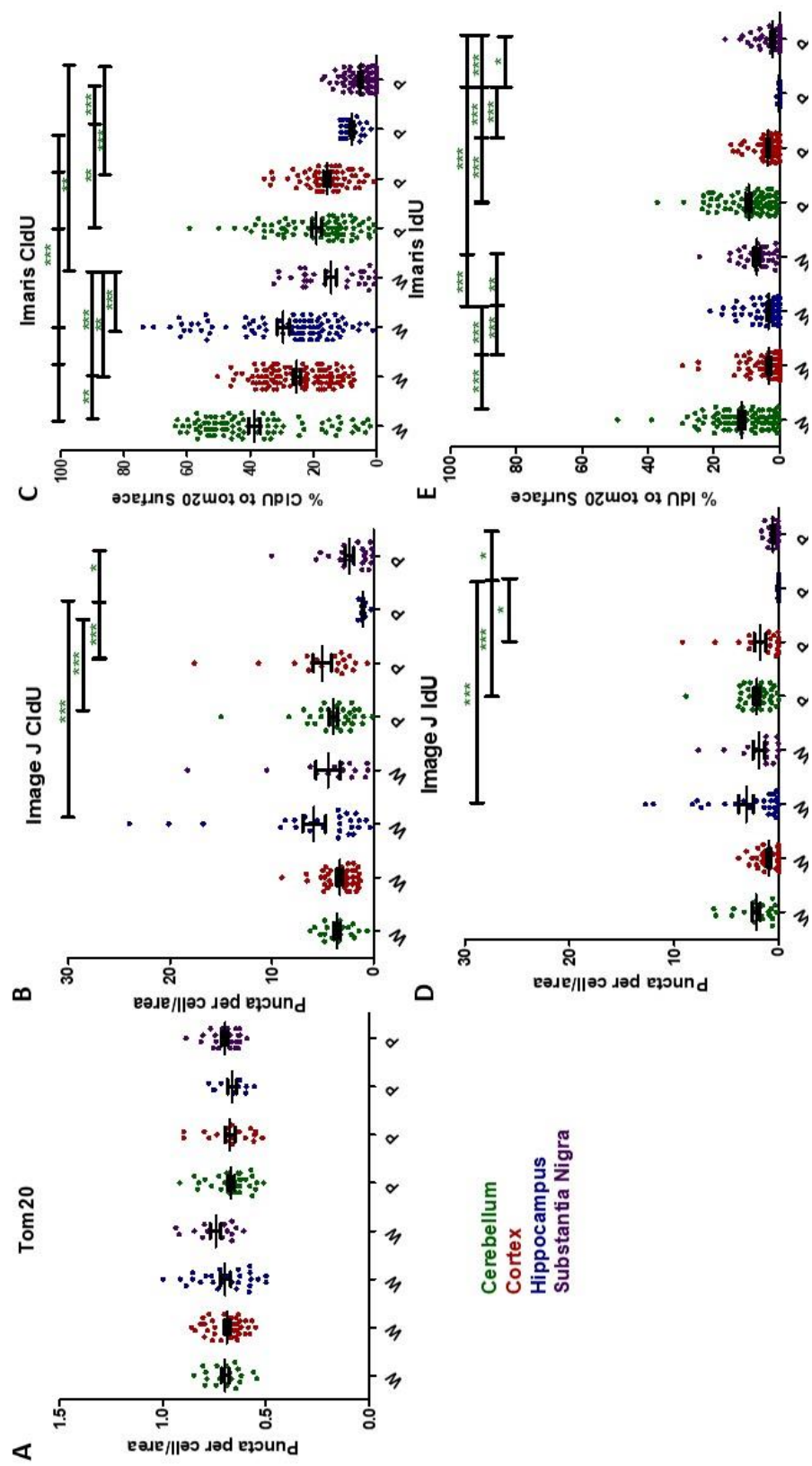
Supplementary figure 8.5 Analysis optimisation: Image J normalised – The puncta per cell analysis after the value were normalised based on the area per cell(based on the Tom20 channel) from Image J. Image A shows the puncta per cell of Tom20 values after normalising to area, suggesting this is a valid method to observe reliable values with cells different in sizes. Images B and D presents the CldU values after normalisation with Image J. Images C and E presents the surface values for the CldU and the IdU channel normalised to the Tom20 surface. The tissue type is indicated by colour with the key in the Figure. All these mice were from the young group, W indicates wild type mouse and P indicates PolgA^{mut/mut}. The N is at least 5 images for each area. * indicates p < 0.05, ** indicates p < 0.01 and *** indicates p < 0.001.

8.5 Differentiating between replication and repair

One of the concerns against using thymidine analogue labelling to study DNA replication is that thymidine incorporation is not exclusive to replication. Thymidine and its analogues can be incorporated into the mtDNA during repair. This is particularly important for this study due to the use of *PolgA^{mut/mut}* mice, since poly is involved in both replication and repair.

Although it is experimentally difficult to distinguish between incorporation due to replication or repair, this may be partially investigated by examining CldU and IdU signal intensities for each individual mitochondria. Analogue incorporation via replication will give a significantly higher signal intensity compared to repair due to the larger number of base pairs involved in replication compared to repair. In replication, 16kbp of mtDNA is available for thymidine analogue incorporation, compared to a single or few nucleotides via repair. To differentiate between the two, intensities of CldU and IdU signal in each mitochondrial surface were analysed. CldU and IdU values were compared from two wild type and two *PolgA^{mut/mut}* mice from the aged group, within the cerebellum and cortex. The ageing cohort was selected as it was hypothesised that more mtDNA repair might be occurring due to age related mtDNA mutations. The graphs in Supplementary figure 6.1 show that the intensities are similar within all surfaces created per mouse. The difference in range is due to the different levels of analogue incorporated into the mtDNA. There were two mice within the CldU graph (Supplementary figure 8.6A): P1 cerebellum and P2 cortex, and 1 mouse within the IdU: P2 cerebellum that produced signal intensities at a much reduced level. These values could potentially represent mtDNA incorporation via repair. This is reiterated by the even further reduction observed in IdU incorporation compared to the CldU as the IdU is labelled for a shorter time period. It is also important to mention that these lower values were observed in *PolgA^{mut/mut}* mice. This could be due to an increase in error prone replication which could result in a higher demand for repair.

All values were <1 in both graphs, hence a threshold value for the intensity was set as 10 per unit area for subsequent analysis. This would potentially eliminate any thymidine analogue incorporation due to repair in the case of CldU.
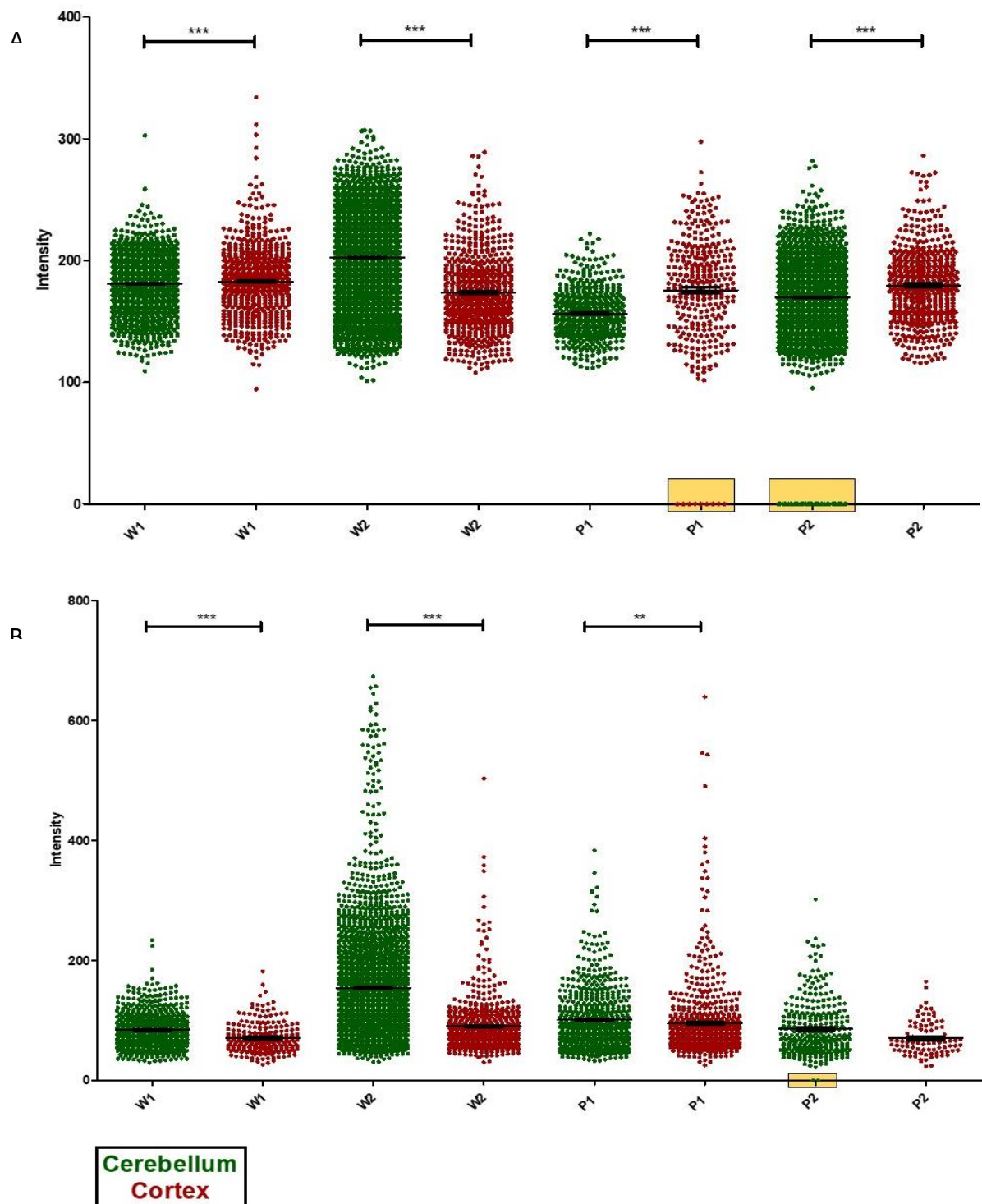
Supplementary figure 8.6 mtDNA replication vs repair – The signal intensity produced by the CldU (A) and IdU (B) channel for each individual Tom20 surface created. This was to distinguish between replication and repair. The yellow boxes represents the values likely due to be incorporated via repair, since they are low. The tissue type is indicated by colour with the key in the Figure. All these mice were from the young group, W indicates wild type mouse and P indicates PolgA^{mut/mut} mice. N=10 images for each area with the total mitochondrial surfaces ranging from 300-4000. * indicates p < 0.05, ** indicates p < 0.01 and *** indicates p < 0.001.

8.6 Normalising datasets

Since the replicates were not normally distributed, as confirmed by Kolmogorov-Smirnov testing ($p<0.05$), quantile normalisation was undertaken to compensate for this. This is a process by which data can be made comparable by rearranging the dataset in numerical ascending order, each value is then given a position within the dataset depending on where it appears on the ascending order. Each value is then averaged by its counterparts in the other datasets. For example is the lowest value is 3,5,and 7 in the three datasets, the average become 5 and the lowest value is all the data sets are then set as three. By doing this, this makes each value comparable, however any differences in the high values and low values between the datasets are still considered. A graphical representation is provided in Supplementary figure 8.7
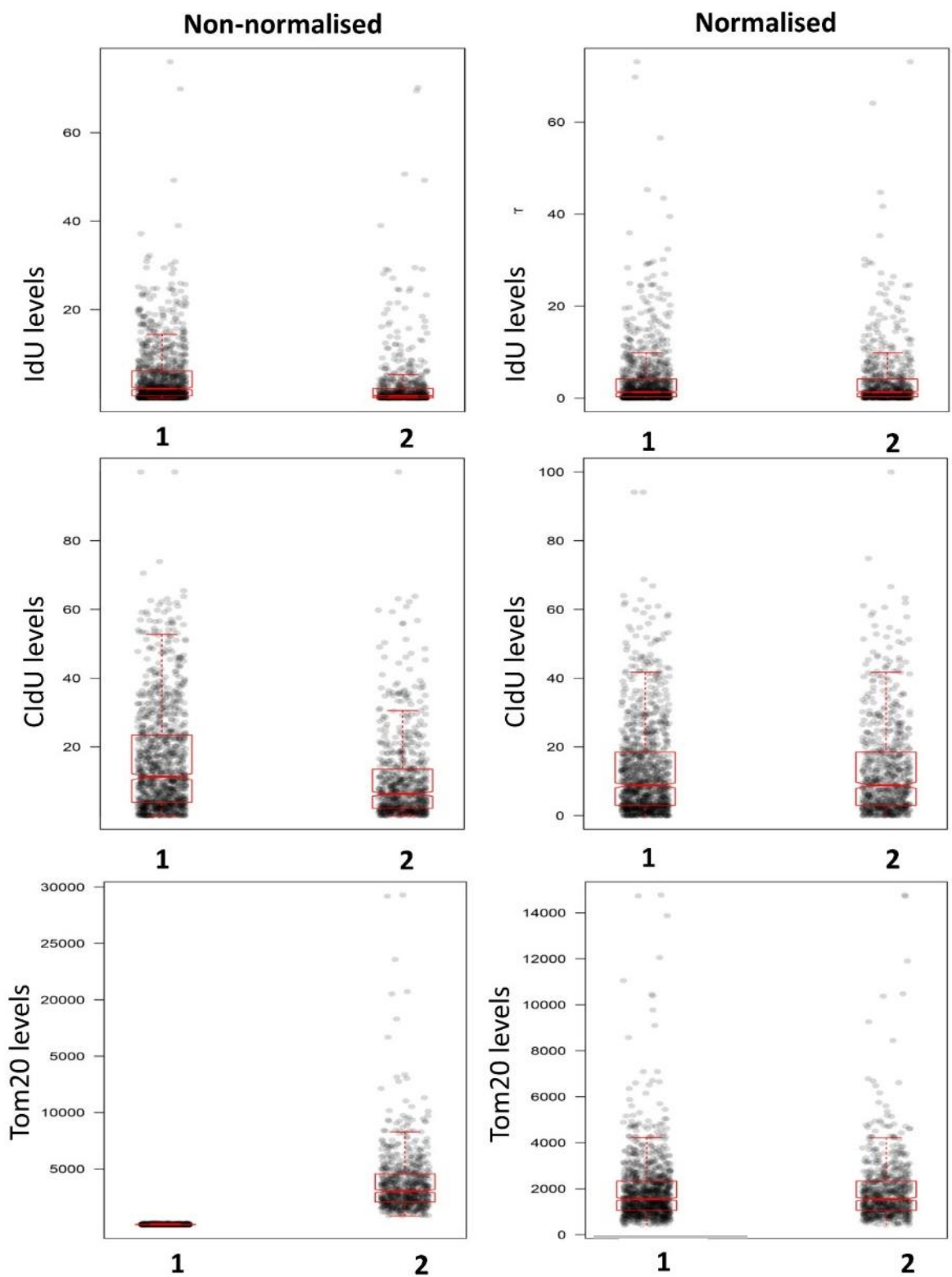
Supplementary figure 8.7 Data normalisation. These scatter plots demonstrates the spread of data prior to and following normalisation to make them comparable between experimental repeats. More details regarding the method for this are provided in section 3.4.6

279

References

ABRAMOV, A. Y., SMULDERS-SRINIVASAN, T. K., KIRBY, D. M., ACIN-PEREZ, R., ENRIQUEZ, J. A., LIGHTOWLERS, R. N., DUCHEN, M. R. & TURNBULL, D. M. 2010. Mechanism of neurodegeneration of neurons with mitochondrial DNA mutations. *Brain,* 133**,** 797-807.

AERBAJINAI, W., GIATTINA, M., LEE, Y. T., RAFFELD, M. & MILLER, J. L. 2003. The proapoptotic factor Nix is coexpressed with Bcl-xL during terminal erythroid differentiation. *Blood,* 102**,** 712-717.

AGARONYAN, K., MOROZOV, Y. I., ANIKIN, M. & TEMIAKOV, D. 2015. Replication-transcription switch in human mitochondria. *Science,* 347**,** 548-551.

AHMAD, Y., BOISVERT, F.-M., LUNDBERG, E., UHLEN, M. & LAMOND, A. I. 2011. Systematic analysis of protein pools, isoforms and modifications affecting turnover and subcellular localisation. *Molecular & Cellular Proteomics***,** mcp. M111. 013680.

AHMED, A. U. & FISHER, P. R. 2009. Import of nuclear-encoded mitochondrial proteins: a cotranslational perspective. *International review of cell and molecular biology,* 273**,** 49-68.

AHMED, S. T., ALSTON, C. L., HOPTON, S., HE, L., HARGREAVES, I. P., FALKOUS, G., OLÁHOVÁ, M., MCFARLAND, R., TURNBULL, D. M. & ROCHA, M. C. 2017. Using a quantitative quadruple immunofluorescent assay to diagnose isolated mitochondrial Complex I deficiency. *Scientific reports,* 7**,** 15676.

AIKEN, J., BUA, E., CAO, Z., LOPEZ, M., WANAGAT, J., MCKENZIE, D. & MCKIERNAN, S. 2002. Mitochondrial DNA deletion mutations and sarcopenia. *Annals of the New York Academy of Sciences,* 959**,** 412-423.

AKBARI, M., KEIJZERS, G., MAYNARD, S., SCHEIBYE-KNUDSEN, M., DESLER, C., HICKSON, I. D. & BOHR, V. A. 2014. Overexpression of DNA ligase III in mitochondria protects cells against oxidative stress and improves mitochondrial DNA base excision repair. *DNA repair,* 16**,** 44-53.

AKBARI, M., VISNES, T., KROKAN, H. E. & OTTERLEI, M. 2008. Mitochondrial base excision repair of uracil and AP sites takes place by single-nucleotide insertion and long-patch DNA synthesis. *DNA repair,* 7**,** 605-616.

ALAM, T. I., KANKI, T., MUTA, T., UKAJI, K., ABE, Y., NAKAYAMA, H., TAKIO, K., HAMASAKI, N. & KANG, D. 2003. Human mitochondrial DNA is packaged with TFAM. *Nucleic Acids Research,* 31**,** 1640-1645.

ALBERTS, B., JOHNSON, A., LEWIS, J., RAFF, M., ROBERTS, K. & WALTER, P. 2002. The cytoskeleton and cell behavior.

ALEXEYEV, M., SHOKOLENKO, I., WILSON, G. & LEDOUX, S. 2013. The maintenance of mitochondrial DNA integrity—critical analysis and update. *Cold Spring Harbor perspectives in biology,* 5**,** a012641.

AMADORO, G., CORSETTI, V., FLORENZANO, F., ATLANTE, A., BOBBA, A., NICOLIN, V., NORI, S. L. & CALISSANO, P. J. F. I. A. N. 2014. Morphological and bioenergetic demands underlying the mitophagy in post-mitotic neurons: the pink–parkin pathway. 6**,** 18.

AMIRI, M. & HOLLENBECK, P. J. 2008. Mitochondrial biogenesis in the axons of vertebrate peripheral neurons. *Developmental neurobiology,* 68**,** 1348-1361.

ANDERSEN, J. K. 2004. Oxidative stress in neurodegeneration: cause or consequence? *Nature medicine,* 10**,** S18.

ANDERSON, S., BANKIER, A. T., BARRELL, B. G., DE BRUIJN, M. H., COULSON, A. R., DROUIN, J., EPERON, I. C., NIERLICH, D. P., ROE, B. A. & SANGER, F. 1981. Sequence and organization of the human mitochondrial genome. *Nature,* 290**,** 457.

ANDERSSON, S. G., ZOMORODIPOUR, A., ANDERSSON, J. O., SICHERITZ-PONTÉN, T., ALSMARK, U. C. M., PODOWSKI, R. M., NÄSLUND, A. K., ERIKSSON, A.-S., WINKLER, H. H. & KURLAND, C. G. 1998. The genome sequence of Rickettsia prowazekii and the origin of mitochondria. *Nature,* 396**,** 133.

ANDREWS, R. M., KUBACKA, I., CHINNERY, P. F., LIGHTOWLERS, R. N., TURNBULL, D. M. & HOWELL, N. 1999. Reanalysis and revision of the Cambridge reference sequence for human mitochondrial DNA. *Nature genetics,* 23**,** 147.

ARNOLD, B., CASSADY, S. J., VANLAAR, V. S. & BERMAN, S. B. 2011. Integrating multiple aspects of mitochondrial dynamics in neurons: age-related differences and dynamic changes in a chronic rotenone model. *Neurobiology of disease,* 41**,** 189-200.

ASANO, M., YAMAMOTO, T., TSURUTA, T., NISHIMURA, N. & SONOYAMA, K. 2015. Dual labeling with 5-bromo-2'-deoxyuridine and 5-ethynyl-2'-deoxyuridine for estimation of cell migration rate in the small intestinal epithelium. *Development, growth & differentiation,* 57**,** 68-73.

ASCHRAFI, A., KAR, A. N., GALE, J. R., ELKAHLOUN, A. G., VARGAS, J. N. S., SALES, N., WILSON, G., TOMPKINS, M., GIOIO, A. E. & KAPLAN, B. B. 2016. A heterogeneous population of nuclear-encoded mitochondrial mRNAs is present in the axons of primary sympathetic neurons. *Mitochondrion,* 30**,** 18-23.

ASHLEY, N., HARRIS, D. & POULTON, J. 2005. Detection of mitochondrial DNA depletion in living human cells using PicoGreen staining. *Experimental cell research,* 303**,** 432-446.

ASHLEY, N. & POULTON, J. 2009. Mitochondrial DNA is a direct target of anti-cancer anthracycline drugs. *Biochemical and biophysical research communications,* 378**,** 450-455.

ATTEIA, A., ADRAIT, A., BRUGIÈRE, S., TARDIF, M., VAN LIS, R., DEUSCH, O., DAGAN, T., KUHN, L., GONTERO, B. & MARTIN, W. 2009. A proteomic survey of Chlamydomonas reinhardtii mitochondria sheds new light on the metabolic plasticity of the organelle and on the nature of the α-proteobacterial mitochondrial ancestor. *Molecular Biology and Evolution,* 26**,** 1533-1548.

BAINES, H. L., STEWART, J. B., STAMP, C., ZUPANIC, A., KIRKWOOD, T. B., LARSSON, N.-G., TURNBULL, D. M. & GREAVES, L. C. 2014. Similar patterns of clonally expanded somatic mtDNA mutations in the colon of heterozygous mtDNA mutator mice and ageing humans. *Mechanisms of ageing and development,* 139**,** 22-30.

BALLARD, D. & VOSS, E. 1985. Base specificity and idiotypy of anti-DNA autoantibodies reactive with synthetic nucleic acids. *The Journal of Immunology,* 135**,** 3372-3380.

BANG, B. & BANG, F. 1957. Graphic reconstruction of the third dimension from serial electron microphotographs. *Journal of ultrastructure research,* 1**,** 138.

BARANOVSKIY, A. G., BABAYEVA, N. D., SUWA, Y., GU, J., PAVLOV, Y. I. & TAHIROV, T. H. 2014. Structural basis for inhibition of DNA replication by aphidicolin. *Nucleic acids research,* 42**,** 14013-14021.

BARAZZONI, R., SHORT, K. R. & NAIR, K. S. 2000. Effects of aging on mitochondrial DNA copy number and cytochromec oxidase gene expression in rat skeletal muscle, liver, and heart. *Journal of Biological Chemistry,* 275**,** 3343-3347.

BARRIENTOS, A., CASADEMONT, J., CARDELLACH, F., ARDITE, E., ESTIVILL, X., URBANO-MÁRQUEZ, A., FERNÁNDEZ-CHECA, J. C. & NUNES, V. 1997. Qualitative and quantitative changes in skeletal muscle mtDNA and expression of mitochondrial-encoded genes in the human aging process. *Biochemical and molecular medicine,* 62**,** 165-171.

BAUMER, A., ZHANG, C., LINNANE, A. W. & NAGLEY, P. 1994. Age-related human mtDNA deletions: a heterogeneous set of deletions arising at a single pair of directly repeated sequences. *American journal of human genetics,* 54**,** 618.

BEAN, B. P. 2007. The action potential in mammalian central neurons. *Nature Reviews Neuroscience,* 8**,** 451.

BELEVICH, I., JOENSUU, M., KUMAR, D., VIHINEN, H. & JOKITALO, E. 2016. Microscopy image browser: a platform for segmentation and analysis of multidimensional datasets. *PLoS biology,* 14**,** e1002340.

BENDER, A., KRISHNAN, K. J., MORRIS, C. M., TAYLOR, G. A., REEVE, A. K., PERRY, R. H., JAROS, E., HERSHESON, J. S., BETTS, J. & KLOPSTOCK, T. 2006a. High levels of mitochondrial DNA deletions in substantia nigra neurons in aging and Parkinson disease. *Nature genetics,* 38**,** 515-517.

BENDER, A., KRISHNAN, K. J., MORRIS, C. M., TAYLOR, G. A., REEVE, A. K., PERRY, R. H., JAROS, E., HERSHESON, J. S., BETTS, J. & KLOPSTOCK, T. 2006b. High levels of mitochondrial DNA deletions in substantia nigra neurons in aging and Parkinson disease. *Nature genetics,* 38**,** 515.

BENDER, A., KRISHNAN, K. J., MORRIS, C. M., TAYLOR, G. A., REEVE, A. K., PERRY, R. H., JAROS, E., HERSHESON, J. S., BETTS, J., KLOPSTOCK, T., TAYLOR, R. W. & TURNBULL, D. M. 2006c. High levels of mitochondrial DNA deletions in substantia nigra neurons in aging and Parkinson disease. *Nat Genet,* 38**,** 515-7.

BENDER, A., SCHWARZKOPF, R.-M., MCMILLAN, A., KRISHNAN, K. J., RIEDER, G., NEUMANN, M., ELSTNER, M., TURNBULL, D. M. & KLOPSTOCK, T. 2008. Dopaminergic midbrain neurons are the prime target for mitochondrial DNA deletions. *Journal of neurology,* 255**,** 1231-1235.

BEREITER-HAHN, J. 1990. Behavior of mitochondria in the living cell. *International review of cytology.* Elsevier.

BERG, I. A. 2011. Ecological aspects of distribution of different autotrophic CO2 fixation pathways. *Applied and Environmental Microbiology*.

BHARATH, S., HSU, M., KAUR, D., RAJAGOPALAN, S. & ANDERSEN, J. K. 2002. Glutathione, iron and Parkinson's disease. *Biochemical pharmacology,* 64**,** 1037-1048.

BIANCO, J. N., POLI, J., SAKSOUK, J., BACAL, J., SILVA, M. J., YOSHIDA, K., LIN, Y.-L., TOURRIÈRE, H., LENGRONNE, A. & PASERO, P. 2012. Analysis of DNA replication profiles in budding yeast and mammalian cells using DNA combing. *Methods,* 57**,** 149-157.

BILBILLE, Y., GUSTILO, E. M., HARRIS, K. A., JONES, C. N., LUSIC, H., KAISER, R. J., DELANEY, M. O., SPREMULLI, L. L., DEITERS, A. & AGRIS, P. F. 2011. The human mitochondrial tRNAMet: structure/function relationship of a unique modification in the decoding of unconventional codons. *Journal of molecular biology,* 406**,** 257-274.

BLACHLY-DYSON, E. & FORTE, M. 2001. VDAC channels. *IUBMB life,* 52**,** 113-118.

BLOKHIN, A., VYSHKINA, T., KOMOLY, S. & KALMAN, B. 2008. Variations in mitochondrial DNA copy numbers in MS brains. *Journal of Molecular Neuroscience,* 35**,** 283-287.

BLOMSTRAND, C. & HAMBERGER, A. 1969. PROTEIN TURNOVER IN CELL-ENRICHED FRACTIONS FROM RABBIT BRAIN 1. *Journal of neurochemistry,* 16**,** 1401-1407.

BODYAK, N. D., NEKHAEVA, E., WEI, J. Y. & KHRAPKO, K. 2001. Quantification and sequencing of somatic deleted mtDNA in single cells: evidence for partially duplicated mtDNA in aged human tissues. *Human molecular genetics,* 10**,** 17-24.

BOGENHAGEN, D. & CLAYTON, D. A. 1977. Mouse L cell mitochondrial DNA molecules are selected randomly for replication throughout the cell cycle. *Cell,* 11**,** 719-727.

BOGENHAGEN, D. F., ROUSSEAU, D. & BURKE, S. 2008. The layered structure of human mitochondrial DNA nucleoids. *Journal of Biological Chemistry,* 283**,** 3665-3675.

BOHR, V. A. 2002. Repair of oxidative DNA damage in nuclear and mitochondrial DNA, and some changes with aging in mammalian cells1, 2. *Free Radical Biology and Medicine,* 32**,** 804-812.

BOHR, V. A., STEVNSNER, T. & DE SOUZA-PINTO, N. C. 2002. Mitochondrial DNA repair of oxidative damage in mammalian cells. *Gene,* 286**,** 127-134.

BOISVERT, F.-M., AHMAD, Y., GIERLIŃSKI, M., CHARRIÈRE, F., LAMOND, D., SCOTT, M., BARTON, G. & LAMOND, A. I. 2011. A quantitative spatial proteomics analysis of proteome turnover in human cells. *Molecular & Cellular Proteomics***,** mcp. M111. 011429.

BOLAM, J. P. & PISSADAKI, E. K. 2012. Living on the edge with too many mouths to feed: why dopamine neurons die. *Movement Disorders,* 27**,** 1478-1483.

BOLDEN, A., NOY, G. P. & WEISSBACH, A. 1977. DNA polymerase of mitochondria is a gamma-polymerase. *Journal of Biological Chemistry,* 252**,** 3351-3356.

BOWMAKER, M., YANG, M. Y., YASUKAWA, T., REYES, A., JACOBS, H. T., HUBERMAN, J. A. & HOLT, I. J. 2003. Mammalian mitochondrial DNA replicates bidirectionally from an initiation zone. *Journal of Biological Chemistry,* 278**,** 50961-50969.

BOYER, P. D. 1997. The ATP synthase-a splendid molecular machine. *Annual review of biochemistry,* 66**,** 717-749.

BRANDON, B. R., DIEDERICH, N. J., SONI, M., WITTE, K., WEINHOLD, M., KRAUSE, M. & JACKSON, S. 2013. Autosomal dominant mutations in POLG and C10orf2: association with late onset chronic progressive external ophthalmoplegia and Parkinsonism in two patients. *Journal of neurology,* 260**,** 1931.

BRAYMER, J. J. & LILL, R. J. J. O. B. C. 2017. Iron–sulfur cluster biogenesis and trafficking in mitochondria. 292**,** 12754-12763.

BROSSAS, J.-Y., BARREAU, E., COURTOIS, Y. & TRÉTON, J. 1994. Multiple deletions in mitochondrial DNA are present in senescent mouse brain. *Biochemical and biophysical research communications,* 202**,** 654-659.

BROWN, T. A., CECCONI, C., TKACHUK, A. N., BUSTAMANTE, C. & CLAYTON, D. A. 2005. Replication of mitochondrial DNA occurs by strand displacement with alternative light-strand origins, not via a strand-coupled mechanism. *Genes & development,* 19**,** 2466-2476.

BROWN, T. A., TKACHUK, A. N., SHTENGEL, G., KOPEK, B. G., BOGENHAGEN, D. F., HESS, H. F. & CLAYTON, D. A. 2011. Super-resolution fluorescence imaging of mitochondrial nucleoids reveals their spatial range, limits, and membrane interaction. *Molecular and cellular biology***,** MCB. 05694-11.

BROWN, W. M., GEORGE, M. & WILSON, A. C. 1979. Rapid evolution of animal mitochondrial DNA. *Proceedings of the National Academy of Sciences,* 76**,** 1967-1971.

BRUNELLE, J. K., BELL, E. L., QUESADA, N. M., VERCAUTEREN, K., TIRANTI, V., ZEVIANI, M., SCARPULLA, R. C. & CHANDEL, N. S. 2005. Oxygen sensing requires mitochondrial ROS but not oxidative phosphorylation. *Cell metabolism,* 1**,** 409-414.

BUA, E., JOHNSON, J., HERBST, A., DELONG, B., MCKENZIE, D., SALAMAT, S. & AIKEN, J. M. 2006. Mitochondrial DNA–deletion mutations accumulate intracellularly to detrimental levels in aged human skeletal muscle fibers. *The American Journal of Human Genetics,* 79**,** 469-480.

BUCKMAN, J. F., HERNÁNDEZ, H., KRESS, G. J., VOTYAKOVA, T. V., PAL, S. & REYNOLDS, I. J. 2001. MitoTracker labeling in primary neuronal and astrocytic cultures: influence of mitochondrial membrane potential and oxidants. *Journal of neuroscience methods,* 104**,** 165-176.

BULGAR, A., WEEKS, L., MIAO, Y., YANG, S., XU, Y., GUO, C., MARKOWITZ, S., OLEINICK, N., GERSON, S. & LIU, L. 2013. Removal of uracil by uracil DNA glycosylase limits pemetrexed cytotoxicity: overriding the limit with methoxyamine to inhibit base excision repair. *Cell death & disease,* 3**,** e252.

CALKINS, M. J. & REDDY, P. H. 2011. Assessment of newly synthesized mitochondrial DNA using BrdU labeling in primary neurons from Alzheimer's disease mice: Implications for impaired mitochondrial biogenesis and synaptic damage. *Biochimica et Biophysica Acta (BBA)-Molecular Basis of Disease,* 1812**,** 1182-1189.

CAMPBELL, G., KRISHNAN, K. J., DESCHAUER, M., TAYLOR, R. W. & TURNBULL, D. M. 2014. Dissecting the mechanisms underlying the accumulation of mitochondrial DNA deletions in human skeletal muscle. *Human molecular genetics,* 23**,** 4612-4620.

CAMPBELL, G. R., KRAYTSBERG, Y., KRISHNAN, K. J., OHNO, N., ZIABREVA, I., REEVE, A., TRAPP, B. D., NEWCOMBE, J., REYNOLDS, R. & LASSMANN, H. 2012. Clonally expanded mitochondrial DNA deletions within the choroid plexus in multiple sclerosis. *Acta neuropathologica,* 124**,** 209-220.

CAMPELLO, S. & SCORRANO, L. 2010. Mitochondrial shape changes: orchestrating cell pathophysiology. *EMBO reports,* 11**,** 678-684.

CANTÓ, C., JIANG, L. Q., DESHMUKH, A. S., MATAKI, C., COSTE, A., LAGOUGE, M., ZIERATH, J. R. & AUWERX, J. 2010. Interdependence of AMPK and SIRT1 for metabolic adaptation to fasting and exercise in skeletal muscle. *Cell metabolism,* 11**,** 213-219.

CANUGOVI, C., MAYNARD, S., BAYNE, A.-C. V., SYKORA, P., TIAN, J., DE SOUZA-PINTO, N. C., CROTEAU, D. L. & BOHR, V. A. 2010. The mitochondrial transcription factor A functions in mitochondrial base excision repair. *DNA repair,* 9**,** 1080-1089.

CAPALDI, R. A. 1990. Structure and function of cytochrome c oxidase. *Annual review of biochemistry,* 59**,** 569-596.

CARDOZO-PELAEZ, F., BROOKS, P. J., STEDEFORD, T., SONG, S. & SANCHEZ-RAMOS, J. 2000. DNA damage, repair, and antioxidant systems in brain regions: a correlative study. *Free Radical Biology and Medicine,* 28**,** 779-785.

CASTRO, M. D. R., SUAREZ, E., KRAISELBURD, E., ISIDRO, A., PAZ, J., FERDER, L. & AYALA-TORRES, S. 2012. Aging increases mitochondrial DNA damage and oxidative stress in liver of rhesus monkeys. *Experimental gerontology,* 47**,** 29-37.

CECCHINI, G. 2003. Function and Structure of Complex II of the Respiratory Chain*. *Annual review of biochemistry,* 72**,** 77-109.

CHANG, D. & REYNOLDS, I. 2006. Differences in mitochondrial movement and morphology in young and mature primary cortical neurons in culture. *Neuroscience,* 141**,** 727-736.

CHANG, D. D. & CLAYTON, D. A. 1985. Priming of human mitochondrial DNA replication occurs at the light-strand promoter. *Proceedings of the National Academy of Sciences,* 82**,** 351-355.

CHATTERJEE, A. & SINGH, K. K. 2001. Uracil-DNA glycosylase-deficient yeast exhibit a mitochondrial mutator phenotype. *Nucleic acids research,* 29**,** 4935-4940.

CHEN, D., CAO, G., HASTINGS, T., FENG, Y., PEI, W., O'HORO, C. & CHEN, J. 2002. Age-dependent decline of DNA repair activity for oxidative lesions in rat brain mitochondria. *Journal of neurochemistry,* 81**,** 1273-1284.

CHEN, H., DETMER, S. A., EWALD, A. J., GRIFFIN, E. E., FRASER, S. E. & CHAN, D. C. 2003a. Mitofusins Mfn1 and Mfn2 coordinately regulate mitochondrial fusion and are essential for embryonic development. *The Journal of cell biology,* 160**,** 189-200.

CHEN, H., VERMULST, M., WANG, Y. E., CHOMYN, A., PROLLA, T. A., MCCAFFERY, J. M. & CHAN, D. C. 2010. Mitochondrial fusion is required for mtDNA stability in skeletal muscle and tolerance of mtDNA mutations. *Cell,* 141**,** 280-289.

285

CHEN, Q., VAZQUEZ, E. J., MOGHADDAS, S., HOPPEL, C. L. & LESNEFSKY, E. J. 2003b. Production of reactive oxygen species by mitochondria central role of complex III. *Journal of Biological Chemistry,* 278**,** 36027-36031.

CHEN, Y. & DORN, G. W. 2013. PINK1-phosphorylated mitofusin 2 is a Parkin receptor for culling damaged mitochondria. *Science,* 340**,** 471-475.

CHINNADURAI, G., VIJAYALINGAM, S. & GIBSON, S. B. 2009. BNIP3 subfamily BH3-only proteins: mitochondrial stress sensors in normal and pathological functions. *Oncogene,* 27**,** S114.

CHINNERY, P., TAYLOR, G., HOWELL, N., BROWN, D., PARSONS, T. J. & TURNBULL, D. 2001. Point mutations of the mtDNA control region in normal and neurodegenerative human brains. *The American Journal of Human Genetics,* 68**,** 529-532.

CHINNERY, P. F., DIMAURO, S., SHANSKE, S., SCHON, E. A., ZEVIANI, M., MARIOTTI, C., CARRARA, F., LOMBES, A., LAFORET, P. & OGIER, H. 2004. Risk of developing a mitochondrial DNA deletion disorder. *The Lancet,* 364**,** 592-596.

CHOURASIA, A. H., TRACY, K., FRANKENBERGER, C., BOLAND, M. L., SHARIFI, M. N., DRAKE, L. E., SACHLEBEN, J. R., ASARA, J. M., LOCASALE, J. W. & KARCZMAR, G. S. 2015. Mitophagy defects arising from BNip3 loss promote mammary tumor progression to metastasis. *EMBO reports,* 16**,** 1145-1163.

CIRCU, M. L. & AW, T. Y. 2010. Reactive oxygen species, cellular redox systems, and apoptosis. *Free Radical Biology and Medicine,* 48**,** 749-762.

CLARK, C. G. & ROGER, A. J. 1995. Direct evidence for secondary loss of mitochondria in Entamoeba histolytica. *Proceedings of the National Academy of Sciences,* 92**,** 6518-6521.

CLARK, I. E., DODSON, M. W., JIANG, C., CAO, J. H., HUH, J. R., SEOL, J. H., YOO, S. J., HAY, B. A. & GUO, M. 2006. Drosophila pink1 is required for mitochondrial function and interacts genetically with parkin. *Nature,* 441**,** 1162.

CLAYTON, D. A. 1982. Replication of animal mitochondrial DNA. *Cell,* 28**,** 693-705.

COCKS, E., TAGGART, M., RIND, F. & WHITE, K. 2018. A guide to analysis and reconstruction of serial block face scanning electron microscopy data. *Journal of microscopy,* 270**,** 217-234.

COOPER, J., MANN, V. & SCHAPIRA, A. 1992. Analyses of mitochondrial respiratory chain function and mitochondrial DNA deletion in human skeletal muscle: effect of ageing. *Journal of the neurological sciences,* 113**,** 91-98.

COPELAND, W. C. & LONGLEY, M. J. 2003. DNA polymerase gamma in mitochondrial DNA replication and repair. *The Scientific World Journal,* 3**,** 34-44.

COPELAND, W. C. & LONGLEY, M. J. 2008. DNA2 resolves expanding flap in mitochondrial base excision repair. *Molecular cell,* 32**,** 457-458.

CORRAL-DEBRINSKI, M., HORTON, T., LOTT, M. T., SHOFFNER, J. M., BEAL, M. F. & WALLACE, D. C. 1992a. Mitochondrial DNA deletions in human brain: regional variability and increase with advanced age. *Nature genetics,* 2**,** 324.

CORRAL-DEBRINSKI, M., HORTON, T., LOTT, M. T., SHOFFNER, J. M., BEAL, M. F. & WALLACE, D. C. 1992b. Mitochondrial DNA deletions in human brain: regional variability and increase with advanced age. *Nature genetics,* 2**,** 324-329.

CORTOPASSI, G., SHIBATA, D., SOONG, N. & ARNHEIM, N. 1992. A pattern of accumulation of a somatic deletion of mitochondrial DNA in aging human tissues. *Proceedings of the National Academy of Sciences,* 89**,** 7370-7374.

CORTOPASSI, G. A. & ARNHEIM, N. 1990. Detection of a specific mitochondrial DNA deletion in tissues of older humans. *Nucleic acids research,* 18**,** 6927-6933.

COTTER, D., GUDA, P., FAHY, E. & SUBRAMANIAM, S. 2004. MitoProteome: mitochondrial protein sequence database and annotation system. *Nucleic acids research,* 32**,** D463-D467.

COTTRELL, D., BLAKELY, E., JOHNSON, M., INCE, P., BORTHWICK, G. & TURNBULL, D. 2001. Cytochrome c oxidase deficient cells accumulate in the hippocampus and choroid plexus with age. *Neurobiology of aging,* 22**,** 265-272.

COTTRELL, D. A., INCE, P. G., BLAKELY, E. L., JOHNSON, M. A., CHINNERY, P. F., HANNA, M. & TURNBULL, D. M. 2000. Neuropathological and histochemical changes in a multiple mitochondrial DNA deletion disorder. *Journal of Neuropathology & Experimental Neurology,* 59**,** 621-627.

COXHEAD, J., KURZAWA-AKANBI, M., HUSSAIN, R., PYLE, A., CHINNERY, P. & HUDSON, G. 2016. Somatic mtDNA variation is an important component of Parkinson's disease. *Neurobiology of aging,* 38**,** 217. e1-217. e6.

DAEMS, W. T. & WISSE, E. 1966. Shape and attachment of the cristae mitochondriales in mouse hepatic cell mitochondria. *Journal of ultrastructure research,* 16**,** 123-140.

DAMAS, J., CARNEIRO, J., AMORIM, A. & PEREIRA, F. 2013. MitoBreak: the mitochondrial DNA breakpoints database. *Nucleic acids research,* 42**,** D1261-D1268.

DAMAS, J., CARNEIRO, J., GONÇALVES, J., STEWART, J. B., SAMUELS, D. C., AMORIM, A. & PEREIRA, F. 2012. Mitochondrial DNA deletions are associated with non-B DNA conformations. *Nucleic acids research***,** gks500.

DAUBNER, S. C., LE, T. & WANG, S. 2011. Tyrosine hydroxylase and regulation of dopamine synthesis. *Archives of biochemistry and biophysics,* 508**,** 1-12.

DAVIDZON, G., GREENE, P., MANCUSO, M., KLOS, K. J., AHLSKOG, J. E., HIRANO, M. & DIMAURO, S. 2006. Early-onset familial parkinsonism due to POLG mutations. *Annals of Neurology: Official Journal of the American Neurological Association and the Child Neurology Society,* 59**,** 859-862.

DAVIS, A. F. & CLAYTON, D. A. 1996. In situ localization of mitochondrial DNA replication in intact mammalian cells. *The Journal of cell biology,* 135**,** 883-893.

DE BRITO, O. M. & SCORRANO, L. 2008. Mitofusin 2 tethers endoplasmic reticulum to mitochondria. *Nature,* 456**,** 605.

DE GREY, A. D. N. J. 1997. A proposed refinement of the mitochondrial free radical theory of aging. *Bioessays,* 19**,** 161-166.

287

DE SOUZA-PINTO, N. C., HOGUE, B. A. & BOHR, V. A. 2001. DNA repair and aging in mouse liver: 8-oxodG glycosylase activity increase in mitochondrial but not in nuclear extracts. *Free Radical Biology and Medicine,* 30**,** 916-923.

DE SOUZA-PINTO, N. C., MASON, P. A., HASHIGUCHI, K., WEISSMAN, L., TIAN, J., GUAY, D., LEBEL, M., STEVNSNER, T. V., RASMUSSEN, L. J. & BOHR, V. A. 2009. Novel DNA mismatch-repair activity involving YB-1 in human mitochondria. *DNA repair,* 8**,** 704-719.

DEGLI ESPOSTI, M. 2016. Late mitochondrial acquisition, really? *Genome biology and evolution,* 8**,** 2031-2035.

DEGLI ESPOSTI, M. 2018. Mitochondria: Where Are They Coming From? *Mitochondrial Biology and Experimental Therapeutics.* Springer.

DELETTRE, C., LENAERS, G., GRIFFOIN, J.-M., GIGAREL, N., LORENZO, C., BELENGUER, P., PELLOQUIN, L., GROSGEORGE, J., TURC-CAREL, C. & PERRET, E. 2000. Nuclear gene OPA1, encoding a mitochondrial dynamin-related protein, is mutated in dominant optic atrophy. *Nature genetics,* 26**,** 207.

DENK, W. & HORSTMANN, H. 2004. Serial block-face scanning electron microscopy to reconstruct three-dimensional tissue nanostructure. *PLoS biology,* 2**,** e329.

DEXTER, D., CARAYON, A., JAVOY-AGID, F., AGID, Y., WELLS, F., DANIEL, S., LEES, A., JENNER, P. & MARSDEN, C. 1991. Alterations in the levels of iron, ferritin and other trace metals in Parkinson's disease and other neurodegenerative diseases affecting the basal ganglia. *Brain,* 114**,** 1953-1975.

DEXTER, D., CARTER, C., WELLS, F., JAVOY-AGID, F., AGID, Y., LEES, A., JENNER, P. & MARSDEN, C. D. 1989. Basal lipid peroxidation in substantia nigra is increased in Parkinson's disease. *Journal of neurochemistry,* 52**,** 381-389.

DI POGGIO, M. B., NESTI, C., BRUNO, C., MESCHINI, M. C., SCHENONE, A. & SANTORELLI, F. M. 2013. Dopamine-agonist responsive Parkinsonism in a patient with the SANDO syndrome caused by POLG mutation. *BMC medical genetics,* 14**,** 105.

DIAZ, F. 2010. Cytochrome c oxidase deficiency: patients and animal models. *Biochimica et Biophysica Acta (BBA)-Molecular Basis of Disease,* 1802**,** 100-110.

DIAZ, F., BAYONA-BAFALUY, M. P., RANA, M., MORA, M., HAO, H. & MORAES, C. T. 2002. Human mitochondrial DNA with large deletions repopulates organelles faster than full-length genomes under relaxed copy number control. *Nucleic acids research,* 30**,** 4626-4633.

DICKINSON, B. C. & CHANG, C. J. 2008. A targetable fluorescent probe for imaging hydrogen peroxide in the mitochondria of living cells. *Journal of the American Chemical Society,* 130**,** 9638-9639.

DIMAURO, S. & DAVIDZON, G. J. A. O. M. 2005. Mitochondrial DNA and disease. 37**,** 222-232.

DIMITROVA, D. S. & GILBERT, D. M. 1999. The spatial position and replication timing of chromosomal domains are both established in early G1 phase. *Molecular cell,* 4**,** 983-993.

DING, J. D., KENNEDY, M. B. & WEINBERG, R. J. 2013. Subcellular organization of camkii in rat hippocampal pyramidal neurons. *Journal of Comparative Neurology,* 521**,** 3570-3583.

DJORDJEVIC, B. & SZYBALSKI, W. 1960. Genetics of human cell lines: III. Incorporation of 5-bromo-and 5-Iododeoxyhridine into the deoxyribonucleic acid of human cells and its effect on radiation sensitivity. *Journal of Experimental Medicine,* 112**,** 509-531.

DÖLLE, C., FLØNES, I., NIDO, G. S., MILETIC, H., OSUAGWU, N., KRISTOFFERSEN, S., LILLENG, P. K., LARSEN, J. P., TYSNES, O.-B. & HAUGARVOLL, K. 2016. Defective mitochondrial DNA homeostasis in the substantia nigra in Parkinson disease. *Nature communications,* 7**,** 13548.

DUBEY, G. P. & BEN-YEHUDA, S. 2011. Intercellular nanotubes mediate bacterial communication. *Cell,* 144**,** 590-600.

DURHAM, S. E., SAMUELS, D. C., CREE, L. M. & CHINNERY, P. F. 2007. Normal levels of wild-type mitochondrial DNA maintain cytochrome c oxidase activity for two pathogenic mitochondrial DNA mutations but not for m. 3243A→ G. *The American Journal of Human Genetics,* 81**,** 189-195.

DUVEZIN-CAUBET, S., JAGASIA, R., WAGENER, J., HOFMANN, S., TRIFUNOVIC, A., HANSSON, A., CHOMYN, A., BAUER, M. F., ATTARDI, G. & LARSSON, N.-G. 2006. Proteolytic processing of OPA1 links mitochondrial dysfunction to alterations in mitochondrial morphology. *Journal of Biological Chemistry,* 281**,** 37972-37979.

ELSON, J. L., SAMUELS, D. C., TURNBULL, D. M. & CHINNERY, P. F. 2001. Random intracellular drift explains the clonal expansion of mitochondrial DNA mutations with age. *The American Journal of Human Genetics,* 68**,** 802-806.

EMPERADOR, S., BAYONA-BAFALUY, M. P., FERNÁNDEZ-MARMIESSE, A., PINEDA, M., FELGUEROSO, B., LÓPEZ-GALLARDO, E., ARTUCH, R., ROCA, I., RUIZ-PESINI, E. & COUCE, M. L. 2017. Molecular-genetic characterization and rescue of a TSFM mutation causing childhood-onset ataxia and nonobstructive cardiomyopathy. *European Journal of Human Genetics,* 25**,** 153.

ENDO, T. & YAMANO, K. 2010. Transport of proteins across or into the mitochondrial outer membrane. *Biochimica Et Biophysica Acta (BBA)-Molecular Cell Research,* 1803**,** 706-714.

ENRÍQUEZ, J. A., FERNÁNDEZ-SILVA, P., PÉREZ-MARTOS, A., LÓPEZ-PÉREZ, M. J. & MONTOYA, J. 1996. The synthesis of mRNA in isolated mitochondria can be maintained for several hours and is inhibited by high levels of ATP. *European journal of biochemistry,* 237**,** 601-610.

ERIKSSON, P. S., PERFILIEVA, E., BJÖRK-ERIKSSON, T., ALBORN, A.-M., NORDBORG, C., PETERSON, D. A. & GAGE, F. H. 1998. Neurogenesis in the adult human hippocampus. *Nature medicine,* 4**,** 1313-1317.

ESCO, M. A., WANG, Z., MCDERMOTT, M. L. & KURPAKUS-WHEATER, M. 2001. Potential role for laminin 5 in hypoxia-mediated apoptosis of human corneal epithelial cells. *Journal of cell science,* 114**,** 4033-4040.

ESCOBAR-HENRIQUES, M. & ANTON, F. 2013. Mechanistic perspective of mitochondrial fusion: tubulation vs. fragmentation. *Biochimica Et Biophysica Acta (BBA)-Molecular Cell Research,* 1833**,** 162-175.

ESCOVITZ, W., FOX, T. & LEVI-SETTI, R. 1975. Scanning transmission ion microscope with a field ion source. *Proceedings of the National Academy of Sciences,* 72**,** 1826-1828.

EUSTAQUIO, T., WANG, C., DUGARD, C. K., GEORGE, N. I., LIU, F., SLIKKER JR, W., PAULE, M. G., HOWARD, P. C. & PAREDES, A. M. 2018. Electron Microscopy Techniques Employed to Explore Mitochondrial Defects in the Developing Rat Brain Following Ketamine Treatment. *Experimental cell research*.

EXNER, N., TRESKE, B., PAQUET, D., HOLMSTRÖM, K., SCHIESLING, C., GISPERT, S., CARBALLO-CARBAJAL, I., BERG, D., HOEPKEN, H.-H. & GASSER, T. 2007. Loss-of-function of human PINK1 results in mitochondrial pathology and can be rescued by parkin. *Journal of Neuroscience,* 27**,** 12413-12418.

FALKENBERG, M., GASPARI, M., RANTANEN, A., TRIFUNOVIC, A., LARSSON, N.-G. & GUSTAFSSON, C. M. 2002. Mitochondrial transcription factors B1 and B2 activate transcription of human mtDNA. *Nature genetics,* 31**,** 289.

FALKENBERG, M., LARSSON, N.-G. & GUSTAFSSON, C. M. 2007. DNA replication and transcription in mammalian mitochondria. *Annu. Rev. Biochem.,* 76**,** 679-699.

FAN, W. & EVANS, R. 2015. PPARs and ERRs: molecular mediators of mitochondrial metabolism. *Current opinion in cell biology,* 33**,** 49-54.

FARGE, G., PHAM, X. H., HOLMLUND, T., KHOROSTOV, I. & FALKENBERG, M. 2007. The accessory subunit B of DNA polymerase γ is required for mitochondrial replisome function. *Nucleic acids research,* 35**,** 902-911.

FAYET, G., JANSSON, M., STERNBERG, D., MOSLEMI, A.-R., BLONDY, P., LOMBÈS, A., FARDEAU, M. & OLDFORS, A. 2002. Ageing muscle: clonal expansions of mitochondrial DNA point mutations and deletions cause focal impairment of mitochondrial function. *Neuromuscular Disorders,* 12**,** 484-493.

FERNÁNDEZ-SILVA, P., ENRIQUEZ, J. A. & MONTOYA, J. 2003. Replication and transcription of mammalian mitochondrial DNA. *Experimental physiology,* 88**,** 41-56.

FILBURN, C. R., EDRIS, W., TAMATANI, M., HOGUE, B., KUDRYASHOVA, I. & HANSFORD, R. G. 1996. Mitochondrial electron transport chain activities and DNA deletions in regions of the rat brain. *Mechanisms of ageing and development,* 87**,** 35-46.

FISCHER, S., LU, Z. & MEINERTZHAGEN, I. A. 2018. From two to three dimensions: The importance of the third dimension for evaluating the limits to neuronal miniaturization in insects. *Journal of Comparative Neurology,* 526**,** 653-662.

FLEISCHER, S., KLOUWEN, H. & BRIERLEY, G. 1961. Studies of the Electron Transfer System XXXVIII. LIPID COMPOSITION OF PURIFIED ENZYME PREPARATIONS DERIVED FROM BEEF HEART MITOCHONDRIA. *Journal of Biological Chemistry,* 236**,** 2936-2941.

FLORY JR, P. J. & VINOGRAD, J. 1973. 5-bromodeoxyuridine labeling of monomeric and catenated circular mitochondrial DNA in HeLa cells. *Journal of molecular biology,* 74**,** 81-94.

FORMOSA, L. E. & RYAN, M. T. 2016. Mitochondrial fusion: Reaching the end of mitofusin's tether. *J Cell Biol**,** jcb. 201611048.

FRAHM, T., MOHAMED, S. A., BRUSE, P., GEMÜND, C., OEHMICHEN, M. & MEISSNER, C. 2005. Lack of age-related increase of mitochondrial DNA amount in brain, skeletal muscle and human heart. *Mechanisms of ageing and development,* 126**,** 1192-1200.

FRANK, M., DUVEZIN-CAUBET, S., KOOB, S., OCCHIPINTI, A., JAGASIA, R., PETCHERSKI, A., RUONALA, M. O., PRIAULT, M., SALIN, B. & REICHERT, A. S. 2012. Mitophagy is triggered by mild oxidative stress in a mitochondrial fission dependent manner. *Biochimica et Biophysica Acta (BBA)-Molecular Cell Research,* 1823**,** 2297-2310.

FREDERICK, R. L. & SHAW, J. M. 2007. Moving mitochondria: establishing distribution of an essential organelle. *Traffic,* 8**,** 1668-1675.

FREY, T. G. & MANNELLA, C. A. 2000. The internal structure of mitochondria. *Trends in biochemical sciences,* 25**,** 319-324.

FUKE, S., KAMETANI, M., YAMADA, K., KASAHARA, T., KUBOTA-SAKASHITA, M., KUJOTH, G. C., PROLLA, T. A., HITOSHI, S. & KATO, T. 2014. Heterozygous Polg mutation causes motor dysfunction due to mt DNA deletions. *Annals of clinical and translational neurology,* 1**,** 909-920.

FUKE, S., KUBOTA-SAKASHITA, M., KASAHARA, T., SHIGEYOSHI, Y. & KATO, T. 2011a. Regional variation in mitochondrial DNA copy number in mouse brain. *Biochimica et Biophysica Acta (BBA)-Bioenergetics,* 1807**,** 270-274.

FUKE, S., KUBOTA-SAKASHITA, M., KASAHARA, T., SHIGEYOSHI, Y. & KATO, T. J. B. E. B. A.-B. 2011b. Regional variation in mitochondrial DNA copy number in mouse brain. 1807**,** 270-274.

FUKUI, H. & MORAES, C. T. 2008. Mechanisms of formation and accumulation of mitochondrial DNA deletions in aging neurons. *Human molecular genetics,* 18**,** 1028-1036.

FUSAKI, N., BAN, H., NISHIYAMA, A., SAEKI, K. & HASEGAWA, M. 2009. Efficient induction of transgene-free human pluripotent stem cells using a vector based on Sendai virus, an RNA virus that does not integrate into the host genome. *Proceedings of the Japan Academy, Series B,* 85**,** 348-362.

FUSTE, J. M., WANROOIJ, S., JEMT, E., GRANYCOME, C. E., CLUETT, T. J., SHI, Y., ATANASSOVA, N., HOLT, I. J., GUSTAFSSON, C. M. & FALKENBERG, M. 2010. Mitochondrial RNA polymerase is needed for activation of the origin of light-strand DNA replication. *Molecular cell,* 37**,** 67-78.

FUSTÉ, J. M., WANROOIJ, S., JEMT, E., GRANYCOME, C. E., CLUETT, T. J., SHI, Y., ATANASSOVA, N., HOLT, I. J., GUSTAFSSON, C. M. & FALKENBERG, M. 2010. Mitochondrial RNA polymerase is needed for activation of the origin of light-strand DNA replication. *Molecular cell,* 37**,** 67-78.

GAARE, J. J., NIDO, G. S., SZTROMWASSER, P., KNAPPSKOG, P. M., DAHL, O., LUND-JOHANSEN, M., MAPLE-GRØDEM, J., ALVES, G., TYSNES, O. B. & JOHANSSON, S. 2018. Rare genetic variation in mitochondrial pathways influences the risk for parkinson's disease. *Movement Disorders*.

GEISLER, S., HOLMSTRÖM, K. M., SKUJAT, D., FIESEL, F. C., ROTHFUSS, O. C., KAHLE, P. J. & SPRINGER, W. 2010. PINK1/Parkin-mediated mitophagy is dependent on VDAC1 and p62/SQSTM1. *Nature cell biology,* 12**,** 119.

GHARRAVI, A. M. 2016. Staining of cerebellar cortex granular layer interneurons with natural dye of Madder. *Cerebellum & ataxias,* 3**,** 12.

291

GILES, R. E., BLANC, H., CANN, H. M. & WALLACE, D. C. 1980. Maternal inheritance of human mitochondrial DNA. *Proceedings of the National academy of Sciences,* 77**,** 6715-6719.

GILKERSON, R., BRAVO, L., GARCIA, I., GAYTAN, N., HERRERA, A., MALDONADO, A. & QUINTANILLA, B. 2013. The mitochondrial nucleoid: integrating mitochondrial DNA into cellular homeostasis. *Cold Spring Harbor perspectives in biology,* 5**,** a011080.

GLANCY, B., HARTNELL, L. M., MALIDE, D., YU, Z.-X., COMBS, C. A., CONNELLY, P. S., SUBRAMANIAM, S. & BALABAN, R. S. 2015. Mitochondrial reticulum for cellular energy distribution in muscle. *Nature,* 523**,** 617.

GOFFART, S., COOPER, H. M., TYYNISMAA, H., WANROOIJ, S., SUOMALAINEN, A. & SPELBRINK, J. N. 2008. Twinkle mutations associated with autosomal dominant progressive external ophthalmoplegia lead to impaired helicase function and in vivo mtDNA replication stalling. *Human molecular genetics,* 18**,** 328-340.

GOOD, P. F., HSU, A., WERNER, P., PERL, D. P. & OLANOW, C. W. 1998. Protein nitration in Parkinson's disease. *Journal of Neuropathology & Experimental Neurology,* 57**,** 338-342.

GOTTLIEB, E., ARMOUR, S. M., HARRIS, M. H. & THOMPSON, C. B. 2003. Mitochondrial membrane potential regulates matrix configuration and cytochrome c release during apoptosis. *Cell Death & Differentiation,* 10**,** 709-717.

GOULD, E., TANAPAT, P., MCEWEN, B. S., FLÜGGE, G. & FUCHS, E. 1998. Proliferation of granule cell precursors in the dentate gyrus of adult monkeys is diminished by stress. *Proceedings of the National Academy of Sciences,* 95**,** 3168-3171.

GRATZNER, H. G. 1982. Monoclonal antibody to 5-bromo-and 5-iododeoxyuridine: a new reagent for detection of DNA replication. *Science,* 218**,** 474-475.

GRAY, M. W. 2012. Mitochondrial evolution. *Cold Spring Harbor perspectives in biology,* 4**,** a011403.

GRAY, M. W. 2015. Mosaic nature of the mitochondrial proteome: Implications for the origin and evolution of mitochondria. *Proceedings of the National Academy of Sciences,* 112**,** 10133-10138.

GRAY, M. W., BURGER, G. & LANG, B. F. 1999. Mitochondrial evolution. *Science,* 283**,** 1476-1481.

GRAZIEWICZ, M. A., LONGLEY, M. J. & COPELAND, W. C. 2006. DNA polymerase γ in mitochondrial DNA replication and repair. *Chemical reviews,* 106**,** 383-405.

GREAVES, L. C., ELSON, J. L., NOOTEBOOM, M., GRADY, J. P., TAYLOR, G. A., TAYLOR, R. W., MATHERS, J. C., KIRKWOOD, T. B. L. & TURNBULL, D. M. 2012. Comparison of mitochondrial mutation spectra in ageing human colonic epithelium and disease: absence of evidence for purifying selection in somatic mitochondrial DNA point mutations. *PLoS Genet,* 8**,** e1003082.

GREAVES, L. C., NOOTEBOOM, M., ELSON, J. L., TUPPEN, H. A., TAYLOR, G. A., COMMANE, D. M., ARASARADNAM, R. P., KHRAPKO, K., TAYLOR, R. W. & KIRKWOOD, T. B. 2014. Clonal expansion of early to mid-life mitochondrial DNA point mutations drives mitochondrial dysfunction during human ageing. *PLoS genetics,* 10**,** e1004620.

GREDILLA, R., GARM, C., HOLM, R., BOHR, V. A. & STEVNSNER, T. 2010. Differential age-related changes in mitochondrial DNA repair activities in mouse brain regions. *Neurobiology of aging,* 31**,** 993-1002.

GRIFFITHS, E. J. & RUTTER, G. A. 2009. Mitochondrial calcium as a key regulator of mitochondrial ATP production in mammalian cells. *Biochimica et Biophysica Acta (BBA)-Bioenergetics,* 1787**,** 1324-1333.

GROSS, N. J., GETZ, G. S. & RABINOWITZ, M. 1969. Apparent turnover of mitochondrial deoxyribonucleic acid and mitochondrial phospholipids in the tissues of the rat. *Journal of Biological Chemistry,* 244**,** 1552-1562.

GROSS, N. J. & RABINOWITZ, M. 1969. Synthesis of new strands of mitochondrial and nuclear deoxyribonucleic acid by semiconservative replication. *Journal of Biological Chemistry,* 244**,** 1563-1566.

GRÜNEWALD, A., LAX, N. Z., ROCHA, M. C., REEVE, A. K., HEPPLEWHITE, P. D., RYGIEL, K. A., TAYLOR, R. W. & TURNBULL, D. M. 2014. Quantitative quadruple-label immunofluorescence of mitochondrial and cytoplasmic proteins in single neurons from human midbrain tissue. *Journal of neuroscience methods,* 232**,** 143-149.

GU, G., REYES, P. F., GOLDEN, G. T., WOLTJER, R. L., HULETTE, C., MONTINE, T. J. & ZHANG, J. 2002. Mitochondrial DNA deletions/rearrangements in parkinson disease and related neurodegenerative disorders. *Journal of Neuropathology & Experimental Neurology,* 61**,** 634-639.

GUENET, L., TOUTAIN, B., GUILLERET, I., CHAUVEL, B., DEAVEN, L. L., LONGMIRE, J. L., LE GALL, J.-Y., DAVID, V. & LE TREUT, A. 1999. Human release factor eRF1: structural organisation of the unique functional gene on chromosome 5 and of the three processed pseudogenes. *FEBS letters,* 454**,** 131-136.

GUPTA, R. S., RAMACHANDRA, N. B., BOWES, T. & SINGH, B. Unusual cellular disposition of the mitochondrial molecular chaperones Hsp60, Hsp70 and Hsp10. Novartis Foundation Symposium, 2008. Chichester; New York; John Wiley; 1999, 59.

HADDAD, D. & NAKAMURA, K. 2015. Understanding the susceptibility of dopamine neurons to mitochondrial stressors in Parkinson's disease. *FEBS letters,* 589**,** 3702-3713.

HAGHNIA, M., CAVALLI, V., SHAH, S. B., SCHIMMELPFENG, K., BRUSCH, R., YANG, G., HERRERA, C., PILLING, A. & GOLDSTEIN, L. S. 2007. Dynactin is required for coordinated bidirectional motility, but not for dynein membrane attachment. *Molecular biology of the cell,* 18**,** 2081-2089.

HAINES, K. M., FELDMAN, E. L. & LENTZ, S. I. 2010a. Visualization of mitochondrial DNA replication in individual cells by EdU signal amplification. *J Vis Exp*.

HAINES, K. M., FELDMAN, E. L. & LENTZ, S. I. 2010b. Visualization of mitochondrial DNA replication in individual cells by EdU signal amplification. *Journal of visualized experiments: JoVE*.

293

HAMILTON, M. L., VAN REMMEN, H., DRAKE, J. A., YANG, H., GUO, Z. M., KEWITT, K., WALTER, C. A. & RICHARDSON, A. 2001. Does oxidative damage to DNA increase with age? *Proceedings of the National Academy of Sciences,* 98**,** 10469-10474.

HANAOKA, F., KATO, H., IKEGAMI, S., OHASHI, M. & YAMADA, M.-A. 1979. Aphidicolin does inhibit repair replication in HeLa cells. *Biochemical and biophysical research communications,* 87**,** 575-580.

HANDSCHIN, C., RHEE, J., LIN, J., TARR, P. T. & SPIEGELMAN, B. M. 2003. An autoregulatory loop controls peroxisome proliferator-activated receptor γ coactivator 1α expression in muscle. *Proceedings of the national academy of sciences,* 100**,** 7111-7116.

HANDSCHIN, C. & SPIEGELMAN, B. M. 2006. Peroxisome proliferator-activated receptor γ coactivator 1 coactivators, energy homeostasis, and metabolism. *Endocrine reviews,* 27**,** 728-735.

HANISCH, F., KORNHUBER, M., ALSTON, C. L., TAYLOR, R. W., DESCHAUER, M. & ZIERZ, S. 2015. SANDO syndrome in a cohort of 107 patients with CPEO and mitochondrial DNA deletions. *Journal of Neurology, Neurosurgery & Psychiatry,* 86**,** 630-634.

HARDIE, D. G., ROSS, F. A. & HAWLEY, S. A. 2012. AMPK: a nutrient and energy sensor that maintains energy homeostasis. *Nature reviews Molecular cell biology,* 13**,** 251.

HARE, D. J. & DOUBLE, K. L. 2016. Iron and dopamine: a toxic couple. *Brain,* 139**,** 1026-1035.

HARRIS, L., ZALUCKI, O. & PIPER, M. 2018. BrdU/EdU dual labeling to determine the cell-cycle dynamics of defined cellular subpopulations. *Journal of molecular histology,* 49**,** 229-234.

HASHIGUCHI, K., STUART, J. A., DE SOUZA-PINTO, N. C. & BOHR, V. A. 2004. The C-terminal αO helix of human Ogg1 is essential for 8-oxoguanine DNA glycosylase activity: the mitochondrial β-Ogg1 lacks this domain and does not have glycosylase activity. *Nucleic acids research,* 32**,** 5596-5608.

HAUGLAND, R. P., YUE, S. T., MILLARD, P. J. & ROTH, B. L. 1995. Cyclic-substituted unsymmetrical cyanine dyes. Google Patents.

HE, L., CHINNERY, P. F., DURHAM, S. E., BLAKELY, E. L., WARDELL, T. M., BORTHWICK, G. M., TAYLOR, R. W. & TURNBULL, D. M. 2002. Detection and quantification of mitochondrial DNA deletions in individual cells by real-time PCR. *Nucleic acids research,* 30**,** e68-e68.

HE, Q., SHUMATE, C. K., WHITE, M. A., MOLINEUX, I. J. & YIN, Y. W. 2013. Exonuclease of human DNA polymerase gamma disengages its strand displacement function. *Mitochondrion,* 13**,** 592-601.

HE, X.-P., YANG, F., XIE, Z.-P. & LU, B. 2000. Intracellular Ca2+ and Ca2+/calmodulin-dependent kinase II mediate acute potentiation of neurotransmitter release by neurotrophin-3. *The Journal of cell biology,* 149**,** 783-792.

HENAULT, J., MARTINEZ, J., RIGGS, J. M., TIAN, J., MEHTA, P., CLARKE, L., SASAI, M., LATZ, E., BRINKMANN, M. M. & IWASAKI, A. 2012. Noncanonical autophagy is required for type I interferon secretion in response to DNA-immune complexes. *Immunity,* 37**,** 986-997.

HENDEE, W. R., ZEBRUN, W. & BONTE, F. J. 1963. Anomalous structures in the cytoplasm of HeLa cells cultured in the presence of 5-bromodeoxyuridine. *The Journal of cell biology,* 17**,** 675.

HIROKAWA, N., NIWA, S. & TANAKA, Y. 2010. Molecular motors in neurons: transport mechanisms and roles in brain function, development, and disease. *Neuron,* 68**,** 610-638.

HIROKAWA, N., SATO-YOSHITAKE, R., YOSHIDA, T. & KAWASHIMA, T. 1990. Brain dynein (MAP1C) localizes on both anterogradely and retrogradely transported membranous organelles in vivo. *The Journal of cell biology,* 111**,** 1027-1037.

HIROTA, K., TSUDA, M., TSURIMOTO, T., COHEN, I. S., LIVNEH, Z., KOBAYASHI, K., NARITA, T., NISHIHARA, K., MURAI, J. & IWAI, S. 2016. In vivo evidence for translesion synthesis by the replicative DNA polymerase δ. *Nucleic acids research,* 44**,** 7242-7250.

HIRST, J., CARROLL, J., FEARNLEY, I. M., SHANNON, R. J. & WALKER, J. E. 2003. The nuclear encoded subunits of complex I from bovine heart mitochondria. *Biochimica et Biophysica Acta (BBA)-Bioenergetics,* 1604**,** 135-150.

HIRST, J., KING, M. S. & PRYDE, K. R. 2008. The production of reactive oxygen species by complex I. Portland Press Limited.

HOLT, I. J., HARDING, A. E. & MORGAN-HUGHES, J. A. 1988. Deletions of muscle mitochondrial DNA in patients with mitochondrial myopathies. *Nature,* 331**,** 717.

HOLT, I. J., LORIMER, H. E. & JACOBS, H. T. 2000. Coupled leading-and lagging-strand synthesis of mammalian mitochondrial DNA. *Cell,* 100**,** 515-524.

HOLT, I. J. & REYES, A. 2012. Human mitochondrial DNA replication. *Cold Spring Harbor perspectives in biology,* 4**,** a012971.

HONRATH, B., METZ, I., BENDRIDI, N., RIEUSSET, J., CULMSEE, C. & DOLGA, A. M. 2017. Glucose-regulated protein 75 determines ER–mitochondrial coupling and sensitivity to oxidative stress in neuronal cells. *Cell death discovery,* 3**,** 17076.

HORTON, T. M., GRAHAM, B. H., CORRAL-DEBRINSKI, M., SHOFFNER, J. M., KAUFMAN, A. E., BEAL, M. F. & WALLACE, D. C. 1995. Marked increase in mitochondrial DNA deletion levels in the cerebral cortex of Huntington's disease patients. *Neurology,* 45**,** 1879-1883.

HOUTEN, S. M. & WANDERS, R. J. 2010. A general introduction to the biochemistry of mitochondrial fatty acid β-oxidation. *Journal of inherited metabolic disease,* 33**,** 469-477.

HOUTGRAAF, J. H., VERSMISSEN, J. & VAN DER GIESSEN, W. J. 2006. A concise review of DNA damage checkpoints and repair in mammalian cells. *Cardiovascular Revascularization Medicine,* 7**,** 165-172.

HU, J., DE SOUZA-PINTO, N. C., HARAGUCHI, K., HOGUE, B. A., JARUGA, P., GREENBERG, M. M., DIZDAROGLU, M. & BOHR, V. A. 2005. Repair of Formamidopyrimidines in DNA Involves Different Glycosylases ROLE OF THE OGG1, NTH1, AND NEIL1 ENZYMES. *Journal of Biological Chemistry,* 280**,** 40544-40551.

HUANG, P., YU, T. & YOON, Y. 2007. Mitochondrial clustering induced by overexpression of the mitochondrial fusion protein Mfn2 causes mitochondrial dysfunction and cell death. *European journal of cell biology,* 86**,** 289-302.

HUANG, X., SUN, L., JI, S., ZHAO, T., ZHANG, W., XU, J., ZHANG, J., WANG, Y., WANG, X. & FRANZINI-ARMSTRONG, C. 2013. Kissing and nanotunneling mediate intermitochondrial communication in the heart. *Proceedings of the National Academy of Sciences,* 110**,** 2846-2851.

HUDSON, G. & CHINNERY, P. F. 2006a. Mitochondrial DNA polymerase-γ and human disease. *Human molecular genetics,* 15**,** R244-R252.

HUDSON, G. & CHINNERY, P. F. J. H. M. G. 2006b. Mitochondrial DNA polymerase-γ and human disease. 15**,** R244-R252.

HÜTTEMANN, M., PECINA, P., RAINBOLT, M., SANDERSON, T. H., KAGAN, V. E., SAMAVATI, L., DOAN, J. W. & LEE, I. 2011. The multiple functions of cytochrome c and their regulation in life and death decisions of the mammalian cell: From respiration to apoptosis. *Mitochondrion,* 11**,** 369-381.

IBORRA, F. J., KIMURA, H. & COOK, P. R. 2004. The functional organization of mitochondrial genomes in human cells. *BMC biology,* 2**,** 9.

IKEBE, S.-I., TANAKA, M., OHNO, K., SATO, W., HATTORI, K., KONDO, T., MIZUNO, Y. & OZAWA, T. 1990. Increase of deleted mitochondrial DNA in the striatum in Parkinson's disease and senescence. *Biochemical and biophysical research communications,* 170**,** 1044-1048.

IMAM, S. Z., KARAHALIL, B., HOGUE, B. A., SOUZA-PINTO, N. C. & BOHR, V. A. 2006. Mitochondrial and nuclear DNA-repair capacity of various brain regions in mouse is altered in an age-dependent manner. *Neurobiology of aging,* 27**,** 1129-1136.

INDO, H. P., DAVIDSON, M., YEN, H.-C., SUENAGA, S., TOMITA, K., NISHII, T., HIGUCHI, M., KOGA, Y., OZAWA, T. & MAJIMA, H. J. 2007. Evidence of ROS generation by mitochondria in cells with impaired electron transport chain and mitochondrial DNA damage. *Mitochondrion,* 7**,** 106-118.

ISHIHARA, N., NOMURA, M., JOFUKU, A., KATO, H., SUZUKI, S. O., MASUDA, K., OTERA, H., NAKANISHI, Y., NONAKA, I. & GOTO, Y.-I. 2009. Mitochondrial fission factor Drp1 is essential for embryonic development and synapse formation in mice. *Nature cell biology,* 11**,** 958.

IWATA, A., MARUYAMA, M., AKAGI, T., HASHIKAWA, T., KANAZAWA, I., TSUJI, S. & NUKINA, N. 2003. Alpha-synuclein degradation by serine protease neurosin: implication for pathogenesis of synucleinopathies. *Human molecular genetics,* 12**,** 2625-2635.

JACOBY, W. G. J. E. S. 2000. Loess:: a nonparametric, graphical tool for depicting relationships between variables. 19**,** 577-613.

JÄGER, S., HANDSCHIN, C., PIERRE, J. S.-. & SPIEGELMAN, B. M. 2007. AMP-activated protein kinase (AMPK) action in skeletal muscle via direct phosphorylation of PGC-1α. *Proceedings of the National Academy of Sciences,* 104**,** 12017-12022.

JAMES, S. A., ROBERTS, B. R., HARE, D. J., DE JONGE, M. D., BIRCHALL, I. E., JENKINS, N. L., CHERNY, R. A., BUSH, A. I. & MCCOLL, G. 2015. Direct in vivo imaging of ferrous iron dyshomeostasis in ageing Caenorhabditis elegans. *Chemical science,* 6**,** 2952-2962.

JANSSEN, R. J. R. J., NIJTMANS, L. G., VAN DEN HEUVEL, L. P. & SMEITINK, J. A. M. 2006. Mitochondrial complex I: structure, function and pathology. *Journal of inherited metabolic disease,* 29**,** 499-515.

JANZEN, D. M. & GEBALLE, A. P. 2004. The effect of eukaryotic release factor depletion on translation termination in human cell lines. *Nucleic acids research,* 32**,** 4491-4502.

JOHANSSON, M. & KARLSSON, A. 1997. Cloning of the cDNA and chromosome localization of the gene for human thymidine kinase 2. *Journal of Biological Chemistry,* 272**,** 8454-8458.

JOHNSON, L. V., WALSH, M. L., BOCKUS, B. J. & CHEN, L. B. 1981. Monitoring of relative mitochondrial membrane potential in living cells by fluorescence microscopy. *The Journal of Cell Biology,* 88**,** 526-535.

JONES, E., HENDRY, S., DEFELIPE, J. & BENSON, D. 1994. GABA neurons and their role in activity-dependent plasticity of adult primate visual cortex. *Primary Visual Cortex in Primates.* Springer.

KAJANDER, O. A., ROVIO, A. T., MAJAMAA, K., POULTON, J., SPELBRINK, J. N., HOLT, I. J., KARHUNEN, P. J. & JACOBS, H. T. 2000. Human mtDNA sublimons resemble rearranged mitochondrial genomes found in pathological states. *Human Molecular Genetics,* 9**,** 2821-2835.

KALIFA, L., BEUTNER, G., PHADNIS, N., SHEU, S.-S. & SIA, E. A. 2009. Evidence for a role of FEN1 in maintaining mitochondrial DNA integrity. *DNA repair,* 8**,** 1242-1249.

KANG, D., NISHIDA, J.-I., IYAMA, A., NAKABEPPU, Y., FURUICHI, M., FUJIWARA, T., SEKIGUCHI, M. & TAKESHIGE, K. 1995. Intracellular localization of 8-oxo-dGTPase in human cells, with special reference to the role of the enzyme in mitochondria. *Journal of Biological Chemistry,* 270**,** 14659-14665.

KANG, J.-S., TIAN, J.-H., PAN, P.-Y., ZALD, P., LI, C., DENG, C. & SHENG, Z.-H. 2008. Docking of axonal mitochondria by syntaphilin controls their mobility and affects short-term facilitation. *Cell,* 132**,** 137-148.

KARAHALIL, B., DE SOUZA-PINTO, N. C., PARSONS, J. L., ELDER, R. H. & BOHR, V. A. 2003. Compromised incision of oxidized pyrimidines in liver mitochondria of mice deficient in NTH1 and OGG1 glycosylases. *Journal of Biological Chemistry,* 278**,** 33701-33707.

KAROL, M. H. & SIMPSON, M. V. 1968. DNA biosynthesis by isolated mitochondria: A replicative rather than a repair process. *Science,* 162**,** 470-473.

KASAHARA, T., KUBOTA, M., MIYAUCHI, T., NODA, Y., MOURI, A., NABESHIMA, T. & KATO, T. 2006. Mice with neuron-specific accumulation of mitochondrial DNA mutations show mood disorder-like phenotypes. *Molecular psychiatry,* 11**,** 577.

KASAMATSU, H. & VINOGRAD, J. 1973. Unidirectionality of replication in mouse mitochondrial DNA. *Nature,* 241**,** 103-105.

KASTNER, A., HIRSCH, E., LEJEUNE, O., JAVOY-AGID, F., RASCOL, O. & AGID, Y. 1992. Is the vulnerability of neurons in the substantia nigra of patients with Parkinson's disease related to their neuromelanin content? *Journal of neurochemistry,* 59**,** 1080-1089.

KAUFMAN, B. A., DURISIC, N., MATIVETSKY, J. M., COSTANTINO, S., HANCOCK, M. A., GRUTTER, P. & SHOUBRIDGE, E. A. 2007. The mitochondrial transcription factor TFAM coordinates the assembly of multiple DNA molecules into nucleoid-like structures. *Molecular biology of the cell,* 18**,** 3225-3236.

KEE, N., SIVALINGAM, S., BOONSTRA, R. & WOJTOWICZ, J. 2002. The utility of Ki-67 and BrdU as proliferative markers of adult neurogenesis. *Journal of neuroscience methods,* 115**,** 97-105.

KETTWIG, M., SCHUBACH, M., ZIMMERMANN, F. A., KLINGE, L., MAYR, J. A., BISKUP, S., SPERL, W., GÄRTNER, J. & HUPPKE, P. 2015. From ventriculomegaly to severe muscular atrophy: expansion of the clinical spectrum related to mutations in AIFM1. *Mitochondrion,* 21**,** 12-18.

KHAIDAKOV, M., HEFLICH, R. H., MANJANATHA, M. G., MYERS, M. B. & AIDOO, A. 2003. Accumulation of point mutations in mitochondrial DNA of aging mice. *Mutation Research/Fundamental and Molecular Mechanisms of Mutagenesis,* 526**,** 1-7.

KHAMBATTA, S., NGUYEN, D. L., BECKMAN, T. J. & WITTICH, C. M. 2014. Kearns–Sayre syndrome: a case series of 35 adults and children. *International journal of general medicine,* 7**,** 325.

KIECHL, S., HORVATH, R., LUOMA, P., KIECHL-KOHLENDORFER, U., WALLACHER-SCHOLZ, B., STUCKA, R., THALER, C., WANSCHITZ, J., SUOMALAINEN, A. & JAKSCH, M. 2004. Two families with autosomal dominant progressive external ophthalmoplegia. *Journal of Neurology, Neurosurgery & Psychiatry,* 75**,** 1125-1128.

KIM, I., RODRIGUEZ-ENRIQUEZ, S. & LEMASTERS, J. J. 2007. Selective degradation of mitochondria by mitophagy. *Archives of biochemistry and biophysics,* 462**,** 245-253.

KIM, J., XU, M., XO, R., MATES, A., WILSON, G., PEARSALL IV, A. & GRISHKO, V. 2010. Mitochondrial DNA damage is involved in apoptosis caused by pro-inflammatory cytokines in human OA chondrocytes. *Osteoarthritis and cartilage,* 18**,** 424-432.

KIRICHOK, Y., KRAPIVINSKY, G. & CLAPHAM, D. E. 2004. The mitochondrial calcium uniporter is a highly selective ion channel. *Nature,* 427**,** 360.

KLINE, E. R., BASSIT, L., HERNANDEZ-SANTIAGO, B. I., DETORIO, M. A., LIANG, B., KLEINHENZ, D. J., WALP, E. R., DIKALOV, S., JONES, D. P. & SCHINAZI, R. F. 2009. Long-term exposure to AZT, but not d4T, increases endothelial cell oxidative stress and mitochondrial dysfunction. *Cardiovascular toxicology,* 9**,** 1-12.

KOC, E. C. & SPREMULLI, L. L. 2002. Identification of mammalian mitochondrial translational initiation factor 3 and examination of its role in initiation complex formation with natural mRNAs. *Journal of Biological Chemistry,* 277**,** 35541-35549.

KOENIG, H. 1958. An autoradiographic study of nucleic acid and protein turnover in the mammalian neuraxis. *The Journal of Cell Biology,* 4**,** 785-792.

KOOPMAN, W. J., VISCH, H.-J., VERKAART, S., VAN DEN HEUVEL, L. W., SMEITINK, J. A. & WILLEMS, P. H. 2005. Mitochondrial network complexity and pathological decrease in complex I activity are tightly correlated in isolated human complex I deficiency. *American Journal of Physiology-Cell Physiology,* 289**,** C881-C890.

KORHONEN, J. A., GASPARI, M. & FALKENBERG, M. 2003. TWINKLE has 5'→ 3' DNA helicase activity and is specifically stimulated by mitochondrial single-stranded DNA-binding protein. *Journal of Biological Chemistry,* 278**,** 48627-48632.

KORHONEN, J. A., PHAM, X. H., PELLEGRINI, M. & FALKENBERG, M. 2004. Reconstitution of a minimal mtDNA replisome in vitro. *The EMBO journal,* 23**,** 2423-2429.

KORR, H., KURZ, C., SEIDLER, T., SOMMER, D. & SCHMITZ, C. 1998. Mitochondrial DNA synthesis studied autoradiographically in various cell types in vivo. *Brazilian journal of medical and biological research,* 31**,** 289-298.

KOSHIBA, T., DETMER, S. A., KAISER, J. T., CHEN, H., MCCAFFERY, J. M. & CHAN, D. C. 2004. Structural basis of mitochondrial tethering by mitofusin complexes. *Science,* 305**,** 858-862.

KRAYTSBERG, Y., KUDRYAVTSEVA, E., MCKEE, A. C., GEULA, C., KOWALL, N. W. & KHRAPKO, K. 2006a. Mitochondrial DNA deletions are abundant and cause functional impairment in aged human substantia nigra neurons. *Nature genetics,* 38**,** 518-520.

KRAYTSBERG, Y., KUDRYAVTSEVA, E., MCKEE, A. C., GEULA, C., KOWALL, N. W. & KHRAPKO, K. 2006b. Mitochondrial DNA deletions are abundant and cause functional impairment in aged human substantia nigra neurons. *Nature genetics,* 38**,** 518.

KREBS, H. & EGGLESTON, L. 1940a. Biological synthesis of oxaloacetic acid from pyruvic acid and carbon dioxide. *Biochemical Journal,* 34**,** 1383.

KREBS, H. A. & EGGLESTON, L. V. 1940b. The oxidation of pyruvate in pigeon breast muscle. *Biochemical journal,* 34**,** 442.

KRISHNAN, K. J., RATNAIKE, T. E., DE GRUYTER, H. L., JAROS, E. & TURNBULL, D. M. 2012. Mitochondrial DNA deletions cause the biochemical defect observed in Alzheimer's disease. *Neurobiology of aging,* 33**,** 2210-2214.

KRISHNAN, K. J., REEVE, A. K., SAMUELS, D. C., CHINNERY, P. F., BLACKWOOD, J. K., TAYLOR, R. W., WANROOIJ, S., SPELBRINK, J. N., LIGHTOWLERS, R. N. & TURNBULL, D. M. 2008. What causes mitochondrial DNA deletions in human cells? *Nature genetics,* 40**,** 275-279.

KUHN, H. G., DICKINSON-ANSON, H. & GAGE, F. H. 1996. Neurogenesis in the dentate gyrus of the adult rat: age-related decrease of neuronal progenitor proliferation. *Journal of Neuroscience,* 16**,** 2027-2033.

KUJOTH, G., HIONA, A., PUGH, T., SOMEYA, S., PANZER, K., WOHLGEMUTH, S., HOFER, T., SEO, A., SULLIVAN, R. & JOBLING, W. J. S. 2005. Mitochondrial DNA mutations, oxidative stress, and apoptosis in mammalian aging. 309**,** 481-484.

KUKAT, C., WURM, C. A., SPÅHR, H., FALKENBERG, M., LARSSON, N.-G. & JAKOBS, S. 2011. Super-resolution microscopy reveals that mammalian mitochondrial nucleoids have a uniform size and frequently contain a single copy of mtDNA. *Proceedings of the National Academy of Sciences,* 108**,** 13534-13539.

KUNKEL, T. A. & LOEB, L. A. 1981. Fidelity of mammalian DNA polymerases. *Science,* 213**,** 765-767.

LADNER, R. D. & CARADONNA, S. J. 1997. The human dutpase gene encodes both nuclear and mitochondrial isoforms differential expression of the isoforms and characterization of a cdna encoding the mitochondrial species. *Journal of Biological Chemistry,* 272**,** 19072-19080.

LAKSHMIPATHY, U. & CAMPBELL, C. 1999. The human DNA ligase III gene encodes nuclear and mitochondrial proteins. *Molecular and cellular biology,* 19**,** 3869-3876.

LAUQUIN, G. J.-M., BRANDOLIN, G., BOULAY, F., BLOCK, M. R. & VIGNAIS, P. V. 2017. Molecular Aspects Of Structure-Function Relationships In Mitochondrial Adenine Nucleotide Carrier. *Structure and Properties of Cell Membrane Structure and Properties of Cell Membranes.* CRC Press.

LAX, N. Z., WHITTAKER, R. G., HEPPLEWHITE, P. D., REEVE, A. K., BLAKELY, E. L., JAROS, E., INCE, P. G., TAYLOR, R. W., FAWCETT, P. R. W. & TURNBULL, D. M. 2012. Sensory neuronopathy in patients harbouring recessive polymerase γ mutations. *Brain,* 135**,** 62-71.

LEE, H.-C., PANG, C.-Y., HSU, H.-S. & WEI, Y.-H. 1994. Differential accumulations of 4,977 bp deletion in mitochondrial DNA of various tissues in human ageing. *Biochimica et Biophysica Acta (BBA)-Molecular Basis of Disease,* 1226**,** 37-43.

LEGROS, F., MALKA, F., FRACHON, P., LOMBÈS, A. & ROJO, M. 2004. Organization and dynamics of human mitochondrial DNA. *Journal of cell science,* 117**,** 2653-2662.

LEIGH-BROWN, S., ENRIQUEZ, J. A. & ODOM, D. T. 2010. Nuclear transcription factors in mammalian mitochondria. *Genome biology,* 11**,** 215.

LENTZ, S. I., EDWARDS, J. L., BACKUS, C., MCLEAN, L. L., HAINES, K. M. & FELDMAN, E. L. 2010. Mitochondrial DNA (mtDNA) biogenesis: visualization and duel incorporation of BrdU and EdU into newly synthesized mtDNA in vitro. *Journal of Histochemistry & Cytochemistry,* 58**,** 207-218.

LEONE, T. C., LEHMAN, J. J., FINCK, B. N., SCHAEFFER, P. J., WENDE, A. R., BOUDINA, S., COURTOIS, M., WOZNIAK, D. F., SAMBANDAM, N. & BERNAL-MIZRACHI, C. 2005. PGC-1α deficiency causes multi-system energy metabolic derangements: muscle dysfunction, abnormal weight control and hepatic steatosis. *PLoS biology,* 3**,** e101.

LEVKOFF, L. H., MARSHALL II, G. P., ROSS, H. H., CALDEIRA, M., REYNOLDS, B. A., CAKIROGLU, M., MARIANI, C. L., STREIT, W. J. & LAYWELL, E. D. 2008. Bromodeoxyuridine inhibits cancer cell proliferation in vitro and in vivo. *Neoplasia,* 10**,** 804-IN13.

LIANG, F.-Q. & GODLEY, B. F. 2003. Oxidative stress-induced mitochondrial DNA damage in human retinal pigment epithelial cells: a possible mechanism for RPE aging and age-related macular degeneration. *Experimental eye research,* 76**,** 397-403.

LIBOSKA, R., LIGASOVÁ, A., STRUNIN, D., ROSENBERG, I. & KOBERNA, K. 2012. Most anti-BrdU antibodies react with 2'-deoxy-5-ethynyluridine—the method for the effective suppression of this cross-reactivity. *PloS one,* 7**,** e51679.

LIGHTOWLERS, R. N., CHINNERY, P. F., TURNBULL, D. M. & HOWELL, N. 1997. Mammalian mitochondrial genetics: heredity, heteroplasmy and disease. *Trends in Genetics,* 13**,** 450-455.

LIGON, L. A. & STEWARD, O. 2000. Role of microtubules and actin filaments in the movement of mitochondria in the axons and dendrites of cultured hippocampal neurons. *Journal of Comparative Neurology,* 427**,** 351-361.

LILL, R., HOFFMANN, B., MOLIK, S., PIERIK, A. J., RIETZSCHEL, N., STEHLING, O., UZARSKA, M. A., WEBERT, H., WILBRECHT, C. & MÜHLENHOFF, U. 2012. The role of mitochondria in cellular iron–sulfur protein biogenesis and iron metabolism. *Biochimica et Biophysica Acta (BBA)-Molecular Cell Research,* 1823**,** 1491-1508.

LINNANE, A., OZAWA, T., MARZUKI, S. & TANAKA, M. 1989. Mitochondrial DNA mutations as an important contributor to ageing and degenerative diseases. *The Lancet,* 333**,** 642-645.

LISMAN, J., YASUDA, R. & RAGHAVACHARI, S. 2012. Mechanisms of CaMKII action in long-term potentiation. *Nature reviews neuroscience,* 13**,** 169.

LIU, P., QIAN, L., SUNG, J.-S., DE SOUZA-PINTO, N. C., ZHENG, L., BOGENHAGEN, D. F., BOHR, V. A., WILSON, D. M., SHEN, B. & DEMPLE, B. 2008. Removal of oxidative DNA damage via FEN1-dependent long-patch base excision repair in human cell mitochondria. *Molecular and cellular biology,* 28**,** 4975-4987.

LONGLEY, M. J., GRAZIEWICZ, M. A., BIENSTOCK, R. J. & COPELAND, W. C. J. G. 2005. Consequences of mutations in human DNA polymerase γ. 354**,** 125-131.

LOSÓN, O. C., SONG, Z., CHEN, H. & CHAN, D. C. 2013. Fis1, Mff, MiD49, and MiD51 mediate Drp1 recruitment in mitochondrial fission. *Molecular biology of the cell,* 24**,** 659-667.

LU, B., YADAV, S., SHAH, P. G., LIU, T., TIAN, B., PUKSZTA, S., VILLALUNA, N., KUTEJOVÁ, E., NEWLON, C. S. & SANTOS, J. H. 2007. Roles for the human ATP-dependent Lon protease in mitochondrial DNA maintenance. *Journal of Biological Chemistry,* 282**,** 17363-17374.

LUARTE, A., CORNEJO, V. H., BERTIN, F., GALLARDO, J. & COUVE, A. 2018. The axonal endoplasmic reticulum: One organelle—many functions in development, maintenance, and plasticity. *Developmental neurobiology,* 78**,** 181-208.

LUOMA, P., MELBERG, A., RINNE, J. O., KAUKONEN, J. A., NUPPONEN, N. N., CHALMERS, R. M., OLDFORS, A., RAUTAKORPI, I., PELTONEN, L. & MAJAMAA, K. 2004. Parkinsonism, premature menopause, and mitochondrial DNA polymerase γ mutations: clinical and molecular genetic study. *The Lancet,* 364**,** 875-882.

LYRAS, L., CAIRNS, N. J., JENNER, A., JENNER, P. & HALLIWELL, B. 1997. An assessment of oxidative damage to proteins, lipids, and DNA in brain from patients with Alzheimer's disease. *Journal of neurochemistry,* 68**,** 2061-2069.

MA, W., RESNICK, M. A. & GORDENIN, D. A. 2008. Apn1 and Apn2 endonucleases prevent accumulation of repair-associated DNA breaks in budding yeast as revealed by direct chromosomal analysis. *Nucleic acids research,* 36**,** 1836-1846.

MACAO, B., UHLER, J. P., SIIBAK, T., ZHU, X., SHI, Y., SHENG, W., OLSSON, M., STEWART, J. B., GUSTAFSSON, C. M. & FALKENBERG, M. 2015. The exonuclease activity of DNA polymerase γ is required for ligation during mitochondrial DNA replication. *Nature communications,* 6**,** 7303.

MAGNUSSON, J., ORTH, M., LESTIENNE, P. & TAANMAN, J.-W. 2003. Replication of mitochondrial DNA occurs throughout the mitochondria of cultured human cells. *Experimental cell research,* 289**,** 133-142.

MALKA, F., GUILLERY, O., CIFUENTES-DIAZ, C., GUILLOU, E., BELENGUER, P., LOMBÈS, A. & ROJO, M. 2005. Separate fusion of outer and inner mitochondrial membranes. *EMBO reports,* 6**,** 853-859.

MANCZAK, M., CALKINS, M. J. & REDDY, P. H. 2011. Impaired mitochondrial dynamics and abnormal interaction of amyloid beta with mitochondrial protein Drp1 in neurons from patients with Alzheimer's disease: implications for neuronal damage. *Human molecular genetics,* 20**,** 2495-2509.

MANCZAK, M., JUNG, Y., PARK, B. S., PARTOVI, D. & REDDY, P. H. 2005. Time-course of mitochondrial gene expressions in mice brains: implications for mitochondrial dysfunction, oxidative damage, and cytochrome c in aging. *Journal of neurochemistry,* 92**,** 494-504.

MANDAL, S. M., HEGDE, M. L., CHATTERJEE, A., HEGDE, P. M., SZCZESNY, B., BANERJEE, D., BOLDOGH, I., GAO, R., FALKENBERG, M. & GUSTAFSSON, C. M. 2012. Role of human DNA glycosylase Nei-like 2 (NEIL2) and single strand break repair protein polynucleotide kinase 3'-phosphatase in maintenance of mitochondrial genome. *Journal of Biological Chemistry,* 287**,** 2819-2829.

MANIURA-WEBER, K., GOFFART, S., GARSTKA, H. L., MONTOYA, J. & WIESNER, R. J. 2004. Transient overexpression of mitochondrial transcription factor A (TFAM) is sufficient to stimulate mitochondrial DNA transcription, but not sufficient to increase mtDNA copy number in cultured cells. *Nucleic acids research,* 32**,** 6015-6027.

MANN, D. M. & YATES, P. O. 1983. Possible role of neuromelanin in the pathogenesis of Parkinson's disease. *Mechanisms of ageing and development,* 21**,** 193-203.

MANNELLA, C. A., MARKO, M. & BUTTLE, K. 1997. Reconsidering mitochondrial structure: new views of an old organelle. *Trends in biochemical sciences,* 22**,** 37-38.

MANNELLA, C. A., MARKO, M., PENCZEK, P., BARNARD, D. & FRANK, J. 1994. The internal compartmentation of rat-liver mitochondria: Tomographic study using the high-voltage transmission electron microscope. *Microscopy research and technique,* 27**,** 278-283.

MARCHINGTON, D., MACAULAY, V., HARTSHORNE, G., BARLOW, D. & POULTON, J. 1998. Evidence from human oocytes for a genetic bottleneck in an mtDNA disease. *The American Journal of Human Genetics,* 63**,** 769-775.

MARGOLIS, E. B., LOCK, H., HJELMSTAD, G. O. & FIELDS, H. L. 2006. The ventral tegmental area revisited: is there an electrophysiological marker for dopaminergic neurons? *The Journal of physiology,* 577**,** 907-924.

MARGULIS, L. 1971. Symbiosis and evolution. *Scientific American,* 225**,** 48-61.

MARTIN, W., HOFFMEISTER, M., ROTTE, C. & HENZE, K. 2001. An overview of endosymbiotic models for the origins of eukaryotes, their ATP-producing organelles (mitochondria and hydrogenosomes), and their heterotrophic lifestyle. *Biological chemistry,* 382**,** 1521-1539.

MARTIN, W. & MÜLLER, M. 1998. The hydrogen hypothesis for the first eukaryote. *Nature,* 392**,** 37.

MARTIN, W. F., GARG, S. & ZIMORSKI, V. 2015. Endosymbiotic theories for eukaryote origin. *Phil. Trans. R. Soc. B,* 370**,** 20140330.

MASON, P. A., MATHESON, E. C., HALL, A. G. & LIGHTOWLERS, R. N. 2003. Mismatch repair activity in mammalian mitochondria. *Nucleic acids research,* 31**,** 1052-1058.

MATSUDA, W., FURUTA, T., NAKAMURA, K. C., HIOKI, H., FUJIYAMA, F., ARAI, R. & KANEKO, T. 2009. Single nigrostriatal dopaminergic neurons form widely spread and highly dense axonal arborizations in the neostriatum. *Journal of Neuroscience,* 29**,** 444-453.

MATTSON, M. P. & CHAN, S. L. 2003. Neuronal and glial calcium signaling in Alzheimer's disease. *Cell calcium,* 34**,** 385-397.

MAWRIN, C., KIRCHES, E., KRAUSE, G., SCHNEIDER-STOCK, R., BOGERTS, B., VORWERK, C. K. & DIETZMANN, K. 2004. Region-specific analysis of mitochondrial DNA deletions in neurodegenerative disorders in humans. *Neuroscience letters,* 357**,** 111-114.

MCCOMMIS, K. S. & FINCK, B. N. J. B. J. 2015. Mitochondrial pyruvate transport: a historical perspective and future research directions. 466**,** 443-454.

MCEWEN, B. F. & MARKO, M. 2001. The emergence of electron tomography as an important tool for investigating cellular ultrastructure. *Journal of Histochemistry & Cytochemistry,* 49**,** 553-563.

MCWILLIAMS, T. G., PRESCOTT, A. R., ALLEN, G. F., TAMJAR, J., MUNSON, M. J., THOMSON, C., MUQIT, M. M. & GANLEY, I. G. 2016. mito-QC illuminates mitophagy and mitochondrial architecture in vivo. *J Cell Biol,* 214**,** 333-345.

MECOCCI, P., MACGARVEY, U., KAUFMAN, A. E., KOONTZ, D., SHOFFNER, J. M., WALLACE, D. C. & BEAL, M. F. 1993. Oxidative damage to mitochondrial DNA shows marked age-dependent increases in human brain. *Annals of Neurology: Official Journal of the American Neurological Association and the Child Neurology Society,* 34**,** 609-616.

MEEUSEN, S., DEVAY, R., BLOCK, J., CASSIDY-STONE, A., WAYSON, S., MCCAFFERY, J. M. & NUNNARI, J. 2006. Mitochondrial inner-membrane fusion and crista maintenance requires the dynamin-related GTPase Mgm1. *Cell,* 127**,** 383-395.

MEEUSEN, S., MCCAFFERY, J. M. & NUNNARI, J. 2004. Mitochondrial fusion intermediates revealed in vitro. *Science,* 305**,** 1747-1752.

MEHTA, A. R., FOX, S. H., TARNOPOLSKY, M. & YOON, G. 2011. Mitochondrial mimicry of multiple system atrophy of the cerebellar subtype. *Movement Disorders,* 26**,** 753-755.

MEISSNER, C., BRUSE, P., MOHAMED, S. A., SCHULZ, A., WARNK, H., STORM, T. & OEHMICHEN, M. 2008. The 4977 bp deletion of mitochondrial DNA in human skeletal muscle, heart and different areas of the brain: a useful biomarker or more? *Experimental gerontology,* 43**,** 645-652.

MEISSNER, C., BRUSE, P. & OEHMICHEN, M. 2006. Tissue-specific deletion patterns of the mitochondrial genome with advancing age. *Experimental gerontology,* 41**,** 518-524.

MICHIKAWA, Y., MAZZUCCHELLI, F., BRESOLIN, N., SCARLATO, G. & ATTARDI, G. 1999. Aging-dependent large accumulation of point mutations in the human mtDNA control region for replication. *Science,* 286**,** 774-779.

MILLER, F. J., ROSENFELDT, F. L., ZHANG, C., LINNANE, A. W. & NAGLEY, P. 2003. Precise determination of mitochondrial DNA copy number in human skeletal and cardiac muscle by a PCR-based assay: lack of change of copy number with age. *Nucleic acids research,* 31**,** e61-e61.

MILLER, W. L. 2013. Steroid hormone synthesis in mitochondria. *Molecular and cellular endocrinology,* 379**,** 62-73.

MIMAKI, M., WANG, X., MCKENZIE, M., THORBURN, D. R. & RYAN, M. T. 2012. Understanding mitochondrial complex I assembly in health and disease. *Biochimica et Biophysica Acta (BBA)-Bioenergetics,* 1817**,** 851-862.

MINIS, A., DAHARY, D., MANOR, O., LESHKOWITZ, D., PILPEL, Y. & YARON, A. 2014. Subcellular transcriptomics—Dissection of the mRNA composition in the axonal compartment of sensory neurons. *Developmental neurobiology,* 74**,** 365-381.

MONTOYA, J., GAINES, G. L. & ATTARDI, G. 1983. The pattern of transcription of the human mitochondrial rRNA genes reveals two overlapping transcription units. *Cell,* 34**,** 151-159.

MORAES, C. T., ANDREETTA, F., BONILLA, E., SHANSKE, S., DIMAURO, S. & SCHON, E. A. 1991. Replication-competent human mitochondrial DNA lacking the heavy-strand promoter region. *Molecular and cellular biology,* 11**,** 1631-1637.

MORAES, C. T., KENYON, L. & HAO, H. 1999. Mechanisms of human mitochondrial DNA maintenance: the determining role of primary sequence and length over function. *Molecular biology of the cell,* 10**,** 3345-3356.

MORAWSKI, M., KIRILINA, E., SCHERF, N., JÄGER, C., REIMANN, K., TRAMPEL, R., GAVRIILIDIS, F., GEYER, S., BIEDERMANN, B. & ARENDT, T. J. N. 2018. Developing 3D microscopy with CLARITY on human brain tissue: Towards a tool for informing and validating MRI-based histology. 182**,** 417-428.

MOROZOV, Y. M., DATTA, D., PASPALAS, C. D. & ARNSTEN, A. F. 2017. Ultrastructural evidence for impaired mitochondrial fission in the aged rhesus monkey dorsolateral prefrontal cortex. *Neurobiology of aging,* 51**,** 9-18.

MORTIBOYS, H., THOMAS, K. J., KOOPMAN, W. J., KLAFFKE, S., ABOU-SLEIMAN, P., OLPIN, S., WOOD, N. W., WILLEMS, P. H., SMEITINK, J. A. & COOKSON, M. R. 2008. Mitochondrial function and morphology are impaired in parkin-mutant fibroblasts. *Annals of Neurology: Official Journal of the American Neurological Association and the Child Neurology Society,* 64**,** 555-565.

MOZDY, A., MCCAFFERY, J. & SHAW, J. 2000. Dnm1p GTPase-mediated mitochondrial fission is a multi-step process requiring the novel integral membrane component Fis1p. *The Journal of cell biology,* 151**,** 367-380.

MUFTUOGLU, M., MORI, M. P. & DE SOUZA-PINTO, N. C. 2014. Formation and repair of oxidative damage in the mitochondrial DNA. *Mitochondrion,* 17**,** 164-181.

NAÏMI, M., BANNWARTH, S., PROCACCIO, V., POUGET, J., DESNUELLE, C., PELLISSIER, J.-F., RÖTIG, A., MUNNICH, A., CALVAS, P. & RICHELME, C. J. E. J. O. H. G. 2006. Molecular analysis of ANT1, TWINKLE and POLG in patients with multiple deletions or depletion of mitochondrial DNA by a dHPLC-based assay. 14**,** 917.

NAKABEPPU, Y. 2001. Molecular genetics and structural biology of human MutT homolog, MTH1. *Mutation Research/Fundamental and Molecular Mechanisms of Mutagenesis,* 477**,** 59-70.

NAKAMURA, K., NEMANI, V. M., AZARBAL, F., SKIBINSKI, G., LEVY, J. M., EGAMI, K., MUNISHKINA, L., ZHANG, J., GARDNER, B. & WAKABAYASHI, J. 2011. Direct membrane association drives mitochondrial fission by the Parkinson disease-associated protein α-synuclein. *Journal of Biological Chemistry***,** jbc. M110. 213538.

NAKAMURA, Y. & ARAKAWA, H. 2017. Discovery of Mieap-regulated mitochondrial quality control as a new function of tumor suppressor p53. *Cancer science,* 108**,** 809-817.

NARENDRA, D., TANAKA, A., SUEN, D.-F. & YOULE, R. J. 2008. Parkin is recruited selectively to impaired mitochondria and promotes their autophagy. *The Journal of cell biology,* 183**,** 795-803.

NARENDRA, D. P., JIN, S. M., TANAKA, A., SUEN, D.-F., GAUTIER, C. A., SHEN, J., COOKSON, M. R. & YOULE, R. J. 2010. PINK1 is selectively stabilized on impaired mitochondria to activate Parkin. *PLoS biology,* 8**,** e1000298.

NASS, M. M. 1969. Mitochondrial DNA: II. Structure and physicochemical properties of isolated DNA. *Journal of molecular biology,* 42**,** 529-545.

NAVIAUX, R. K. & NGUYEN, K. V. 2004. POLG mutations associated with Alpers' syndrome and mitochondrial DNA depletion. *Annals of neurology,* 55**,** 706-712.

NGO, H. B., KAISER, J. T. & CHAN, D. C. 2011a. The mitochondrial transcription and packaging factor Tfam imposes a U-turn on mitochondrial DNA. *Nature structural & molecular biology,* 18**,** 1290.

NGO, H. B., KAISER, J. T. & CHAN, D. C. 2011b. The mitochondrial transcription and packaging factor Tfam imposes a U-turn on mitochondrial DNA. *Nature structural & molecular biology,* 18**,** 1290-1296.

NGO, H. B., KAISER, J. T. & CHAN, D. C. 2011c. Tfam, a mitochondrial transcription and packaging factor, imposes a U-turn on mitochondrial DNA. *Nature structural & molecular biology,* 18**,** 1290-1296.

NGO, H. B., LOVELY, G. A., PHILLIPS, R. & CHAN, D. C. 2014. Distinct structural features of TFAM drive mitochondrial DNA packaging versus transcriptional activation. *Nature communications,* 5**,** 3077.

NGUYEN, L. H., ERZBERGER, J. P., ROOT, J. & WILSON, D. M. 2000. The human homolog of Escherichia coli Orn degrades small single-stranded RNA and DNA oligomers. *Journal of Biological Chemistry,* 275**,** 25900-25906.

NILSEN, H., OTTERLEI, M., HAUG, T., SOLUM, K., NAGELHUS, T. A., SKORPEN, F. & KROKAN, H. E. 1997. Nuclear and mitochondrial uracil-DNA glycosylases are generated by alternative splicing and transcription from different positions in the UNG gene. *Nucleic acids research,* 25**,** 750-755.

NISHIOKA, K., OHTSUBO, T., ODA, H., FUJIWARA, T., KANG, D., SUGIMACHI, K. & NAKABEPPU, Y. J. M. B. O. T. C. 1999. Expression and differential intracellular localization of two major forms of human 8-oxoguanine DNA glycosylase encoded by alternatively spliced OGG1 mRNAs. 10, 1637-1652.

NISSANKA, N., BACMAN, S. R., PLASTINI, M. J. & MORAES, C. T. 2018. The mitochondrial DNA polymerase gamma degrades linear DNA fragments precluding the formation of deletions. *Nature communications,* 9, 2491.

NUNNARI, J. & SUOMALAINEN, A. 2012. Mitochondria: in sickness and in health. *Cell,* 148, 1145-1159.

OHTSUBO, T., NISHIOKA, K., IMAISO, Y., IWAI, S., SHIMOKAWA, H., ODA, H., FUJIWARA, T. & NAKABEPPU, Y. 2000. Identification of human MutY homolog (hMYH) as a repair enzyme for 2-hydroxyadenine in DNA and detection of multiple forms of hMYH located in nuclei and mitochondria. *Nucleic acids research,* 28, 1355-1364.

OLICHON, A., BARICAULT, L., GAS, N., GUILLOU, E., VALETTE, A., BELENGUER, P. & LENAERS, G. 2003. Loss of OPA1 perturbates the mitochondrial inner membrane structure and integrity, leading to cytochrome c release and apoptosis. *Journal of Biological Chemistry,* 278, 7743-7746.

ORRENIUS, S., ZHIVOTOVSKY, B. & NICOTERA, P. 2003. Calcium: Regulation of cell death: the calcium–apoptosis link. *Nature reviews Molecular cell biology,* 4, 552.

OSELLAME, L. D., RAHIM, A. A., HARGREAVES, I. P., GEGG, M. E., RICHARD-LONDT, A., BRANDNER, S., WADDINGTON, S. N., SCHAPIRA, A. H. & DUCHEN, M. R. 2013. Mitochondria and quality control defects in a mouse model of Gaucher disease—links to Parkinson's disease. *Cell metabolism,* 17, 941-953.

OTERA, H., WANG, C., CLELAND, M. M., SETOGUCHI, K., YOKOTA, S., YOULE, R. J. & MIHARA, K. 2010. Mff is an essential factor for mitochondrial recruitment of Drp1 during mitochondrial fission in mammalian cells. *The Journal of cell biology,* 191, 1141-1158.

PACELLI, C., GIGUÈRE, N., BOURQUE, M.-J., LÉVESQUE, M., SLACK, R. S. & TRUDEAU, L.-É. 2015. Elevated mitochondrial bioenergetics and axonal arborization size are key contributors to the vulnerability of dopamine neurons. *Current Biology,* 25, 2349-2360.

PALADE, G. E. 1953. An electron microscope study of the mitochondrial structure. *Journal of Histochemistry & Cytochemistry,* 1, 188-211.

PARK, J., LEE, S. B., LEE, S., KIM, Y., SONG, S., KIM, S., BAE, E., KIM, J., SHONG, M. & KIM, J.-M. 2006. Mitochondrial dysfunction in Drosophila PINK1 mutants is complemented by parkin. *Nature,* 441, 1157.

PARK, S. J., SCHERTEL, A., LEE, K. E. & HAN, S. S. 2013. Ultra-structural analysis of the brain in a Drosophila model of Alzheimer's disease using FIB/SEM microscopy. *Microscopy,* 63, 3-13.

PARSONS, P. & SIMPSON, M. V. 1967. Biosynthesis of DNA by isolated mitochondria: incorporation of thymidine triphosphate-2-C14. *Science,* 155, 91-93.

PATHAK, D., SEPP, K. J. & HOLLENBECK, P. J. 2010. Evidence that myosin activity opposes microtubule-based axonal transport of mitochondria. *Journal of Neuroscience,* 30, 8984-8992.

PEDDIE, C. J. & COLLINSON, L. M. 2014. Exploring the third dimension: volume electron microscopy comes of age. *Micron,* 61**,** 9-19.

PEEVA, V., BLEI, D., TROMBLY, G., CORSI, S., SZUKSZTO, M. J., REBELO-GUIOMAR, P., GAMMAGE, P. A., KUDIN, A. P., BECKER, C. & ALTMÜLLER, J. 2018. Linear mitochondrial DNA is rapidly degraded by components of the replication machinery. *Nature communications,* 9.

PENG, T.-I., YU, P.-R., CHEN, J.-Y., WANG, H.-L., WU, H.-Y., WEI, Y.-H. & JOU, M.-J. 2006. Visualizing common deletion of mitochondrial DNA-augmented mitochondrial reactive oxygen species generation and apoptosis upon oxidative stress. *Biochimica et Biophysica Acta (BBA)-Molecular Basis of Disease,* 1762**,** 241-255.

PERIER, C., BENDER, A., GARCÍA-ARUMÍ, E., MELIA, M. J., BOVE, J., LAUB, C., KLOPSTOCK, T., ELSTNER, M., MOUNSEY, R. B. & TEISMANN, P. 2013. Accumulation of mitochondrial DNA deletions within dopaminergic neurons triggers neuroprotective mechanisms. *Brain,* 136**,** 2369-2378.

PERSSON, Ö., MUTHUKUMAR, Y., BASU, S., JENNINGER, L., UHLER, J. P., BERGLUND, A.-K., MCFARLAND, R., TAYLOR, R. W., GUSTAFSSON, C. M. & LARSSON, E. J. N. C. 2019. Copy-choice recombination during mitochondrial L-strand synthesis causes DNA deletions. 10**,** 759.

PESCE, V., CORMIO, A., FRACASSO, F., VECCHIET, J., FELZANI, G., LEZZA, A. M., CANTATORE, P. & GADALETA, M. N. 2001. Age-related mitochondrial genotypic and phenotypic alterations in human skeletal muscle. *Free Radical Biology and Medicine,* 30**,** 1223-1233.

PFAFF, E., HELDT, H. & KLINGENBERG, M. 1969. Adenine nucleotide translocation of mitochondria. *European journal of biochemistry,* 10**,** 484-493.

PFEIFER, C., SHOMORONY, A., ARONOVA, M., ZHANG, G., CAI, T., XU, H., NOTKINS, A. & LEAPMAN, R. 2015. Quantitative analysis of mouse pancreatic islet architecture by serial block-face SEM. *Journal of structural biology,* 189**,** 44-52.

PFEIFFER, K., GOHIL, V., STUART, R. A., HUNTE, C., BRANDT, U., GREENBERG, M. L. & SCHÄGGER, H. 2003. Cardiolipin stabilizes respiratory chain supercomplexes. *Journal of biological chemistry,* 278**,** 52873-52880.

PHILLIPS, A. F., MILLET, A. R., TIGANO, M., DUBOIS, S. M., CRIMMINS, H., BABIN, L., CHARPENTIER, M., PIGANEAU, M., BRUNET, E. & SFEIR, A. 2017. Single-molecule analysis of mtDNA replication uncovers the basis of the common deletion. *Molecular cell,* 65**,** 527-538. e6.

PHILLIPS, J., LAUDE, A., LIGHTOWLERS, R., MORRIS, C. M., TURNBULL, D. M. & LAX, N. Z. 2016. Development of passive CLARITY and immunofluorescent labelling of multiple proteins in human cerebellum: understanding mechanisms of neurodegeneration in mitochondrial disease. *Scientific reports,* 6**,** 26013.

PHILLIPS, N. R., SIMPKINS, J. W. & ROBY, R. K. 2014. Mitochondrial DNA deletions in Alzheimer's brains: a review. *Alzheimer's & Dementia,* 10**,** 393-400.

PICKRELL, A. M., FUKUI, H., WANG, X., PINTO, M. & MORAES, C. T. 2011. The striatum is highly susceptible to mitochondrial oxidative phosphorylation dysfunctions. *Journal of neuroscience,* 31**,** 9895-9904.

PILLING, A. D., HORIUCHI, D., LIVELY, C. M. & SAXTON, W. M. 2006. Kinesin-1 and Dynein are the primary motors for fast transport of mitochondria in Drosophila motor axons. *Molecular biology of the cell,* 17**,** 2057-2068.

PILZER, D. & FISHELSON, Z. 2005. Mortalin/GRP75 promotes release of membrane vesicles from immune attacked cells and protection from complement-mediated lysis. *International immunology,* 17**,** 1239-1248.

PONAMAREV, M. V., LONGLEY, M. J., NGUYEN, D., KUNKEL, T. A. & COPELAND, W. C. 2002. Active site mutation in DNA polymerase γ associated with progressive external ophthalmoplegia causes error-prone DNA synthesis. *Journal of Biological Chemistry,* 277**,** 15225-15228.

POOVATHINGAL, S. K., GRUBER, J., LAKSHMANAN, L., HALLIWELL, B. & GUNAWAN, R. 2012. Is mitochondrial DNA turnover slower than commonly assumed? *Biogerontology,* 13**,** 557-564.

POPOV, V., MEDVEDEV, N. I., DAVIES, H. A. & STEWART, M. G. 2005. Mitochondria form a filamentous reticular network in hippocampal dendrites but are present as discrete bodies in axons: A three-dimensional ultrastructural study. *Journal of Comparative Neurology,* 492**,** 50-65.

PRADOS, M. D., SEIFERHELD, W., SANDLER, H. M., BUCKNER, J. C., PHILLIPS, T., SCHULTZ, C., URTASUN, R., DAVIS, R., GUTIN, P. & CASCINO, T. L. 2004. Phase III randomized study of radiotherapy plus procarbazine, lomustine, and vincristine with or without BUdR for treatment of anaplastic astrocytoma: final report of RTOG 9404. *International Journal of Radiation Oncology* Biology* Physics,* 58**,** 1147-1152.

PRESTON, C. C., OBERLIN, A. S., HOLMUHAMEDOV, E. L., GUPTA, A., SAGAR, S., SYED, R. H. K., SIDDIQUI, S. A., RAGHAVAKAIMAL, S., TERZIC, A. & JAHANGIR, A. 2008. Aging-induced alterations in gene transcripts and functional activity of mitochondrial oxidative phosphorylation complexes in the heart. *Mechanisms of ageing and development,* 129**,** 304-312.

PSARRA, A.-M. G. & SEKERIS, C. E. 2008. Nuclear receptors and other nuclear transcription factors in mitochondria: regulatory molecules in a new environment. *Biochimica et Biophysica Acta (BBA)-Molecular Cell Research,* 1783**,** 1-11.

PUSCHMANN, A. 2013. Monogenic Parkinson's disease and parkinsonism: clinical phenotypes and frequencies of known mutations. *Parkinsonism & related disorders,* 19**,** 407-415.

PYLE, A., BRENNAN, R., KURZAWA-AKANBI, M., YARNALL, A., THOUIN, A., MOLLENHAUER, B., BURN, D., CHINNERY, P. F. & HUDSON, G. 2015. Reduced cerebrospinal fluid mitochondrial DNA is a biomarker for early-stage Parkinson's disease. *Annals of neurology,* 78**,** 1000-1004.

RAFELSKI, S. M. & MARSHALL, W. F. 2008. Building the cell: design principles of cellular architecture. *Nature Reviews Molecular Cell Biology,* 9**,** 593.

REEVE, A. K. 2007. *The molecular basis of neurodegeneration: the role of mitochondrial DNA mutations,* University of Newcastle upon Tyne.

REEVE, A. K., KRISHNAN, K. J., ELSON, J. L., MORRIS, C. M., BENDER, A., LIGHTOWLERS, R. N. & TURNBULL, D. M. 2008. Nature of mitochondrial DNA deletions in substantia nigra neurons. *The American Journal of Human Genetics,* 82**,** 228-235.

REYES, A., KAZAK, L., WOOD, S. R., YASUKAWA, T., JACOBS, H. T. & HOLT, I. J. 2013. Mitochondrial DNA replication proceeds via a 'bootlace'mechanism involving the incorporation of processed transcripts. *Nucleic acids research,* 41**,** 5837-5850.

RIZZUTO, R., BRINI, M., DE GIORGI, F., ROSSI, R., HEIM, R., TSIEN, R. Y. & POZZAN, T. 1996. Double labelling of subcellular structures with organelle-targeted GFP mutants in vivo. *Current Biology,* 6**,** 183-188.

ROBIN, E. D. & WONG, R. 1988. Mitochondrial DNA molecules and virtual number of mitochondria per cell in mammalian cells. *Journal of cellular physiology,* 136**,** 507-513.

ROCHA, M. C., GRADY, J. P., GRÜNEWALD, A., VINCENT, A., DOBSON, P. F., TAYLOR, R. W., TURNBULL, D. M. & RYGIEL, K. A. 2015. A novel immunofluorescent assay to investigate oxidative phosphorylation deficiency in mitochondrial myopathy: understanding mechanisms and improving diagnosis. *Scientific reports,* 5**,** 15037.

RODGER, C. E., MCWILLIAMS, T. G. & GANLEY, I. G. 2018. Mammalian mitophagy–from in vitro molecules to in vivo models. *The FEBS journal,* 285**,** 1185-1202.

RODRIGUEZ-ACEBES, S., MOURÓN, S. & MÉNDEZ, J. 2018. Uncoupling fork speed and origin activity to identify the primary cause of replicative stress phenotypes. *Journal of Biological Chemistry,* 293**,** 12855-12861.

RODRIGUEZ-MORENO, J., ROLLENHAGEN, A., ARLANDIS, J., SANTUY, A., MERCHAN-PÉREZ, A., DEFELIPE, J., LÜBKE, J. H. & CLASCA, F. 2017. Quantitative 3D ultrastructure of thalamocortical synapses from the "Lemniscal" ventral posteromedial nucleus in mouse barrel cortex. *Cerebral Cortex***,** 1-17.

ROGER, A. J. 1999. Reconstructing early events in eukaryotic evolution. *the american naturalist,* 154**,** S146-S163.

ROSSIGNOL, R., FAUSTIN, B., ROCHER, C., MALGAT, M., MAZAT, J.-P. & LETELLIER, T. 2003. Mitochondrial threshold effects. *Biochemical Journal,* 370**,** 751-762.

ROSSMANITH, W. & KARWAN, R. M. 1998. Characterization of human mitochondrial RNase P: novel aspects in tRNA processing. *Biochemical and biophysical research communications,* 247**,** 234-241.

ROUAULT, T. A. & TONG, W.-H. 2005. Iron–sulphur cluster biogenesis and mitochondrial iron homeostasis. *Nature Reviews Molecular Cell Biology,* 6**,** 345.

RUBIO-COSIALS, A., SYDOW, J. F., JIMÉNEZ-MENÉNDEZ, N., FERNÁNDEZ-MILLÁN, P., MONTOYA, J., JACOBS, H. T., COLL, M., BERNADÓ, P. & SOLÀ, M. 2011. Human mitochondrial transcription factor A induces a U-turn structure in the light strand promoter. *Nature structural & molecular biology,* 18**,** 1281.

RUHANEN, H., BORRIE, S., SZABADKAI, G., TYYNISMAA, H., JONES, A. W., KANG, D., TAANMAN, J.-W. & YASUKAWA, T. 2010. Mitochondrial single-stranded DNA binding protein is required for maintenance of mitochondrial DNA and 7S DNA but is not required for mitochondrial nucleoid organisation. *Biochimica et Biophysica Acta (BBA)-Molecular Cell Research,* 1803**,** 931-939.

RUSSELL, O. M., FRUH, I., RAI, P. K., MARCELLIN, D., DOLL, T., REEVE, A., GERMAIN, M., BASTIEN, J., RYGIEL, K. A. & CERINO, R. 2018. Preferential amplification of a human mitochondrial DNA deletion in vitro and in vivo. *Scientific reports,* 8**,** 1799.

RUSSO, G. J., LOUIE, K., WELLINGTON, A., MACLEOD, G. T., HU, F., PANCHUMARTHI, S. & ZINSMAIER, K. E. 2009. Drosophila Miro is required for both anterograde and retrograde axonal mitochondrial transport. *Journal of Neuroscience,* 29**,** 5443-5455.

RYGIEL, K. A., TUPPEN, H. A., GRADY, J. P., VINCENT, A., BLAKELY, E. L., REEVE, A. K., TAYLOR, R. W., PICARD, M., MILLER, J. & TURNBULL, D. M. 2016. Complex mitochondrial DNA rearrangements in individual cells from patients with sporadic inclusion body myositis. *Nucleic Acids Research***,** gkw382.

SAADA, A., SHAAG, A., MANDEL, H., NEVO, Y., ERIKSSON, S. & ELPELEG, O. J. N. G. 2001. Mutant mitochondrial thymidine kinase in mitochondrial DNA depletion myopathy. 29**,** 342.

SABHARWAL, S. S. & SCHUMACKER, P. T. 2014. Mitochondrial ROS in cancer: initiators, amplifiers or an Achilles' heel? *Nature Reviews Cancer,* 14**,** 709.

SAFIULINA, D., VEKSLER, V., ZHARKOVSKY, A. & KAASIK, A. 2006. Loss of mitochondrial membrane potential is associated with increase in mitochondrial volume: physiological role in neurones. *Journal of cellular physiology,* 206**,** 347-353.

SAGE, J. M., GILDEMEISTER, O. S. & KNIGHT, K. L. 2010. Discovery of a novel function for human Rad51 maintenance of the mitochondrial genome. *Journal of Biological Chemistry,* 285**,** 18984-18990.

SAMUELS, D. C., SCHON, E. A. & CHINNERY, P. F. 2004. Two direct repeats cause most human mtDNA deletions. *Trends in Genetics,* 20**,** 393-398.

SANDOVAL, H., THIAGARAJAN, P., DASGUPTA, S. K., SCHUMACHER, A., PRCHAL, J. T., CHEN, M. & WANG, J. 2008. Essential role for Nix in autophagic maturation of erythroid cells. *Nature,* 454**,** 232.

SANTEL, A., FRANK, S., GAUME, B., HERRLER, M., YOULE, R. J. & FULLER, M. T. 2003. Mitofusin-1 protein is a generally expressed mediator of mitochondrial fusion in mammalian cells. *Journal of cell science,* 116**,** 2763-2774.

SANTEL, A. & FULLER, M. T. 2001. Control of mitochondrial morphology by a human mitofusin. *Journal of cell science,* 114**,** 867-874.

SATOH, M. & KUROIWA, T. 1991. Organization of multiple nucleoids and DNA molecules in mitochondria of a human cell. *Experimental cell research,* 196**,** 137-140.

SAZANOV, L. A. 2007. Respiratory complex I: mechanistic and structural insights provided by the crystal structure of the hydrophilic domain. *Biochemistry,* 46**,** 2275-2288.

SCHÄGGER, H., BRANDT, U., GENCIC, S. & VON JAGOW, G. 1995. [7] Ubiquinol-cytochrome-c reductase from human and bovine mitochondria. *Methods in enzymology,* 260**,** 82-96.

SCHINDELIN, J., ARGANDA-CARRERAS, I., FRISE, E., KAYNIG, V., LONGAIR, M., PIETZSCH, T., PREIBISCH, S., RUEDEN, C., SAALFELD, S. & SCHMID, B. 2012. Fiji: an open-source platform for biological-image analysis. *Nature methods,* 9**,** 676.

SCHON, E. A., DIMAURO, S. & HIRANO, M. 2012. Human mitochondrial DNA: roles of inherited and somatic mutations. *Nature Reviews Genetics,* 13**,** 878.

SCHORL, C. & SEDIVY, J. M. 2007. Analysis of cell cycle phases and progression in cultured mammalian cells. *Methods,* 41**,** 143-150.

SCHULTZ, R. A., SWOAP, S. J., MCDANIEL, L. D., ZHANG, B., KOON, E. C., GARRY, D. J., LI, K. & WILLIAMS, R. S. 1998. Differential expression of mitochondrial DNA replication factors in mammalian tissues. *Journal of Biological Chemistry,* 273**,** 3447-3451.

SCHWARZ, T. L. 2013. Mitochondrial trafficking in neurons. *Cold Spring Harbor perspectives in biology,* 5**,** a011304.

SCHWARZER, C., BARNIKOL-WATANABE, S., THINNES, F. P. & HILSCHMANN, N. 2002. Voltage-dependent anion-selective channel (VDAC) interacts with the dynein light chain Tctex1 and the heat-shock protein PBP74. *The international journal of biochemistry & cell biology,* 34**,** 1059-1070.

SCRUGGS, E. R. & NAYLOR, A. J. D. 2008. Mechanisms of zidovudine-induced mitochondrial toxicity and myopathy. *Pharmacology,* 82**,** 83-88.

SEKERKOVÁ, G., ILIJIC, E. & MUGNAINI, E. 2004. Bromodeoxyuridine administered during neurogenesis of the projection neurons causes cerebellar defects in rat. *Journal of Comparative Neurology,* 470**,** 221-239.

SENA, L. A. & CHANDEL, N. S. 2012. Physiological roles of mitochondrial reactive oxygen species. *Molecular cell,* 48**,** 158-167.

SHAFIT-ZAGARDO, B. & KALCHEVA, N. 1998. Making sense of the multiple MAP-2 transcripts and their role in the neuron. *Molecular neurobiology,* 16**,** 149-162.

SHAN, Y. & CORTOPASSI, G. 2016. Mitochondrial Hspa9/Mortalin regulates erythroid differentiation via iron-sulfur cluster assembly. *Mitochondrion,* 26**,** 94-103.

SHANSKE, S., TANG, Y., HIRANO, M., NISHIGAKI, Y., TANJI, K., BONILLA, E., SUE, C., KRISHNA, S., CARLO, J. R. & WILLNER, J. J. T. A. J. O. H. G. 2002. Identical mitochondrial DNA deletion in a woman with ocular myopathy and in her son with Pearson syndrome. 71**,** 679-683.

SHAW, G. C., COPE, J. J., LI, L., CORSON, K., HERSEY, C., ACKERMANN, G. E., GWYNN, B., LAMBERT, A. J., WINGERT, R. A. & TRAVER, D. 2006. Mitoferrin is essential for erythroid iron assimilation. *Nature,* 440**,** 96.

SHENG, Z.-H. 2014. Mitochondrial trafficking and anchoring in neurons: new insight and implications. *J Cell Biol,* 204**,** 1087-1098.

SHENG, Z.-H. & CAI, Q. 2012. Mitochondrial transport in neurons: impact on synaptic homeostasis and neurodegeneration. *Nature Reviews Neuroscience,* 13**,** 77.

SHI, Y., DIERCKX, A., WANROOIJ, P. H., WANROOIJ, S., LARSSON, N.-G., WILHELMSSON, L. M., FALKENBERG, M. & GUSTAFSSON, C. M. 2012. Mammalian transcription factor A is a core component of the mitochondrial transcription machinery. *Proceedings of the National Academy of Sciences***,** 201119738.

SHIGEOKA, T., JUNG, J., HOLT, C. E. & JUNG, H. 2018. Axon-TRAP-RiboTag: Affinity Purification of Translated mRNAs from Neuronal Axons in Mouse In Vivo. *RNA Detection.* Springer.

SHORT, K. R., BIGELOW, M. L., KAHL, J., SINGH, R., COENEN-SCHIMKE, J., RAGHAVAKAIMAL, S. & NAIR, K. S. 2005. Decline in skeletal muscle mitochondrial function with aging in humans. *Proceedings of the National Academy of Sciences,* 102**,** 5618-5623.

SHOSHAN-BARMATZ, V., DE PINTO, V., ZWECKSTETTER, M., RAVIV, Z., KEINAN, N. & ARBEL, N. 2010. VDAC, a multi-functional mitochondrial protein regulating cell life and death. *Molecular aspects of medicine,* 31**,** 227-285.

SIMCOX, E. M., REEVE, A. & TURNBULL, D. 2013. Monitoring mitochondrial dynamics and complex I dysfunction in neurons: implications for Parkinson's disease. Portland Press Limited.

SINGER, V. L., JONES, L. J., YUE, S. T. & HAUGLAND, R. P. 1997. Characterization of PicoGreen reagent and development of a fluorescence-based solution assay for double-stranded DNA quantitation. *Analytical biochemistry,* 249**,** 228-238.

SLUPPHAUG, G., KAVLI, B. & KROKAN, H. E. 2003. The interacting pathways for prevention and repair of oxidative DNA damage. *Mutation Research/Fundamental and Molecular Mechanisms of Mutagenesis,* 531**,** 231-251.

SMALE, S. T. 2009. Nuclear run-on assay. *Cold Spring Harbor Protocols,* 2009**,** pdb. prot5329.

SMIRNOVA, E., GRIPARIC, L., SHURLAND, D.-L. & VAN DER BLIEK, A. M. 2001. Dynamin-related protein Drp1 is required for mitochondrial division in mammalian cells. *Molecular biology of the cell,* 12**,** 2245-2256.

SOFIC, E., LANGE, K. W., JELLINGER, K. & RIEDERER, P. 1992. Reduced and oxidized glutathione in the substantia nigra of patients with Parkinson's disease. *Neuroscience letters,* 142**,** 128-130.

SOLTYS, D. T., PEREIRA, C. P., ROWIES, F. T., FARFEL, J. M., GRINBERG, L. T., SUEMOTO, C. K., LEITE, R. E., RODRIGUEZ, R. D., ERICSON, N. G. & BIELAS, J. H. 2019. Lower mitochondrial DNA content but not increased mutagenesis associates with decreased base excision repair activity in brains of AD subjects. *Neurobiology of Aging,* 73**,** 161-170.

SONG, W., BOSSY, B., MARTIN, O. J., HICKS, A., LUBITZ, S., KNOTT, A. B. & BOSSY-WETZEL, E. 2008. Assessing mitochondrial morphology and dynamics using fluorescence wide-field microscopy and 3D image processing. *Methods,* 46**,** 295-303.

SOONG, N. W., HINTON, D. R., CORTOPASSI, G. & ARNHEIM, N. 1992. Mosaicism for a specific somatic mitochondrial DNA mutation in adult human brain. *Nature genetics,* 2**,** 318.

SPEIT, G., SCHÜTZ, P. & BAUSINGER, J. 2016. Different sensitivities of cultured mammalian cells towards aphidicolin-enhanced DNA effects in the comet assay. *Mutation Research/Genetic Toxicology and Environmental Mutagenesis,* 803**,** 22-26.

SPELBRINK, J. N., LI, F.-Y., TIRANTI, V., NIKALI, K., YUAN, Q.-P., TARIQ, M., WANROOIJ, S., GARRIDO, N., COMI, G. & MORANDI, L. 2001. Human mitochondrial DNA deletions associated with mutations in the gene encoding Twinkle, a phage T7 gene 4-like protein localized in mitochondria. *Nature genetics,* 28**,** 223.

SPILLANE, M., KETSCHEK, A., MERIANDA, T. T., TWISS, J. L. & GALLO, G. 2013. Mitochondria coordinate sites of axon branching through localized intra-axonal protein synthesis. *Cell reports,* 5**,** 1564-1575.

STAMP, C. 2016. Determining the impact of mitochondrial dysfunction on stem cell dynamics and proliferation within the colon.

STANKOV, M. V., PANAYOTOVA-DIMITROVA, D., LEVERKUS, M., SCHMIDT, R. E. & BEHRENS, G. M. 2013. Thymidine analogues suppress autophagy and adipogenesis in cultured adipocytes. *Antimicrobial agents and chemotherapy,* 57**,** 543-551.

STEWART, J. B. & CHINNERY, P. F. 2015. The dynamics of mitochondrial DNA heteroplasmy: implications for human health and disease. *Nature Reviews Genetics,* 16**,** 530.

SUN, T., QIAO, H., PAN, P.-Y., CHEN, Y. & SHENG, Z.-H. 2013. Motile axonal mitochondria contribute to the variability of presynaptic strength. *Cell reports,* 4**,** 413-419.

SURMEIER, D. J. & SCHUMACKER, P. T. 2013. Calcium, bioenergetics, and neuronal vulnerability in Parkinson's disease. *Journal of Biological Chemistry,* 288**,** 10736-10741.

SZABO, I. & ZORATTI, M. 2014. Mitochondrial channels: ion fluxes and more. *Physiological reviews,* 94**,** 519-608.

SZCZESNY, B., TANN, A. W., LONGLEY, M. J., COPELAND, W. C. & MITRA, S. 2008. Long patch base excision repair in mammalian mitochondrial genomes. *Journal of Biological Chemistry,* 283**,** 26349-26356.

TAHBAZ, N., SUBEDI, S. & WEINFELD, M. 2011. Role of polynucleotide kinase/phosphatase in mitochondrial DNA repair. *Nucleic acids research***,** gkr1245.

TAKAHASHI, K., TANABE, K., OHNUKI, M., NARITA, M., ICHISAKA, T., TOMODA, K. & YAMANAKA, S. 2007. Induction of pluripotent stem cells from adult human fibroblasts by defined factors. *cell,* 131**,** 861-872.

TAKAO, M., ABURATANI, H., KOBAYASHI, K. & YASUI, A. J. N. A. R. 1998. Mitochondrial targeting of human DNA glycosylases for repair of oxidative DNA damage. 26**,** 2917-2922.

TAKEUCHI, N., TOMITA, N. & UEDA, T. 2010. EF-G2mt is an exclusive recycling factor in mammalian mitochondrial protein synthesis. *Seikagaku. The Journal of Japanese Biochemical Society,* 82**,** 825.

TAMADA, H., KIRYU-SEO, S., HOSOKAWA, H., OHTA, K., ISHIHARA, N., NOMURA, M., MIHARA, K., NAKAMURA, K. I. & KIYAMA, H. 2017. Three-dimensional analysis of somatic mitochondrial dynamics in fission-deficient injured motor neurons using FIB/SEM. *Journal of Comparative Neurology,* 525**,** 2535-2548.

TANAKA, Y., KANAI, Y., OKADA, Y., NONAKA, S., TAKEDA, S., HARADA, A. & HIROKAWA, N. 1998. Targeted disruption of mouse conventional kinesin heavy chain kif5B, results in abnormal perinuclear clustering of mitochondria. *Cell,* 93**,** 1147-1158.

TAUPIN, P. 2007. BrdU immunohistochemistry for studying adult neurogenesis: paradigms, pitfalls, limitations, and validation. *Brain research reviews,* 53**,** 198-214.

TAYLOR, J. H., WOODS, P. S. & HUGHES, W. L. 1957. The organization and duplication of chromosomes as revealed by autoradiographic studies using tritium-labeled thymidinee. *Proceedings of the National Academy of Sciences,* 43**,** 122-128.

TAYLOR, R. W., BARRON, M. J., BORTHWICK, G. M., GOSPEL, A., CHINNERY, P. F., SAMUELS, D. C., TAYLOR, G. A., PLUSA, S. M., NEEDHAM, S. J. & GREAVES, L. C. 2003a. Mitochondrial DNA mutations in human colonic crypt stem cells. *Journal of Clinical Investigation,* 112**,** 1351.

TAYLOR, R. W., BARRON, M. J., BORTHWICK, G. M., GOSPEL, A., CHINNERY, P. F., SAMUELS, D. C., TAYLOR, G. A., PLUSA, S. M., NEEDHAM, S. J. & GREAVES, L. C. 2003b. Mitochondrial DNA mutations in human colonic crypt stem cells. *The Journal of clinical investigation,* 112**,** 1351-1360.

TAYLOR, R. W. & TURNBULL, D. M. 2005. Mitochondrial DNA mutations in human disease. *Nature Reviews Genetics,* 6**,** 389-402.

TELL, G., CRIVELLATO, E., PINES, A., PARON, I., PUCILLO, C., MANZINI, G., BANDIERA, A., KELLEY, M. R., DI LORETO, C. & DAMANTE, G. 2001. Mitochondrial localization of APE/Ref-1 in thyroid cells. *Mutation Research/DNA Repair,* 485**,** 143-152.

TELL, G., DAMANTE, G., CALDWELL, D. & KELLEY, M. R. 2005. The intracellular localization of APE1/Ref-1: more than a passive phenomenon? *Antioxidants & redox signaling,* 7**,** 367-384.

TIGHILET, B., HASHIKAWA, T. & JONES, E. G. 1998. Cell-and lamina-specific expression and activity-dependent regulation of type II calcium/calmodulin-dependent protein kinase isoforms in monkey visual cortex. *Journal of Neuroscience,* 18**,** 2129-2146.

TONG, W. H. & ROUAULT, T. 2000. Distinct iron–sulfur cluster assembly complexes exist in the cytosol and mitochondria of human cells. *The EMBO journal,* 19**,** 5692-5700.

TRIFUNOV, S., PYLE, A., VALENTINO, M. L., LIGUORI, R., YU-WAI-MAN, P., BURTÉ, F., DUFF, J., KLEINLE, S., DIEBOLD, I. & RUGOLO, M. 2018. Clonal expansion of mtDNA deletions: different disease models assessed by digital droplet PCR in single muscle cells. *Scientific reports,* 8**,** 11682.

TRIFUNOVIC, A., WREDENBERG, A., FALKENBERG, M., SPELBRINK, J. N., ROVIO, A. T., BRUDER, C. E., BOHLOOLY-Y, M., GIDLÖF, S., OLDFORS, A. & WIBOM, R. 2004. Premature ageing in mice expressing defective mitochondrial DNA polymerase. *Nature,* 429**,** 417-423.

TUTTLE, A. H., RANKIN, M. M., TETA, M., SARTORI, D. J., STEIN, G. M., KIM, G. J., VIRGILIO, C., GRANGER, A., ZHOU, D. & LONG, S. H. 2010. Immunofluorescent detection of two thymidine analogues (CldU and IdU) in primary tissue. *Journal of visualized experiments: JoVE*.

TWIG, G., ELORZA, A., MOLINA, A. J., MOHAMED, H., WIKSTROM, J. D., WALZER, G., STILES, L., HAIGH, S. E., KATZ, S. & LAS, G. 2008. Fission and selective fusion govern mitochondrial segregation and elimination by autophagy. *The EMBO journal,* 27**,** 433-446.

TWIG, G., GRAF, S. A., WIKSTROM, J. D., MOHAMED, H., HAIGH, S. E., ELORZA, A., DEUTSCH, M., ZURGIL, N., REYNOLDS, N. & SHIRIHAI, O. S. 2006. Tagging and tracking individual networks within a complex mitochondrial web with photoactivatable GFP. *American Journal of Physiology-Cell Physiology,* 291**,** C176-C184.

TYYNISMAA, H., MJOSUND, K. P., WANROOIJ, S., LAPPALAINEN, I., YLIKALLIO, E., JALANKO, A., SPELBRINK, J. N., PAETAU, A. & SUOMALAINEN, A. 2005. Mutant mitochondrial helicase Twinkle causes multiple mtDNA deletions and a late-onset mitochondrial disease in mice. *Proceedings of the National Academy of Sciences,* 102**,** 17687-17692.

TYYNISMAA, H., SEMBONGI, H., BOKORI-BROWN, M., GRANYCOME, C., ASHLEY, N., POULTON, J., JALANKO, A., SPELBRINK, J. N., HOLT, I. J. & SUOMALAINEN, A. 2004. Twinkle helicase is essential for mtDNA maintenance and regulates mtDNA copy number. *Human molecular genetics,* 13**,** 3219-3227.

UCHIC, M. D., GROEBER, M. A., DIMIDUK, D. M. & SIMMONS, J. 2006. 3D microstructural characterization of nickel superalloys via serial-sectioning using a dual beam FIB-SEM. *Scripta Materialia,* 55**,** 23-28.

VALKO, M., LEIBFRITZ, D., MONCOL, J., CRONIN, M. T., MAZUR, M. & TELSER, J. 2007. Free radicals and antioxidants in normal physiological functions and human disease. *The international journal of biochemistry & cell biology,* 39**,** 44-84.

VAN DEN HEUVEL, L. & SMEITINK, J. 2001. The oxidative phosphorylation (OXPHOS) system: nuclear genes and human genetic diseases. *Bioessays,* 23**,** 518-525.

VAN DER BLIEK, A. M., SHEN, Q. & KAWAJIRI, S. 2013. Mechanisms of mitochondrial fission and fusion. *Cold Spring Harbor perspectives in biology,* 5**,** a011072.

VAN GOETHEM, G., DERMAUT, B., LÖFGREN, A., MARTIN, J.-J. & VAN BROECKHOVEN, C. 2001. Mutation of POLG is associated with progressive external ophthalmoplegia characterized by mtDNA deletions. *Nature genetics,* 28**,** 211.

VAN LAAR, V. S., ARNOLD, B., HOWLETT, E. H., CALDERON, M. J., CROIX, C. M. S., GREENAMYRE, J. T., SANDERS, L. H. & BERMAN, S. B. 2018. Evidence for compartmentalized axonal mitochondrial biogenesis: Mitochondrial DNA replication increases in distal axons as an early response to Parkinson's disease-relevant stress. *Journal of Neuroscience***,** 0541-18.

VAN SPRONSEN, M., MIKHAYLOVA, M., LIPKA, J., SCHLAGER, M. A., VAN DEN HEUVEL, D. J., KUIJPERS, M., WULF, P. S., KEIJZER, N., DEMMERS, J. & KAPITEIN, L. C. 2013. TRAK/Milton motor-adaptor proteins steer mitochondrial trafficking to axons and dendrites. *Neuron,* 77**,** 485-502.

VARADI, A., JOHNSON-CADWELL, L. I., CIRULLI, V., YOON, Y., ALLAN, V. J. & RUTTER, G. A. 2004. Cytoplasmic dynein regulates the subcellular distribution of mitochondria by controlling the recruitment of the fission factor dynamin-related protein-1. *Journal of cell science,* 117**,** 4389-4400.

VINCENT, A. E. 2017. Investigating the pathogenesis of mitochondrial dysfunction in mitochondrial and other myopathies.

VINCENT, A. E., ROSA, H. S., PABIS, K., LAWLESS, C., CHEN, C., GRÜNEWALD, A., RYGIEL, K. A., ROCHA, M. C., REEVE, A. K. & FALKOUS, G. 2018. Subcellular origin of mitochondrial DNA deletions in human skeletal muscle. *Annals of neurology,* 84**,** 289-301.

VINCENT, A. E., TURNBULL, D. M., EISNER, V., HAJNÓCZKY, G. & PICARD, M. 2017. Mitochondrial nanotunnels. *Trends in cell biology,* 27**,** 787-799.

315

VINCENT, A. E., WHITE, K., DAVEY, T., PHILIPS, J., OGDEN, R. T., LAWESS, C., WARREN, C., HALL, M. G., NG, Y. S. & FALKOUS, G. J. C. R. 2019. Quantitative 3D Mapping of the Human Skeletal Muscle Mitochondrial Network. 26**,** 996-1009. e4.

WAKABAYASHI, J., ZHANG, Z., WAKABAYASHI, N., TAMURA, Y., FUKAYA, M., KENSLER, T. W., IIJIMA, M. & SESAKI, H. 2009. The dynamin-related GTPase Drp1 is required for embryonic and brain development in mice. *The Journal of cell biology,* 186**,** 805-816.

WALLACE, D. C. 1989. Mitochondrial DNA mutations and neuromuscular disease. *Trends in Genetics,* 5**,** 9-13.

WALLACE, D. C. 1992. Mitochondrial genetics: a paradigm for aging and degenerative diseases? *Science,* 256**,** 628-632.

WAN-XIN, T., TIAN-LEI, C., BEN, W., WEI-HUA, W. & PING, F. 2012. Effect of mitofusin 2 overexpression on the proliferation and apoptosis of high-glucose-induced rat glomerular mesangial cells. *Journal of nephrology,* 25**,** 1023-1030.

WANDERS, R. J., RUITER, J. P., IJLST, L., WATERHAM, H. R. & HOUTEN, S. M. J. J. O. I. M. D. 2010. The enzymology of mitochondrial fatty acid beta-oxidation and its application to follow-up analysis of positive neonatal screening results. 33**,** 479-494.

WANG, C. & YOULE, R. J. 2009. The role of mitochondria in apoptosis. *Annual review of genetics,* 43**,** 95-118.

WANG, G. J., NUTTER, L. M. & THAYER, S. A. 1997. Insensitivity of cultured rat cortical neurons to mitochondrial DNA synthesis inhibitors: evidence for a slow turnover of mitochondrial DNA. *Biochemical pharmacology,* 54**,** 181-187.

WANG, J. & PANTOPOULOS, K. 2011. Regulation of cellular iron metabolism. *Biochemical Journal,* 434**,** 365-381.

WANG, W., BAKER, P. & SEAH, S. Y. 2010. Comparison of two metal-dependent pyruvate aldolases related by convergent evolution: substrate specificity, kinetic mechanism, and substrate channeling. *Biochemistry,* 49**,** 3774-3782.

WANG, X., SU, B., LEE, H.-G., LI, X., PERRY, G., SMITH, M. A. & ZHU, X. 2009. Impaired balance of mitochondrial fission and fusion in Alzheimer's disease. *Journal of Neuroscience,* 29**,** 9090-9103.

WANG, X., ZHANG, C., SZÁBO, G. & SUN, Q.-Q. 2013. Distribution of CaMKIIα expression in the brain in vivo, studied by CaMKIIα-GFP mice. *Brain research,* 1518**,** 9-25.

WANROOIJ, S., FUSTÉ, J. M., FARGE, G., SHI, Y., GUSTAFSSON, C. M. & FALKENBERG, M. 2008. Human mitochondrial RNA polymerase primes lagging-strand DNA synthesis in vitro. *Proceedings of the National Academy of Sciences,* 105**,** 11122-11127.

WANROOIJ, S., LUOMA, P., VAN GOETHEM, G., VAN BROECKHOVEN, C., SUOMALAINEN, A. & SPELBRINK, J. N. 2004. Twinkle and POLG defects enhance age-dependent accumulation of mutations in the control region of mtDNA. *Nucleic acids research,* 32**,** 3053-3064.

WELLE, S., BHATT, K., SHAH, B., NEEDLER, N., DELEHANTY, J. M. & THORNTON, C. A. 2003. Reduced amount of mitochondrial DNA in aged human muscle. *Journal of applied physiology,* 94**,** 1479-1484.

WERNITZNIG, S., SELE, M., URSCHLER, M., ZANKEL, A., PÖLT, P., RIND, F. C. & LEITINGER, G. 2016. Optimizing the 3D-reconstruction technique for serial block-face scanning electron microscopy. *Journal of neuroscience methods,* 264**,** 16-24.

WESTERMANN, B. 2010. Mitochondrial fusion and fission in cell life and death. *Nature reviews Molecular cell biology,* 11**,** 872.

WIEMERSLAGE, L. & LEE, D. 2016. Quantification of mitochondrial morphology in neurites of dopaminergic neurons using multiple parameters. *Journal of neuroscience methods,* 262**,** 56-65.

WIESNER, R. J., RÜEGG, J. C. & MORANO, I. 1992. Counting target molecules by exponential polymerase chain reaction: copy number of mitochondrial DNA in rat tissues. *Biochemical and biophysical research communications,* 183**,** 553-559.

WILKE, S. A., ANTONIOS, J. K., BUSHONG, E. A., BADKOOBEHI, A., MALEK, E., HWANG, M., TERADA, M., ELLISMAN, M. H. & GHOSH, A. 2013. Deconstructing complexity: serial block-face electron microscopic analysis of the hippocampal mossy fiber synapse. *Journal of Neuroscience,* 33**,** 507-522.

WILLIAMS, K. P., SOBRAL, B. W. & DICKERMAN, A. W. 2007. A robust species tree for the alphaproteobacteria. *Journal of bacteriology,* 189**,** 4578-4586.

WILLIAMS, P. A., MORGAN, J. E. & VOTRUBA, M. 2010. Opa1 deficiency in a mouse model of dominant optic atrophy leads to retinal ganglion cell dendropathy. *Brain,* 133**,** 2942-2951.

WILLIS, D. E., XU, M., DONNELLY, C. J., TEP, C., KENDALL, M., ERENSTHEYN, M., ENGLISH, A. W., SCHANEN, N. C., KIRN-SAFRAN, C. B. & YOON, S. O. 2011. Axonal localization of transgene mRNA in mature PNS and CNS neurons. *Journal of Neuroscience,* 31**,** 14481-14487.

WONG-RILEY, M. T. 1989. Cytochrome oxidase: an endogenous metabolic marker for neuronal activity. *Trends in neurosciences,* 12**,** 94-101.

WONG, L. J. C., NAVIAUX, R. K., BRUNETTI-PIERRI, N., ZHANG, Q., SCHMITT, E. S., TRUONG, C., MILONE, M., COHEN, B. H., WICAL, B. & GANESH, J. 2008. Molecular and clinical genetics of mitochondrial diseases due to POLG mutations. *Human mutation,* 29**,** E150-E172.

WU, Z., PUIGSERVER, P., ANDERSSON, U., ZHANG, C., ADELMANT, G., MOOTHA, V., TROY, A., CINTI, S., LOWELL, B. & SCARPULLA, R. C. 1999. Mechanisms controlling mitochondrial biogenesis and respiration through the thermogenic coactivator PGC-1. *Cell,* 98**,** 115-124.

YAKES, F. M. & VAN HOUTEN, B. 1997. Mitochondrial DNA damage is more extensive and persists longer than nuclear DNA damage in human cells following oxidative stress. *Proceedings of the National Academy of Sciences,* 94**,** 514-519.

YAKUBOVSKAYA, E., MEJIA, E., BYRNES, J., HAMBARDJIEVA, E. & GARCIA-DIAZ, M. 2010. Helix unwinding and base flipping enable human MTERF1 to terminate mitochondrial transcription. *Cell,* 141**,** 982-993.

YAMASHITA, S., NISHINO, I., NONAKA, I. & GOTO, Y.-I. 2008. Genotype and phenotype analyses in 136 patients with single large-scale mitochondrial DNA deletions. *Journal of human genetics,* 53**,** 598-606.

YANG, D., OYAIZU, Y., OYAIZU, H., OLSEN, G. J. & WOESE, C. R. 1985. Mitochondrial origins. *Proceedings of the National Academy of Sciences,* 82**,** 4443-4447.

YANG, M. Y., BOWMAKER, M., REYES, A., VERGANI, L., ANGELI, P., GRINGERI, E., JACOBS, H. T. & HOLT, I. J. 2002. Biased incorporation of ribonucleotides on the mitochondrial L-strand accounts for apparent strand-asymmetric DNA replication. *Cell,* 111**,** 495-505.

YASUKAWA, T., REYES, A., CLUETT, T. J., YANG, M. Y., BOWMAKER, M., JACOBS, H. T. & HOLT, I. J. 2006. Replication of vertebrate mitochondrial DNA entails transient ribonucleotide incorporation throughout the lagging strand. *The EMBO Journal,* 25**,** 5358-5371.

YEN, T.-C., SU, J.-H., KING, K.-L. & WEI, Y.-H. 1991. Ageing-associated 5 kb deletion in human liver mitochondrial DNA. *Biochemical and biophysical research communications,* 178**,** 124-131.

YOUNG, M. J. & COPELAND, W. C. 2016. Human mitochondrial DNA replication machinery and disease. *Current opinion in genetics & development,* 38**,** 52-62.

YU, W. H., WOLFGANG, W. & FORTE, M. 1995. Subcellular localization of human voltage-dependent anion channel isoforms. *Journal of Biological Chemistry,* 270**,** 13998-14006.

YUZEFOVYCH, L. V., KAHN, A. G., SCHULER, M. A., EIDE, L., ARORA, R., WILSON, G. L., TAN, M. & RACHEK, L. I. 2016. Mitochondrial DNA repair through OGG1 activity attenuates breast cancer progression and metastasis. *Cancer research,* 76**,** 30-34.

ZANNA, C., GHELLI, A., PORCELLI, A. M., KARBOWSKI, M., YOULE, R. J., SCHIMPF, S., WISSINGER, B., PINTI, M., COSSARIZZA, A. & VIDONI, S. 2007. OPA1 mutations associated with dominant optic atrophy impair oxidative phosphorylation and mitochondrial fusion. *Brain,* 131**,** 352-367.

ZEVIANI, M., MORAES, C., DIMAURO, S., NAKASE, H., BONILLA, E., SCHON, E. & ROWLAND, L. 1988. Deletions of mitochondrial DNA in Kearns-Sayre syndrome. *Neurology,* 38**,** 1339-1339.

ZHANG, C., BAUMER, A., MAXWELL, R. J., LINNANE, A. W. & NAGLEY, P. 1992. Multiple mitochondrial DNA deletions in an elderly human individual. *FEBS letters,* 297**,** 34-38.

ZHANG, J., MONTINE, T. J., SMITH, M. A., SIEDLAK, S. L., GU, G., ROBERTSON, D. & PERRY, G. 2002. The mitochondrial common deletion in Parkinson's disease and related movement disorders. *Parkinsonism & related disorders,* 8**,** 165-170.

ZHANG, J. & NEY, P. A. 2009. Role of BNIP3 and NIX in cell death, autophagy, and mitophagy. *Cell death and differentiation,* 16**,** 939.

ZHANG, L., TRUSHIN, S., CHRISTENSEN, T. A., BACHMEIER, B. V., GATENO, B., SCHROEDER, A., YAO, J., ITOH, K., SESAKI, H. & POON, W. W. 2016. Altered brain energetics induces mitochondrial fission arrest in Alzheimer's Disease. *Scientific reports,* 6**,** 18725.

ZHANG, Y., PAK, C., HAN, Y., AHLENIUS, H., ZHANG, Z., CHANDA, S., MARRO, S., PATZKE, C., ACUNA, C. & COVY, J. 2013. Rapid single-step induction of functional neurons from human pluripotent stem cells. *Neuron,* 78**,** 785-798.

ZHENG, L., ZHOU, M., GUO, Z., LU, H., QIAN, L., DAI, H., QIU, J., YAKUBOVSKAYA, E., BOGENHAGEN, D. F. & DEMPLE, B. 2008. Human DNA2 is a mitochondrial nuclease/helicase for efficient processing of DNA replication and repair intermediates. *Molecular cell,* 32**,** 325-336.

ZHU, J., VINOTHKUMAR, K. R. & HIRST, J. 2016. Structure of mammalian respiratory complex I. *Nature,* 536**,** 354.

ZONG, H., REN, J. M., YOUNG, L. H., PYPAERT, M., MU, J., BIRNBAUM, M. J. & SHULMAN, G. I. 2002. AMP kinase is required for mitochondrial biogenesis in skeletal muscle in response to chronic energy deprivation. *Proceedings of the national academy of sciences,* 99**,** 15983-15987.

ZUCCA, F. A., SEGURA-AGUILAR, J., FERRARI, E., MUÑOZ, P., PARIS, I., SULZER, D., SARNA, T., CASELLA, L. & ZECCA, L. 2017. Interactions of iron, dopamine and neuromelanin pathways in brain aging and Parkinson's disease. *Progress in neurobiology,* 155**,** 96-119.

ZÜCHNER, S., DE JONGHE, P., JORDANOVA, A., CLAEYS, K. G., GUERGUELTCHEVA, V., CHERNINKOVA, S., HAMILTON, S. R., VAN STAVERN, G., KRAJEWSKI, K. M. & STAJICH, J. 2006. Axonal neuropathy with optic atrophy is caused by mutations in mitofusin 2. *Annals of Neurology: Official Journal of the American Neurological Association and the Child Neurology Society,* 59**,** 276-281.